

## Distribution Agreement

In presenting this thesis or dissertation as a partial fulfillment of the requirements for an advanced degree from Emory University, I hereby grant to Emory University and its agents the non-exclusive license to archive, make accessible, and display my thesis or dissertation in whole or in part in all forms of media, now or hereafter known, including display on the world wide web. I understand that I may select some access restrictions as part of the online submission of this thesis or dissertation. I retain all ownership rights to the copyright of the thesis or dissertation. I also retain the right to use in future works (such as articles or books) all or part of this thesis or dissertation.

Signature:

---

Debresha Auriel Shelton

---

Date

The Role of the Retinal Pigment Epithelium and *serpinf1* in  
Visual Outcomes after Light Damage Exposure

By

Debresha Auriel Shelton  
Doctor of Philosophy

Graduate Division of Biological and Biomedical Science  
Genetics and Molecular Biology

---

John M. Nickerson  
Advisor

---

Jeffrey H. Boatright  
Committee Member

---

Andrew Escayg  
Committee Member

---

Peng Jin  
Committee Member

---

Steven Sloan  
Committee Member

Accepted:

---

Kimberly Jacob Arriola, Ph.D.  
Dean of the James T. Laney School of Graduate Studies

---

Date

The Role of the Retinal Pigment Epithelium and *serpinf1* in  
Visual Outcomes after Light Damage Exposure

By

Debresha Auriel Shelton  
B.A. Fisk University, 2014  
M.A. Fisk University, 2018

Advisor: John M. Nickerson, PhD

An abstract of  
A dissertation submitted to the Faculty of the  
James T. Laney School of Graduate Studies of Emory University  
in partial fulfillment of the requirements for the degree of  
Doctor of Philosophy in  
Genetics and Molecular Biology  
2024

## Abstract

The Role of the Retinal Pigment Epithelium and *serpinf1* in  
Visual Outcomes after Light Damage Exposure  
By Debresha Auriel Shelton

Increasing evidence highlights the retinal pigment epithelium (RPE) in ocular inflammation and the complex, nuanced presentation of retinal degenerative diseases involving RPE pathobiology. Multiple retinal degenerative diseases, characterized by significant loss of retinal function and supportive tissue, demonstrate either primary or secondary RPE involvement in disease progression. Mammalian systems, including humans, lack the ability to regenerate damaged RPE cells, making it crucial to understand how the RPE modulates inflammation to protect visual structures and preserve vision. RPE cells serve dual roles in inflammation, exhibiting both immunogenic and immunosuppressive functions depending on the conditions. Many immunosuppressive properties of RPE are mediated by secreted factors, such as Pigment epithelium-derived factor (PEDF), encoded by *serpinf1*, and Insulin-like growth factor-1 (IGF-1). However, the expression of these factors is altered in disease, leading to a more advanced pathological state. Studies have linked up-regulated Galectin-3 (Gal-3) expression to poor prognosis in retinal degeneration, particularly in subretinal immune cells interacting with RPE.

This study aimed to 1) characterize changes in RPE morphometric features related to structural and functional vision aberrations with age, and 2) explore the immunomodulatory effects of PEDF on Galectin-3 signaling and RPE-microglia interactions after damage. While the roles of these factors in various diseases have been examined, there is limited data on their interactions in ocular damage. The findings from this study indicated that loss of PEDF increased the vulnerability of C57BL/6J mice to light damage, led to severe retinal degeneration, elevated recruitment of subretinal immune cells, and resulted in defects in damage-associated IGF-1 expression after light stress. Additionally, without damage, PEDF-deficient mice showed lower Gal-3 expression at both gene and protein levels compared to wildtypes. Interestingly, light damage exposure significantly increased Galectin-3 expression in PEDF-deficient mice, a phenotype opposite of PEDF wildtypes after the initial insult. Additionally, pharmacological inhibition of Gal-3 in PEDF wildtype mice mimicked the effects seen in PEDF-deficient mice. These results suggest that PEDF and Galectin-3 may co-regulate ocular inflammatory responses and influence visual outcomes following light damage.

The Role of the Retinal Pigment Epithelium and *serpinf1* in  
Visual Outcomes after Light Damage Exposure

By

Debresha Auriel Shelton  
B.A. Fisk University, 2014  
M.A. Fisk University, 2018

Advisor: John M. Nickerson, PhD

A dissertation submitted to the Faculty of the  
James T. Laney School of Graduate Studies of Emory University  
in partial fulfillment of the requirements for the degree of  
Doctor of Philosophy  
in Genetics and Molecular Biology  
2024

### **Acknowledgments**

First, I would like to give glory and honor to GOD for his influence in my life and for guiding me during this challenging feat. Everything I've accomplished and written in this dissertation resulted from his grace and mercy and for that I would like to thank HIM. Next, I would like to thank my wonderful, supportive parents for encouraging me to pursue my passions and cultivating my sense of curiosity about the world. Thank you for the late-night phone calls and the motivational speeches that pushed me never to give up. I want to give a special acknowledgment to my grandparents, who are no longer here to share in the celebration of my work but without whom I could never have dreamt of chasing such a huge ambition. I would also like to thank my friends, Drs. Salma Ferdous and Trenell Mosley, thank you for mentoring, motivating, and advocating for me during this process. The two of you inspire me daily to be the best scientist I can be. I'd also like to thank Yana and Jack for helping me finish my projects within a tight deadline. You guys are fantastic; this work could not have been completed without you. I want to thank the Fisk-Vanderbilt Bridge program for believing in me and instilling the grit I needed to finish my Ph.D. Next, I would also like to thank my colleagues and mentors in the Emory Eye Center for their support of my work and for being like a secondary family to me for the last 5 years. Finally, I would like to give a huge thank you to my mentor, Dr. John Nickerson, for allowing me to be your final graduate student. You allowed me to pursue my passionate questions and always imparted sagacious advice. I will forever be grateful that I had the opportunity to work with you.

## **Dissertation Table of Contents**

|             |   |     |
|-------------|---|-----|
| Chapter I.  | Abstract  | 4   |
|             | Introduction  | 9   |
|             | Premise of this dissertation  | 15  |
|             | Premise for Aim 1: The role of <i>Lsd1</i> in normal retinal development  | 16  |
|             | Premise of Aim 2: <i>Lsd1</i> is a potential therapeutic target in retinoblastoma   | 16  |
|             | Outline of the dissertation   | 16  |
|             |   |     |
| Chapter II  | Deletion of histone demethylase Lsd1(Kdm1a) during retinal development leads to visual function and morphological defects | 18  |
|             | Abstract  | 19  |
|             | Introduction  | 20  |
|             | Methods   | 22  |
|             | Results   | 29  |
|             | Discussion  | 32  |
|             | Figures and Tables  | 36  |
|             | References  | 42  |
|             |   |     |
| Chapter III | Age-related RPE Changes in C57BL/6J Mice Between 2 and 32 Months of Age   | 46  |
|             | Abstract  | 47  |
|             | Introduction  | 48  |
|             | Methods   | 50  |
|             | Results   | 55  |
|             | Discussion  | 58  |
|             | Figures & tables  | 64  |
|             |   |     |
| Chapter IV  | Comparing Light Damage-Induced Phenotype Variation in RPE65 hyper- and hypomorphs   | 72  |
|             | Abstract  | 73  |
|             | Introduction  | 75  |
|             | Methods   | 77  |
|             | Results   | 85  |
|             | Discussion  | 87  |
|             | Figures & tables  | 89  |
|             |   |     |
| Chapter V   | Loss of Pigment Epithelium Derived Factor Sensitizes C57BL/6J to Light-Induced Retinal Damage                             | 100 |
|             | Abstract  | 101 |
|             | Introduction  | 103 |
|             | Methods   | 104 |
|             | Results   | 113 |
|             | Discussion  | 120 |
|             | Figures & Tables  | 126 |

|            |                             |     |
|------------|-----------------------------|-----|
|            |                             |     |
| Chapter VI | Discussion and Summary      | 144 |
|            | Future Directions           | 148 |
|            | Significant and Impact      | 149 |
|            | References (Chapter 1, 3-5) | 150 |

## CHAPTER 1.1 INTRODUCTION

The goal of this dissertation is to characterize the functional, immunological, and molecular characteristics of pigmented animals during acute and low-grade phototoxic damage(Aim 1), and investigate PEDF as a potential regulator of damage outcomes via IGF-1-Galectin-3 signaling paradigm(Aim 2).

### 1 Importance of Understanding RPE Function During Pathology for Advancements in Therapeutics for Vision Loss

The retinal pigment epithelium (RPE) is a collective monolayer of polarized, hexagonal-shaped cells that overlay Bruch's membrane in the posterior segment of the eye, acting as the secondary site of the blood-retinal barrier. RPE selectively facilitates the exchange of nutrients, ions, and water between the retina and the choriocapillaris. The apical portion of the RPE contains microvilli, which intercalates between the outer segment of photoreceptors within the neuroretina and extends into the interphotoreceptor matrix, the compartment between the neuroretina and the RPE. The microvilli, each composed of a densely packed core of actin filaments, enclose the termini of rod- and cone photoreceptors. The RPE is the seat of multiple cellular processes required for ocular homeostasis, including waste management and regeneration of components used in phototransduction<sup>1-3</sup>. In addition to its role as a semi-permeable barrier, the RPE protects the neurosensory cells from excessive light exposure and nourishes the neuroretina with neurotropic factors that aid in its development and maintenance. Due to the myriads of functions held by the RPE, damage or dysfunction to this tissue can have devastating, adverse effects on vision<sup>4-6</sup>. Unfortunately, as a predominantly quiescent tissue, the RPE has limited mechanisms to mitigate stress or resolve damage<sup>7-9</sup>. Currently, there are no curatives to replace dead RPE cells or restore their function.

The risk of RPE dysfunction increases with age, and the consequences manifest in retinal pathologies like Age-related Macular Degeneration (AMD), Retinitis Pigmentosa (RP), and Leber's Congenital Amaurosis (LCA)<sup>10-15</sup>. Although the phenotypes of these two pathologies manifest differently, both involve etiologies that originate with RPE dysfunction and issues with the inflammatory response<sup>16-21</sup>. Thus, identifying molecular mechanisms that consider the coordinated influence of immune cells and RPE on damage phenotypes and outcomes is needed to develop new, early therapeutic interventions to protect vision in affected individuals.

### **1.1 Discovery of RPE function and structure**

The retinal pigment epithelium was first observed and described as a "real membrane" using rudimentary microscopic techniques in the late 1700s by anatomist Carlo Mondini in his "Commentationes Bononienses." In Mondini's work, he described what would later be coined the "pigmentum nigrum" by English anatomist Thomas Wharton as a "delicate network" of "innumerable globules." In the early 19<sup>th</sup> century, Wharton would describe the RPE as a "dark-colored matter...with uniform character" that lined the inner surface of the choroid of cow and sheep eyes<sup>22,23</sup>.

### **1.2 Development of the RPE**

The RPE arises from epithelial cell progenitors derived from the diencephalon, which also gives rise to the optic stalk, retina, and anterior structures of the forebrain, like the thalamus<sup>24</sup>. The RPE differentiates alongside the retina and aids in its development. In early and late RPE ablation studies, the eyecup is either reabsorbed or there is retinal disorganization, respectively<sup>25</sup>. Retinogenesis begins around embryonic day E8 in mice, with the retina and RPE beginning to differentiate around E11.5<sup>26</sup>. In addition to its roles in secreting neurotropic factors that help with retina differentiation<sup>27</sup>, waste management, and retinoid storage and regeneration, the RPE also contains melanosomes, heavily pigmented cells that protect the neural retina from oxidative stress and extraneous light exposure<sup>28</sup>.

### 1.3 Pathology of the RPE

Many of the functions of the RPE are affected during pathology involving or affecting the RPE. For example, in age-related macular degeneration (AMD), drusen, which are extracellular deposits of lipids, proteins, and debris not degraded during proteolysis, accumulates under the RPE as an early sign of age-related macular degeneration. An essential function of RPE is the phagocytosis of photoreceptor outer segments via phagocytosis, specifically LC-3-associated phagocytosis, a non-canonical form of autophagy. Studies of drusen accumulation in humans and RPE impairment models in mice show that defects in phagocytosis and autophagy result in increased sub-RPE lipofuscin and drusen deposits: a pathological phenotype of age-related macular degeneration and correlated with a significant decrease in visual function<sup>29,30</sup>.

Both Retinitis Pigmentosa (RP) and Leber's Congenital Amaurosis (LCA) are inherited retinal diseases that involve mutations in Rpe65, an isomerase found in the RPE that converts all-trans retinyl esters to 11-cis retinols required for phototransduction<sup>31</sup>. Loss of or mutations in this gene result in a diverse range of phenotypes ranging from mild to severe, resulting in progressive photoreceptor death and vision loss. The etiology of these conditions involves loss of proper vitamin A cycle regeneration in the RPE, resulting in RPE stress and photoreceptor death<sup>32-34</sup>. Environmental factors, like light stress, exacerbate the pathological phenotypes of LCA and RP<sup>35,36</sup>.

### 1.4 Immunomodulation via the RPE

Many mammalian systems, including those found in humans, cannot regenerate damaged RPE cells or accommodate their loss, depending on initial lesion size. Consequently, studying the innate molecular pathway that modulates the immune response to limit ocular damage may be an alternative therapeutic method of preserving RPE cells.

In the presentation of AMD, chronic para-inflammation, low-level noxious inflammatory stress, and deficits in RPE function are familiar hallmarks of disease<sup>37-40</sup>. Previous studies have shown that the RPE plays a role in immunomodulation. The central nervous system, and by extension the eye, employs immune privilege to limit toxic inflammation from destroying critical, post-mitotic tissues via immunosuppression<sup>41,42</sup>. The term “immune privilege” was coined by Nobel prize-winning biologist Sir Peter Medawar in the mid-20<sup>th</sup> century. In his lecture on immune tolerance, he expressed that the degree of immunological tolerance via limited or non-reactivity differs between tissues. He also described the tolerance within the eye as “special.” In the ocular microenvironment, injections into the eye's vitreous results in anterior chamber-associated immune deviation (ACAID), which protects the eye by suppressing the immune response<sup>43,44</sup>. The ACAID-like phenotype manifests during the introduction of foreign bodies into the subretinal space. An intact RPE is required for this immune tolerance to occur<sup>42,43,45-47</sup>. The RPE secretes immunosuppressive neuropeptides that aid in modulating the activity of T-cells and macrophages, like Neuropeptide Y and MSH-1<sup>48-50</sup>. The RPE also secretes neurotrophic factors implicated in immune regulation, PEDF, and IGF-1. However, the mechanism by which these factors influence eye inflammation requires elucidation.

### 1.5 Pigment epithelium-derived factor (PEDF or gene: *serpinf1*)

PEDF (also known as SerpinF1) is a member of the serpin family of proteins, known for their serine protease inhibitor function; however, PEDF is unique because it is a non-inhibitory member of this family. There are 16 clades, or subclasses, of eukaryotic serpins: PEDF exists in Clade F along with SerpinF2 or alpha-2 antiplasmin. PEDF is only expressed in vertebrates and evolutionarily and structurally conserved<sup>51</sup>. PEDF has two functional domains; one has neurotrophic activities, and the other has anti-angiogenic functions as a counterbalance to VEGF-mediated vascularization<sup>52</sup>.

Pigment epithelium-derived factor (PEDF) is a crucial multifunctional protein in RPE cell function. PEDF was initially described by *Tombran-Tink et al.* for its capability of inducing differentiation in

retinoblastoma cell lines, suggesting that PEDF is necessary for the organization and maintenance of the intraocular environment<sup>53,54</sup>. PEDF has anti-inflammatory effects, which may involve inhibition of the MAPK signaling cascade and activation of the Lamin receptor signaling in myeloma cells<sup>55</sup>. Studies in dry eye disease (DED) have postulated that the 29-mer of PEDF has protective effects via the immunosuppression of proinflammatory cytokines and reduced activity of matrix metalloproteinase-9(MMP9)<sup>56</sup>.

PEDF influences the proliferative capacity and metabolism of microglia and astrocytes collected from rat brains, suggesting that PEDF plays a role in suppressing the proliferation of these cell types<sup>57</sup>. PEDF suppresses dry eye disease-associated (DED) damage severity, enhancing T-regulatory frequency and functional capacity<sup>58</sup>. PEDF expression is vital to maintain the differentiated phenotype in epithelial cells. For example, in low metastatic cancer cells, high expression of PEDF was accompanied by increased alpha-catenin expression, a structural protein that works with F-actin to form a mechanosensory junction needed for cell-cell contact of healthy cells<sup>59-61</sup>. PEDF also functions to influence microglia morphology<sup>62</sup>. The ability of PEDF to modulate both RPE cell responses and microglia morphology and function suggests that it participates in the selective recruitment of microglia subclasses from the retina during the onset and progression of disease<sup>57,63</sup>.

## **1.6 Insulin-like Growth Factor-1 (IGF-1)**

The insulin-like growth factor (IGF) system consists of hormone peptide ligands IGF-1 and IGF-2, which share more than 50% homology with insulin, their respective receptors, and several protein binding partners. IGF-1/IGF-1 receptor modulates multiple cellular processes, including growth and development, cell survival, and proangiogenic and anti-apoptotic properties through localized paracrine/autocrine signaling in various tissues<sup>64</sup>. IGF-1 facilitates proper retina vascularization, even in the presence of VEGF. Due to the conserved homology that IGF-1 shares with insulin, the IGF-1/IGF-1 receptor

complex is also involved in the pathogenic presentation of metabolic disorders involving insulin resistance, like diabetic retinopathy<sup>65</sup>.

Studies have also implicated IGF-1 in modulating innate and adaptative immune responses via a STAT3-mediated signaling cascade<sup>64</sup>. Additionally, IGF-1/insulin is associated with the prolonged proinflammation associated with aging. Other studies have posited that IGF-1 can shift proinflammatory microglia from an M1 cell fate to an M2 phenotype associated with protection<sup>66</sup>. Interestingly, PEDF may regulate IGF-1 expression, repressing IGF-1 activity, and indirectly regulating microglia activity in an IGF-dependent manner<sup>67</sup>.

### 1.7 Galectin-3(Gal-3 or gene: *Lgals3*)

In 2006, An et al. studied the secreted proteome of RPE cell cultures isolated from patients with AMD and compared them to control eyes<sup>17,68</sup>. Interestingly, they found a 3-fold increase in the secretion of four proteins in AMD eyes compared to controls; among them were galectin-3 (*Lgals3*) and pigment epithelium-derived factor (PEDF). Galectin-3, a member of the  $\beta$ -galactosidase binding protein family, expressed in the cytosol and the nucleus of the RPE, can be secreted via a non-classical pathway to the cell surface of the RPE, where it participates in a cell lattice formation and cell-cell interaction<sup>69,70</sup>. Galectin-3 fine-tunes inflammatory responses due to its increased affinity for  $\beta$ -1, 6-N- glycosylation on the cell surface of RPE cells undergoing epithelial-to-mesenchymal transition ( EMT) and its increased secretion of Galectin-3 from RPE cells after damage<sup>69-71</sup>. While the complete list of galectin-3 binding partners is still incomplete, there is evidence that galectin-3 can bind to receptors like TGF- $\beta$  receptors and interact to form complexes with neurotrophic factor receptors associated with inflammatory functions<sup>71,72</sup>. Co-culturing microglia with galectin-3 can change their secretory profile and morphology, suggesting that galectin-3 is essential in fine-tuning immune cell response<sup>72</sup>. *O'koren et al.* showed that microglia reside in two anatomically distinct niches within the retina and display different dependencies

on IL-34 to survive. They describe that microglia from both niches are recruited to the subretinal space where the RPE resides<sup>73</sup> during damage.

Multiple studies other studies have also suggested there is transcriptional heterogeneity in microglia during neurodegenerative diseases, including those performed in the eye, and have identified a subpopulation of proliferating microglia enriched with galectin-3 transcripts and another gene that is often co-expressed with galectin-3, insulin-like growth factor (*Igfl*)<sup>73-76</sup>. IGF-1 is associated with neuroprotective functions, and functional studies have shown it co-expressed in galectin-3-positive microglia<sup>72</sup>. *Lalancette-Hebert et al.* showed that IGF-1 may be an upstream regulator of galectin-3 expression in microglia and can induce microglia proliferation after damage<sup>77-79</sup>.

Multiple organs in the body express PEDF. Additionally, several cell types in the eye express PEDF, but it is preferentially secreted by the RPE in the eye. PEDF is a secreted neurotrophic factor expressed at high levels in healthy, fully differentiated RPE cells and downregulated during damage, aging, and EMT found in cancerous cells<sup>80-82</sup>.

With PEDF counterbalance to VEGF-A, a prominent focus of current therapeutic intervention in AMD and other retinal diseases, it is essential to characterize the possible immunomodulatory influence of PEDF secreted by RPE cells within the damaged ocular environment.

## **1.8 PREMISE**

Based on the literature, our central hypothesis is that the RPE influences immune responses via a PEDF-Galectin-3 mediated signaling paradigm. This study addresses the gap in knowledge around the immunomodulatory effects of PEDF on Galectin-3 signaling and the RPE-microglia interactions mediating immune privilege in the eye after damage.

**1.8.1 Aim 1: Evaluate pigmented animals' functional, immunological, and molecular characteristics during acute and low-grade phototoxic damage.**

***Hypothesis:*** Common molecular signatures are subverted during pathology; thus, identifying damage kinetics and molecular determinants involved in modifying damage outcomes will provide therapeutic targets for sigh-saving intervention.

**1.8.2 Aim 2: Investigate PEDF as a potential regulator of immune responses via IGF-1-Galectin-3 signaling. *Hypothesis:*** Dysregulation of PEDF expression is associated with RPE damage and increased inflammation during AMD progression in humans; thus, loss of PEDF will increase Galectin-3 mediated inflammation and down-regulate neuroprotective factor, IGF-1, in the subretinal space

**1.9 Dissertation Outline**

This dissertation is divided into six chapters. The introduction serves as the first chapter and is a brief review of seminal works covering RPE structure, importance in normal eye development and pathology, and key secreted factors discussed in the body of this work. The second chapter is a primary scientific article published in *Frontiers Neuroscience* that investigates the role of the lysine demethylase, *Lsd1*, in proper retina development and retinal subtype speciation. This chapter is unrelated to PEDF or RPE. The third chapter is a primary scientific article, preprinted in *BioRxiv*, characterizing morphological changes in RPE that correspond with changes in functional and immunological patterning in *C57BL/6J* mice aged over 24 months, a distinctly understudy demographic. This chapter is unrelated to PEDF but has some relevance to RPE structures. The fourth chapter investigates the functional, immunological, and molecular changes in congenic pigmented photosensitive versus pigmented photoresistant animals via manipulation of the vitamin A cycle. Chapter four details the phenotypic differences in pigmented *C57BL/6J* animals with a conservative, single nucleotide substitution in the *Rpe65* gene, an isomerase

that is expressed in the RPE and needed for phototransduction. We showed that the substitution of amino acid 450 within the RPE65 protein from methionine (which confers photoresistance) to leucine confers photosensitivity in mice. We also investigate the requirement of PEDF in the photoresistant phenotype. The fifth chapter examines the facilitation of protection from phototoxic damage via a novel function of PEDF in regulating IGF-1 and Galectin-3 expression. Chapter five posits that PEDF and Galectin-3 may co-regulate each other to confer a photoresistant phenotype and may be therapeutic targets for further studies of immune privilege. The sixth, and final, chapter is the summary and overall discussion of the implications of the work included in document, how it differs from previous studies, and adds important insights to the field.

**2 CHAPTER 2: Deletion of histone demethylase Lsd1 (Kdm1a) during retinal development leads to visual function and morphological defects**

Salma Ferdous<sup>1†</sup>, Debresha A. Shelton<sup>1†</sup>, Tatiana E. Getz<sup>1</sup>, Micah A. Cherek<sup>1</sup>, Nancy L'Hernault<sup>1</sup>, Jana T. Sellers<sup>1</sup>, Vivian R. Summers<sup>1</sup>, P. Michael Iuvone<sup>1</sup>, Jeremy M. Boss<sup>2</sup>, Jeffrey H. Boatright<sup>1,3</sup>, John M. Nickerson<sup>1</sup>

†These authors contributed equally to this work and share first authorship

<sup>1</sup>Emory University, Department of Ophthalmology, Atlanta, Ga, United States

<sup>2</sup>Emory University, Department of Microbiology and Immunology, Atlanta, Georgia, United States

<sup>3</sup> Atlanta Veterans Administration Center for Visual and Neurocognitive Rehabilitation, Decatur, Georgia, United States

## 2.1 ABSTRACT

### Purpose:

This study aimed to investigate the role of Lsd1 in proper retinal development. Lysine-specific demethylase 1 (Lsd1) is a histone demethylase that can demethylate mono- and di-methyl groups on H3K4 and H3K9. Using Chx10-Cre and Rho-iCre75 driver lines, we generated novel transgenic mouse lines to delete Lsd1 in all progenitor cells or specifically in rod photoreceptors. We hypothesize that Lsd1 deletion will cause global morphological and functional defects due to its importance in neuronal development.

### Methods:

We tested young adult mice for visual function, with electroretinograms (ERGs), and *in vivo* imaging to obtain Fundus and SD-OCT images. Afterwards, eyes were enucleated and fixed for H&E and immunofluorescent staining or electron microscopy.

### Results:

In adult Chx10-Cre Lsd1(lox/lox) animals, we observed a marked reductions in a-, b-, and c- wave magnitudes in scotopic conditions. Raw photopic and flicker ERG waveforms were even more sharply reduced. These decreases in visual function were corroborated with modest reductions in total retinal thickness and outer nuclear layer thickness as observed in SD-OCT and H&E images. Lastly, electron microscopy revealed significantly shorter inner and outer segments and immunofluorescence showed modestly reduced cell type populations. We did not observe any obvious functional or morphological defects in the adult Rho-iCre75 Lsd1 (lox/lox) animals.

### Conclusions:

Lsd1 is necessary for neuronal development specifically in the retina as adult Chx10-Cre Lsd1 (lox/lox) mice show greatly impaired visual function and retinal morphology. These effects were fully manifested in young adults (P30) suggesting that Lsd1 affects early mouse retina development.



## 2.2 INTRODUCTION

Lysine-specific demethylase 1 (Lsd1) can demethylate mono- and di- methyl groups on H3K4 (Shi, 2004), H3K9 (Laurent, 2015), and H4K20 (Wang, 2007) on Histone H3 and H4 in nucleosomes as well as demethylate non-histone proteins (Gu, 2020). Although it is ubiquitously expressed throughout the body, Lsd1 has an acutely important role in the development of neurons, particularly due to a neuron specific isoform, neuroLsd1 (nLsd1) (Zibetti, 2010 Rusconi, 2016, Toffolo, 2014). Lsd1 promotes neurite growth and branching (Zibetti, 2010) and plays a role in spatial learning and long-term memory formation (Rusconi, 2016). Dysregulation of Lsd1 in animal models cause a variety of neuronal specific abnormalities including reduced cell proliferation in the hippocampal dentate gyri (Sun, 2010), abnormal development of pyramidal cortical neurons (Fuentes, 2012), paralysis related to degeneration of the hippocampus and cortex (Christopher, 2017), and an anxiety-like emotional behavior (Rusconi, 2016 (emotional)). In humans, mutations in Lsd1 are associated with a wide array of neurodevelopmental, psychiatric, and addiction disorders (Collins, 2019). Human patients who have dominant missense mutations in Lsd1 have neurodevelopmental delays and craniofacial abnormalities (Chong, 2016 Pilotto, 2016) and features of KBG syndrome (OMIM #148050) and Kabuki syndrome (OMIM #147920) (Tunovic, 2014).

Lsd1 is in the top 2% of evolutionarily constrained genes, which are genes that exhibit no sequence changes among widely diverse species (Samocha, 2014). Consequently, global homozygous deletion of Lsd1 in mice results in embryonic lethality at embryonic day 9.5 (E9.5), likely due to cardiac problems, whereas heterozygous deletion has no profound consequences (Wang, 20??). During normal retinal development, Lsd1 is expressed in all retinal progenitor cells (RPCs) during retinal development and in most mature retinal neurons after development is complete (Ferdous, 2019). Lsd1 is also expressed in all other major ocular structures, such as the cornea, lens, and retinal pigmented epithelium (RPE) (Ferdous, 2019). Based on the importance of Lsd1 in proper brain neuronal development and function as well as its

ubiquitous expression in retinal neurons during and after development, we hypothesize that Lsd1 is required for the development, maintenance, and function of the retina. The deletion of Lsd1 could result in either: 1) Retinal degeneration due to retinal progenitor cells being unable to proliferate and/or cells undergoing cell death due to aberrant epigenomic regulation, or 2) Improper differentiation of retinal progenitor cells into mature retinal neurons leading to an over- or under-representation of certain neuronal populations, specifically photoreceptors. This hypothesis is based on work done by Popova et al. in which pharmacological inhibition of Lsd1 in retinal explants inhibited proper rod photoreceptor development via misexpression of the Notch/Hes1 pathway (Popova, 2016). This group then went on to discover that pharmacological inhibition of Lsd1 in the rd10 mouse prevented rod photoreceptor death and improved visual function, indicating that Lsd1 inhibitors may be a viable option for treating retinal degenerations (Popova, 2021). 3) A third possibility is that roughly the correct number of cells are born and terminally differentiate but due to abnormalities in gene expression, wiring among “normal” appearing cells is incorrect. Therefore, the retina would look morphologically normal, but does not function correctly.

To test our hypotheses, we used the Cre-Lox system (Nagy, 2000) to delete Lsd1 in most retinal progenitor cells using the Chx10-Cre driver mouse line (Rowan, 2004). Afterwards, we tested juvenile post-natal day 30 (P30) adult mice for visual function (ERGs), examined in vivo morphology (fundus and SD-OCT), and conducted post-mortem morphology (H&E staining, immunofluorescence staining, and electron microscopy) to understand the effects of loss of Lsd1. We found substantial functional abnormalities and losses in ERGs but comparatively modest structural changes at the microscopic level. We also tested whether deletion of Lsd1 in a rod-specific manner using the Rho-iCre75 driver mouse would have any effect on proper rod development or function; however, those animals did not show signs of obvious phenotype.

## 2.3 METHODS

### 2.3.1 Animal studies:

Mouse housing, experiments, and handling were approved by the Emory University Institutional Animal Care and Use Committee, and the studies were conducted in adherence with Association for Research in Vision and Ophthalmology (ARVO) and followed guidance and principles of the Association for Assessment and Accreditation of Laboratory Animal Care (AAALAC). Mice were maintained on a 12-h light/dark cycle at 22 °C, and standard mouse chow (Lab Diet 5001; PMI Nutrition Inc., LLC, Brentwood, MO) and water was provided ad libitum. The mice were managed and housed by Emory University Division of Animal Resources. Roughly equal number of male and female mice were used in all experiments. Adult mice were euthanized using CO<sub>2</sub> gas asphyxiation for 5 minutes followed by cervical dislocation.

### 2.3.2 Breeding scheme:

Chx10-Cre animals (JAX Stock #005105) obtained from Dr. Michael Iuvone at the Emory University were bred with Lsd1 (lox/lox) animals obtained from Dr. Jeremy Boss at Emory University. This breeding scheme produced litters that were 50% Lsd1 (lox/lox) (controls) and 50% Chx10-Cre Lsd1 (lox/lox) (experimental). These mice were produced to specifically delete Lsd1 in most retinal progenitor cells during development. Chx10-Cre control animals were bred separately. Additionally, Rho-iCre75 (JAX Stock #015850) (Li 2005) were also bred with Lsd1 (lox/lox) animals to produce litters that were 50% Lsd1 (lox/lox) (controls) and 50% Rho-iCre75 Lsd1 (lox/lox). These mice were produced to specifically delete Lsd1 in rod photoreceptors. Results from genotyping for Cre recombinase were hidden from the experimental biologists until after in vivo experiments were complete and samples were collected to remove any possible implicit bias.

### 2.3.3 Electroretinograms:

Equal numbers of male and female mice were dark-adapted overnight the day before ERGs were performed (Mazzoni 2019). In darkness (under infrared lighting), each mouse was anesthetized using intraperitoneal (IP) injections of 100 mg/kg of ketamine and 15 mg/kg xylazine (ketamine; KetaVed from Patterson Veterinary, Greeley, CO; xylazine from Patterson Veterinary, Greeley, CO).

Once anesthetized, proparacaine (1%; Akorn Inc.) and tropicamide (1%; Akorn Inc.) eye drops were administered to reduce eye sensitivity and dilate pupils. Mice were placed on a heating pad (39 °C) under dim red light provided by the overhead lamp of the Diagnosys Celeris system (Diagnosys, LLC, Lowell, MA, USA). The light guided electrodes were placed in contact with individual eyes; the corneal electrode for the contralateral eye acts the reference electrode. Full-field ERGs were recorded for the scotopic condition (stimulus intensity: 0.001, 0.005, 0.01, 0.1, 1, and 10 cd s/m<sup>2</sup>; flash duration 4 milliseconds). Signals were collected for 0.3 seconds in steps 1 to 5 and 5 seconds for step 6 after light flashes. Scotopic a-, b-, and c-waves were captured and analyzed. After scotopic testing, mice were light-adapted for 10 minutes, and then full-field ERGs were recorded for the photopic conditions (stimulus intensity: 3 and 10 cd s/m<sup>2</sup>) to capture photopic a- and b-waves as well as cone flicker responses at 10 Hz. After recordings, each mouse was placed in its home cage on top of a heating pad (39 °C) to recover from anesthesia.

#### **2.3.4 In vivo ocular imaging:**

Mice were anesthetized using IP injections of ketamine and xylazine as described above. Once anesthetized, proparacaine and tropicamide eye drops were administered as described above. A MICRON<sup>®</sup> IV SD-OCT system with fundus camera (Phoenix Research Labs, Pleasanton, CA) was used to obtain both fundus photos and OCT images for both eyes. Images were taken after clear visualization of the fundus with a centered optic nerve. Circular scans approximately 100 microns from the optic nerve head were taken and fifty scans were averaged together. The OCT images were analyzed for both total retinal thickness and photoreceptor layer thickness using Photoshop CS6 (Adobe Systems Inc., San Jose,

CA) by an individual who was masked to sample identity. The number of pixels were converted into micrometers by multiplying by a conversion factor (1 pixel = 1.3 microns).

### 2.3.5 Immunoblotting:

Immunoblot experiments were performed as previously described (Ferdous 2019). In brief, two dissected retinas were collected for each sample. Protein was extracted using mechanical shearing of the tissue by a QIAGEN TissueLyser. Protein concentration of the supernatant was determined using a Pierce Bicinchoninic Acid (BCA) Assay<sup>28</sup> and absorbance was measured at 562 nm using a Synergy H1 Hybrid Plate Reader (BioTek). After protein quantification, samples were diluted to a protein concentration of 0.8 mg/mL and immediately before electrophoresis samples were heated for 5 minutes at 95 °C in a thermocycler. Samples were run on a pre-cast Criterion gel (BioRad TGX Stain Free Gel 4-15% Catalog #567-1083) as well as 10 mL of a molecular weight ladder (Bio-Rad Catalog #1610376) and run at 100 V for 90 min. Samples were transferred for 7 minutes onto PVDF blotting membrane using Trans-blot turbo pack (Bio-Rad Catalog #170-4157) and Trans-blot Turbo Transfer System (Bio-Rad). Membranes were blocked for 2 hours at room temperature in 5% (W/V) instant nonfat dry milk (Quality Biological Catalog #A614-1005) in TBST (Tris buffered saline (TBS) (Bio-Rad #1706435) with 0.1% (V/V) Tween 20 (Fisher Scientific BP337-100)). Afterwards, primary antibodies (anti-Lsd1 (Abcam 129195 [1:1000]) and anti-GAPDH (GeneTex GTX627408 [1:1000]) were diluted with 5% milk in TBST, and membranes were incubated overnight on a 4 °C shaker. The membrane was washed three times for 5 minutes each using TBST. HRP conjugated secondary antibodies (mouse anti-rabbit HRP (Santa Cruz sc-2357 [1:5000]) and goat anti-mouse HRP (Abcam ab7068 [1:5000])) were diluted with 5% milk in TBST and membranes were incubated 1-2 hours at room temperature on a shaker. The membrane was washed three times for 5 minutes each using TBST. 10 mL of Luminata Crescendo Western HRP substrate (EMD Millipore Catalog #WBLUR0500) was applied to the membrane for 5 min. The membrane was imaged in chemiluminescence mode using MP ChemiDoc Imaging System (Bio-Rad). Exposure times varied from 30 to 180 seconds. In order to re-probe the same membrane with multiple antibodies, after imaging, 10

mL of Restore western blot stripping buffer (Thermo Scientific Catalog #21059) was applied to the blot for 10 minutes, the blot was washed for 5 minutes using TBST, and then blocked with 5% milk (W/V) in TBST and incubated with the appropriate primary and secondary antibody as described above.

### **2.3.6 Ocular sectioning and histology:**

Eyes were enucleated and processed for histology by a freeze substitution method in 10 mL of dry-ice chilled 97% methanol + 3% acetic acid for 4 days at -80 °C (Sun, 2015). Afterwards, samples were exchanged for 20 minutes in each of the following solutions (100% ethanol twice, followed by 100% xylene twice) at room temperature and then embedded in paraffin. 5-micron sagittal plane sections were cut on a microtome with a fresh blade, and sections containing the optic nerve and the center of the cornea were selected for further staining to ensure consistency across all samples. Sections were stained with hematoxylin and eosin (H&E) to visualize retinal morphology. Nuclei in the outer nuclear layer (ONL), inner nuclear layer (INL), and retinal ganglion cell layer (RGCL) were counted manually by an individual who was masked to sample identity. Only nuclei within a 100-micron region were counted using Photoshop CS6 at regularly spaced intervals 500 microns apart from the optic nerve in both the inferior and superior directions. For retinal arc length, Photoshop CS6 was used to measure the distance along the retina between the inferior and superior most peripheral retina.

### **2.3.7 Immunofluorescence:**

Antibody staining was performed on eyes that were enucleated and processed by a freeze substitution method in 10 mL of dry-ice chilled 97% methanol + 3% acetic acid for 4 days at -80 °C (Sun, 2015) and embedded in paraffin as above. Afterwards 5-micron sections were cut, and slides were soaked for 2 minutes each in 5 steps of xylene, an ethanol rehydration series (100%, 90%, 80%, 70%, 60%, 50%), and TBS (Corning 46-012-CM). A Sequenza staining system (Thermo Scientific 73310017, 72110017) was used for immunostaining the slides. Slides were incubated at room temperature (RT; ~23°C) for 30 minutes in blocking buffer (2.5% normal donkey serum in TBS (Corning 46-012-CM with

0.01% NaAzide)). Slides were stained for 1 hour at RT, washed twice for 5 minutes each with TBST (TBS + 0.1% Tween-20; Biorad 1706531), incubated with secondary antibody for RT for 1 hour, washed twice for 5 minutes each with TBST, counterstained with 2.5  $\mu$ M Hoechst 33342 in TBS for 10 minutes, and rinsed once with TBS. Vectashield Vibrance (Vector Labs H-1700) was used to mount the coverslip and then the sections were imaged using an A1R confocal on a Nikon Ti2 microscope. All primary and secondary antibodies used for this study are listed in Table 1.

### **2.3.8** TUNEL Staining:

The manufacturer instructions for the Promega DeadEnd TUNEL Fluorometric kit (Promega G3250) were followed. In brief, tissue sections were deparaffinized in 5 steps of xylene for 2 minutes each. The tissue sections were then rehydrated in a graded ethanol series (100%, 90%, 80%, 70%, 60%, 50%) for 2 minutes each. The slides were then washed for 5 minutes in PBS (Corning 46-013-CM) and mounted in the Sequenza system. Sections were incubated for 15 minutes in Z-fix (Anatech, Fisher Scientific NC935141), washed twice in PBS for 5 minutes each, incubated in Proteinase K solution for 8 minutes, washed with PBS for 5 minutes, fixed with Z-fix for 5 minutes, washed with PBS for 5 minutes, incubated with rTDT enzyme and nucleotide mix in equilibration buffer for 2 hours, washed with 2x SSC for 5 minutes, counterstained with 2.5 mHoechst 33342 in TBS for 10 minutes, and rinsed with TBS for 5 minutes. Coverslips were then mounted using VectaShield Vibrance and imaged using an A1R confocal on a Nikon Ti2 microscope.

### **2.3.9** Electron microscopy:

Eyes are enucleated and fixed in 0.1M Cacodylate buffer for 2 hours at RT and then overnight at 4 °C. Afterwards, tissue was washed in 0.1 M sodium cacodylate buffer for 15 minutes before being post-fixed in 1% OsO<sub>4</sub> in 0.1M sodium cacodylate buffer for 2 hours at RT. The tissue was washed in deionized water for 10 minutes and then dehydrated in a graded ethanol series (35%, 50%, 70%, 95%, and 100% twice) for 15 minutes each. The tissue was washed in propylene oxide twice for 15 minutes

before being placed overnight in a 1:1 mixture of propylene oxide: LX 112 embedding resin (Ladd Research, Williston, VT) overnight. The next day, the tissue was placed in pure resin within a vacuum desiccator for 3-4 hours. Finally, the tissue was embedded in fresh resin and placed at 60 °C for two days to polymerize. A Lecia UCT was used to cut 1-micron thick sections, which were stained in an aqueous solution of 1% toluidine blue and 1% sodium borate. Ultrathin sections (silver-gray) were cut from areas of interest, placed on 300 mesh copper grids and stained with 2% aqueous uranyl acetate for 30 minutes, before being washed in distilled water, stained with Reynold's lead citrate for 2 minutes, washed and air dried. Finally, images were taken with a JEOL 100 CX-11 transmission electron microscope and photographed with an SIA L12C Peltier-cooled CCD digital camera (Scientific Instruments and Applications, Inc., Duluth, GA 30096).

#### **2.3.10 Statistical Analysis:**

Statistical analysis was conducted using Prism 8.4.2 (GraphPad Software, Inc., La Jolla, CA, USA) on Mac OS 11.6.8. All data are summarized as mean  $\pm$  standard deviation (SD), and individual statistical tests and sample sizes are listed in the figure legends. P values  $< 0.05$  were statistically significant. Each sample group member is an independent mouse.

## **2.4 RESULTS**

The Chx10 Cre driver mouse line expresses Cre recombinase as early as E14.5 in most retinal progenitor cells (Rowan, 2004). Expression of Chx10 (Vsx2) increases by 3-4-fold between P0 – P6 (Liu, 1994) but is absent in most post-mitotic retinal cells except bipolar cells and some Muller glial cells in mice (Rowan, 2004). After breeding Chx10-Cre mice with Lsd1 (lox/lox) mice, we first tested the efficiency of Lsd1 deletion in the retina via western immunoblotting. Retinas were isolated from P30 mice from two control lines, Chx10-Cre only and Lsd1 (lox/lox) only to serve as negative controls that have normal Lsd1 expression and function, and one experimental line Chx10-Cre Lsd1 (lox/lox). All

mouse lines were on a C57Bl/6J background to eliminate any potential genetic confounding factors. We probed for Lsd1 protein (Figure 1A) and used GAPDH as a loading control (Figure 1B). All eight control retinas exhibited Lsd1 protein bands at the expected molecular weight of 107 kDa. Although there was some Lsd1 protein expression in the four Chx10 – Cre Lsd1 lox samples, quantification via densitometry showed a statistically significant 86% reduction in Lsd1 in the experimental animals compared to the control groups (Figure 1C and Supplemental Table 1). This indicates that Lsd1 was deleted in a high percentage of retinal cells and is consistent with known expression patterns of Chx10 (Vsx2) in most retinoblasts and mature inner retinal cells, particularly bipolar cells (Liu, 1994; Rowan, 2004).

After Lsd1 deletion was confirmed via immunoblotting, adult P30 animals were tested for visual function using full field electroretinograms (ERGs). Animals were tested in both scotopic and photopic conditions and both a- and b-waves were measured. For both scotopic and photopic conditions, raw ERG waveforms in response to a 10 cd s/m<sup>2</sup> light flash showed relatively normal ERG responses in the Chx10-Cre and Lsd1 (lox/lox) control animals; however, the Chx10-Cre Lsd1 (lox/lox) animals had sharply reduced and abnormal visual responses (Figure 2A – 2B). In scotopic conditions with increasing light flash intensities, we observed significant decreases in the a-waves (~75%) and b-waves (~89%) of the Chx10-Cre Lsd1 (lox/lox) animals when compared to controls, indicating dysfunction in the rod photoreceptors and rod bipolar cells (Figure 2C – 2D and Supplemental Table 2 & 3). Additionally, scotopic c-waves were significantly reduced (Figure 2E and Supplemental Table 4) and cone flicker responses were abolished, and oscillatory potentials data were profoundly reduced (Figure 2F-2G) indicating proportional dysfunction in the RPE and abolishment of cone photoreceptors signals.

The significant visual function defects in the Chx10-Cre Lsd1 (lox/lox) mice suggest that there may be developmental abnormalities in photoreceptors and bipolar cells. To detect *in vivo* retinal morphology defects, animals were tested at P30 with fundus photography and SD-OCT images and total retinal thickness and outer nuclear layer (ONL) thickness were quantified by a masked individual. In the fundus

photos, we observed a more mottled and speckled appearance in the Chx10-Cre Lsd1 (lox/lox) animals compared to the controls (Figure 3A, 3C, 3E). The SD-OCT images revealed substantial degeneration and increased hyper-reflectivity in the ONL in the Chx10-Cre Lsd1 (lox/lox) animals compared to the controls (Figure 3B, 3D, 3F). There was a statistically significant reduction in total retinal thickness (~26% loss) and ONL thickness (~22% loss) (Figure 3G - 3H and Supplemental Table 5 & 6). The significant 22% reduction in the ONL likely contributes in part to the 75% loss of scotopic a-waves.

After *in vivo* measurements, we collected P30 eyes for post-mortem analysis. We first stained sagittal retinal sections with hematoxylin & eosin (H&E) to observe retinal morphology (Figure 4A – 4F). In these sections, we found the same retinal thinning that was observed in the SD-OCT images. We also found that, on average, cell nuclei quantification of the ONL and inner nuclear layer (INL) showed statistically significant losses (~19% and ~30% respectively) between the experimental group and control groups (Figure 4G – 4H and Supplemental Table 7 & 8); however, there were no statistical differences in the retinal ganglion cell layer (RGCL) (Figure 4I and Supplemental Table 9). This may indicate that Lsd1 protein functionality is more important in the proper development of photoreceptors and inner neurons such as bipolar cells and horizontal cells, rather than retinal ganglion cells or displaced amacrine cells. Alternatively, it may indicate that because retinal ganglion cells and amacrine cells, along with horizontal cells, are the first cells to develop in the retina, these cell types are fully committed and differentiated before Lsd1 enzyme activity is knocked out of those cells by Chx10-Cre mediated deletion (Cepko, 1996 ; Bassett, 2012). Lastly, on average the retinal arc lengths of the Chx10-Cre Lsd1 (lox/lox) mice were statistically shorter by ~7% compared to both control groups (Figure 4J and Supplemental Table 10).

To obtain more detailed information on the abnormal morphology of the area between the RPE and the external limiting membrane (ELM), we took electron microscopy images. Based on the images, we observed a substantial degeneration and disorganization of the inner and outer segments (Figure 5C and 5F), which is the likely cause of the visual function loss in the experimental animals compared to the

controls (Figure 5A - 5B and 5D - 5E). We observe large vacuoles and no clear demarcation between the inner and outer segments in the experimental animals compared to controls. On average, we found that the inner segments and outer segments of the Chx10-Cre Lsd1 (lox/lox) animals were significantly shorter compared to both control groups (~31% and 47% respectively, Supplemental Table 11 and 12). The average length of the outer segments in the Chx10-Cre Lsd1 (lox/lox) animals was 15.4um, compared to 27.9um for the Chx10-Cre controls and 29.7um for the Lsd1 (lox/lox) controls (Figure 5G). The average inner segments in the Chx10-Cre Lsd1 (lox/lox) animals was 14.1um, compared to 20.8um for the Chx10-Cre controls and 19.8um for the Lsd1 (lox/lox) controls (Figure 5H).

Because of the significant decreases in cell nuclei observed in the ONL and INL, we wanted to see if certain cell types were uniquely sensitive to Lsd1 deletion. Through immunofluorescence, we stained for Lsd1, TUNEL, and major cell type specific markers across all three groups. There was little Lsd1 protein expressed in the Chx10-Cre Lsd1 (lox/lox) animals compared to control groups (Figure 6A – 6F) which corroborate the western blot results in Figure 1. When we examined cell-type specific markers for photoreceptors (Figure 6G – 6L), horizontal and amacrine cells (Figure 6M – 6R), and rod bipolar cells and retinal ganglion cells (Figure 6S – 6X) we observed qualitative reductions in the expression of calbindin and PKCalpha in the Chx10-Cre Lsd1 (lox/lox) animals compared to controls. We also observed TUNEL staining, which labels DNA breaks during apoptosis, in the experimental Chx10-Cre Lsd1 (lox/lox) group in the ONL which is consistent with active photoreceptor cell death. As expected, no TUNEL staining was observed in either control group (Figure 6Y – 6DD).

In addition to the Chx10-Cre driver line, we also used a Rho-Cre driver mouse to delete Lsd1 in a rod-specific manner. In order to determine whether the deletion of Lsd1 in rods has any effect on proper retinal function, we performed ERGs in scotopic conditions. Looking at the raw waveforms (S1A), there was virtually no difference between the controls and the experimental animals. When looking specifically at the a-wave, b-wave, and c-waves (S1B-S1D), there was no statistically significant difference between

the control *Lsd1* (lox/lox) and experimental Rho-iCre75 *Lsd1* (lox/lox) animals across the different parameters. Additionally, we performed *in vivo* imaging to determine whether there were any morphological defects. Based on the Fundus photos (S2A-S2B) and SD-OCT photos (S2C-S2D), there were no obvious signs of degeneration. Those *in vivo* results were corroborated with post-mortem results with H&E staining of whole eye (S3A-S3B) and retina (S3C-S3D) that showed no statistical difference in ONL nuclei counts (S3E).

## 2.5 DISCUSSION

Overall, the goal of this study was to determine the role of *Lsd1* in ocular development by genetically ablating *Lsd1* throughout the retina early during development or specifically in rods. This was achieved by using either a Chx10-Cre driver mouse to delete *Lsd1* specifically in most RPCs or by a Rho-iCre75 driver mouse for the rod photoreceptors. We hypothesized that deletion could cause ocular abnormalities which would be observed through visual function tests, *in vivo* imaging, and post-mortem analyses. Through immunoblotting, we observed a large and significant reduction in *Lsd1* protein expression (~86%) in the experimental Chx10-Cre *Lsd1* (lox/lox) animals compared to the two control groups (Figure 1). After observing successful *Lsd1* deletion, we tested the mice for visual function and retinal morphology, both *in vivo* and post-mortem. We observed significant reductions in ERG amplitudes from the experimental animals compared to controls in both scotopic and photopic conditions (Figure 2). In scotopic conditions, the a- and b-wave amplitudes decreased by ~75% and ~89% respectively in the Chx10-Cre *Lsd1* (lox/lox) animals compared to controls. These decreases in ERG amplitudes suggest photoreceptor and bipolar cell dysfunction (Granit, 1933; Weymouth, 2008). There were also sharp reductions in c-waves (which mirror and depend on a- wave signals), cone flicker response (which was extinguished), and oscillatory potentials (which were virtually eliminated) (Figure 2). We also observed significant but lesser decreases in total retinal thickness (~26%) and ONL thickness (~21%) in SD-OCT images and a more mottled and speckled appearance of fundus photos in the Chx10-Cre *Lsd1* (lox/lox) animals compared to their littermate controls (Figure 3). Those results were corroborated with results

from H&E staining which showed modest degeneration in the experimental animals and significant decreases in cell nuclei quantification in the ONL (~19%) and INL (~30%) accompanied by mild but distinct disorganization, but not RGCL (Figure 4). Retinal lengths also decreased by ~7% in the Chx10-Cre Lsd1 (lox/lox) animals compared to controls. Based on the electron microscopy images, we observed significant decreases in outer segment length (~47%) and inner segment length (~31%) in the experimental animals compared to controls and apparently important loss of normal organization, shape and continuity that may account for most of the lost ERG and functional signals (Figure 5). Through antibody staining, we determined that Lsd1 deletion during retinal development affects many major neuronal cell types in the retina and there was increased apoptosis in the experimental animals compared to controls (Figure 6). When looking at the Rho-iCre75 Lsd1 (lox/lox) animals, we did not observe any statistical differences in the scotopic a-, b-, or c-waves (Supplemental Figure 1). Additionally, there were no obvious signs of degeneration when looking at Fundus and SD-OCT images (Supplemental Figure 2) or H&E retinal images and ONL nuclei counts (Supplemental Figure 3). We hypothesize that the lack of an obvious phenotype in the Rho-iCre75 Lsd1 (lox/lox) animals is because Lsd1 activity was reduced after the retinal cells had committed and differentiated, thus the retinal cells and circuitry were able to properly develop.

One interesting note is that we observed small, but statistically significant differences between the Chx10-Cre and Lsd1 (lox/lox) control groups for a few parameters, including Lsd1 protein expression (Figure 1C), scotopic b-waves (Figure 2D), and total retinal thickness as measured by OCT imaging (Figure 3E). Although unexpected, it is possible that the Chx10-Cre only animals may experience some retinal toxicity due to the presence of Cre recombinase. Although rare, there have been reports about differences in recombinase efficiency in different tissues and Cre recombinase toxicity (Loonstra, 2001; Hameyer, 2007 ; Naiche, 2007 ; Lexow, 2013). Importantly, three different Nestin-Cre mouse strains were shown to develop hydrocephaly due to high amounts of Cre recombinase expression in neural progenitor cells (Forni, 2006). It is possible that the Chx10-Cre animals have slight Cre toxicity resulting in lower

protein expression, overstimulation of bipolar cells, and small amounts of edema in the retina which accounts for the small, but significant differences we observe between the control groups. Overall, it does not detract from the important role of Lsd1 in proper retinal development but should be noted.

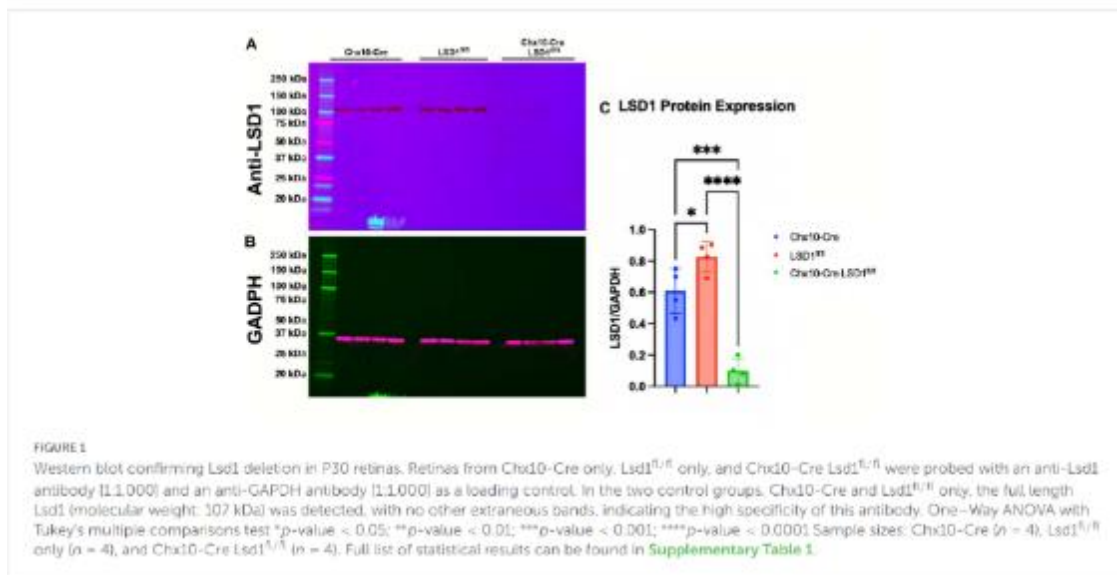
Earlier we hypothesized that Lsd1 ablation could result in either: 1) retinal degeneration due to RPC apoptosis or abnormalities in RPC proliferation or 2) irregularities in the relative proportion of various mature retinal neuron subtypes due to improper RPC differentiation. For now, we are unable to differentiate between these two possibilities and will be the subject of future studies. RPCs are heterogenous in their individual transcriptome and this allows for multipotency (Trimarchi, 2008 ; Bassett, 2012 ; Cepko, 2014). Under the influence of different cell fate determinants, the RPCs undergo asymmetrical cell division and become increasingly restricted and specified before committing to a particular cell fate (Cepko, 1996 ; Livesey, 2001 ; Saito, 2003 ; Kechard, 2012). These restricted RPCs often have distinct molecular and transcriptional profiles compared to their multipotent counterparts (Blackshaw, 2004 ; Aldiri, 2017 ; Buenaventura, 2018 ; Clark, 2019 ; Shiao, 2021). Thus, during retinal development, the 7 major and ~130 subtypes of mature retinal cells are born in distinct, but overlapping windows of time in a stereotypical order (Young, 1985; Cepko, 1996 ; Bassett, 2012 ; Shekhar, 2016 ; Tran, 2019 ; Yan, 2020). Therefore, we posited that the loss of Lsd1 would affect the proliferation, specification, and differentiation of the RPCs due to global abnormalities in the epigenetic environment. Future studies will investigate how RPCs cope with the epigenetic dysregulation that possibly occurs with the loss of Lsd1 by studying timepoints during retinal development. This can be achieved looking at the global retinal morphology and specific differentiation of specific major and minor cell types during embryonic and post-natal retinal development. One limitation of the present study is the relatively crude identification of the loss of specific major cell types via immunofluorescence. More sophisticated methods such as RNAscope (Wang, 2012), or single-cell spatial technologies such as MERFISH (Chen, 2015; Moffitt, 2016), Seq-Scope (Cho, 2021), or SABER-FISH (Kishi, 2019), which has already been applied to the retina to investigate bipolar cell subtype identify, location, and birthdate (West, 2022),

could be used to elucidate precisely which retinal subtypes are missing following *Lsd1* deletion during retinal development.

Additionally, it is crucial to study how the global transcriptome and epigenome are altered in these animals both during and after development through RNA-seq (Mortazavi, 2008; Nagalakshmi, 2008), ChIP-seq (Johnson, 2007 ; Robertson, 2007) / CUT&RUN (Skene, 2017), and ATAC-seq (Buenrostro, 2013) methods. This could lead to significant insights on the mechanistic role of *Lsd1* in the proper development and differentiation of the retina.

## 2.6 FIGURES AND TABLES

## 2.6.1 Figure 1 Retinal LSD1 Protein Expression at P30



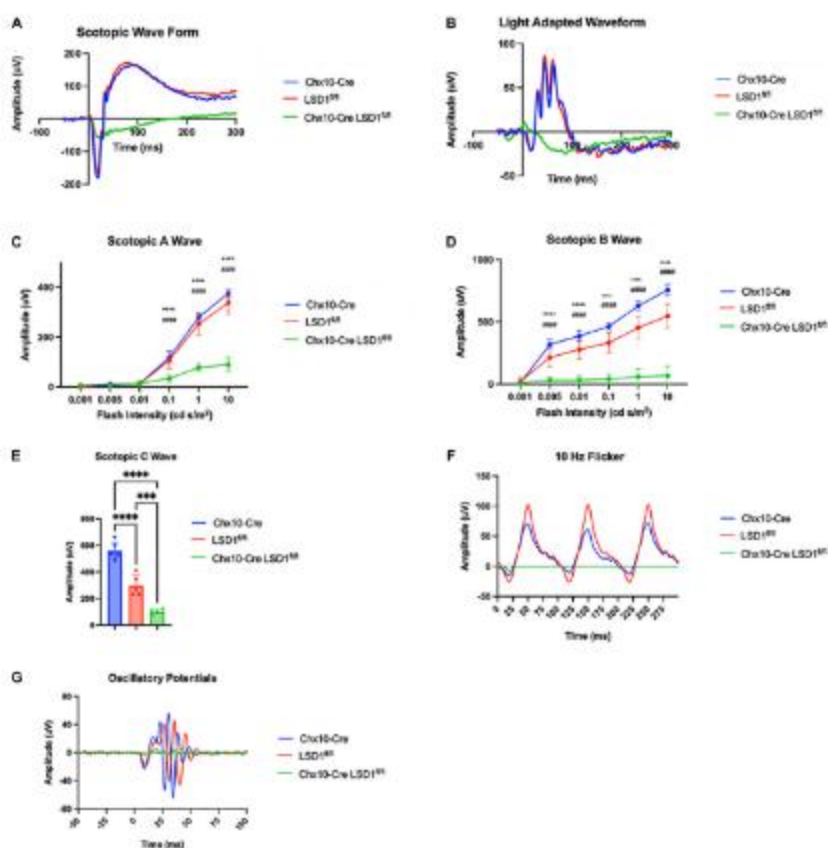
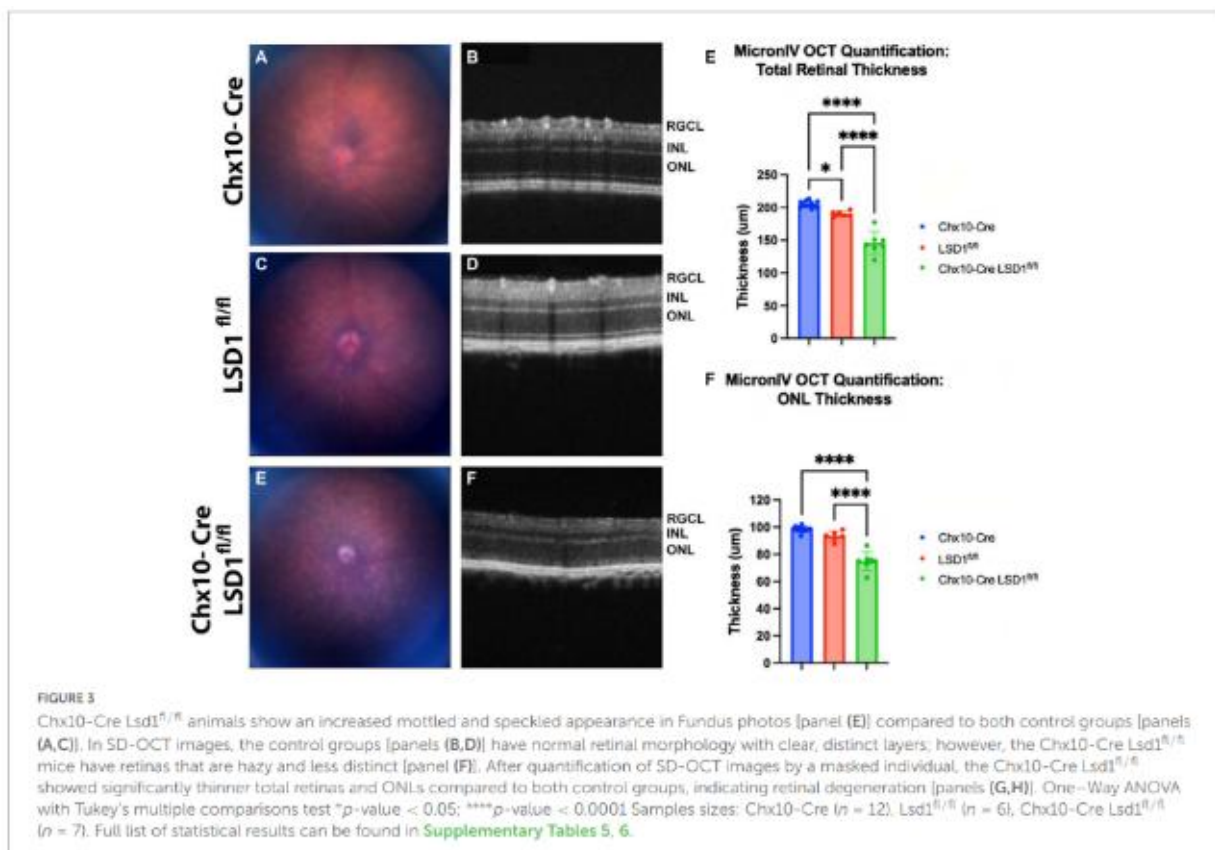
2.6.2 Figure 2: Chx-10 Lsd1<sup>fl/fl</sup> Show Deficits in ERG Responses

FIGURE 2

Chx10-Cre Lsd1<sup>fl/fl</sup> mice have relatively flat ERG response in scotopic and photopic conditions compared to controls. Raw electroretinogram waveforms from Chx10-Cre controls, Lsd1<sup>fl/fl</sup> controls and Chx10-Cre Lsd1<sup>fl/fl</sup> in scotopic [panel (A)] and photopic [panel (B)] conditions after a 10 cd s/m<sup>2</sup> light flash. At multiple flash intensities, both control groups show a relatively normal response for scotopic a-wave [panel (C)], scotopic b-wave [panel (D)] and scotopic c-wave [panel (E)]; however, the Chx10-Cre Lsd1<sup>fl/fl</sup> mice have significant reductions in ERG response, suggesting dysfunctional photoreceptors and bipolar cells. The Chx10-Cre Lsd1<sup>fl/fl</sup> mice also have profound reductions in cone flicker response at 10 Hz compared to controls [panel (F)] as well as reductions in oscillatory potentials [panel (G)]. Two-Way ANOVA with Tukey's multiple comparisons test \*\*\*p-value < 0.001; \*\*\*\*p-value < 0.0001. Sample sizes: Chx10-Cre (n = 6-7), Lsd1<sup>fl/fl</sup> (n = 5), Chx10-Cre Lsd1<sup>fl/fl</sup> (n = 4-5). Full list of statistical results can be found in [Supplementary Tables 2-4](#).

### 2.6.3 Figure 3: Chx10-Lds1<sup>fl/fl</sup> Show Abnormalities in Retinal Structures



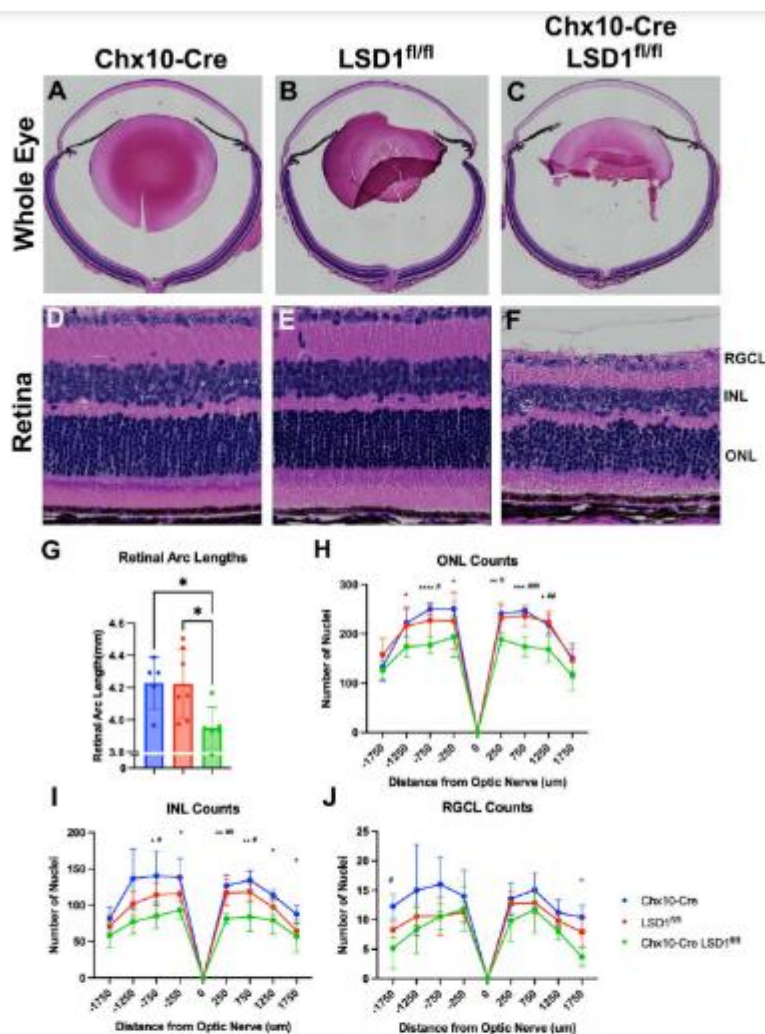
2.6.4 Figure 4: Chx10-Lds1<sup>fl/fl</sup> Exhibit Significant Loss of Retinal Thickness

FIGURE 4

Chx10-Cre Lsd1<sup>fl/fl</sup> showed modest signs of retinal thinning and irregular morphology in Hematoxylin and Eosin (H&E) staining compared to controls; however, the laminar structure and organization was present. Whole eye images (panels [A–C]) and high magnification retina images (panels [D–F]) are shown for all three groups. Chx10-Cre Lsd1<sup>fl/fl</sup> mice show significant total retinal thinning and disorganized ONL and INL (panel [F]) compared to both control groups (panels [D,E]). Quantification of nuclei in the ONL (panel [G]), INL (panel [H]), and RGCL (panel [I]) show significant decreases in cell number in ONL and INL, but not RGCL, of Lsd1<sup>fl/fl</sup> mice compared to both control groups. Quantification of total retinal arc length (panel [G]) show significant decrease in retinal arc length in Chx10-Cre Lsd1<sup>fl/fl</sup> mice compared to control groups. One-Way ANOVA with Tukey's multiple comparisons test for retinal lengths and Two-Way ANOVA with Tukey's multiple comparisons test for ONL, INL, and RGCL cell nuclei quantification \**p*-value < 0.05; \*\**p*-value < 0.01; \*\*\**p*-value < 0.001; \*\*\*\**p*-value < 0.0001; #*p*-value < 0.05; ##*p*-value < 0.01; ###*p*-value < 0.001; ####*p*-value < 0.0001 (\* symbols indicate significance between Chx10-Cre controls and Chx10-Cre Lsd1<sup>fl/fl</sup>; # symbols indicate significant between Lsd1<sup>fl/fl</sup> controls and Chx10-Cre Lsd1<sup>fl/fl</sup>). Sample sizes: Chx10-Cre (*n* = 5), Lsd1<sup>fl/fl</sup> (*n* = 7), Chx10-Cre Lsd1<sup>fl/fl</sup> (*n* = 6). Full list of statistical results can be found in [Supplementary Tables 7–10](#).

## 2.6.5 Figure 5: Chx10-Lds1<sup>fl/fl</sup> Exhibit Shortening of Inner and Outer Photoreceptor Segments

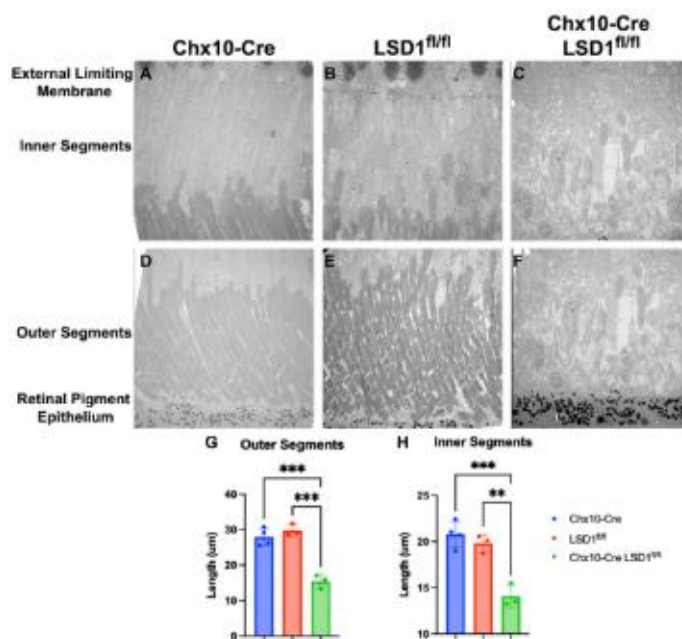


FIGURE 5

Electron microscopy of the area between RPE and external limiting membrane (ELM) show decreased lengths of inner and outer segments in Chx10-Cre Lsd1<sup>fl/fl</sup> animals compared to controls. Using 1400X magnification, we observed disorganization and significant reductions of the inner and outer segments lengths [panels (C,F)]; however, no abnormalities were observed in the Chx10-Cre only controls [panels (A,D)] or the Lsd1<sup>fl/fl</sup> only controls [panels (B,E)]. Additionally, no abnormalities, such as drusenoid like deposits or vacuoles, were observed in the ELM, RPE, or choroid in any mouse strain. Two-Way ANOVA with Tukey's multiple comparisons test for the outer segments and inner segments \*\**p*-value < 0.01; \*\*\**p*-value < 0.001. Samples sizes: Chx10-Cre (*n* = 4), Lsd1<sup>fl/fl</sup> (*n* = 4), Chx10-Cre Lsd1<sup>fl/fl</sup> (*n* = 5). Full list of statistical results can be found in [Supplementary Tables 11, 12](#).

## 2.6.6 Figure 6: Chx Chx10-Lds1<sup>fl/fl</sup> Show Loss of Retinal Subtypes and Increased Apoptosis

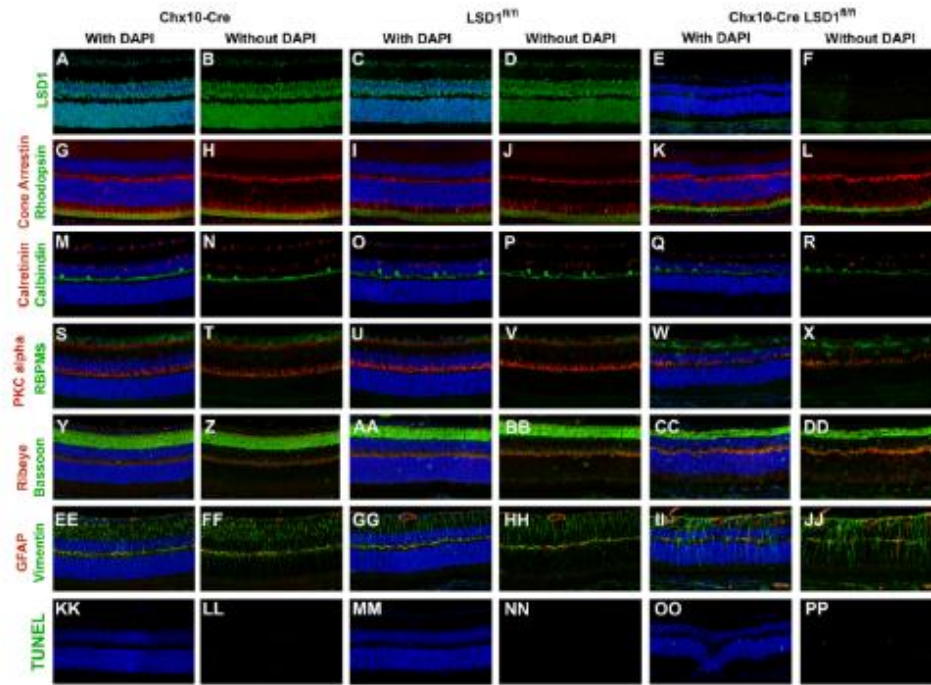


FIGURE 6

Immunofluorescence staining of Lsd1, various major cell specific markers, and TUNEL show decreased presence of specific retinal neurons and increased apoptosis in Chx10-Cre Lsd1<sup>fl/fl</sup> animals compared to controls. Lsd1 protein has little to no expression in Chx10-Cre Lsd1<sup>fl/fl</sup> animals [panels (E,F)] compared to both control groups [panels (A-D)]. Qualitatively, expression of photoreceptor marker cone arrestin and rhodopsin [panels (G-L)] are relatively consistent across the three groups. Expression of calretinin was qualitatively uniform across the three groups, however, calbindin positive cell bodies seem reduced in the Chx10-Cre Lsd1<sup>fl/fl</sup> animals [panels (Q,R)] compared to controls [panels (M-P)]. RBPMs expression was qualitatively uniform across the three groups, but PKCalpha was reduced in the Chx10-Cre Lsd1<sup>fl/fl</sup> animals [panels (W,X)] compared to controls [panels (S-V)]. Bassoon and Ribeye staining [panels (CC,DD)] seems qualitatively different in the Chx10-Cre Lsd1<sup>fl/fl</sup> compared to controls [panels (Y-BB)]. Expression of Muller glia cell markers Vimentin and GFAP had a qualitatively increased co-localization in the Chx10-Cre Lsd1<sup>fl/fl</sup> [panels (II,JJ)] compared to controls [panels (EE-HH)]. No TUNEL positive cells were observed in the control groups [panels (KK-NN)], but several were observed in the Chx10-Cre Lsd1<sup>fl/fl</sup> animals [panels (OO,PP)]. Samples sizes: Chx10-Cre (n = 5), Lsd1<sup>fl/fl</sup> (n = 5), Chx10-Cre Lsd1<sup>fl/fl</sup> (n = 5).

## 2.7 REFERENCES

- Aldiri I, Xu B, Wang L, et al. The Dynamic Epigenetic Landscape of the Retina During Development, Reprogramming, and Tumorigenesis. *Neuron*. 2017;94(3):550-568.e10. doi:10.1016/j.neuron.2017.04.022
- Bassett EA, Wallace VA. Cell fate determination in the vertebrate retina. *Trends Neurosci* 2012;35:565–73. PMID:22704732.
- Blackshaw S, Harpavat S, Trimarchi J, et al. Genomic analysis of mouse retinal development. *PLoS Biol*. 2004;2(9):E247. doi:10.1371/journal.pbio.0020247
- Buenaventura DF, Ghinia-Tegla MG, Emerson MM. Fate-restricted retinal progenitor cells adopt a molecular profile and spatial position distinct from multipotent progenitor cells. *Dev Biol*. 2018 Nov 1;443(1):35-49. doi: 10.1016/j.ydbio.2018.06.023. Epub 2018 Aug 24. PMID: 30145104; PMCID: PMC6441625.
- Buenrostro JD, Giresi PG, Zaba LC, Chang HY, Greenleaf WJ. Transposition of native chromatin for fast and sensitive epigenomic profiling of open chromatin, DNA-binding proteins and nucleosome position. *Nat Methods*. 2013 Dec;10(12):1213-8. doi: 10.1038/nmeth.2688. Epub 2013 Oct 6. PMID: 24097267; PMCID: PMC3959825.
- Cepko CL, Austin CP, Yang X, Alexiades M, Ezzeddine D. Cell fate determination in the vertebrate retina 1996;93:589–95.
- Cepko C. Intrinsically different retinal progenitor cells produce specific types of progeny. *Nat Rev Neurosci* 2014;15:615–27. PMID:25096185.
- Chen KH, Boettiger AN, Moffitt JR, Wang S, Zhuang X. RNA imaging. Spatially resolved, highly multiplexed RNA profiling in single cells. *Science*. 2015 Apr 24;348(6233):aaa6090. doi: 10.1126/science.aaa6090. Epub 2015 Apr 9. PMID: 25858977; PMCID: PMC4662681.
- Cho CS, Xi J, Si Y, Park SR, Hsu JE, Kim M, Jun G, Kang HM, Lee JH. Microscopic examination of spatial transcriptome using Seq-Scope. *Cell*. 2021 Jun 24;184(13):3559-3572.e22. doi: 10.1016/j.cell.2021.05.010. Epub 2021 Jun 10. PMID: 34115981; PMCID: PMC8238917.
- Chong JX, Yu J, Lorentzen P, Park KM, Jamal SM, Tabor HK, et al. Gene discovery for Mendelian conditions via social networking: de novo variants in KDM1A cause developmental delay and distinctive facial features. *Genet Med* 2016;18:788–95. PMID:26656649
- Christopher MA, Myrick DA, Barwick BG, Engstrom AK, Porter-Stransky KA, Boss JM, et al. LSD1 protects against hippocampal and cortical neurodegeneration. *Nat Commun* 2017;8:1–13. PMID:28993646.
- Clark BS, Stein-O'Brien GL, Shiao F, Cannon GH, Davis-Marcisak E, Sherman T, Santiago CP, Hoang TV, Rajaii F, James-Esposito RE, Gronostajski RM, Fertig EJ, Goff LA, Blackshaw S. Single-Cell RNA-Seq Analysis of Retinal Development Identifies NFI Factors as Regulating Mitotic Exit and Late-Born Cell Specification. *Neuron*. 2019 Jun 19;102(6):1111-1126.e5. doi: 10.1016/j.neuron.2019.04.010. Epub 2019 May 22. PMID: 31128945; PMCID: PMC6768831.
- Collins BE, Greer CB, Coleman BC, Sweatt JD. Histone H3 lysine K4 methylation and its role in learning and memory. *Epigenetics and Chromatin* 2019;12:1–16. PMID:30616667.
- Forni PE, Scuoppo C, Imayoshi I, Taulli R, Dastrù W, Sala V, Betz UA, Muzzi P, Martinuzzi D, Vercelli AE, Kageyama R, Ponzetto C. High levels of Cre expression in neuronal progenitors cause defects in brain development leading to microencephaly and hydrocephaly. *J Neurosci*. 2006 Sep 13;26(37):9593-602. doi: 10.1523/JNEUROSCI.2815-06.2006. PMID: 16971543; PMCID: PMC6674592.
- Fuentes P, Cánovas J, Berndt FA, Noctor SC, Kukuljan M. CoREST/LSD1 control the development of pyramidal cortical neurons. *Cereb Cortex* 2012;22:1431–41. PMID:21878487.
- Granit R. The Components of the retinal action potential in mammals and their relation to the discharge in the optic nerve. *J Physiol* 1933;77:207–39.
- Gu F, Lin Y, Wang Z, Wu X, Ye Z, Wang Y, et al. Biological roles of LSD1 beyond its demethylase activity. *Cell Mol Life Sci* 2020;77:3341–50. PMID:32193608.
- Hameyer D, Loonstra A, Eshkind L, Schmitt S, Antunes C, Groen A, Bindels E, Jonkers J, Krimpenfort P, Meuwissen R, Rijswijk L, Bex A, Berns A, Bockamp E. Toxicity of ligand-dependent Cre recombinases and generation of a conditional Cre deleter mouse allowing mosaic recombination in peripheral tissues. *Physiol Genomics*. 2007 Sep 19;31(1):32-41. doi: 10.1152/physiolgenomics.00019.2007. Epub 2007 Apr 24. PMID: 17456738.
- Johnson DS, Mortazavi A, Myers RM, Wold B. Genome-wide mapping of in vivo protein-DNA interactions. *Science*. 2007 Jun 8;316(5830):1497-502. doi: 10.1126/science.1141319. Epub 2007 May 31. PMID: 17540862.

- Kechad A, Jolicoeur C, Tufford A, Mattar P, Chow RWY, Harris WA, Cayouette M. Numb is required for the production of terminal asymmetric cell divisions in the developing mouse retina. *J Neurosci*. 2012 Nov 28;32(48):17197-17210. doi: 10.1523/JNEUROSCI.4127-12.2012. PMID: 23197712; PMCID: PMC4650329.
- Kishi JY, Lapan SW, Beliveau BJ, West ER, Zhu A, Sasaki HM, Saka SK, Wang Y, Cepko CL, Yin P. SABER amplifies FISH: enhanced multiplexed imaging of RNA and DNA in cells and tissues. *Nat Methods*. 2019 Jun;16(6):533-544. doi: 10.1038/s41592-019-0404-0. Epub 2019 May 20. PMID: 31110282; PMCID: PMC6544483.
- Laurent B, Ruitu L, Murn J, Hempel K, Ferraro R, Xiang Y, et al. A Specific LSD1/KDM1A Isoform Regulates Neuronal Differentiation through H3K9 Demethylation. *Mol Cell* 2015;57:957–70. PMCID:26928661.
- Lexow J, Poggioli T, Sarathchandra P, Santini MP, Rosenthal N. Cardiac fibrosis in mice expressing an inducible myocardial-specific Cre driver. *Dis Model Mech*. 2013;6(6):1470-1476. doi:10.1242/dmm.010470
- Li S, Chen D, Sauvé Y, McCandless J, Chen YJ, Chen CK. Rhodopsin-iCre transgenic mouse line for Cre-mediated rod-specific gene targeting. *Genesis*. 2005 Feb;41(2):73-80. doi: 10.1002/gene.20097. PMID: 15682388.
- Liu ISC, Chen J de, Ploder L, Vidgen D, van der Kooy D, Kalnins VI, et al. Developmental expression of a novel murine homeobox gene (Chx10): Evidence for roles in determination of the neuroretina and inner nuclear layer. *Neuron* 1994;13:377–93.
- Livesey FJ, Cepko CL. Vertebrate neural cell-fate determination: Lessons from the retina. *Nat Rev Neurosci* 2001;2:109–18. PMCID:11252990.
- Loonstra A, Vooijs M, Beverloo HB, Allak BA, van Drunen E, Kanaar R, Berns A, Jonkers J. Growth inhibition and DNA damage induced by Cre recombinase in mammalian cells. *Proc Natl Acad Sci U S A*. 2001 Jul 31;98(16):9209-14. doi: 10.1073/pnas.161269798. PMID: 11481484; PMCID: PMC55399.
- Mazzoni F, Tombo T, Finnemann SC. No Difference Between Age-Matched Male and Female C57BL/6J Mice in Photopic and Scotopic Electroretinogram a- and b-Wave Amplitudes or in Peak Diurnal Outer Segment Phagocytosis by the Retinal Pigment Epithelium. *Adv Exp Med Biol*. 2019;1185:507-511. doi: 10.1007/978-3-030-27378-1\_83. PMID: 31884662.
- Moffitt JR, Zhuang X. RNA Imaging with Multiplexed Error-Robust Fluorescence In Situ Hybridization (MERFISH). *Methods Enzymol*. 2016;572:1-49. doi: 10.1016/bs.mie.2016.03.020. Epub 2016 Apr 27. PMID: 27241748; PMCID: PMC5023431.
- Mortazavi A, Williams BA, McCue K, Schaeffer L, Wold B. Mapping and quantifying mammalian transcriptomes by RNA-Seq. *Nat Methods*. 2008 Jul;5(7):621-8. doi: 10.1038/nmeth.1226. Epub 2008 May 30. PMID: 18516045.
- Nagalakshmi U, Wang Z, Waern K, et al. The transcriptional landscape of the yeast genome defined by RNA sequencing. *Science*. 2008;320(5881):1344-1349. doi:10.1126/science.1158441
- Nagy A. Cre recombinase: The universal reagent for genome tailoring. *Genesis* 2000;26:99–109. PMCID:10686599.
- Naiche LA, Papaioannou VE. Cre activity causes widespread apoptosis and lethal anemia during embryonic development. *Genesis*. 2007 Dec;45(12):768-75. doi: 10.1002/dvg.20353. PMID: 18064676.
- Pilotto S, Speranzini V, Marabelli C, Rusconi F, Toffolo E, Grillo B, et al. LSD1/KDM1A mutations associated to a newly described form of intellectual disability impair demethylase activity and binding to transcription factors. *Hum Mol Genet* 2016;25:2578–87. PMCID:27094131.
- Popova EY, Pinzon-Guzman C, Salzberg AC, Zhang SS, Barnstable CJ. LSD1-Mediated Demethylation of H3K4me2 Is Required for the Transition from Late Progenitor to Differentiated Mouse Rod Photoreceptor. *Mol Neurobiol*. 2016 Sep;53(7):4563-81. doi: 10.1007/s12035-015-9395-8. Epub 2015 Aug 23. PMID: 26298666; PMCID: PMC6910084.
- Popova EY, Imamura Kawasaki Y, Zhang SS, Barnstable CJ. Inhibition of Epigenetic Modifiers LSD1 and HDAC1 Blocks Rod Photoreceptor Death in Mouse Models of Retinitis Pigmentosa. *J Neurosci*. 2021 Aug 4;41(31):6775-6792. doi: 10.1523/JNEUROSCI.3102-20.2021. Epub 2021 Jun 30. PMID: 34193554; PMCID: PMC8336706.
- Robertson G, Hirst M, Bainbridge M, Bilenky M, Zhao Y, Zeng T, Euskirchen G, Bernier B, Varhol R, Delaney A, Thiessen N, Griffith OL, He A, Marra M, Snyder M, Jones S. Genome-wide profiles of STAT1 DNA association using chromatin immunoprecipitation and massively parallel sequencing. *Nat Methods*. 2007 Aug;4(8):651-7. doi: 10.1038/nmeth1068. Epub 2007 Jun 11. PMID: 17558387.
- Rowan S, Cepko CL. Genetic analysis of the homeodomain transcription factor Chx10 in the retina using a novel multifunctional BAC transgenic mouse reporter. *Dev Biol*. 2004 Jul 15;271(2):388-402. doi: 10.1016/j.ydbio.2004.03.039. PMID: 15223342.

- Rusconi F, Grillo B, Toffolo E, Mattevi A, Battaglioli E. NeuroLSD1: Splicing-Generated Epigenetic Enhancer of Neuroplasticity. *Trends Neurosci* 2016;40:1–11. PMID:27986293.
- Rusconi F, Grillo B, Ponzoni L, Bassani S, Toffolo E, Paganini L, et al. LSD1 modulates stress-evoked transcription of immediate early genes and emotional behavior. *Proc Natl Acad Sci U S A* 2016;113:1511974113-. PMID:26976584.
- Saito K, Kawaguchi A, Kashiwagi S, Yasugi S, Ogawa M, Miyata T. Morphological asymmetry in dividing retinal progenitor cells. *Dev Growth Differ*. 2003 Jun;45(3):219-29. doi: 10.1046/j.1524-4725.2003.690.x. PMID: 12828683
- Samocha KE, Robinson EB, Sanders SJ, Stevens C, Sabo A, McGrath LM, et al. A framework for the interpretation of de novo mutation in human disease. *Nat Genet* 2014;46:944–50.
- Skene, P. J. & Henikoff, S. An efficient targeted nuclease strategy for high-resolution mapping of DNA binding sites. *eLife* 6, e21856 (2017).
- Shekhar K, Lapan SW, Whitney IE, Tran NM, Macosko EZ, Kowalczyk M, Adiconis X, Levin JZ, Nemesh J, Goldman M, McCarroll SA, Cepko CL, Regev A, Sanes JR, 2016. Comprehensive classification of retinal bipolar neurons by single-cell transcriptomics. *Cell* 166, 1308–1323. 10.1016/j.cell.2016.07.054 e30
- Shi Y, Lan F, Matson C, Mulligan P, Whetstone JR, Cole PA, et al. Histone demethylation mediated by the nuclear amine oxidase homolog LSD1. *Cell* 2004; 119:941–53. PMID:15620353.
- Shiau F, Ruzyccki PA, Clark BS. A single-cell guide to retinal development: Cell fate decisions of multipotent retinal progenitors in scRNA-seq. *Dev Biol*. 2021 Oct;478:41-58. doi: 10.1016/j.ydbio.2021.06.005. Epub 2021 Jun 17. PMID: 34146533; PMID: PMC8386138.
- Sun G, Alzayady K, Stewart R, Ye P, Yang S, Li W, et al. Histone Demethylase LSD1 Regulates Neural Stem Cell Proliferation. *Mol Cell Biol* 2010;30:1997–2005. PMID:20123967.
- Sun N, Shibata B, Hess JF, FitzGerald PG. An alternative means of retaining ocular structure and improving immunoreactivity for light microscopy studies. *Mol Vis*. 2015 Apr 16;21:428-42. PMID: 25991907; PMID: PMC4403009.
- Toffolo E, Rusconi F, Paganini L, Tortorici M, Pilotto S, Heise C, et al. Phosphorylation of neuronal Lysine-Specific Demethylase 1LSD1/KDM1A impairs transcriptional repression by regulating interaction with CoREST and histone deacetylases HDAC1/2. *J Neurochem* 2014;128:603–16. PMID:24111946.
- Tran NM, Shekhar K, Whitney IE, Jacobi A, Benhar I, Hong G, Yan W, Adiconis X, Arnold ME, Lee JM, Levin JZ, Lin D, Wang C, Lieber CM, Regev A, He Z, Sanes JR, 2019. Single-cell profiles of retinal ganglion cells differing in resilience to injury reveal neuroprotective genes. *Neuron* 104, 1039–1055. 10.1016/j.neuron.2019.11.006 e12.
- Trimarchi JM, Stadler MB, Cepko CL. Individual retinal progenitor cells display extensive heterogeneity of gene expression. *PLoS One* 2008;3: PMID:18270576.
- Tunovic S, Barkovich J, Sherr EH, Slavotinek AM. De novo ANKRD11 and KDM1A gene mutations in a male with features of KBG syndrome and Kabuki syndrome. *Am J Med Genet Part A* 2014;164:1744–9. PMID:24838796
- Wang J, Scully K, Zhu X, Cai L, Zhang J, Prefontaine GG, et al. Opposing LSD1 complexes function in developmental gene activation and repression programs. *Nature* 2007;446:882–7. PMID:17392792.
- Wang F, Flanagan J, Su N, et al. RNAscope: a novel in situ RNA analysis platform for formalin-fixed, paraffin-embedded tissues. *J Mol Diagn*. 2012;14(1):22-29. doi:10.1016/j.jmoldx.2011.08.002
- Wang J, Telese F, Tan Y, Li W, Jin C, He X, et al. LSD1 is an H4K20 demethylase regulating memory formation via transcriptional elongation control. *Nat Neurosci* 2015;18:1256–64. PMID:26214369.
- West ER, Lapan SW, Lee C, Kajderowicz KM, Li X, Cepko CL. Spatiotemporal patterns of neuronal subtype genesis suggest hierarchical development of retinal diversity. *Cell Rep*. 2022 Jan 4;38(1):110191. doi: 10.1016/j.celrep.2021.110191. PMID: 34986354.
- Weymouth AE, Vingrys AJ. Rodent electroretinography: Methods for extraction and interpretation of rod and cone responses. *Prog Retin Eye Res* 2008;27:1–44. PMID:18042420.
- Yan W, Laboulaye MA, Tran NM, Whitney IE, Benhar I, Sanes JR, 2020a. Mouse retinal cell atlas: molecular identification of over sixty amacrine cell types. *J. Neurosci* 40, 5177–5195. 10.1523/JNEUROSCI.0471-20.2020.
- Young RW. Cell differentiation in the retina of the mouse. *Anat Rec*. 1985 Jun;212(2):199-205. doi: 10.1002/ar.1092120215. PMID: 3842042.
- Zibetti C, Adamo A, Binda C, Forneris F, Toffolo E, Verpelli C, et al. Alternative splicing of the histone demethylase LSD1/KDM1 contributes to the modulation of neurite morphogenesis in the mammalian nervous system. *J Neurosci* 2010;30:2521–32. PMID:20164337.



### 3 CHAPTER 3: Title: Age-related RPE Changes in C57BL/6J Mice Between 2 and 32 Months of Age

**Authors:** Debresha A. Shelton<sup>1</sup>, Isabelle Gefke<sup>1</sup>, Vivian Summers<sup>1</sup>, Yong-Kyu Kim<sup>1,3</sup>, Hanyi Yu<sup>1,4</sup>, Tatiana Getz<sup>1</sup>, Salma Ferdous<sup>1,6</sup>, Kevin Donaldson<sup>1</sup>, Kristie Liao<sup>1</sup>, Jack T. Papania<sup>1</sup>, Micah A. Chrenek<sup>1</sup>, Jeffrey H. Boatright<sup>1,5</sup>, John M. Nickerson<sup>1</sup>

Affiliations:

<sup>1</sup>Department of Ophthalmology, Emory University, Atlanta, Georgia, United States

<sup>2</sup>Atlanta Veterans Administration Center for Visual and Neurocognitive Rehabilitation, Decatur, Georgia, United States

<sup>3</sup>Department of Ophthalmology, Hallym University College of Medicine, Kangdong Sacred Heart Hospital, Seoul, South Korea

<sup>4</sup>Department of Computer Science, Emory University, Atlanta, Georgia, United States

<sup>5</sup>Atlanta VA Center for Visual and Neurocognitive Rehabilitation, Decatur, Georgia, United States

<sup>6</sup> Human Genome Sequencing Center, Baylor College of Medicine, Houston, Texas, United States

Correspondence to: Please address all correspondence to Dr. John M. Nickerson; Department of Ophthalmology, Emory University, B5602, 1365B Clifton Road, NE, Atlanta, GA, 30322; Phone 404-778-4411; email: litjn@emory.edu

Funding: Supported by National Institutes of Health (NIH) grants R01EY028450, R01EY021592, P30EY006360, R01EY028859, T32EY07092, and T32GM008490, the Abraham and Phyllis Katz Foundation, VA RR&D I01RX002806 and I21RX001924, VA RR&D C9246C (Atlanta Veterans Administration Center for Excellence in Vision and Neurocognitive Rehabilitation), and a challenge grant to the Department of Ophthalmology at Emory University from Research to Prevent Blindness, Inc.



### 3.1 ABSTRACT:

**Purpose:** Using C57BL6/J mice ranging in age from P60-P970, we sought to evaluate how regional changes in RPE shape reflect incremental losses in RPE cell function with advancing age. We hypothesize that tracking morphological changes in RPE is predictive of functional defects over time.

**Methods:** We examined three groups of C57BL/6J mice (young: P60-180; middle-aged: P365-544; aged: P730- 970) for function and structural defects using electroretinograms, immunofluorescence, and phagocytosis assays.

**Results:** The most significant changes in RPE morphology were evident between the young and aged groups, while the middle-aged group exhibited lesser but notable region-specific differences. We observed a 1.9-fold increase in cytoplasmic alpha-catenin expression, specifically in the region proximal-medial of the optic nerve, in the aged group compared to the young. Cells expressing cytoplasmic alpha-catenin in the aged group had increased cell area and eccentricity compared to the young group. Additionally, there was a 9-fold increase in IBA-1-positive immune cell density in the subretinal space and a significant decrease in visual function in aged mice compared to young mice. Functional defects in the RPE are corroborated by changes in phagocytotic capacity, possibly suggesting a slower turnover of phagosomes.

**Conclusions:** There was a marked increase in cytoplasmic alpha-catenin expression in the RPE of aged mice compared to the young group. There was a regional increase of cytoplasmic alpha-catenin in aged mice proximal-medial of the optic nerve; additionally, these cells also exhibited increased cell area and eccentricity compared to cells in the same region in young animals. Similarly, the regional increase of subretinal immune cell density and decreased visual output coincide with changes in RPE cell morphometrics when stratified by age. These cumulative changes in the regional RPE morphology and stress marker patterns are associated with the loss of RPE integrity and function.

### 3.2 INTRODUCTION

The retinal pigment epithelium (RPE) is a monolayer of hexagonal cells between the neurosensory retina and the choroid that interacts with Bruch's membrane<sup>83-87</sup>. Primary functions of the RPE include supplying the retina with nutrients via basal infoldings and removing waste by-products from the phototransduction processes of photoreceptor cells<sup>86,87</sup>. RPE phagocytosis recycles the outer segments of rod and cone photoreceptors and secretes growth hormones that are critical in maintaining the morphological integrity of multiple retinal structures<sup>1,88,89</sup>. The role of the RPE is evident beginning at the very early stages of ocular development. Ablation of the RPE results in absent or abnormal ocular development<sup>90,91</sup>. Due to the plethora of functions that the RPE performs, its density, structure, and function are critical to visual signaling. Consequently, studying age-related changes in RPE structure can serve as a predictive measure for retinal degeneration and progressive vision loss<sup>4,91-93</sup>.

Aging affects many tissues of the human body, including the RPE. In healthy adults, RPE cell density decreases uniformly from the second to the ninth decade of life<sup>94</sup>, declining by about 0.3% per year, increasing the photoreceptor-to-RPE cell ratio<sup>95,96</sup>. In addition to reduced density of the RPE, other hallmarks of aging include the thickening of RPE-Bruch's membrane complex at the foveal minimum, subretinal accumulation of lipofuscin, decreased visual acuity, increased circulation of profibrotic macrophages, increased choroidal neovascularization, and the formation of hard drusen<sup>39,97-103</sup>. While these are expected changes in natural aging, they overlap with disease hallmarks, suggesting a partially conserved mechanism between normal and abnormal aging<sup>1,104-106</sup>. For example, age is the primary demographic risk factor for age-related macular degeneration (AMD), followed by race, iris color, and dysregulation of inflammation-associated genes (e.g., *CFH* and *ARMS/HRTAI*, and *C3b*<sup>107-114</sup> and lipoproteins<sup>14,106</sup>).

Structural changes in RPE cells can also be indicators of future RPE dysfunction and progressive loss of vision. During increased apoptosis, neighboring RPE cells expand their borders to maintain contact, increasing polymegathism and pleomorphism in aging and damaged RPE cells. A study by Rashid *et al.* showed a region-specific increase in cell size and loss of hexagonal shape of the RPE during normal

aging and AMD<sup>86</sup>. Further research is needed to understand the association between increased age, abnormal RPE structure, decreased phagocytic capacity, and AMD<sup>15,115,116</sup>. Understanding familiar hallmarks of normal and abnormal aging mechanisms can aid in early detection of pathogenesis and preserve vision.

Further study of age-related structural RPE heterogeneity and its molecular underpinnings is required to target the RPE-mediated initiation of age-related retinopathies. This study employed a natural aging model to examine unique structural patterns in RPE associated with age and deterioration. Previous aging studies compared relatively young animals with animals that were ~1 to 2 years old<sup>117-119</sup>. However, this excludes a crucial advanced aged demographic (mice older than 24 months) that may better capture the overall progression of ocular differences due to aging that recapitulates human disease. After 24 months of age, the probability of survivorship in mice drops markedly from roughly 50% before 24 months to less than 20% after that time point<sup>120</sup>.

Additionally, many studies focused on retinal dysfunction and may have missed critical changes in RPE structure that are also important in visual function outcomes. Currently, many studies explicitly characterizing changes in the aging RPE of mice are limited to data before or around the age of 24 months (correlating to 56-69 human years), which limits our understanding of changes in RPE morphology resulting in the cumulative loss of vision in seniors over 80 years of age<sup>121-124</sup>. In humans, RPE morphology is intact into middle age (38-47 years); however, by 80 years of age, there is a sudden decrease in visual function due to subtle changes in the RPE monolayer arrangement, integrity, and geometry, resulting in vision loss<sup>125</sup>. The timeframe of RPE morphological changes corresponds with a significant spike in the rate of visual disability in adults that are 80 years or older<sup>126</sup>. Weikal *et al.* described substantial differences in the frequencies of age-related lesions and structural aberrations in animals that were 23.5 months compared to 17 months old, a phenotype exacerbated by high-fat diet exposure<sup>127</sup>. Thus, the data loss in this maturational gap between 17 months and 32 months limits our understanding of early signs of aging and distress in RPE cells, resulting in vision loss. To address this gap, we utilized C57BL/6J mice divided into three groups: young (P60-180), middle-aged (P365-P544),

and aged (P730-P970), providing a comprehensive analysis of RPE aging. Our study expands on previous work by correlating RPE dysmorphia with immune cell recruitment, stress-related protein expression changes, and RPE dysfunction over time<sup>128</sup>.

### 3.3 METHODS

#### 3.3.1 Animal Husbandry:

Mouse housing, experiments, and handling were approved by the Emory University Institutional Animal Care and Use Committee. Studies were conducted in adherence with Association for Research in Vision and Ophthalmology (ARVO). The studies conducted followed the guidance and principles of the Association for Assessment and Accreditation of Laboratory Animal Care (AAALAC). C57BL/6J (WT) mice were maintained on a 12-h light/dark cycle at 22°C, and standard mouse chow (Lab Diet 5001; PMI Nutrition Inc., LLC, Brentwood, MO) and water were provided *ad libitum*. Animal breeding pairs were purchased from Jackson Laboratories (JAX) and bred in-house for three generations before experimental use. The mice used in each group were collected from different litters, and all samples represent an independent animal; therefore, we expect no batch effects. The mice were managed and housed by Emory University Division of Animal Resources. Adult mice were euthanized using CO<sub>2</sub> gas asphyxiation for 5 minutes followed by cervical dislocation. All mice used for this study were divided up into the following groups: Group 1 (Young: post-natal day 60-180); Group 2 (Middle-aged: post-natal day 365-544); Group 3 (Aged: post-natal day 730-P970).

#### 3.3.2 RPE and Visual Function Studies:

##### 3.3.2.1 Electroretinography (ERGs) – a-, b-, and c-waves

Scotopic electroretinograms were performed on mice that were dark-adapted overnight. Each mouse was anesthetized using intraperitoneal (IP) injections of 100 mg/kg of ketamine and 15 mg/kg xylazine (ketamine; KetaVed from Patterson Veterinary, Greeley, CO; xylazine from Patterson Veterinary,

Greeley, CO). Once anesthetized, the pupils were dilated with proparacaine (1%; Akorn Inc., Ann Arbor, MI) and tropicamide (1% Tropicamide Ophthalmic Solution, USP; Akorn Inc., Ann Arbor, MI or 0.5% Tropicamide Ophthalmic Solution, USP, Sandoz, Princeton, NJ) eye drops, which were administered topically. Mice were placed on a heating pad under red light, and function was analyzed with Diagnosys Celeris System (Diagnosys, LLC, Lowell, MA). Full-field ERGs were assessed at the following stimulus intensities (0.001, 0.005, 0.01, 1, and 10 cd s/m<sup>2</sup>). Signals were collected for 0.3 sec after each step to test for scotopic a- and b-wave function. The c-wave was tested at a flash intensity of 10 cd s/m<sup>2</sup>, and the signal was collected for 5 sec. The c-wave was measured from baseline to the peak of the waveform. After recording, each mouse was placed in its home cage on top of a heating pad (39°C) to recover from anesthesia. Afterward, mice were injected with a reversal agent (0.5 mg/mL atipamezole, injection volume 5 µL per gram mouse weight; Patterson Veterinary, Greeley, CO) and placed individually in cages on top of heated water pads to recover.

### **3.3.3 Rhodopsin Metabolism Assay**

Murine eyes were enucleated and placed in glass tubes of “freeze-sub” solution of 97% methanol (Fisher Scientific A433p-4) and 3% acetic acid that was chilled with dry ice, following the method of Sun and coworkers<sup>129</sup>. Tubes were placed at -80°C for at least four days to dehydrate the tissue. After at least four days, tubes were allowed to reach room temperature before the eye samples were placed into tissue cassettes (Fisher Scientific, Catalog # 15200403D). The cassettes were placed in 100% ethanol for 20 minutes and then fresh 100% ethanol for another 20 minutes. Next, the cassettes were placed in xylene (Fisher Scientific X3S-4) for 20 minutes and then in fresh xylene for another 20 minutes. Afterwards, the cassettes were placed in a paraffin bath for 45 to 60 minutes before being transferred to a fresh paraffin bath for another 45-60 minutes. Eyes were then embedded in paraffin and sectioned for immunofluorescence.

The paraffin sections were then deparaffinized and rehydrated with xylene and decreasing ethanol concentrations, then finally in Tris-buffered saline (TBS) (#1706435; Bio-Rad). The slides were covered in a blocking solution made up of Tris-buffered saline (#1706435; Bio-Rad) with 0.1% (vol/vol) Tween 20 (pH 6.0) (BP337-100; Fisher Scientific) (TBST)] with 2% Bovine Serum Albumin (BSA) [catalog #BP9703-100]. The primary antibodies (mouse anti-rhodopsin, Abcam, catalog #ab3267, [1:250] and Rabbit anti-BEST1, Abcam, catalog # ab14927 [1:250]) are then added to the blocking solution and put on the slides overnight at room temperature in a humidified chamber. The next day, the secondary antibody is added to the blocking solution. The slides were washed three times in TBST, and then the secondary antibody was placed on the slides and incubated for four hours. Slides were washed and nuclei stained before mounting in fluoromount G (catalog #0100-01; SouthernBiotech, Birmingham, AL, USA). We used counts of rhodopsin deposits within the RPE from shed rod outer segments as a proxy for phagosome production which were quantified. Counts were performed by three independent, blinded observers using Photoshop (Adobe Photoshop, Version 27.4.0 release), and each count was averaged for final counts per sample.

### **3.3.4 RPE flat mount preparation for ZO-1/alpha-catenin immunohistochemistry**

Murine eyes were enucleated and fixed with either zinc and formaldehyde (Z-fix) (Anatach, Battle Creek, MI Catalog # 622) for 10 minutes at room temperature for alpha-catenin staining or 4% paraformaldehyde (PFA; 16% solution stored under argon from Electron Microscopy Sciences Catalog # 15710) diluted in 1X PBS (Fisher Scientific #50-980-487 and Corning 46-013-CM) for 1 hour at room temperature. Afterward, the eyes were washed five times in Hanks' Balanced Salt Solution (HBSS Cat #14025092 Gibco by Life Technologies, Grant Island, NY) and stored at 4°C for up to 24 hours before dissection. RPE flat mounts were dissected and prepared as described in Zhang et al. (2021)<sup>130</sup>. After the removal of the retina, each RPE flat mount was individually transferred into a well created by attaching a silicone gasket (Sigma Aldrich #GBL665104-25EA) to a SuperFrost Plus microscope glass slide (Fisher

Scientific #12-550-15). Flat mounts were incubated in 300  $\mu$ L of blocking buffer (3% (W/V) bovine serum albumin (BSA) (Catalog #BP9703-100) and 0.1% (V/V) Triton X-100 (Sigma) in HBSS (Fisher Scientific Catalog # MT21023CV) for 1 hour at room temperature in a humidified chamber. Primary antibodies (anti-ZO1 EMD Millipore Cat #MABT11 and anti-CTNNA1 (alpha-catenin) Abcam Cat #ab51032) or (anti-ZO-1 EMD Millipore Cat #MABT11 and anti-Iba1 [EPR16589] (ab178847)) were diluted and pre-blocked in the blocking buffer for 1 hour before being applied to the flat mounts. Flat mounts were incubated in the primary antibody overnight at room temperature. The primary antibodies were aspirated, and the flat mounts were washed five times with wash buffer (HBSS and 0.1% V/V Triton X-100). Secondary antibodies (see Table 2) were diluted and pre-blocked in the blocking buffer for 1 hour at room temperature before being applied to the flat mounts overnight at room temperature. The flat mounts were then rinsed three times with the nuclear stain, Hoechst 33258 (Thermo-Fisher H3569, Waltham, MA), in the wash buffer, followed by two additional washes with the wash buffer. Afterward, the wash buffer was aspirated, the gasket was removed from the glass slide, and the flat mounts were mounted with Fluoromount-G (Southern Biotech; Catalog #0100-01; Birmingham, AL) and covered with a 22X40 mm coverslip (Thermo Fisher #152250). Flat mounts were dried overnight on flat surfaces in the dark.

### **3.3.5** Confocal microscopy:

The Nikon Ti2 with an A1R confocal scanner microscope was used for imaging. The processing software used for imaging was NIS Elements 5.2. Imaging was done in resonance mode at 1024x1024 with 8x averaging, and a Denoise.ai filter was applied to the images. Lasers were 405, 488, 560, and 640 nm. Images were collected using a 20x objective, and 25 images were usually photomerged together using Adobe Photoshop CS6.

### 3.3.6 Morphometry

#### 3.3.6.1 CellProfiler Segmentation Analysis

CellProfiler, a free, open-sourced cell image analysis software, is designed to analyze different images through customizable scripts, or “pipelines.” A pipeline was explicitly created to examine the morphology of the retinal pigment epithelium cells in murine eyes (used with Cellprofiler version 4.2.5), specifically the area, eccentricity, and radius of cells expressing alpha-catenin. The pipeline first converted the staining of ZO-1 (green), alpha-catenin (red), and Hoechst 33258 (blue) to grayscale, inverted the image, identified the primary object in the image, collected metrics of each cell (including the number of neighbors and eccentricity), and saved all morphometric analysis information of each cell to a spreadsheet that can be exported from the program for analysis.

#### 3.3.6.2 Imaris for alpha-catenin intensity

The intensity of cytoplasmic alpha-catenin was analyzed using Bitplane's Imaris software 10.0.0. Maximum intensity projection images of each RPE flat mount were processed using IMARIS 10.0.0 (Bitplane, Inc.), in which individual cells were segmented, identified, and quantified morphologically. Before converting and uploading images to Imaris, the corneal flaps and optic nerve heads were removed via the crop tool in Photoshop. Cropped flat mounts were uploaded to Imaris, and segmentation was customized based on target cell characteristics. The Imaris software allowed for thresholding based on cell size. Incorrectly segmented cells and artifacts were manually corrected. ZO-1 was used to segment each RPE cell, and cells were filtered based on alpha-catenin intensities in the cytosol.

### 3.3.7 Iba-1 quantification

Sub-retinal immune cells were manually counted using the Photoshop count function (Adobe Photoshop, Version 27.4.0 release) by three independent, masked observers.

### 3.3.8 Statistical analysis

Statistical analysis was conducted using Prism 9.1.0 (on Mac OS X 14 Sonoma) (GraphPad Software, Inc., La Jolla, CA, USA). Data are presented as mean +/- standard deviation (SD), with statistical testing for individual datasets described in the Figure legends. A p-value <0.05 was considered statistically significant. Demographic distributions and sample sizes are summarized in Table 1. All statistical tests used are detailed in supplemental data Figures. Note: Regional analysis of cell counts and fluorescence intensity for proteins of interest was averaged over the total number of cells within that partition and normalized to the partition containing the most significant number of cells by partition area.

## 3.4 RESULTS

### 3.4.1 **Natural aging of the retinal pigment epithelium resulted in ectopic localization of structural protein alpha-catenin.**

To examine if increased age is accompanied by cytoplasmic mislocalization of alpha-catenin (Acat or CTNNA1), a force-sensing protein that interacts with F-actin and cadherins of the actin cytoskeleton<sup>61,131</sup>, we stained RPE flat mounts from young and aged mice. With increased age, we found that Acat immunoreactivity was more prevalent in the RPE cytoplasm in aged mice than in young mice [Figure 1]. The oldest mice showed a 1.9-fold increase (young mean: 24.7 A.U. ±9.93; Aged mean: 48.1 A.U. ± 9.31; p-value\*\*\*<0.001; One-way ANOVA with Tukey's multiple comparison test.) in cytoplasmic alpha-catenin signal compared to the young mice; while middle-aged mice showed a ~16 percent increase in cytoplasmic alpha-catenin compared to the young group (middle-aged mean: 28.67 A.U. ±3.55 vs. young mean: 24.7 A.U. ±9.93; p-value: not significant; One-way ANOVA with Tukey's multiple comparison test). This increased accumulation coincided with increased numbers of enlarged, multinucleated RPE cells (see white arrows, Figure 1). Enlarged cells were mainly concentrated in the central portion of the RPE sheet. However, the aged group's peripheral cells also showed cytoplasmic alpha-catenin signs. These changes in alpha-catenin localization were a sign of RPE stress as the cells undergo structural

modification (breakdown of adherens junctions in the cell membrane) in response to age-related damage<sup>131 132</sup>.

### **3.4.2 Cytoplasmic alpha-catenin localization has regional distribution patterns and is highly expressed in aging animals in the central medial to the optic nerve.**

The morphometric analysis of RPE eccentricity and mean area averaged across the entire flat mount showed no statistically significant differences among age groups [data not shown]. However, we hypothesized that by comparing RPE morphology by regional subcategories, there would be a considerable difference in morphometric features among age groups due to notable empirical observations of regional patches of RPE cells that looked morphometrically distinct. To test this, we made five circular, concentric partitions around the optic nerve expanding into the periphery. We observed an interesting trend in regional subcategories when compared between age groups. When comparing regions proximal to the optic nerve, alpha-catenin expression significantly increased when stratified by age group [See Figure 2B]. This trend was further evident when assessing the eccentricity and mean area of the cells expressing cytoplasmic alpha-catenin within each group partition. In the aged group, cells expressing cytoplasmic alpha-catenin displayed regional increases in cell area and eccentricity proximal-medial to the optic nerve compared to cells from the young group (Figure 2C-2D). A similar trend was observed between the middle-aged and young groups, indicating that these localization changes in the force-sensing protein, alpha-catenin, are an early feature of RPE stress preceding age-related visual decline and functional loss of RPE. These data align with previous studies that show central RPE cells exhibit more cell death and stress signals than peripheral RPE cells<sup>133</sup>.

### **3.4.3 Inflammatory cell recruitment to the RPE increases with advanced age.**

To assess whether the number of immune cells recruited to the RPE increases in the natural aging of mice, we quantified the total number of IBA-1 positive cells in the RPE sheets of young and aged mice. We found that there was a more than 9-fold increase of IBA-1+ immune cells within the RPE sheets of mice

in the aged group compared to younger groups (aged: mean  $438.85 \pm 350$ ; young: mean  $46.5 \pm 40.3$ ; p-value  $< 0.05$ ; Kruskal-Willis ANOVA with Dunn's multiple comparison test) [see Figure 3A and B]. Additionally, the deposition of immune cells was two-fold higher in the mid-periphery of the RPE within the aged group represented by zones 3 and 4 (Zone 3: young mean:  $4.25 \pm 3.9$  cells v.s. aged:  $72.6 \pm 53.5$  IBA1 cells; p-value  $< 0.05$ ; Two-way ANOVA with Tukey's multiple comparison. Zone 4: young mean:  $8.25 \pm 9.6$  IBA1 cells v.s. aged:  $78.6 \pm 74.7$  IBA1 cells; p-value  $< 0.05$ ; Two-way ANOVA with Tukey's multiple comparison [ see Figure 3C] compared to the young group.

#### **3.4.4 Loss of Retinal and RPE Function Occurs with Aging.**

Comparative analysis of functional output between age groups found that there was a ~40% to 50% loss of function in both scotopic a- and b-wave function, respectively, between the young and aged groups (young a-wave mean:  $257.5 \mu\text{V} \pm 46.3$  vs. aged a-wave mean:  $148.75 \mu\text{V} \pm 18.5$ ; p-value  $**** < 0.0001$ . young b-wave mean:  $534.0 \mu\text{V} \pm 105.0$  vs. aged b-wave:  $264.83 \mu\text{V} \pm 36.9$ .; p-value  $**** < 0.0001$ . One-way ANOVA with Tukey's multiple comparisons test). We observed a more modest but significant reduction in scotopic a- and b-waves between the middle-aged and aged groups and the young and middle-aged groups. (29% and 22% loss, respectively p-value  $*** < 0.001$ ; young mean:  $257.5 \mu\text{V} \pm 46.3$  middle-aged mean:  $210.3 \mu\text{V} \pm 34.3$ ; aged mean:  $148.75 \mu\text{V} \pm 18.5$ ; One-way ANOVA with Tukey's multiple comparisons test). When assessing RPE function via c-wave amplitude analysis, only the aged group showed a significant reduction in function compared to the youngest group (30% loss, p-value  $**0.001$ ; mean young:  $258.9 \text{ nV} \pm 59.58$ ; aged mean  $182.3 \text{ nV} \pm 25.98$ ; One-way ANOVA with Brown-Forsythe test), while there was no difference between the young and middle-aged group.

#### **3.4.5 Aging animals show modest retinal and RPE morphological irregularity.**

Mice in the aged group showed marginal differences in retinal architecture compared to the youngest group. At ~500 to 1000 microns from the optic nerve on the superior side, there is as much as a 34% increase in retinal thickness (young group: average:  $6.2 \pm 0.8 \mu\text{m}$ ; Aged group: average  $8.3 \pm 0.87 \mu\text{m}$ . p-

value  $** < 0.01$ . Two-way ANOVA with Dunnett's comparison test) in the aged group compared to the youngest group. This difference in regional retinal thickness appeared near the optic nerve on the superior portion of the retina. Additionally, the retinas of older mice showed abnormalities of the RPE layer with enlarged cells compared to young animals and loss of cell-cell contacts between the RPE cells, indicating irregularities in the cell structures (See Figure 5A: see white arrows; Figure 5B). There were also changes in the morphology of the inner and outer segments of the photoreceptors in the aged group compared to the younger groups. These data also suggested that isolated, regional changes correlate with increased age<sup>15,116,134</sup>.

#### **3.4.6 Natural aging resulted in the retention of phagosomes within the RPE.**

A significant function of the RPE is to provide cellular waste management of the photoreceptor outer segments via phagocytosis. Studies of RPE function in human donor eyes with AMD showed dysregulation of phagocytosis in the RPE eyes. Due to the significant loss of RPE function in the aged group compared to the young group, we evaluated RPE function via a rod outer segment phagocytosis assay. Based on previous studies, we hypothesized that there would be a reduction in phagosomes within the RPE of aged mice compared to the young group<sup>15,134-136</sup>. However, we found an increase of ~68% (in phagosomes retained within the RPE of the aged group compared to the youngest group (young mean:  $\sim 239.6 \pm 57.6$  phagosomes/animal; aged group:  $\sim 406.8 \pm 107.8$  phagosomes/animal; p-value  $** < 0.01$ ; Unpaired t-test) (Figure 6A and 6B). These data suggest phagosome processing in RPE cells may be slower in old mice.

### **3.5 DISCUSSION**

This study aimed to define the changes in RPE morphology during natural aging in the C57BL/6J older than 24 months of age. We sought to systematically dissect these morphological characteristics to look for discrete regional changes that may account for the loss of central vision during natural aging. Our previous work analyzed changes in RPE organization in aging animals using morphometric analysis<sup>128</sup>.

In that study, we described RPE morphology as relatively conserved characteristics between young and aged animals: 1) cells at the periphery radiated outward along an axis and showed high levels of variability in cell shape, and 2) the cells located at the central to mid-peripheral RPE sheet are densely packed and show little change in density over time, possibly due to cells from the periphery elongating and pushing into the center. Thus, the accumulation of subtle RPE changes over time is most correlated with the detrimental effects seen in aging. While mice lack a macula and cannot provide a direct comparison to human AMD, they have been effectively used to study AMD-like manifestations of disease in RPE cells (<sup>127,137</sup>). Weikal et al. described apparent phenotypic differences in mice at 23.5 months compared to 17-month-old C57BL/6J mice, suggesting that the study animals older than 24 months is warranted. Additionally, studying the maturational gap after 24 months will aid in identifying abnormal patterns in cell morphology and function coupled with early intervention, which may be adequate to delay age-associated pathology resulting in vision loss.

While we have explored multiple methodologies to optimize the tracking of subtle changes in RPE morphology that correlate with genetic and age-related manifestations of vision loss and pathology <sup>138-140</sup>, our understanding of very early signs of RPE distress and damage remains elusive. This study builds on these methods by evaluating increased regional pleomorphism and polymegathism of cytosolic, alpha-catenin expressing RPE cells and regional increases of immune cell recruitment as indicators of RPE stress preceding the overall decline in RPE function with age.

The RPE consists of a monolayer of post-mitotic cells that do not readily increase; consequently, the RPE has adopted other stress responses to accommodate the loss of cell density with age <sup>119</sup>. We first evaluated alpha-catenin localization in conjunction with changes in the peripheral membrane, tight-junction associated protein, Zonula Occludens 1 (ZO-1), as a metric for early signs of RPE damage. The RPE of young mice was of uniform cell size and shape, and alpha-catenin was restricted to the cell borders, indicating healthy RPE morphology. In contrast, the RPE in the aged group showed increased cytoplasmic alpha-catenin compared to the young group [See Figure 1A-B], likely indicating a higher degree of disassembly of adherens junction protein complexes associated with pathology. Multiple studies

have validated the role of alpha-catenin in controlling actin skeleton dynamics via its ability to bind actin bundles and act as a stabilizer at sites of adherens junction force-sensors<sup>61,132,141–143</sup>. We also assessed cell area and eccentricity (level of shape irregularity) of cells with cytoplasmic alpha-catenin. Still, we found no significant differences between groups when averaged over the entire flat mount (data not shown). We conducted a regional analysis using five concentric partitions for cytoplasmic alpha-catenin expression and the cell area and shape irregularity in the RPE expressing cytoplasmic alpha-catenin among each group. We found distinct regional differences by age when assessing the morphometrics of RPE cells expressing cytoplasmic alpha-catenin. In the aged group, the RPE in zones 1, 2, and 3 showed significantly higher cytoplasmic alpha-catenin expression than the young group [ See Figure 2A and 2B]. Additionally, the aged RPE expressing cytoplasmic alpha-catenin displayed increased numbers of pleomorphic (increased eccentricity) cells and polymegathism (non-uniform cell area) in zones 1, 2, and 3 compared to the young group [See Figure 2C-2D]. Our findings further validate previous studies that have examined regional differences in RPE morphology<sup>119,128,133</sup>, regional heterogeneity of stress markers<sup>5,19,112,144–147</sup>, and increased apoptosis in areas with higher photoreceptor density. Our previous morphometric analysis, cited in *Kim et al*, assessed RPE morphometrics and topology using ZO-1 analysis and found increased eccentricity and cell size in the peripheral RPE, near the cornea, with increasing age<sup>128</sup>. The present study, incorporates alpha-catenin, an indicator of stress-associated breakdown of RPE adherens junctions, in the RPE morphometric analysis and shows that there are regional increases in RPE cell irregularities proximal-medial to the optic nerve that accumulate with age and precede age-related deficits in vision. These data support a link between the mislocalized alpha-catenin and age-related stress changes in RPE structure and size. An alternative explanation for the elevated cytoplasmic alpha-catenin levels could be the age-related loss of melanosomes, potentially enhancing the detection of cytosolic alpha-catenin<sup>146</sup>

Next, we analyzed subretinal immune cell deposition in each group by staining flat mounts for IBA-1+ cells. Our study found the aged group (P730+) displayed increased attachment of these cells to the apical face of the RPE compared to younger groups [See Figure 3AB]. Additionally, the regional

analysis revealed higher deposition in zones 3 and 4, corresponding to the mid-periphery and far periphery, with fewer cells near the optic nerve. Interestingly, this deposition pattern aligned with the increased alpha-catenin expression and increased eccentricity data shown in Figure 2A-D, suggesting that there may be a correlation between RPE stress indicators and increased regional accumulation of immune cells [ See Figure 3C-D.] Previous studies have proposed that interactions between RPE cells and microglia/macrophages contribute to retinal damage, with inflammation being a hallmark of aging and AMD. Multiple genome-wide association and functional studies have described increased inflammation as a hallmark of aging,<sup>102,148–152</sup> and increased risk for AMD and subretinal damage in humans<sup>19,112,147,153</sup>.

Several studies have documented age-related deterioration in visual function in mice<sup>151,152,154,155</sup>. Marola *et al.* identified conserved, overlapping transcriptomic and proteomic signatures associated with visual defects in aging mouse retinas<sup>156</sup>. We evaluated visual function robustness using electroretinogram (ERG) scotopic a-, b-, and c-waves. We observed a significant decline in a- and b-wave output starting in the middle-aged group (P365-P544) and continuing into the aged group (P730-P970). RPE function assessed via c-wave amplitude showed a ~30% decrease in the aged group compared to the young [See Figure 4A-C]. These findings suggest a correlation between early RPE stress indicators and significant loss of visual function between the young and aged groups. Interestingly, the middle-aged group also showed deviations in a- and b-wave function, correlating with changes in RPE morphology and cytoplasmic alpha-catenin, preceding increased immune cell infiltration or changes in c-wave in the middle-aged group.

Then, we quantified retinal thinning and cell loss over time to examine age-related structural changes. Surprisingly, we found an increase in retinal thickness in the aged group compared to both young and middle-aged groups, particularly in the superior mid-periphery. There was a regional component to this distinction, with the retina from the superior portion of the eye cup within the mid-periphery being thicker in the aged group than in the young group [Figure 5B]. These data may indicate retinal edema or swelling proximal to the optic nerve due to cellular distress, potentially explaining the

regional thickness increase in the aged group<sup>157,158</sup>. Additionally, structural abnormalities in RPE were observed only in the aged group [Figure 4A, denoted by white arrows]. These findings suggest that although RPE is resilient and shows functional damage later than the retina, accumulated age-related structural changes in RPE contribute to functional decline and inflammation.

Finally, to assess RPE function in response to the loss of electroretinogram output, we studied RPE phagocytic activity in young and aged groups by proxy of rhodopsin metabolism. Phagocytosis, a critical function of the RPE, was evaluated by staining samples for rhodopsin within 1 hour of light onset and assessing changes in rhodopsin metabolism by the RPE. We found a significantly increased presence of rhodopsin in the RPE of the aged group compared to the young, demonstrating age-related dysfunction in the RPE (see Fig. 6). Previous studies have described a similar aberration in RPE phagocytic capacity, increased stress markers, and accumulation of iron and drusen deposits with growing age or damage<sup>136,159,160–164</sup>. We hypothesize that the increased presence of phagosomes in the aged group may lie in phagosome turnover rather than increased production or reduced maturation. Incomplete proteolysis of phagosomes by the RPE in advanced age has been described and could result in cellular stress, leading to RPE loss of function and death<sup>165</sup>. This explanation may also partially account for the manifestation of regional differences. Central RPE cells are responsible for recycling the waste of a more densely packed population of photoreceptors. As a result, the central RPE is more affected, and defects are evident before those in the periphery.

Limitations: This study is limited by the increased attrition rate of the study as animals age and drop out due to death by natural causes. Very few of the animals survived to be included in the oldest group, which may result in an age and sex bias in the data. We didn't perform multifocal ERGs, which would have been an additional method of topographically mapping changes in visual function with age. Another limitation of this study is that the morphometric analysis of RPE cells and immune cells is contingent on the adherence to the surface of the flat mount preparation. Thus, our methods could not analyze nonadherent

cells that might weakly interact with the RPE and may be involved in the damage response. Analysis of the flat mounts was restricted to the apical face, which may miss phenomena that contribute to pathology that lie on the basal face of the cells. Data analysis was also limited by the study's nature, only incorporating static, post-mortem analysis of cellular changes. Longitudinal, live-imaging data may complement this study and monitor dynamic changes in labeled immune cell localization over time. Additionally, studies of the dynamics of RPE cells and subretinal immune cells may differ between humans and mice during aging. We also used the inbred C57BL/6J mouse strain so that the observations may vary in other inbred strains or outbred mice. Last, in this study, we did not delineate between microglia and macrophages, which may play different roles in the onset of pathology associated with aging.

### 3.6 FIGURES AND TABLES

**3.6.1 Table 1: Animal Sample Sizes by Age Group and Outcome Measure**

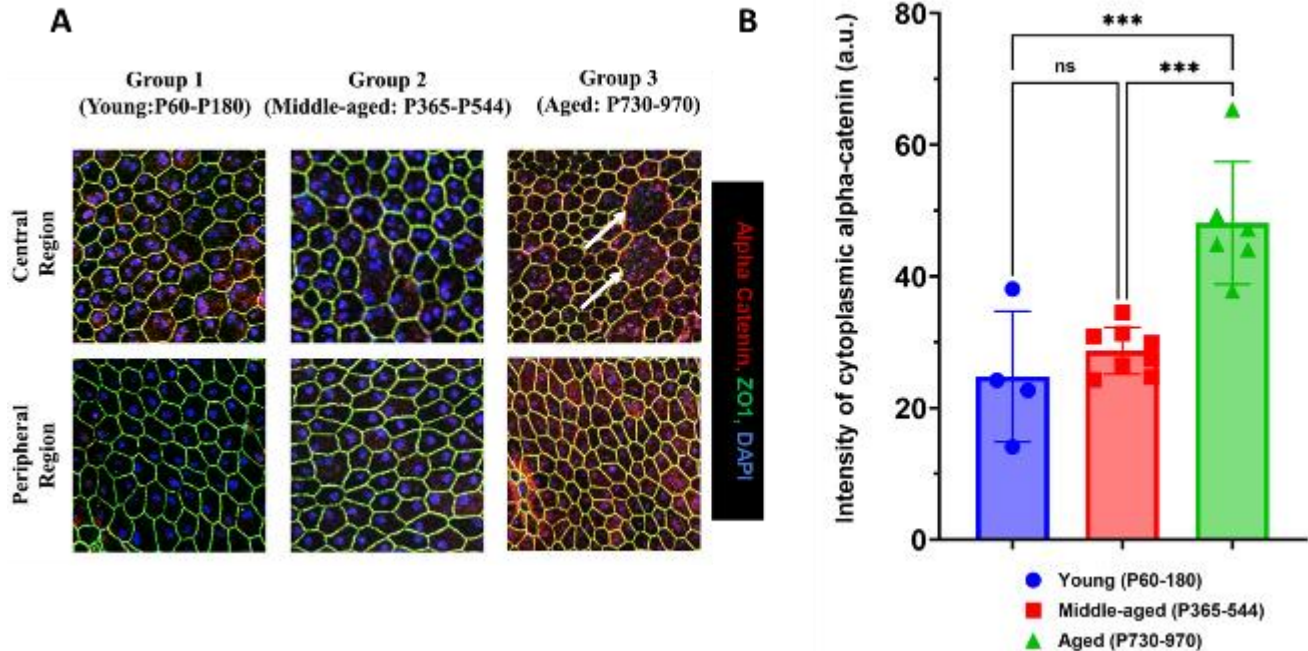
| <b>Group</b>                 | <b>Immunofluorescence<br/>(Alpha-catenin)</b> | <b>Immunofluorescence<br/>(IBA-1)</b> | <b>ERG</b> | <b>Phagocytosis</b> |
|------------------------------|---|---------------------------------------|------------|---------------------|
| <b>Young: P60-180</b>        | N=6   | N=4                                   | N=10       | N=6                 |
| <b>Middle-aged: P365-544</b> | N=11  | N=7                                   | N=13       | N/A                 |
| <b>Aged: P730-P970</b>       | N=4   | N=7                                   | N=8        | N=5                 |

Table Legend: Numbers of individual mice are provided. Approximately equal numbers of males and females were collected per sample group. Average Body Weight per group: Young: 19.4 grams  $\pm$  3.4; Middle-aged: 30.5 grams  $\pm$  1.9; Aged: 35.5 grams  $\pm$  4.8. N/A indicates none available.

**3.6.2 Table 2: Primary and Secondary Antibodies and Reagents used for immunofluorescence**

| Antibody  | Antibody type           | Vendor + Catalog #                     | Concentration |
|---|-------------------------|--|---------------|
| Rat Anti-ZO1  | Primary                 | EMD Millipore, Catalog # MABT11        | [1:200]       |
| Rabbit Anti-CTNNA1 (Alpha-catenin)                          | Primary                 | Abcam, Catalog #AB51032                | [1:500]       |
| Rabbit Anti-Iba1 (ionized calcium binding adaptor molecule) | Primary                 | Abcam, Catalog #ab178847               | [1:1000]      |
| Mouse anti- Rhodopsin                                       | Primary                 | Abcam, ab3267                          | [1:250]       |
| Rabbit anti-Best1   | Primary                 | Abcam, ab14927                         | [1:250]       |
| Pentahydrate (bis-Benzamide)<br>Hoechst 33258               | DNA<br>nuclear<br>Stain | Thermo-Fisher<br>Catalog #: H3569      | [1:250]       |
| Donkey anti-Rat (AF488)                                     | Secondary               | Life Technologies,<br>Catalog # A21208 | [1:1000]      |
| Donkey anti-rabbit (AF568)                                  | Secondary               | Life Technologies,<br>Catalog # A10042 | [1:1000]      |
| Donkey Anti-Mouse (AF488)                                   | Secondary               | Life Technologies<br>Catalog #A21202   | [1:1000]      |

### 3.6.3 Figure 1: Natural Aging of the Retinal Epithelium Results in Ectopic Localization of Structural Protein, Alpha-catenin



**Figure 1: Natural aging of the retinal pigment epithelium resulted in ectopic localization of the structural**

**protein alpha-catenin.** RPE flat mounts from animals in young (P60-180), middle-aged (P365-729), and aged (P730-970) were collected and stained for anti-alpha-catenin [1:500; red], anti-ZO1[1:200; green], and Hoechst 33258 [blue]. The figure shows a representative image of alpha-catenin localization into the cytoplasm of RPE cells exhibiting atypical morphology [Figure 1A; Representative Full flat mounts are shown in Supplemental Fig.1].

White arrows show examples of enlarged RPE cells with cytoplasmic expression of alpha-catenin. The prevalence of these cells increased in the aged group and is quantified in Fig 1B. N =4-8 animals/group. One-way ANOVA with Tukey's multiple comparison test was used for analysis. Error bars: standard deviation (SD). An \* represents p-value <0.05; \*\* represents p-value <0.01; \*\*\* represents p value <0.001; \*\*\*\* represents p-value <0.0001. Sample size: 4-8 animals/group. Statistical test details are in Supplemental Table 1.

### 3.6.4 Figure 2: Cytoplasmic Alpha-catenin Localization has Regional Distribution Patterns and is Highly Expressed in the Mid-Periphery of Aging Animals.

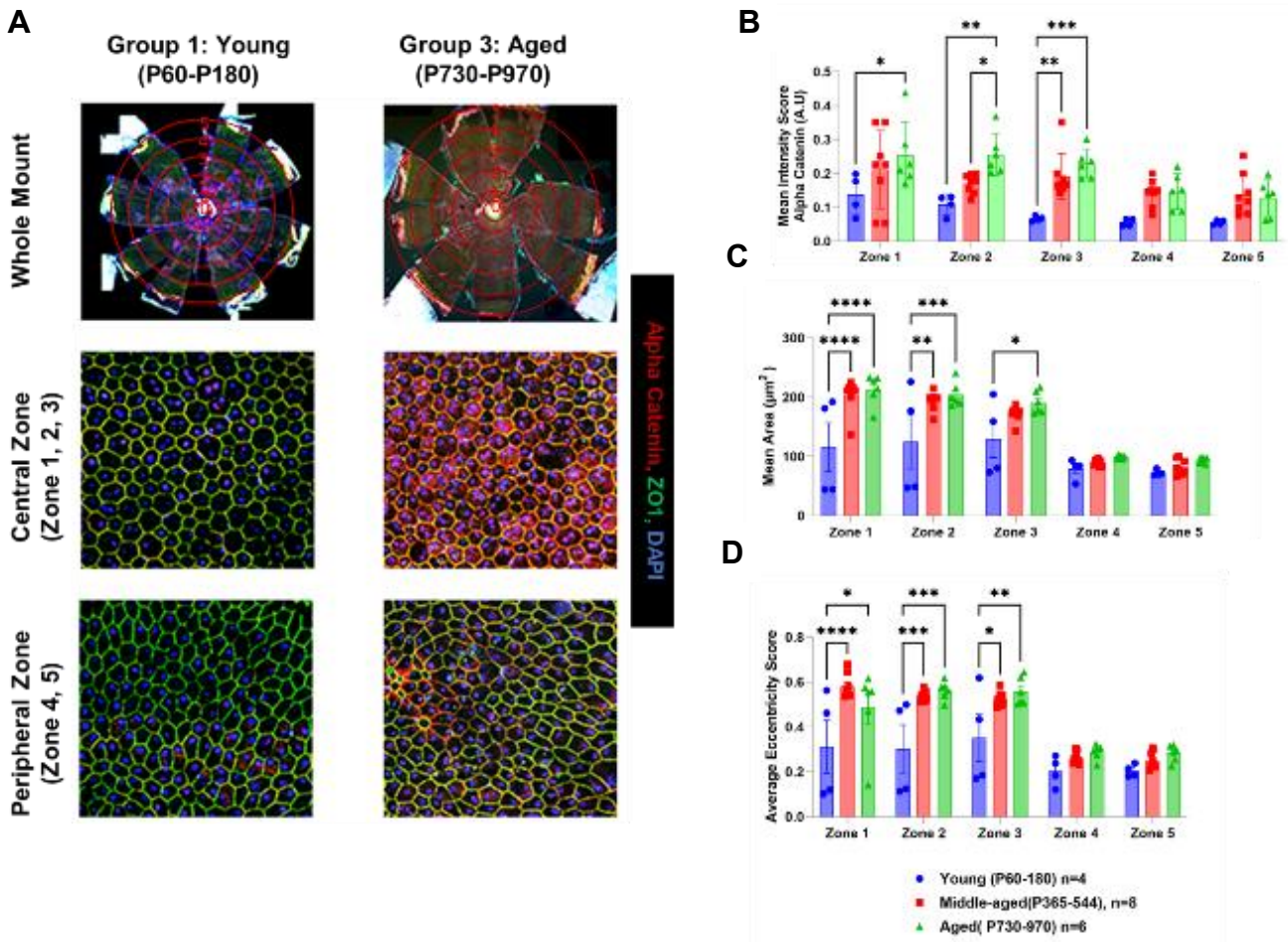


**Figure 2: Cytoplasmic Alpha-catenin localization displayed regional distribution patterns and was highly expressed centrally in aging animals.** RPE flat mounts were segmented into concentric zones around the optic nerve and cropped for segmentation using CellProfiler. Zone locations are shown in a representative image in Figure 2A. Multiple parameters were analyzed, including the mean intensity of alpha-catenin within the cytoplasm of the RPE cells (See Figure 2B), the average area of cells expressing cytoplasmic alpha-catenin (Figure 2C), and cell shape of RPE cells expressing cytoplasmic alpha-catenin (eccentricity) (Figure 2D). Sample sizes: N=4-11/group. Analysis: Two-way ANOVA with Tukey's comparison (2B,2C, and 2D); error bars: SD, \*= $p < 0.05$ , \*\*= $p < 0.01$ , \*\*\*= $p < 0.001$ . Statistical test details are in Supplemental Tables 2-4.

### 3.6.5 Figure 3: Inflammatory Cell Deposition Within the RPE Sheet was Increased with Advanced Age.

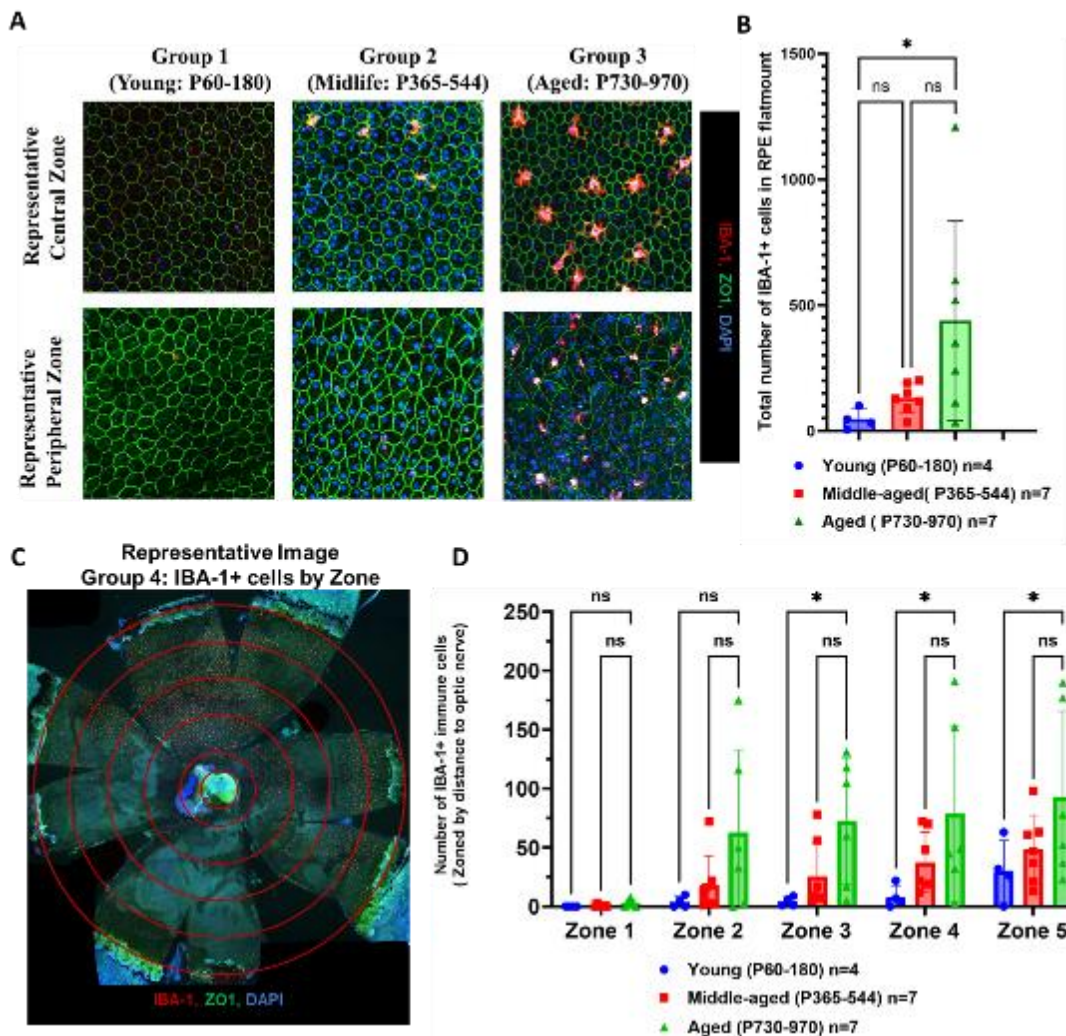


**Figure 3: Inflammatory cell deposition within the RPE sheet increased with age.**

RPE flat mounts were stained with an inflammatory cell marker, IBA-1[1:1000; red], ZO1(1:200; green], and Hoechst 33258 [blue]. Representative images show increased deposition of IBA-1 positive cells both centrally and peripherally in the aged group compared to the young group in Figure 3A [Representative whole flat mounts shown in Supplemental Fig.2]. The total IBA-1-positive cells were counted using Imaris [Figure 3B]. The flat mounts were then segmented into zones as previously mentioned and quantified with CellProfiler pipeline per zone.

Quantification of these results is shown in Figure 3C and 3D. N=3-7 animals/group. Analysis: Kruskal-Wallis with Dunn's Correction test (3B) and Two-way ANOVA with Tukey's multiple comparison test(3D); error bars: SD

\*=p<0.05, \*\*= p<0.01, \*\*\*= p<0.001. Statistical test details are in Supplemental Tables 5 and 6.

### 3.6.6 Figure 4: Loss of Retinal and RPE Function Increases with Natural Aging

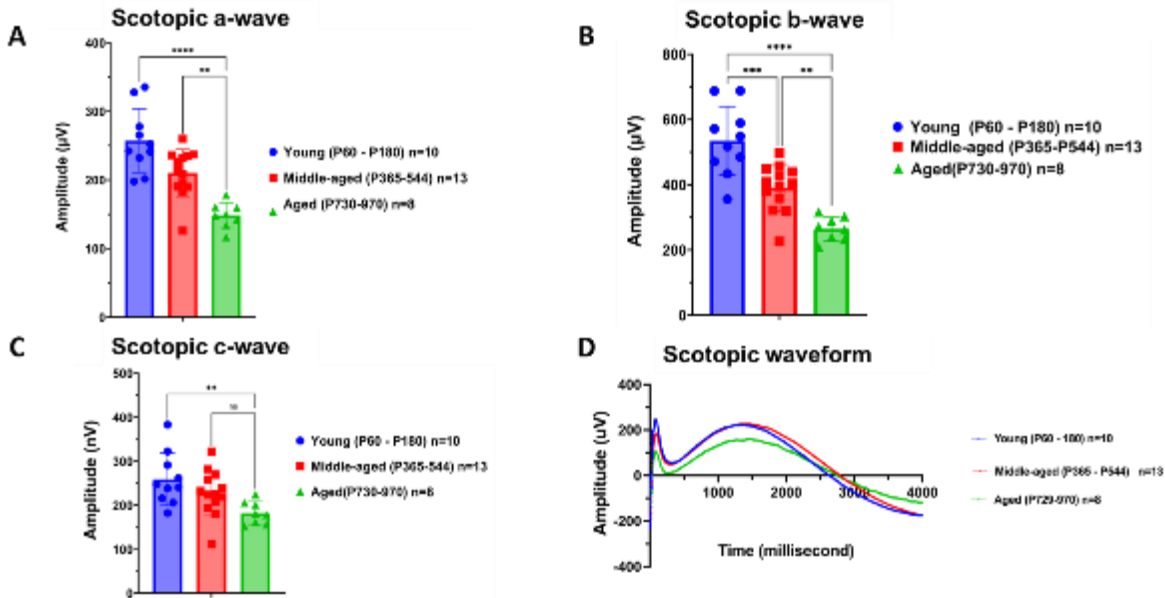
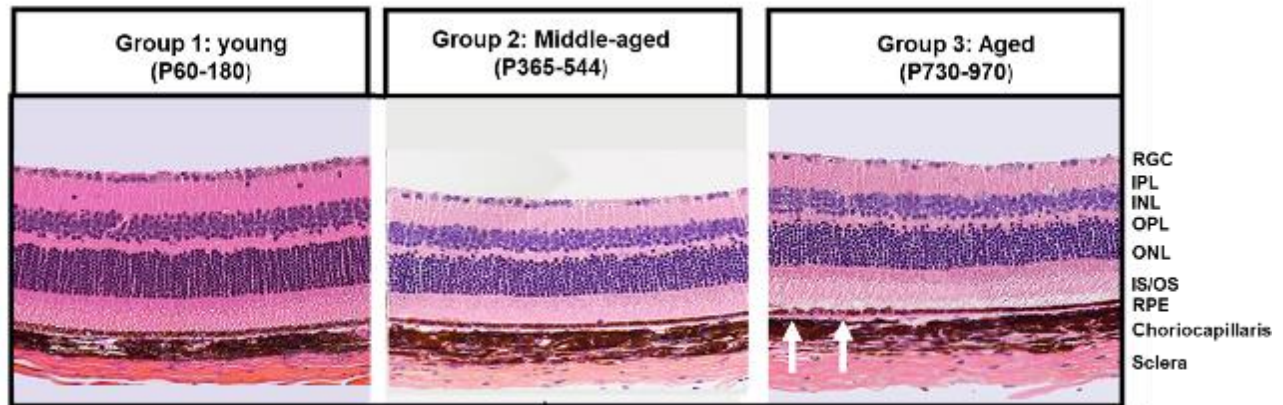


**Figure 4: Significant loss of visual function with natural aging with moderate loss of function within the RPE.**

Raw electroretinogram waveforms from the young, middle-aged, and aged groups under scotopic conditions and after a  $10\text{-cd s/m}^2$  light flash are shown (Panel D). At multiple flash intensities, there were significant differences between all groups and group 1 for scotopic *a-wave* and scotopic *b-wave*. In contrast, the scotopic *c-wave* was only modestly significant between the young and aged groups. The significant reductions in ERG response suggest that there were dysfunctional photoreceptors and bipolar cells. Additionally, the reduction in RPE c-wave response at 10Hz compared to the young group suggests that the age-related changes in the RPE also affected visual function. One-way ANOVA with Tukey's multiple comparison test. \*\*\* represents p-value  $<0.001$ ; \*\*\*\* represents p value  $<0.0001$ . Samples sizes: 8-13 animals/group. Statistical test details are in Supplemental Tables 7-9.

### 3.6.7 Figure 5: Aging Animals show Irregularities in Retinal and RPE Morphology

A



B

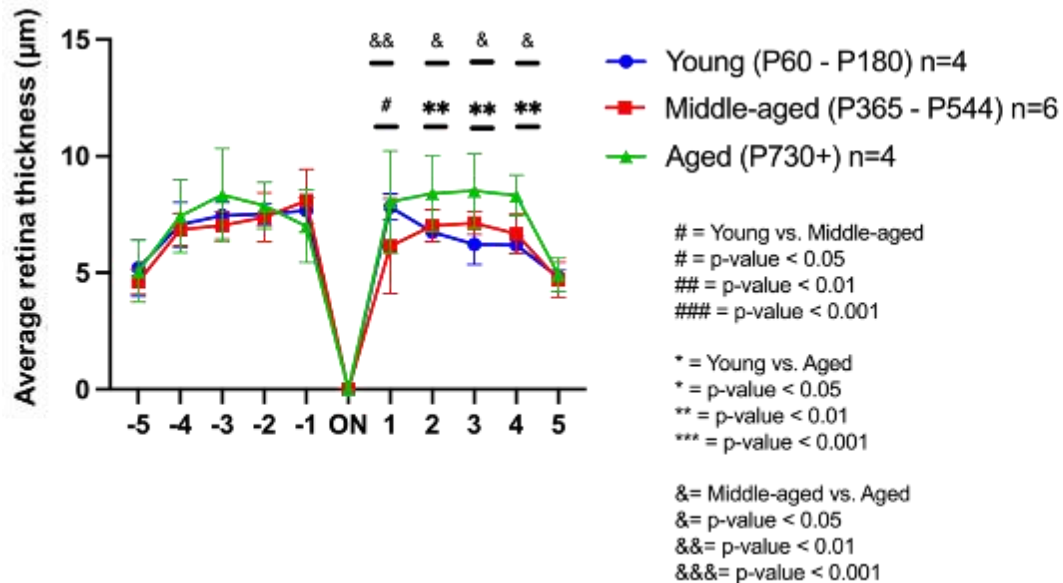


**Figure 5: Aging animals showed irregular morphology and retinal swelling in Hematoxylin & Eosin (H&E) staining compared to young animals.** Representative H&E-stained retina (Figure 5A: panels 1-3) are shown by age group. Notably, the aged group shows significant perturbations to the RPE (denoted by white arrows) compared to the young and middle-aged groups. The quantification of total retinal thickness is shown in Figure 5B. It shows regional changes in the retinal thickness of aged mice compared to the youngest group. Two – Way ANOVA with Dunnett’s correction multiple comparisons test for retinal thickness analysis\*, # = p-value < 0.05; \*\*, ### = p-value < 0.01; \*\*\*, #### = p-value < 0.001; \*\*\*\*, ##### = p value < 0.0001 (\* symbols indicate significance between young group vs . aged group; # symbols indicate significant between the young and middle-aged group. Samples sizes: 4-6 animals/ group). Statistical test details are in Supplemental Table 10.

### 3.6.8 Figure 6: Natural Aging Results in Reduced Rhodopsin Metabolism within the RPE compared to Young Animals

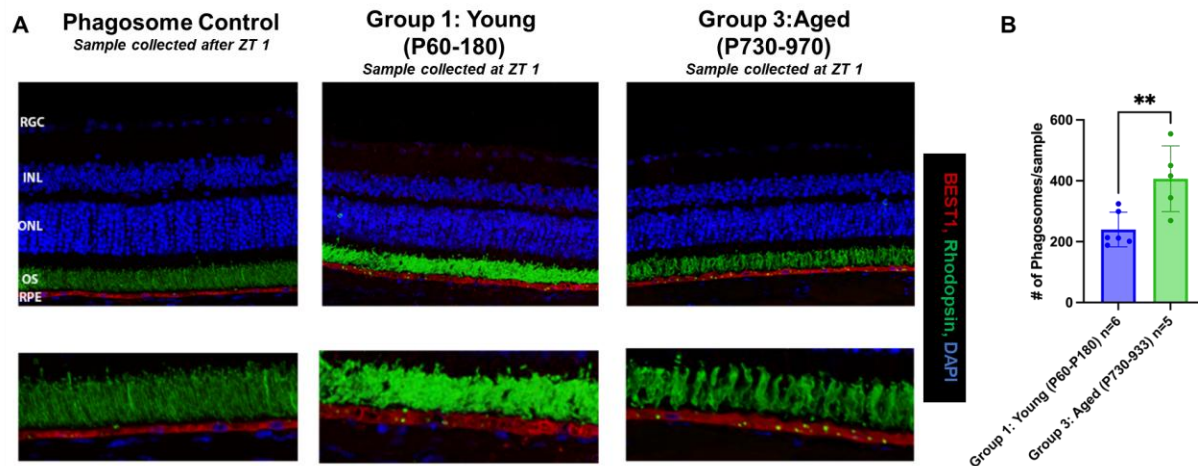


**Figure 6: Natural aging results in Reduced Rhodopsin Metabolism within the RPE compared to Young Animals**

In each group, whole eyes were extracted from animals at Zeitgeber 1 [ZT1] within 1 hour of environmental light cue onset [ZT0]. The sections were stained with Rhodopsin [green], Best1 [red], and DAPI [blue]. Representative images of a rhodopsin metabolism in the healthy control animal group (See Figure 6A). [Note: Control samples were collected outside the maximal phagosome production time after ZT1 (far left panel). The young group (middle panel) and aged group (far right panel) were collected between ZT0 and ZT1 or within 1 hour of lights on at 7 AM, which is during the maximal phagosome production period.] Rhodopsin-containing granules within the RPE were counted manually by three blinded observers and quantified (Figure 6B). Results showed increased phagosomes within the RPE of the oldest group compared to the youngest animals or the ZT control, suggesting that there may be aberrant turnover or maturation of the RPE phagosomes in aging mice. N=5-6/group. Analysis: Unpaired t-test; error bars: Standard deviation \*= $p$ -value $<0.05$ , \*\*= $p$ -value $<0.01$ , \*\*\*= $p$ -value $<0.001$ . Statistical test details are in Supplemental Table 11.

### **3.7 Conclusion:**

In this study, we sought to understand further how regional changes in the RPE sheet due to aging may affect the functional and structural outcomes of the subretinal space in mice older than 24 months. Our study found that RPE cells within the mid-periphery exhibit more eccentricity changes [Figure 2D], increased cytoplasmic alpha-catenin accumulation [Figure 1A-B, 2A-B], and increased deposition of IBA-1+ immune cells than the far periphery or central RPE cells in the advance age group [Figure 3A-D]. Our study also highlights how changes in regional stress responses and cell structure precede notable loss of RPE function over time. These morphological changes correlated with the loss of visual function via ERGs and defects in phagosome turnover in the RPE in the aged group and were associated with pathology onset. Aging C57BL/6J studies that include ages over two years are needed to examine the full range of age-associated RPE pathology to mirror clinical phenotypes found in at-risk persons within the crucial advanced age demographic of 80 to 95. Further study of potential mechanisms of RPE-immune cell communication during aging may give greater insight into targets for early intervention to preserve the sight of an increasing number of geriatric patients.

### **3.8 Acknowledgments:**

This work was supported by Grants from the National Institutes of Health (R01EY028450, R01EY021592, P30EY006360, U01CA242936, R01EY028859, T32EY07092, T32GM008490); by the Abraham J. and Phyllis Katz Foundation; by grants from the U.S. Department of Veterans Affairs and Atlanta Veterans Administration Center for Excellence in Vision and Neurocognitive Rehabilitation (RR&D I01RX002806, I21RX001924; VA RR&D C9246C); and an unrestricted grant to the Department of Ophthalmology at Emory University from Research to Prevent Blindness, Inc.

#### **4 CHAPTER 4: Comparing Light Damage-induced Phenotype Variation in pigmented, C57BL/6J animals with single nucleotide substitution in RPE65 gene**

**Authors:** Debresha A. Shelton<sup>1</sup>, Jack Papania<sup>1</sup>, Tatiana Getz<sup>1</sup>, Jana T. Sellers<sup>1</sup>, Preston Giradot<sup>1</sup>, Micah A. Chrenek<sup>1</sup>, Hans E. Grossniklaus<sup>1</sup>, Jeffrey H. Boatright<sup>1,2</sup>, John M. Nickerson<sup>1</sup>

Affiliations:

<sup>1</sup>Department of Ophthalmology, Emory University, Atlanta, Georgia, United States

<sup>2</sup>Atlanta Veterans Administration Center for Visual and Neurocognitive Rehabilitation, Decatur, Georgia, United States

Correspondence to: Please address all correspondence to Dr. John M. Nickerson; Department of Ophthalmology, Emory University, B5602, 1365B Clifton Road, NE, Atlanta, GA, 30322; Phone 404-778-4411; email: [litjn@emory.edu](mailto:litjn@emory.edu)

Funding: Supported by National Institutes of Health (NIH) grants R01EY028450, R01EY021592, P30EY006360, R01EY028859, T32EY07092, and T32GM008490, the Abraham and Phyllis Katz Foundation, VA RR&D I01RX002806 and I21RX001924, VA RR&D C9246C (Atlanta Veterans Administration Center for Excellence in Vision and Neurocognitive Rehabilitation), and a challenge grant to the Department of Ophthalmology at Emory University from Research to Prevent Blindness, Inc.

## 4.1 ABSTRACT:

### **Purpose:**

Light-induced retinal damage (LIRD), an ocular damage model that uses light stress to initiate retinal degeneration and study damage-associated changes in cellular processes and signaling, has traditionally used albino animals due to their increased light sensitivity. However, albino and pigmented animals differ significantly in retinal development and visual signaling, with the visual processing in pigmented animals more closely resembling human processes. Pigmentation is critical for retinal structure and function. This study aims to establish a light damage model reflecting pigmentation's impact on retinal degeneration and investigate the role of RPE65 and Pigment Epithelium Derived Factor (PEDF) in light stress responses. We hypothesized that (1) rhodopsin regeneration via RPE65 SNPs modulates LIRD susceptibility in pigmented C57BL/6J mice; (2) galectin-3 (Gal-3) expression correlates with damage severity; and (3) PEDF expression is essential for resistance to LIRD.

### **Methods:**

C57BL/6J mice with high (RPE65<sup>L450/L450</sup>) or low (RPE65<sup>M450/M450</sup>) activity RPE65 variants were bred with Cx3CR1-GFP mice. Light damage was induced at 50,000 lux for 5 hours during the dark phase. Mice were analyzed at 1-, 3-, and 7-days post-damage using electroretinography(ERG), spectral domain optical coherence tomography (SD-OCT), confocal scanning laser ophthalmoscopy (cSLO), histology, and western blotting. GFP+ (microglia/macrophages) and Gal-3+ cells were quantified using RPE flat mounts.

### **Results:**

RPE65<sup>L450/L450</sup> mice exhibited greater retinal damage and higher Gal-3 expression compared to RPE65<sup>M450/M450</sup> mice. Retinal thinning and ERG wave amplitude loss was more severe in RPE65<sup>L450/L450</sup> animals at day 7 compared to RPE65<sup>M450/M450</sup> (p-value <0.0001 and p-value 0.0001). GFP+ cell counts

increased by day 7 post-damage in RPE65<sup>L450/L450</sup> mice (p-value <0.0001). Gal-3 expression, initially comparable between genotypes, remained elevated in RPE65L/L mice on day 7 but decreased in RPE65<sup>M450/M450</sup> mice. Knocking out PEDF expression systemically in mice with the RPE65<sup>M450/M450</sup> allele resulted in increased vulnerability to light stress. The loss of protection from light stress in RPE65<sup>M450/M450</sup> animals suggests that PEDF expression was necessary for resistance to phototoxic damage.

**Conclusion:**

RPE65<sup>L450/L450</sup> increases photosensitivity and damage-associated Gal-3 expression in pigmented C57BL/6J mice. PEDF is crucial for the protective effects against phototoxic damage in RPE65M450/M450 mice, providing insights into the role of factors secreted by the RPE in the ocular response to light stress.

## 4.2 INTRODUCTION

Multiple genome-wide association and proteomic studies have implicated dysfunction in immune cell regulation and decline in retinal pigment epithelium (RPE) function as common characteristics of retinal degenerative diseases<sup>17-20</sup>. Visual disease etiology often subverts normal molecular mechanisms, leading to disease-associated phenotypes. Light damage studies have been integral in modeling the conditions under which molecular determinants evoke normal versus pathological phenotypes, deepening our understanding of cellular and molecular mechanisms contributing to disease progression.

However, previous phototoxicity studies predominantly relied on findings from albino animals as they are more susceptible to light damage. Pigmented mice and rats, which process visual stimuli more like humans, are resistant to light damage, requiring extended exposure time<sup>166,167</sup> to display minimal damage phenotypes, a characteristic attributed to slower regeneration of rhodopsin<sup>168-170</sup>. Additionally, previous studies have reported innate differences in ocular responses in albino strains compared to pigmented ones, e.g., the reduced density and distribution of photoreceptors and altered speciation of retinal ganglion cells in albino compared to pigmented animals, suggesting that strain differences may have a confounding influence on how these studies should be interpreted<sup>171-175</sup>. To create a model that is more like the pigmented vision of most humans, we made a pigmented, photosensitive C57BL/6J mouse by creating a single nucleotide polymorphism in the gene *Rpe65* at amino acid 450. As a result of substituting the methionine at position 450 with leucine, we can shift the photoresistance exhibited in C57BL/6J mice to conferred photosensitivity respectively<sup>33</sup>. This method eliminates potential strain differences since the mice will be on the same background and possess congenic features at every other gene locus. This study examined the functional, morphological, and molecular differences in pigmented animals with putative-conferred photosensitivity compared to putative photoresistance. This study found that pigmented, RPE65<sup>L450/L450</sup> animals are conferred photosensitivity and exhibit more susceptibility to damage, have increased subretinal immune cell recruitment, and increased galectin-3 expression compared to RPE65<sup>M450/M450</sup> controls, which exhibit photoresistance. Galectin-3, a  $\beta$ -galactoside-binding

protein, is significantly increased in multiple progressive degenerative diseases affecting both the brain and eye, including Huntington's disease, ischemic injury, glaucoma, uveitis, and advanced age-related macular degeneration<sup>68,176–182</sup>. *O'koren et al.* reported the preferential recruitment of Gal-3 expressing immune cells to the subretinal space where the RPE in a both light damage and genetic model of retinal degeneration<sup>73,75</sup>.

Previous studies of light damage have implicated pigment epithelium derived factor (PEDF) in the protection of photoreceptors and neurons after damage-associated oxidative stress.<sup>183–185</sup> PEDF, a neurotropic protein preferentially secreted by the RPE, has been shown to have many neuroprotective effects, in both the eye and brain<sup>186–188</sup>. Previous studies of the secreted proteome of eyes collected from patients diagnosed with retinal degeneration also showed disruption of both galectin-3 and PEDF expression compared to age-matched controls, suggesting that they both may be involved in disease pathology<sup>17</sup>. Loss of PEDF has also been linked to increased activation of proinflammatory signaling in the retina<sup>189</sup>. Due to the role that PEDF and the RPE play in the maintenance of homeostatic ocular signaling, as well as the links to increased inflammatory signaling when depleted or dysfunctional, we hypothesized that the putative photoprotective phenotype observed in RPE65<sup>M450/M450</sup> animals requires PEDF expression. In the following data we show that photoprotective phenotype in RPE65<sup>M450/M450</sup> requires PEDF expression. Deficiencies in PEDF expression in RPE65<sup>M450/M450</sup> and RPE<sup>L450/L450</sup>, result in severe deficits in visual function after light damage exposure. RPE65<sup>M450/M450</sup> animals that don't express PEDF show a similar photosensitive phenotype to RPE65<sup>L450/L450</sup>. Taken together, these findings suggest that the comparative analysis of congenic, pigmented photosensitive and photoresistant animals is a promising model to study and identify early biomarkers of disease outcome and targets for therapeutic interventions that may preserve vision.

## 4.3 METHODS

### 4.3.1 Breeding Scheme

To generate the C57BL/6J mouse line expressing the RPE65<sup>L450/L450</sup> allele, the donor strain, 129-SV, was bred to the recipient strain, C57BL/6J. The resultant progeny were backcrossed to the C57BL/6J strain for five generations until homozygosity was reached. We maintained separate homozygous sublines of RPE65<sup>L450/L450</sup> and RPE65<sup>M450/M450</sup> mice on the C57BL/6J background. In order to study immune cell activity *in vivo* and histology, we crossed CX3CR1<sup>GFP</sup> knock-in mice on the C57BL/6J background, acquired from Jackson Laboratory (Stock NO. 005582), to both the RPE65<sup>L450/L450</sup> and RPE65<sup>M450/M450</sup> sublines to homozygosity. The breeding scheme resulted in RPE65<sup>L450/L450</sup>; CX3CR1<sup>GFP/+</sup> and RPE65<sup>M450/M450</sup>; CX3CR1<sup>GFP/+</sup> genotypes which were maintained. In order to study the effects of the RPE-secreted factor, Pigment Epithelium Derived Factor (PEDF), on changes in visual function and immune cell recruitment after light stress, we generated PEDF-null sublines of our RPE65<sup>M450/M450</sup> and RPE65<sup>L450/L450</sup> mice. The PEDF knockout/null (PEDF<sup>KO/KO</sup> or PEDF-null) mice used in this study were gifted from Dr. Hans Grossniklaus and Dr. Sue Crawford at Northwestern University Feinberg School of Medicine (JAX Laboratory Stock No. 030065). This mouse strain has had exons 3-6 of the PEDF gene replaced by an IRES-lacZ cassette systemically. We bred PEDF (ko/+) x PEDF (ko/+) with either RPE65<sup>M450/M450</sup> or RPE65<sup>L450/L450</sup> on C57BL/6J background. The breeding scheme resulted in litters that were approximately 25% PEDF<sup>KO/KO</sup> (experimental) and 25% PEDF<sup>+/+</sup> (wildtype controls). All experiments were conducted on animals that were P60-P380. Experimental biologists were masked of genotyping results until after *in vivo* experiments and samples were collected to limit bias.

#### 4.3.2 Genotyping:

Genotyping was performed using a polymerase chain reaction to confirm the deletion of the PEDF gene expression. To limit ascertainment biases, PCR genotyping results were masked from experimental biologists until after in vivo experimental data and tissue samples were collected, and analyzed.

#### 4.3.3 Immunofluorescence staining and Histology.

##### 4.3.3.1 RPE Flat mounts

Immunofluorescence was used to detect galectin-3 positive cells and RPE cells to assess the extent of immune cell recruitment and damage. Eyes were micro-dissected using the technique reported by Zhang et al.<sup>130,140,190</sup>. In brief, after enucleation, the eye was fixed with 4% Paraformaldehyde/Phosphate buffered saline (PBS) solution to incubate for 30 minutes before being washed three times with HBSS and stored in PBS at 4°C until dissection. After lens removal, four flaps were made to flatten the RPE sheet to a conventional slide with an adhered silicon gasket (Grace Bio-Labs, Cat # GBL665104, Bend, OR). The RPE flat mounts were blocked in Hank's Balanced salt solution (Hyclone, Cat #SH30588.01, Logan, UT) containing 0.3 % (V/V) Triton X-100 and 1% (W/V) bovine serum albumin for 1 hour at 22 °C or overnight at 4°C in a humidified chamber. The next day, the flat mounts were washed in buffer and then incubated with secondary antibodies [See Section 4.6.1: Table 1] in HBSS/ Triton 100 X/BSA solution for 1 hour at 22°C. After secondary incubation, samples were washed with Hoechst 333258/HBSS/Triton 100 X solution before mounting with fluoromount G.

##### 4.3.3.2 Retinal Sections

Eyes were fixed in using a freeze-substitution protocol<sup>129</sup> at -80 °C for 4 days, embedded in paraffin, and sectioned through the sagittal plane on a microtome at thickness of 5 µm. Sections were stained with hematoxylin and eosin (H&E) to visualize the retinal morphology. Nuclei in the outer nuclear layer (ONL) were counted manually by three individuals that were blinded to the sample identity. Only nuclei within a 100-micron region were counted using Photoshop CS6 at regularly spaced intervals of 500 microns apart from the optic nerve in both the inferior and superior directions. Deparaffinized retinal

sections were also stained for immunofluorescence. Slides were incubated at room temperature (RT; ~23°C) for 30 min in blocking buffer containing 2.5% normal donkey serum in a humidified chamber. Slides were stained with primary for 1 hr at room temperature (RT), washed twice for 5 min, and incubated with secondary antibody for RT for 1 hr. The slides were then counterstained with Hoechst 333258 in TBS for 10 min, and rinsed once with buffer before Vectashield Vibrance (Vector Labs, Cat # H-1700, Newark, CA) used to mount the coverslip. The sections were imaged using an A1R confocal on a Nikon Ti2 microscope. All primary and secondary antibodies used for this study are listed in [Table 1](#).

#### 4.3.4 Electoretinography (ERG)

Mice were dark-adapted overnight for electroretinographic (ERG) testing, conducted under dim red-light conditions as previously described<sup>191</sup>. Anesthesia was administered intraperitoneally with a 100 mg/kg ketamine and 15 mg/kg xylazine solution ketamine solution. Topical eyedrops of Proparacaine (1%; Akorn Inc.) and Tropicamide (1%; Akorn Inc.) were used to numb the eye and pupil dilation, respectively. ERGs were recorded using the Diagnosys Celeris system (Diagnosys, LLC, Lowell, MA, USA), with corneal electrodes on each eye and the contralateral eye as the reference. Full-field ERGs were recorded for scotopic conditions at stimulus intensities of 0.001, 0.005, 0.01, 0.1, and 10 cd s/m<sup>2</sup> with a 4 ms flash duration, collecting signals for 0.3 sec to assess a- and b-wave function. For c-wave analysis, a 10 cd s/m<sup>2</sup> flash was used, with a 5-sec signal collection. After light adaptation for 10 minutes, photopic ERGs were captured 10 cd s/m<sup>2</sup>. Post-recording, mice were placed in their home cages on heating pads to recover from anesthesia unless animals require further preparation for SD-OCT and cSLO examinations.

#### 4.3.5 In Vivo Ocular Imaging

##### 4.3.5.1 Spectral Domain Optical Coherence Tomography (SD-OCT):

Mice were anesthetized during the previous ERG examination, and a ketamine booster was administered to extend the examination period. The procedure for in vivo ocular posterior segment morphology analysis described previously<sup>130</sup>. In brief, spectral domain optical coherence tomography (SD-OCT) using the MICRON<sup>®</sup> IV Spectral Domain Optical Coherence Tomography (SD-OCT) system with a fundus camera (Phoenix Research Labs, Pleasanton, CA, USA) was used sequentially to examine the retinal anatomy. Micron IV system, circular scans ~100  $\mu$ m from the optic nerve head were collected (50 scans averaged together) to generate image-guided OCT images of the retinal layers and fundus. Retinal layers were annotated according to previously published nomenclature<sup>192</sup>. Total retinal thickness and photoreceptor (outer nuclear layer thickness) were analyzed using Photoshop (Adobe Photoshop 2024 version 25.5) as previously described<sup>130</sup>.

#### 4.3.5.2 Confocal Scanning Laser Ophthalmoscopy (cSLO):

Immediately after ERG analysis, a rigid, contact lens adapted for mouse imaging (Heidelberg Engineering) was placed on the eye (back optic zone radius, 1.7 mm; diameter, 3.2 mm; power, Plano), and blue autofluorescence (BAF) imaging at the layer of the photoreceptor-RPE was obtained using Heidelberg Spectralis HRA and SD-OCT instrument with a 25 D lens (HRA)CT2-MC; Heidelberg Engineering, Heidelberg, Germany). After live imaging and ERG analyses, mice were injected with a reversal agent (0.5 mg/mL atipamezole, injection volume 5  $\mu$ L per gram mouse weight; Patterson Veterinary, Greeley, CO) and placed individually in cages on top of heated water pads to recover.

#### 4.3.6 Western Blot Analysis:

As described in Ferdous et al. 2019 and Ferdous et al. 2023, immunoblot experiments were conducted<sup>191,193</sup>. In brief, two dissected eye cups (containing the retina and RPE/ Sclera) were collected from each animal. Protein was extracted via mechanical rending of tissue by a QIAGEN TissueLyser in a

solution of radioimmunoprecipitation (RIPA) buffer containing protease inhibitors (completed mini protein inhibitor catalog #118361530001) and phosphatase inhibitors (PhosSTOP EASypack #04906845001). Protein concentration was determined using Pierce bicinchonic Acid (BCA) Assay, and absorbance was measured at 562 nm using a Synergy H1 Hybrid Plate Reader (Biotek). After ascertaining the protein concentration, the samples were diluted to 0.8 mg/mL and heated to 95 °C for 10 minutes to denature proteins before electrophoresis. Samples were run on a pre-cast Criterion gel (Bio-Rad TGX Stain free Gel 4%-20%, Catalog # 567-8094, (Bio-Rad Laboratories, Inc., Hercules, CA)) along with 10 $\mu$ L of a molecular weight ladder (Bio-Rad Catalog # 1610376) and run at 120V for 90 mins.

## 4.4 RESULTS

### 4.4.1 **Figure 1: Light-induced retinal damage results in increased recruitment of subretinal immune cells.**

It has been well documented that increased inflammation and the recruitment of immune cells from the retina into the subretinal space are associated with damage and aging<sup>37,38,194–196</sup>. Figure 1A shows a cartoon schematic of the general location of neural retina-associated immune cells compared to the RPE in the standard, undamaged ocular environment. These anatomical relationships change during pathology, where a subset of these immune cells traverse the retina, deposit in the subretinal space, and interact with the RPE. The recruitment of these cells also appears to follow a particular kinetic profile, with Day 7 post-light-damage displaying the peak number of recruited cells.

### 4.4.2 **Figure 2: C57BL/6J mice with RPE65 Met450Leu substitution show photosensitive phenotype after Light Damage exposure.**

Most studies that utilize phototoxic models of ocular damage use albino animals since they are susceptible to light stress<sup>166,197</sup>. Very few of these studies have used pigmented animals, and of those that have, the treatment requires multiple consecutive days of light exposure to elicit an appreciable visual defect<sup>198,199</sup>. Previous studies using pigmented and albino rats show differences in responses and susceptibility to elevations in intraocular pressure, suggesting differences in strains may partially confound the findings<sup>171,172</sup>. Additionally, albino animals display developmental differences compared to pigmented animals, e.g., reduced number of photoreceptors and loss of retinal ganglion cell subtype speciation, leading to differences in visual function and responses to light damage<sup>175,200,201</sup>. Differential strain confounders were redressed by generating a congenic putative photosensitive pigmented animal subline (Rpe65<sup>L450/L450</sup>), donated from 129SV mouse strain). This line was back-crossed ten times to the parental C57BL/6J lineage. We detected severe damage with only one 5-hour treatment period during the dark cycle (when mice spend the least time sleeping to maximize damage exposure) of the animals in the L450 line.

In contrast, there was negligible damage to the retina in the M450 line. Figure 2 shows that when assessed by electroretinogram at baseline, the light-sensitive (RPE65 L450/L450) animals have no significant visual defects compared to their photoresistant (RPE65 M450/M450) counterparts. Additionally, at early points after LIRD, both sublines of animals have similar a-, b-, and c-wave ERG responses until three days post-damage. However, on day 5, photosensitive animals exhibit severe loss of visual function, which peaks on day seven after the damage. In contrast, the Rpe65 M450 allele exhibits minor damage at any timepoint from Day 0 to Day 7 following light stress, suggesting a photoresistant phenotype.

#### **4.4.3 Figure 3: RPE65<sup>L450/L450</sup> animals Exhibits Severe Retinal Thinning and Morphological Differences in Retinal Structure *in vivo* Compared to RPE65<sup>M450/M450</sup> after LIRD.**

In addition to the loss of function, photosensitive (RPE65<sup>L450/L450</sup>) animals display significant morphological changes in the retina compared to photoresistant (RPE65<sup>M450/M450</sup>) animals. There was a substantial loss of RPE-photoreceptor attachment, increasing the space of the interphotoreceptor matrix, and an overall loss of retinal thickness of RPE65<sup>L450/L450</sup> animals after LIRD compared to the RPE65<sup>M450/M450</sup> at the same time (See Figure 3A-F). There is a considerable loss of the outer nuclear layer density compared to controls and an increase in the damage-associated autofluorescent backscattering of light, indicating an increase in the disorganization of retinal structures. Retinal thicknesses were also significantly depleted compared to photoresistant animals at the same time point, quantified in 3H.

#### **4.4.4 Figure 4: Histology Confirms More Severe Depletion Of Photoreceptor Outer Nuclear Layer In RPE65<sup>L450/L450</sup> Than RPE65<sup>M450/M450</sup> After LIRD.**

As shown in Figure 4, at baseline, there were no morphological or structural differences between photosensitive and photoresistant animals (see Fig. 4A-4B). However, when analyzing changes in retinal architecture at day seven between photosensitive (RPE65<sup>L450/L450</sup>) and photoresistant animals (RPE65<sup>M450/M450</sup>), there are striking changes in the gross anatomy. RPE65<sup>M450/M450</sup> animals showed minimal

retinal thinning or loss of integrity in the retinal layers (see Fig.4D). Conversely, the RPE65<sup>L450/L450</sup> animals lost over 80-90% of the photoreceptors in the outer nuclear layer and irregularities in the RPE monolayer (See Fig. 4C). These data are quantified in Figure 4E.

#### 4.4.5 **Figure 5 : RPE65<sup>L450/L450</sup> have increased Gal-3+ immune cell recruitment to the subretinal space after LIRD compared to RPE65<sup>M450/M450</sup>**

RPE flat mounts were collected at multiple time points to test whether the subretinal immune cells found at the RPE interface of photosensitive mice are enriched in galectin-3. The data show that the RPE sheets from RPE65<sup>L450/L450</sup> animals look like those from RPE65<sup>M450/M450</sup> animals before light damage (See Fig. 5A and 5B).

Similarly, at day three post-LIRD, the number of subretinal immune cells present and the number of immune cells expressing high levels of galectin-3 are similar between sublines. Notably, there are also more RPE cells expressing cytoplasmic galectin-3 in the putative photosensitive animals (RPE65<sup>L450/L450</sup>) compared to the photoresistant (RPE65<sup>M450/M450</sup>) simultaneously. However, at seven days post light exposure, Gal-3 expression is almost exclusively found in immune cells. Interestingly, the photosensitive animals have significantly more immune cells expressing Gal-3 than the photoresistant animals, which are predominantly green (Fig.5E and 5F). Photosensitive animals had markedly more subretinal immune recruitment than photoresistant animals; the number of GFP+ immune cells which is quantified in Fig. G.

#### 4.4.6 **Figure 6: RPE65<sup>M450/M450</sup> dampen Galectin-3 expression after LIRD, while Galectin-3 expression remains high in RPE65<sup>L450/L450</sup> after light damage exposure.**

We analyzed the overall level of ocular Galectin-3 in the photosensitive (RPE65<sup>L450/L450</sup>) compared to the photoresistant (RPE65<sup>M450/M450</sup>) animals via western blot. We found that photoresistant animals had significantly reduced expression of galectin-3 protein after LIRD exposure compared to RPE65<sup>L450/L450</sup> at the same time. Differential expression of Galectin-3 protein began three days post-LIRD and persisted until day 7. Notably, Galectin-3 expression is similar in RPE65<sup>L450/L450</sup> and RPE 65

$M450/M450$  animals before damage initiation. Gal-3 expression is actively suppressed in Photoresistant ( $RPE65^{M450/M450}$ ) animals in response to damage, which may be a compensatory response to prevent the overactivation of the galectin-3-mediated inflammatory responses. This dampening response was not observed in  $RPE65^{L450/L450}$  animals during the time points we assessed, suggesting a prolonged immune response.

#### **4.4.7 Figure 7: Loss of PEDF ablated the photoprotective phenotype of $RPE65^{M450/M450}$ exposed to light damage.**

Once we established that the hypomorphic  $RPE65^{M450/M450}$  allelic variant was protective against phototoxic damage, we wanted to test if the secreted neurotrophic protein, pigment epithelium-derived factor (PEDF), would influence the conferred protective phenotype observed. To test this, we compared the visual function of photosensitive animals with normal levels of PEDF expression with the photoresistant  $RPE65^{M450/M450}$  animals containing a loss of function mutation in the *serpinfl* gene, which encodes PEDF. We found that in the absence of PEDF, the hypomorphic  $RPE65^{M450/M450}$  allelic variant lost its resistance to light damage and phenocopied the damaged response of the photosensitive  $RPE65^{L450/L450}$ , which had normal PEDF expression (see Fig. 7A-7C).

#### **4.4.8 Figure 8: Loss of PEDF in $RPE65^{L450/L450}$ animals results in baseline deficits in visual function compared to $PEDF^{+/+}$ .**

In the previous section, we assessed the influence of PEDF on the photoresistant phenotype and found that it was important for neuroprotection to be observed, even if there was minimal damage as a result of the slower rhodopsin regeneration cycle. We also tested if the loss of PEDF would have an increased effect on photosensitive animals, further sensitizing the animals to light damage stress. Interestingly, we found that even at baseline, loss of PEDF leads to a significant reduction in visual function in the photosensitive animal over  $PEDF^{+/+}$  littermates, a phenomenon that we did not observe in the photoresistant animals lacking PEDF expression. This was an unexpected finding since in the presence of

PEDF and the absence of damage, the photosensitive and photoresistant animals have similar visual function. We postulate that the accumulation of low-grade light damage due to ambient room light exposure sustained by photosensitive animals under normal lighting conditions may be exacerbated by the loss of PEDF, leading to a more severe phenotype than either the PEDF<sup>KO/KO</sup> or RPE65<sup>L450/L450</sup> mutation alone.

#### 4.4.9 **Figure 9: Distribution of Galectin-3 May Differ in PEDF<sup>KO/KO</sup> compared to PEDF<sup>+/+</sup> animals at Day 7**

Finally, we assessed if Galectin-3 expression patterns and subretinal immune cell recruitment were different in the PEDF knockout animals compared to wildtype (PEDF<sup>+/+</sup>) animals on the same background at the same time point after LIRD. When we compared the two photosensitive sublines, RPE65<sup>L450/L450</sup>; PEDF<sup>+/+</sup> and RPE65<sup>L450/L450</sup>; PEDF<sup>KO/KO</sup> at day seven post-LIRD, we found that there were notable differences in : 1) the amount of galectin-3 expressing cells observed, 2) which cells were expressing Galectin-3 at the time, 3) and where within those cells Galectin-3 was being expressed. The PEDF<sup>KO/KO</sup> photosensitive animal had significantly more galectin-3 expression and subretinal immune cells. The immune cells aggregated together, with more signs of gliosis than with the PEDF<sup>+/+</sup>. Additionally, in the PEDF<sup>KO/KO</sup> animals, there was significantly more localization of galectin-3 at the cell borders of the RPE cells compared to the PEDF<sup>+/+</sup>, which only expressed galectin-3 in the subretinal immune cells. .

#### 4.4.10 **Figure 10: Summary Figure of the General Phenotypes observed in this study**

RPE cells are stressed, hypomorphic RPE65<sup>M450/M450</sup> allelic variant or PEDF<sup>+/+</sup> confer resistance to phototoxic damage and protect visual function. However, if the hypermorphic RPE65<sup>L450/L450</sup> variant or PEDF<sup>KO/KO</sup> is present, this confers photosensitivity to light damage, resulting in increased loss of retinal morphology, and a more severe loss of visual function.

## 4.5 DISCUSSION

In this study, we utilized a single nucleotide substitution in RPE65 to take advantage of the vitamin A cycle and generate a photosensitive and photoresistant pigmented pair of congenic mice. We then performed a comparative study of changes in visual function and immune responses in the RPE65<sup>M450/M450</sup> (photoresistant hypomorph) and RPE65<sup>L450/L450</sup> (photosensitive morph). The changes in light damage susceptibility observed in this study were correlated with both Galectin-3 expression and expression of PEDF, suggesting a hypothesis that both proteins may be involved in the manifestation of light damage.

This study found that photosensitive (RPE65<sup>L450/L450</sup>) and photoresistant (RPE65<sup>M450/M450</sup>) animals are structurally and functionally the same at baseline. However, after acute light damage, the photosensitive (RPE65<sup>L450/L450</sup>) animals experience progressive loss of visual function, loss of photoreceptors, and increased retinal thinning compared to the photoresistant (RPE65<sup>M450/M450</sup>) counterpart, which peaks on Day 7 (See Figures 1-4)

The functional and structural deficits in photosensitive (RPE65<sup>L450/L450</sup>) animals correspond with an increased presence of Galectin-3 positive subretinal immune cells and elevated ocular galectin-3 protein expression compared to photoresistant (RPE65<sup>M450/M450</sup>) (See. Fig. 5-6). Increased galectin-3 expression is associated with progressive damage and poor prognosis in several disorders. Galectin-3 plays a role in the epithelial-to-mesenchymal transition of the RPE, recruited by the increased N-glycosylated sugar residues expressed on RPE cells undergoing EMT<sup>69</sup>. Galectin-3 can then aid in forming multimeric protein complexes that influence RPE responses<sup>202</sup>.

Due to the integral role that the RPE and PEDF play in both homeostasis and pathology, as well as their relationship to inflammation, we tested if the protection conferred by RPE65<sup>M450/M450</sup> variant required expression of PEDF. We found the RPE65<sup>M450/M450</sup>; PEDF<sup>KO/KO</sup> phenocopy RPE65<sup>L450/L450</sup>,

PEDF<sup>+/+</sup> after light damage, suggesting the loss of PEDF ameliorates the phototoxic protection of the RPE65 hypomorph (See Fig. 7A-C). Additionally, when comparing photoresistant lines with or without PEDF expression, the hypomorph that expresses PEDF retains photoresistance. At the same time, the PEDF-null mouse shows severe loss of function by five days post damage and peaks at day 7 (See Fig 7D-F). Interestingly, when comparing photosensitive morphs with and without PEDF expression, we observed significant deficits at baseline in the photosensitive PEDF<sup>KO/KO</sup> animals compared to photosensitive PEDF<sup>+/+</sup> and persisted up until three days post damage (See Fig. 8). Notably, we did not observe the same phenomenon in the photoresistant PEDF<sup>KO/KO</sup> when compared to photoresistant PEDF<sup>+/+</sup>. Taken together these data show that PEDF plays a large part in the neuroprotective phenotype observed in both the RPE65<sup>(L450/L450)</sup> and RPE65<sup>(M450/M450)</sup> since loss of PEDF exacerbated the presentation of light damage in both sublines. These data suggest that although loss of PEDF under homeostatic conditions does not result in significant changes to visual function, PEDF plays a large role in the protection of retinal structures and the resolution outcomes after damage is initiated. The role of PEDF in influencing these processes requires further study.

Lastly, galectin-3 expression patterns significantly differ in the PEDF<sup>KO/KO</sup> animals compared to the PEDF<sup>+/+</sup> at day 7 Post LIRD. In the PEDF<sup>+/+</sup> animals, at day 7, Galectin-3 is exclusively expressed by the subretinal immune cells; there is little to no galectin-3 expression in the RPE cells. Conversely, the RPE flat mounts from the PEDF<sup>KO/KO</sup> animals at day 7 show robust expression of Galectin-3, increased subretinal immune cell deposition, and significant sequestration of Galectin-3 at the cell borders of the RPE (See Fig. 9A-D and Fig. 10). Taken together, these data may suggest that PEDF plays a role in influencing Galectin-3 localization after damage and modulates sensitivity to light damage.

## 4.6 FIGURES AND TABLES

4.6.1 Table 1: Primary and Secondary Antibody

| <b>Antibody</b>                                 | <b>Antibody Type</b>       | <b>Species</b> | <b>Company and Catalog information</b> | <b>Concentration</b> |
|---|----------------------------|----------------|--|----------------------|
| <b>Galectin-3</b>                               | Primary                    | Goat           | R&D Systems ( AF1197)                  | 1:250                |
| <b>ZO-1</b>                                     | Primary                    | Rat            | Sigma                                  | 1:250                |
| <b>IGF-1</b>                                    | Primary (conjugated AF546) | Mouse          | Santa Cruz (sc-518040)                 | 1:100                |
| <b>IBA-1</b>                                    | Primary                    | Rabbit         | Abcam (ab178847)                       | (1:1000)             |
| <b>Pentahydrate(bis-Benzamide)Hoechst 33258</b> | DNA nuclear Stain          | N/A            | Thermo-Fisher Catalog #: H3569         | [1:250]              |
| <b>Donkey anti-Rat (AF488)</b>                  | Secondary                  | Rat            | Life Technologies, Catalog # A21208    | [1:1000]             |
| <b>Donkey anti-rabbit (AF568)</b>               | Secondary                  | Rabbit         | Life Technologies, Catalog # A10042    | [1:1000]             |
| <b>Donkey Anti-Mouse(AF488)</b>                 | Secondary                  | Mouse          | Life Technologies Catalog #A21202      | [1:1000]             |
| <b>Donkey Anti-Goat(AF568)</b>                  | Secondary                  | Goat           | Abcam Catalog # A-11057                | [1:1000]             |
| <b>Donkey Anti-Rat (AF405)</b>                  | Secondary                  | Rat            | Invitrogen #A48261                     | [1:1000]             |

#### 4.6.2 Figure 1: Light-induced Retinal Damage Results in Increased Recruitment of Subretinal Immune Cells

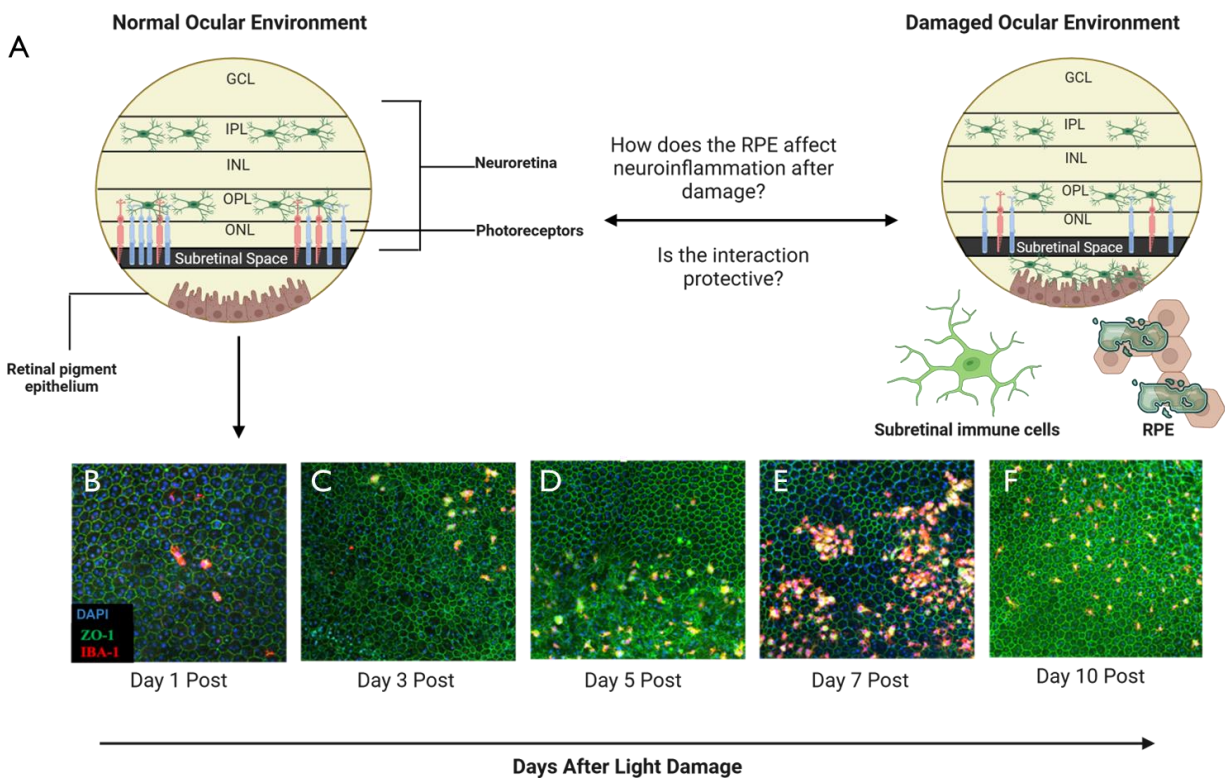


Figure 1: Cartoon schematic of how the ocular architecture changes under the damaged conditions compared to the typical ocular environment. Immune cells form the neural retina and traverse the interphotoreceptor matrix, where they interact with the RPE. The recruitment of these subretinal immune cells appears to have conserved kinetics, with the first cells depositing between days 1-3 and peaking around Day 7. Image made using Biorender.

4.6.3 Figure 2: Retinal Function is significantly reduced in RPE65<sup>L450/L450</sup> (photosensitive) compared to RPE65<sup>M450/M450</sup> (photoresistant) animals at Day 5 Post LIRD

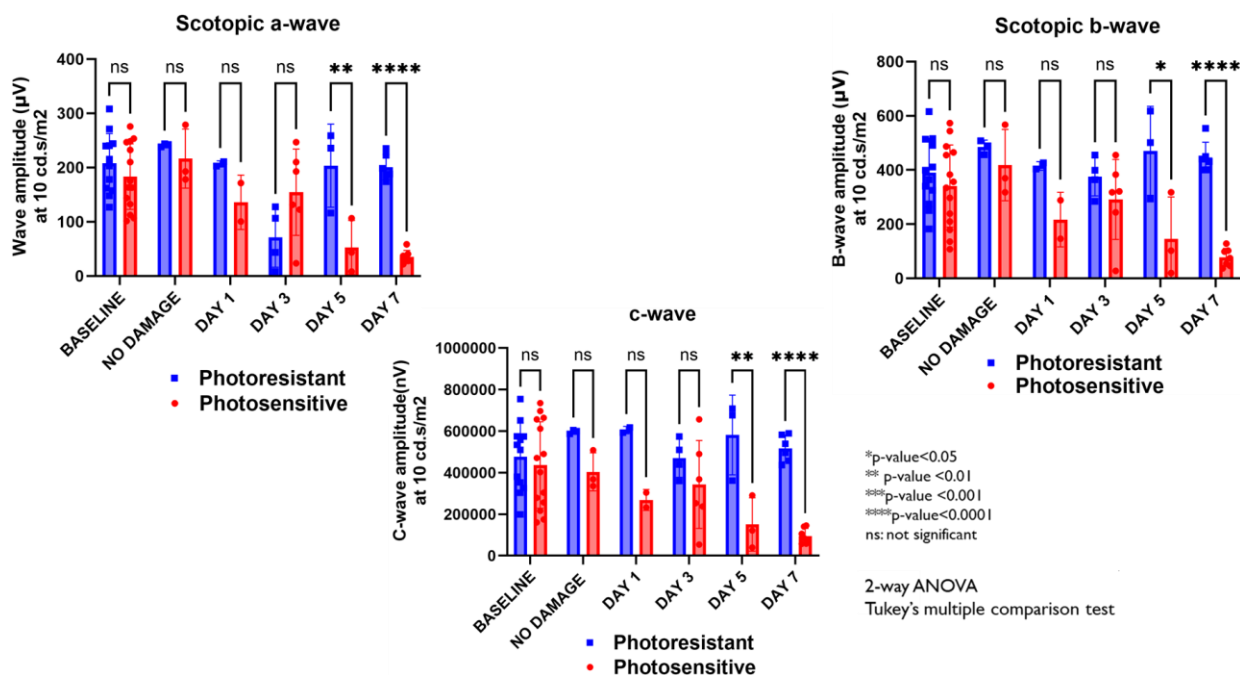


Fig 2: Retinal function drastically differs between photosensitive and photoresistant animals beginning at Day 5 post LIRD. During early LIRD, there are no statistically significant differences in photosensitive and photoresistant mice; however, at day five post-LIRD, there is a notable divergence in the functional ERG output by genotype. Blue= RPE<sup>M450/M450</sup> animals; Red Bars= RPE<sup>L450/L450</sup> animals. Statistical analysis: Multiple t-tests with two-step FDR control using Benjamini, Krieger, and Yekutieli. NS= not significant, \*=p-value of 0.05, \*\*= p-value of 0.01, \*\*\*=p-value of 0.001.

4.6.4 **Figure 3: RPE65<sup>L450/L450</sup> (photosensitive) animals have severe retinal thinning after LIRD compared to RPE65<sup>M450/M450</sup> (photoresistant)**

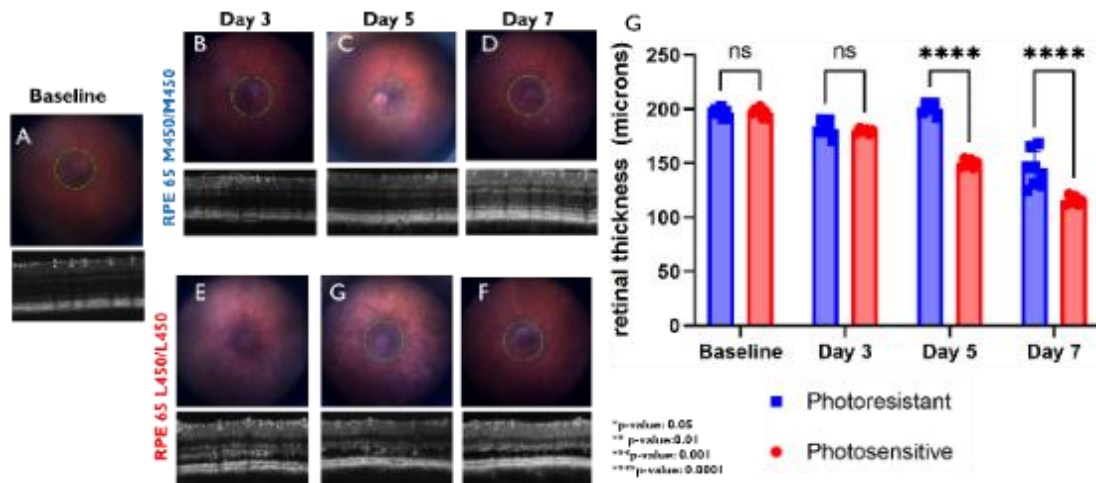
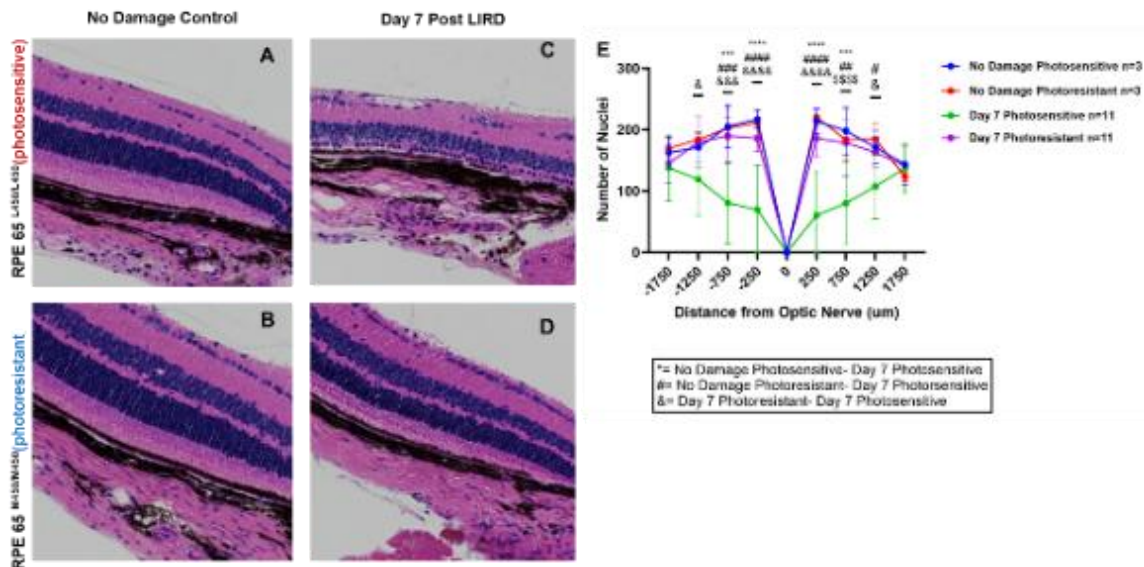


Figure 3: In vivo imaging of retinal architecture via Spectral domain-optical coherence tomography (SD-OCT) shows severe perturbations in photosensitive animals after light damage compared to photoresistant counterparts (Fig. 3A-F). The loss of retinal thickness is quantified in Fig. 3G. Two-way ANOVA with Tukey's correction. \*p-value:0.05, \*\*p-value: 0.01, \*\*\*p-value:0.001, \*\*\*\*p-value: 0.0001,

#### 4.6.5 Figure 4: RPE65<sup>L450/L450</sup> Exhibit Significant Loss of Outer Nuclear Layer Density Compared to RPE65<sup>M450/M450</sup>



**Figure 4:** Representative H&E-stained retinal sections show significant loss of photoreceptor cell cells in the outer nuclear layer density in RPE65<sup>L450/L450</sup> animals compared to the RPE65<sup>M450/M450</sup> animals at the same time point. At baseline, photosensitive and photoresistant animals are morphologically similar with similar retinal layer thicknesses (Fig. 4A-4B). However, after damage initiation, photosensitive animals display significant loss of outer nuclear layer (ONL) photoreceptors compared to photoresistant counterparts at Day 7 post (see Fig 4C-4D). This loss in photoreceptor nuclei is quantified in Fig 4E. Statistical analysis: one-way ANOVA with Barlett's correction test. Comparisons denoted in figure key. \*p-value<0.05, \*\*<p-value 0.01, \*\*\*p-value<0.001, \*\*\*\*p-value<0.0001. Note: the number of symbols signify the degree of significance by comparison.

4.6.6 **Figure 5: RPE65<sup>L450/L450</sup> show increased recruitment of GFP<sup>+</sup>, Gal-3<sup>+</sup> subretinal immune cells after LIRD compared to RPE65<sup>M450/M450</sup> animals**

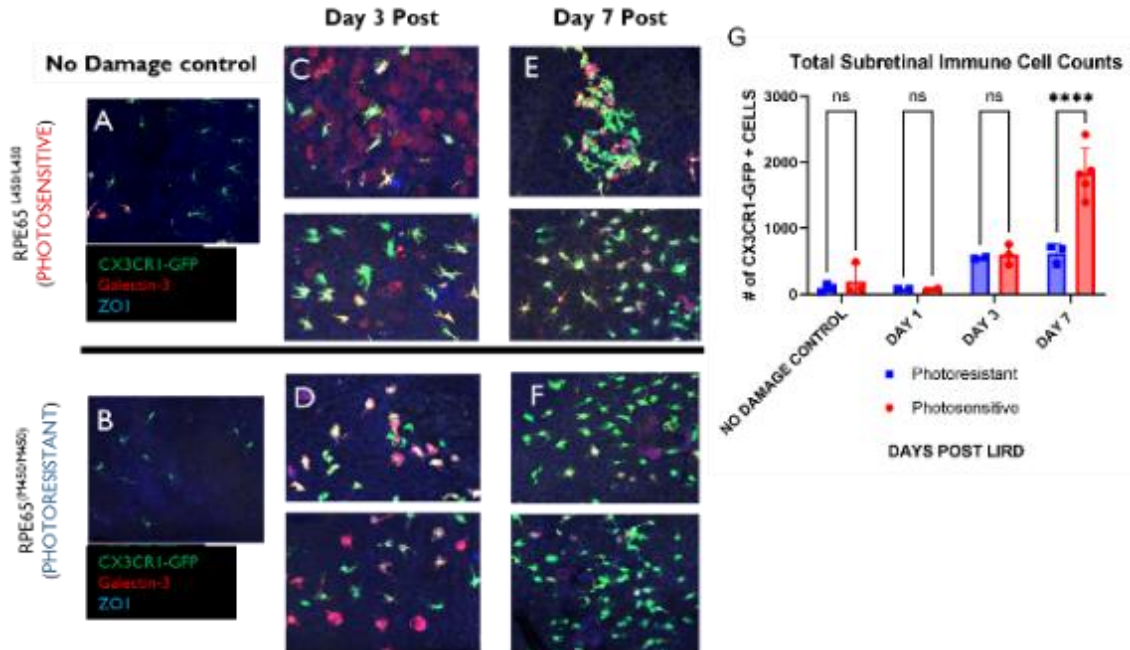


**Figure 5:** Ocular tissue was collected and stained with antibodies against ZO-1 (Zonula Occludins, RPE cell borders, blue), Gal-3, red, and subretinal immune cells tagged with CX3CR1-GFP (Green). n=3-5 samples/group. Graph depicts the number of microglia/macrophages that express high or low levels of Gal-3 at each time point after LIRD. Statistical analysis: 2-way ANOVA with Sidak's multiple comparison test. \*=p-value of 0.05, \*\*= p-value of 0.01, \*\*\*=p-value of 0.001. On Day 3 post-LIRD, the expression of Gal-3 is similar in the photosensitive and photoresistant strains; however, the expression patterns are drastically different by Day 7 post-LIRD.

4.6.7 **Figure 6: Galectin-3 protein expression is dampened in Photoresistant compared to Photosensitive animals after LIRD.**

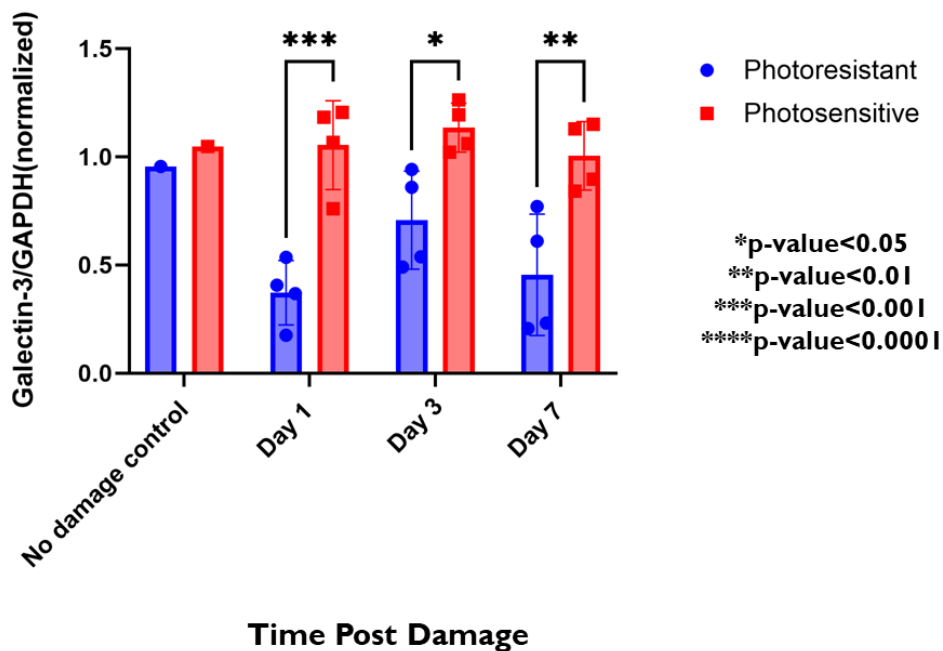


**Figure 6:** Galectin-3 protein expression is dampened in RPE65<sup>M450/M450</sup> (Photoresistant) compared to RPE65<sup>L450/L450</sup> (Photosensitive) animals after LIRD exposure. Ocular Galectin-3 protein expression was assessed via western blot analysis. These data show that in photoresistant animals dampen galectin-3 expression in response to LIRD exposure compared to photosensitive animals. GAPDH was used as the loading control for these experiments. Blue (RPE65<sup>M450/M450</sup>); Red (RPE65<sup>L450/L450</sup>) Statistical analysis: Two-way ANOVA with Sidak's multiple comparison test; n=4/group/timepoint. \*p-value<0.05, \*\*p-value<0.01, \*\*\*p-value<0.001, \*\*\*\*p-value<0.0001, ns=not significant.

#### 4.6.8 Figure 7: PEDF is Required for RPE65<sup>M450/M450</sup> Protection from Light Damage

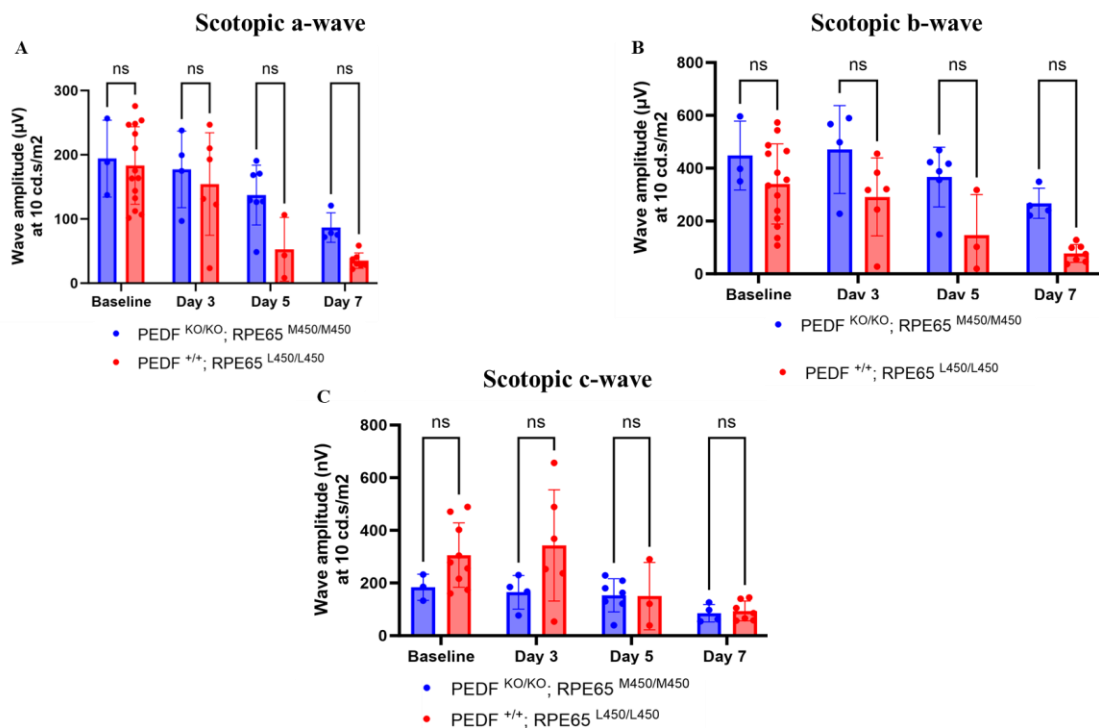


**Figure 7:** Electroretinogram findings suggest that loss of PEDF ablates protection of the RPE65<sup>M450/M450</sup> hypomorph and phenocopies photosensitive animals exposed to light damage (See Fig. 7A-C). When comparing photoresistant subline that are PEDF<sup>KO/KO</sup>, to the Photosensitive subline with normal PEDF expression, there is no significant difference in visual function output before or after LIRD. This suggests that loss of PEDF results in photoresistant animals phenocopying photosensitive animals after LIRD exposure, losing the photoprotective phenotype. These data further confirm that PEDF plays a role in the protective phenotype observed in the photoresistant animals. \*p-value<0.05, \*\*p-value<0.01, \*\*\*p-value<0.001, \*\*\*\*p-value<0.0001, ns=not significant. N=3-14/group/timepoint.

4.6.9 **Figure 8: Loss of PEDF in RPE65<sup>L450/L450</sup> animals results in baseline visual deficits that phenocopy LIRD exposure.**

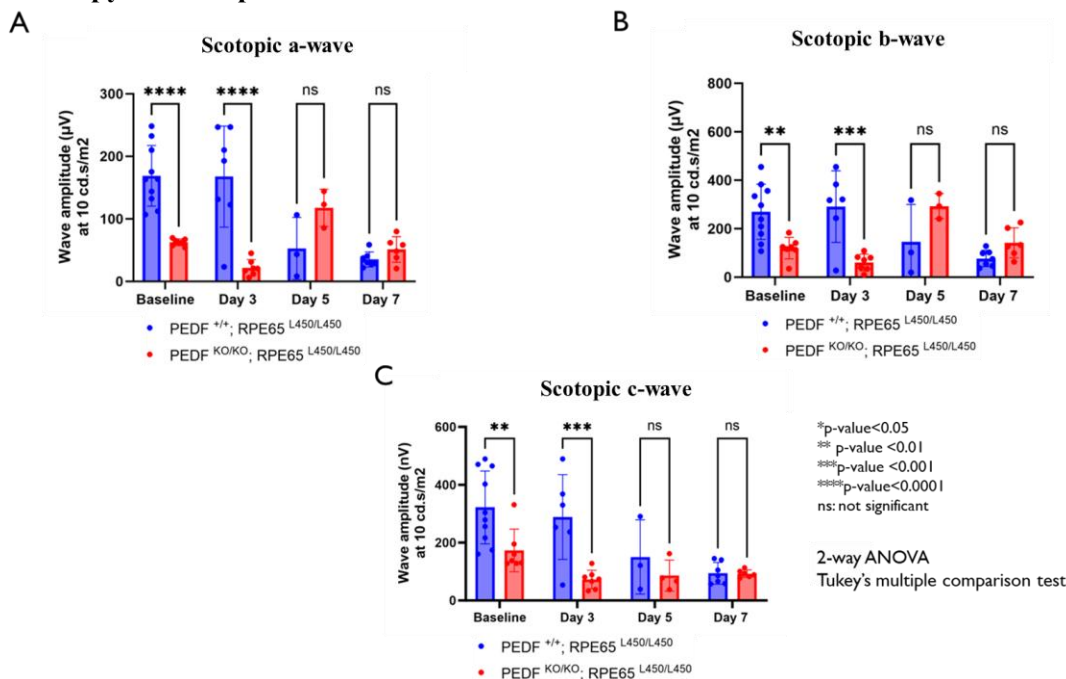


**Figure 8:** Loss of PEDF in photosensitive (RPE65<sup>L450/L450</sup>) animals has a subtractive effect on visual function, leading to baseline deficits in vision. In photosensitive, PEDF<sup>KO/KO</sup> animals, there are significant reductions in a-, b-, and c-wave amplitudes at baseline compared to photosensitive animals with wild-type PEDF expression. Interestingly, by Day 5 post LIRD, the differential is lost, and both lines show severe visual defects that peak at Day 7 post. These data show that the PEDF<sup>KO/KO</sup> and RPE65<sup>L450/L450</sup> have an additive, more severe phenotype than either mutation alone.

4.6.10 **Figure 9: Distribution of Galectin-3 May Differ in PEDF<sup>KO/KO</sup> compared to PEDF<sup>+/+</sup> at Day 7 Post LIRD.**

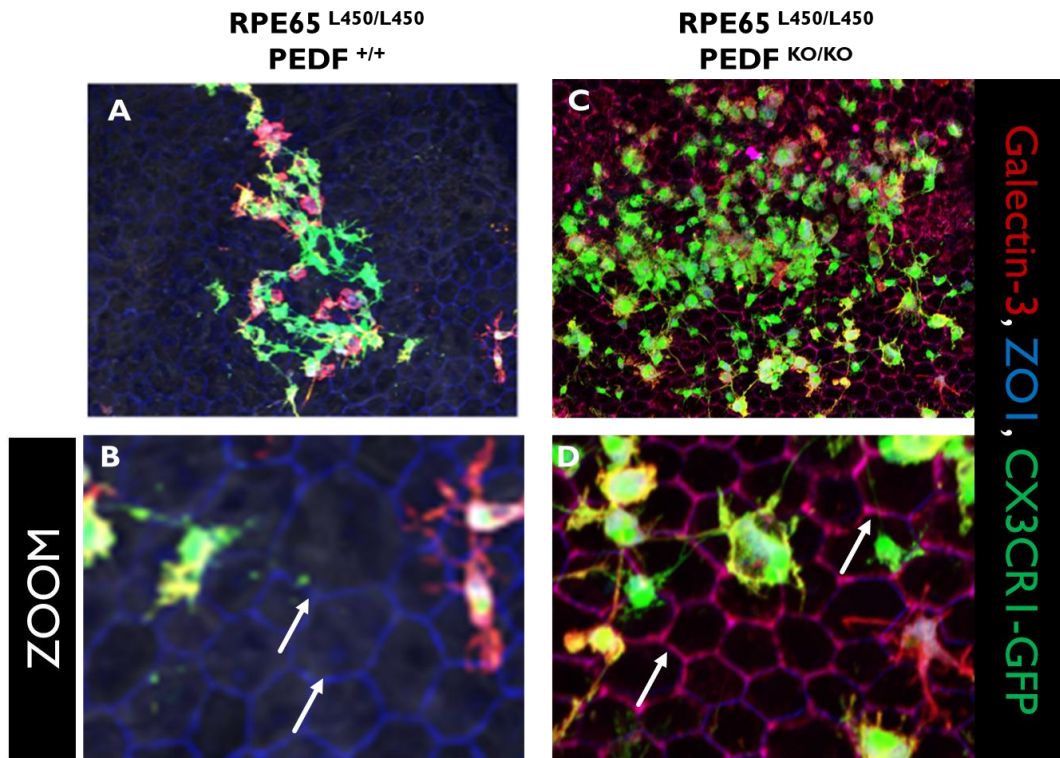
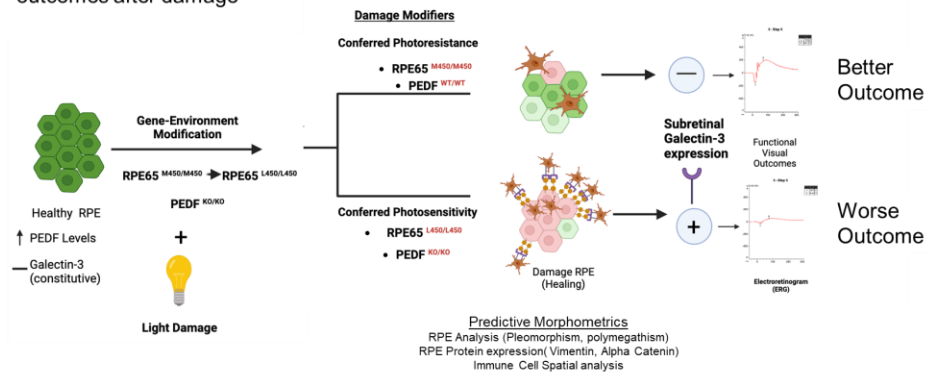


**Figure 9:** PEDF<sup>KO/KO</sup> animal show increased Gal-3+ cell recruitment and differential Gal-3 compartmentalization compared to PEDF<sup>+/+</sup> at the same time point after LIRD. Representative immunoreactivity images at day seven post-LIRD of photosensitive animals with and without PEDF expression show differences in Galectin-3 localization. The images showcase that animals lacking PEDF exhibit a total increase in the number of subretinal immune cells recruited compared to PEDF wildtype animals at the same timepoint after damage. Additionally, the image shows the localization of galectin-3 expression in both the RPE cell borders and in recruited subretinal immune cells of PEDF<sup>KO/KO</sup> animals differs from PEDF<sup>+/+</sup> animals which have restricted galectin-3 localized to the immune cells exclusively. Panels A and B(20X); Panels B and D(40X).

## 4.6.11 Figure Summary Figure of Major Findings in Chapter 4

## Figure 10: Summary Figure Overview

There are conserved characteristics in immune response and RPE morphometrics between different modifiers of LIRD. There may also be evidence that the bidirectional influence of RPE-microglia interactions can affect visual outcomes after damage



Created with BioRender.com

**Figure 10:** Summary figure illustrating significant findings from this study. The presence of either the RPE65<sup>M450/M450</sup> and/ or PEDF expression confers a degree of protection from light damage. Conversely, the presence of RPE65<sup>L450/L450</sup> or loss of PEDF confers a photosensitive phenotype and more severe damage outcomes. Figure made using Biorender.

## 5 CHAPTER 5: Loss of Pigment Epithelium Derived Factor Sensitizes C57BL/6J Mice to Light-Induced Retinal Damage

**Authors:** Debresha A. Shelton<sup>1</sup>, Jack Papania<sup>1</sup>, Tatiana Getz<sup>1</sup>, Jana T. Sellers<sup>1</sup>, Preston Giradot<sup>1</sup>, Micah A. Chrenek<sup>1</sup>, Hans E. Grossniklaus<sup>1</sup>, Jeffrey H. Boatright<sup>1,2</sup>, John M. Nickerson<sup>1</sup>

Affiliations:

<sup>1</sup>Department of Ophthalmology, Emory University, Atlanta, Georgia, United States

<sup>2</sup>Atlanta Veterans Administration Center for Visual and Neurocognitive Rehabilitation, Decatur, Georgia, United States

Correspondence to: Please address all correspondence to Dr. John M. Nickerson; Department of Ophthalmology, Emory University, B5602, 1365B Clifton Road, NE, Atlanta, GA, 30322; Phone 404-778-4411; email: litjn@emory.edu

Funding: Supported by National Institutes of Health (NIH) grants R01EY028450, R01EY021592, P30EY006360, R01EY028859, T32EY07092, and T32GM008490, the Abraham and Phyllis Katz Foundation, VA RR&D I01RX002806 and I21RX001924, VA RR&D C9246C (Atlanta Veterans Administration Center for Excellence in Vision and Neurocognitive Rehabilitation), and a challenge grant to the Department of Ophthalmology at Emory University from Research to Prevent Blindness, Inc.

## 5.1 ABSTRACT

### **Purpose:**

Pigment epithelium-derived factor (PEDF) is a neurotrophic glycoprotein secreted by the retinal pigment epithelium (RPE), a tissue that supports retinal photoreceptor health. Deficits in PEDF are associated with increased inflammation and retinal degeneration in aging and diabetic retinopathy. We hypothesized that light-induced stress in C57BL/6J mice deficient in PEDF would lead to increased retinal neuronal and RPE defects, impaired expression of neurotrophic factor Insulin-like growth factor 1 (IGF-1), and overactivation of Galectin-3-mediated inflammatory signaling.

### **Methods:**

C57BL/6J mice expressing the RPE65 M450/M450 allele were crossed to PEDF<sup>KO/KO</sup> and wildtype (PEDF<sup>+/+</sup>) littermates. Mice were exposed to 50,000 lux light for 5 hours during to initiate acute damage. Changes in visual function outcomes were tracked via electroretinogram (ERG), confocal scanning laser ophthalmoscopy(cSLO), and spectral domain optical coherence tomography (SD-OCT) on days 3, 5, and 7 post-light exposure. Gene and protein expression of Galectin-3 were measured by digital droplet PCR (ddPCR) and western blot. To further investigate the role of Galectin-3 on visual outcomes and PEDF expression after damage, we also used a small-molecule inhibitor to reduce its activity.

### **Results:**

Following light damage, PEDF<sup>KO/KO</sup> mice showed more severe retinal thinning, impaired visual function (reduced a-, b-, and c-wave amplitudes), and increased Galectin-3 expressing immune cell infiltration compared to PEDF<sup>+/+</sup>. PEDF<sup>KO/KO</sup> mice had suppressed damage-associated

increases in IGF-1 expression. Additionally, baseline Galectin-3 mRNA and protein expression were reduced in PEDF<sup>KO/KO</sup> mice compared to PEDF<sup>+/+</sup>. However, after light damage, Galectin-3 expression decreases in PEDF<sup>+/+</sup> mice but increases in PEDF KO/KO mice without reaching PEDF<sup>+/+</sup> levels. Galectin-3 inhibition worsens retinal degeneration, reduces PEDF expression in PEDF<sup>+/+</sup> mice, and mimics the effects seen in PEDF knockouts.

### **Conclusions:**

Loss of PEDF alone does not elicit functional defects in C57BL/6J mice. However, under light stress, PEDF deficiency significantly increases severe retinal degeneration, visual deficits, Galectin-3 expression, and suppression of IGF-1 than PEDF<sup>+/+</sup>. PEDF deficiency reduced baseline expression of Galectin-3, and pharmacological inhibition of Galectin-3 worsens outcomes and suppress PEDF expression in PEDF<sup>+/+</sup>, suggesting a novel co-regulatory relationship between the two proteins in mitigating light-induced retinal damage.

## 5.2 INTRODUCTION

Pigment epithelium-derived factor (PEDF), a secreted 50-kDa glycoprotein with neurotrophic effects, is critical in the development and homeostasis of the vertebrate eye<sup>185,203–205</sup>. While other ocular tissues express PEDF, the retinal pigment epithelium (RPE) is the primary producer of PEDF and is crucial for retinal health and visual signaling.<sup>25,206–209</sup> RPE ablation studies have shown that loss of the RPE leads to disorganization of multiple retinal layers during development; however, supplementation with PEDF is sufficient to rescue this phenotype in *X. leavis* in ex vivo tissue culture models<sup>203</sup>. Similarly, loss of the RPE and PEDF expression in the eye is associated with aging<sup>82,204,210</sup> and ocular pathology<sup>211,212</sup>, including diabetic retinopathy<sup>188,213</sup> and vascular glaucoma<sup>188</sup>.

PEDF has putative anti-inflammatory roles in eye<sup>214,215</sup> and was first described as an anti-tumor factor by Tombran-Tink and colleagues in 1990 because of its ability to differentiate retinoblastoma cells<sup>53,216</sup>. Since then, multiple studies have identified PEDF as a significant support in cellular differentiation, retinal development, inflammation, vascularization, and neuroprotection of photoreceptors and neurons<sup>186,189,207,217–222</sup>. In this study, we asked if PEDF has a protective role in the retina and RPE following LIRD in a C57BL/6J mouse strain that confers resistance to light damage.

In 2006, An et al. studied the secreted proteome of RPE cell cultures isolated from patients with AMD and compared them to control eyes<sup>223,224</sup>. Interestingly, they found a 3-fold increase in the secretion of four proteins in eye patients with age-related macular degeneration (AMD) compared to controls; among them were Galectin-3 (Lgals3) and pigment epithelium-derived factor (PEDF), suggesting that both may be involved in the pathology of the phenotype. Galectin-3, a member of the  $\beta$ -galactosidase binding protein family, is endogenously expressed in the cytosol. Galectin-3 is secreted via a non-classical pathway to the cell surface of the RPE, where it participates in a cell lattice formation and cell-cell interaction observed during epithelial-to-mesenchymal transition (EMT) of myofibroblastic RPE cells<sup>225,226</sup>. Galectin-3 has also been implicated in fine-tuning inflammatory responses of immune cells

during neurodegeneration via its increased affinity for  $\beta$ -1, 6-N-glycosylation on the cell surface of RPE cells undergoing EM; additionally, there is increased secretion of Galectin-3 from the RPE and immune cells after damage<sup>69,180,225–228</sup>. However, the role that PEDF expression may play in the modulation of Galectin-3 after damage in the eye is not fully understood.

This study identified a novel potential molecular target and signaling pathway that connects the RPE and inflammation via a PEDF-Galectin-3 mediated signaling paradigm. The interplay between PEDF and Galectin-3 may reveal an additional level of regulation of ocular immune privilege facilitated by the RPE over immune cell behavior. Using *in vivo* imaging techniques, electroretinograms, protein and gene expression analysis, and immunofluorescence, we examine how the loss of PEDF expression after light damage increases Galectin-3 expression, recruitment of subretinal immune cells, and progressive loss of visual structures and function over time. These findings support the importance of PEDF in protecting eye tissues against LIRD.

## 5.3 METHODS

### 5.3.4 Animal husbandry

The Emory University Institutional Animal Care and Use Committee approved mouse handling, care, housing, and experimental design. The experiments were compiled with the Association for Research in Vision and Ophthalmology (ARVO) and Accreditation of Laboratory Animal Care (AAALAC) guidelines and doctrine. Mice were housed and maintained on a 12-hour light/dark cycle at 22 °C, with standardized rodent chow (Lab Diet 5001; PMI Nutrition Inc., LLC, Brentwood, MO, USA). Mice had access to water *ad libitum*. The Emory University Division of Animal Resources supervised mouse care and housing. A roughly equal representation of male and female mice was used in all experiments. Animals were euthanized using standardized asphyxiation via CO<sub>2</sub> gas for 5 min, followed by confirmatory cervical dislocation.

### 5.3.5 Breeding Scheme

PEDF knockout/null (PEDF<sup>KO/KO</sup> or PEDF-null) mice used in this study were gifted from Dr. Hans Grossniklaus and Dr. Sue Crawford at Northwestern University Feinberg School of Medicine (JAX Laboratory Stock No. 030065). This mouse strain has had exons 3-6 of the PEDF gene replaced by an IRES-lacZ cassette systemically. We bred PEDF (ko/+) x PEDF(ko/+) with RPE65<sup>M450/M450</sup> on C57BL/6J background. The breeding scheme resulted in litters that were approximately 25% PEDF<sup>KO/KO</sup> (experimental) and 25% PEDF<sup>+/+</sup> (wildtype controls). These mice were used for all protein and gene expression analysis. To assess and track immune cell dynamics *in vivo* and immunofluorescence staining data, we used CX3CR1<sup>GFP</sup> knock-in mice on the C57BL/6J background which were acquired from Jackson Laboratory (Stock NO. 005582). We maintained a line that was homozygous for PEDF-ko and another line that was homozygous for PEDF-wt. Both sets of mice were then bred to produce heterozygous CX3CR1(gfp/+) on the RPE65<sup>M450/M450</sup> background. The resultant animals were either PEDF<sup>KO/KO</sup>; CX3CR1<sup>GFP/+</sup>; RPE65<sup>M450/M450</sup> or PEDF<sup>+/+</sup>; CX3CR1<sup>GFP/+</sup>; RPE65<sup>M450/M450</sup>. All PEDF<sup>KO/KO</sup> experiments were conducted in animals that were more than P60 but less than P380. Genotyping was performed using a polymerase chain reaction to confirm the deletion of the PEDF gene product. The genotyping results were masked from experimental biologists until after *in vivo* experiments, and samples were collected to limit ascertainment biases.

### 5.3.6 Light-induced retinal damage (LIRD) conditions and LIRD box information

Mice were dark-adapted overnight before light damage initiation. Phototoxic light damage was induced using Fancier 500-A LED light lamp panels (Fancier Studio, Cat # ACE45330, Haywood, CA), which was modified to fit on transparent polycarbonate model 750 cages. The protocol is a modification of previously described phototoxic damage models<sup>197,229</sup>. The light intensity was calibrated using a VWR® Light Meter with outputs (VWR, Cat# No. 62344-944, Radnor, PA) to 50,000 lux. The mice were

treated with topical 1% Atropine eye drops for two rounds of 10 seconds per eye. Mice were exposed to high-intensity light damage for 5 hours during the dark phase of the animals (7PM-12 AM or ZT12-ZT17). After light damage, animals were returned to their home cages for recovery.

### **5.3.7 Immunofluorescence staining and Histology.**

#### **5.3.7.1 RPE Flat mounts:**

Immunofluorescence was used to detect Galectin-3 positive cells and RPE cells to assess the extent of immune cell recruitment and damage. Samples were dissected using the technique reported by Zhang et al.<sup>130,140,190</sup>. In brief, after enucleation, the eye is placed into a 4% Paraformaldehyde/Phosphate-buffered saline (PBS) mixture to incubate for 30 minutes. The lens was removed, and four flaps were made to flatten the RPE sheet to a conventional slide with an adhered silicon gasket (Grace Bio-Labs, Cat # GBL665104, Bend, OR). The RPE flat mounts were blocked in Hank's Balanced salt solution (HBSS) (Hyclone, Cat #SH30588.01, Logan, UT) containing 0.3 % (V/V) Triton X-100 and 1% (W/V) bovine serum albumin for 1 hour at 22 °C or overnight at 4°C in a humidity chamber. The samples were then stained with Galectin-3 (1:250), Vimentin (1:250), IGF-1(1:250), and ZO-1(1:200) overnight at 4°C. The next day, the flat mounts were washed with HBSS/Triton X-100 solution and incubated in secondary antibody in HBSS/ Triton 100 X/BSA solution for 1 hour at 22°C. After secondary incubation, samples were washed with HBSS/Triton 100 X solution before mounting with fluoromount G.

#### **5.3.7.2 Retinal Sections**

Eyes were fixed in fixation solution (97% methanol, VWR, Cat. # BDH20291GLP, Radnor, PA ; 3% acetic acid, Fisher Scientific, Cat. # BP2401-500, Ottawa, Ontario) at -80 °C for 4 days, embedded in paraffin, and sectioned through the sagittal plane on a microtome at thickness of 5 µm as previously described by Sun et al<sup>230</sup>. Sections were stained with hematoxylin and eosin to assess retinal morphology. Nuclei in the outer nuclear layer (ONL) were counted manually by an individual masked to sample identity. Only nuclei within a 100-micron region were counted using Adobe Photoshop (Version 27.4.0) at regularly spaced intervals of 500 microns apart from the optic nerve in both the inferior and superior

directions. Deparaffinized retinal sections were also stained for immunofluorescence in a humidity chamber as described by Zhang et al<sup>130</sup>. Slides were mounted using Vectashield Vibrance (Vector Labs, Cat # H-1700-2; Newark, CA) was used to mount the coverslip, and the sections were imaged using an A1R confocal on a Nikon Ti2 microscope. All primary and secondary antibodies used for this study are listed in [Table 1](#).

### **5.3.8 Rhodopsin staining /Rhodopsin metabolism assay**

Animals were euthanized, and eye samples were collected within 1 hour of light onset (between ZT0 and ZT1) to capture maximal phagosome production (shed rhodopsin outer segment accumulation) as previously described by Devera et al.<sup>231</sup>. Murine eyes were enucleated and placed in glass tubes of “freeze-sub” solution of 97% methanol and 3% acetic acid that was chilled with dry ice, following the method of Sun and coworkers<sup>129</sup>. Tubes were placed at -80°C for at least four days to dehydrate the tissue. The sections were then treated as described in section 2.4.2. The primary antibodies (mouse anti-rhodopsin, Abcam, Cat #ab3267, [1:250] and Rabbit anti-BEST1, Abcam, Cat # ab14927 [1:250]) are then added to the blocking solution and put on the slides overnight at room temperature in a humidified chamber. The next day, the secondary antibody was added to the blocking solution. Slides were washed and nuclei stained before mounting in fluoromount G (Southern Biotech, Cat #0100-01, Birmingham, AL). The shed rod outer segments (rhodopsin-positive vesicles) within RPE were quantified as phagosomes and used to compare rhodopsin metabolism by RPE. Counts were performed by three independent, masked observers using Photoshop (Adobe Photoshop, Version 27.4.0), and each count was averaged for final counts per sample.

### **5.3.9 Electroretinography (ERG)**

Mice were dark-adapted overnight for ERG testing, conducted under dim red-light conditions as previously described<sup>191</sup>. Anesthesia was administered intraperitoneally with a 100 mg/kg ketamine and 10 mg/kg xylazine solution ketamine (KetaVed from Boehringer Ingelheim Vetmedica, Inc., Cat # 1867-

66-9, Fort Dodge, IA; xylazine from PivotalVet, Cat # 04606-6750-02, Greeley, CO, USA). Proparacaine (0.5 %; Akorn Inc., Cat # 17478-0263-12, Decatur, IL) and tropicamide (0.5 %; Akorn Inc., 17478-0101-12, Decatur, IL) eyedrops were used for topical anesthesia and pupil dilation. Mice were kept on a 39 °C heating pad during the procedure. ERGs were recorded using the Diagnosys Celeris system (Diagnosys, LLC, Lowell, MA, USA), with corneal electrodes on each eye and the contralateral eye as the reference. Full-field ERGs were recorded for scotopic conditions at stimulus intensities of 0.001, 0.005, 0.01, 0.1, and 10 cd s/m<sup>2</sup> with a 4 ms flash duration, collecting signals for 0.3 sec to assess a- and b-wave function. For c-wave analysis, a 10-cd s/m<sup>2</sup> flash was used, with a 5-sec signal collection. After light adaptation for 10 minutes, photopic ERGs were captured at 3 and 10 cd s/m<sup>2</sup>. Post-recording, mice were placed in their home cages on heating pads to recover from anesthesia unless further prepared for SD-OCT and cSLO examinations.

### **5.3.10 In Vivo Ocular Imaging**

#### **5.3.10.1 Spectral Domain Optical Coherence Tomography (SD-OCT):**

Mice were anesthetized during the previous ERG examination, and a ketamine booster was administered to extend the examination period. The procedure for in vivo ocular posterior segment morphology analysis has been previously described<sup>130</sup>. In brief, spectral domain optical coherence tomography (SD-OCT) using the MICRON<sup>®</sup> IV Spectral Domain Optical Coherence Tomography (SD-OCT) system with a fundus camera (Phoenix Research Labs, Pleasanton, CA, USA) was used sequentially to examine the retinal anatomy. Micron IV system, circular scans ~100 μm from the optic nerve head were collected (50 scans averaged together) to generate image-guided OCT images of retinal layers and fundus. Retinal layers were annotated according to previously published nomenclature<sup>192</sup>. Total retinal thickness and photoreceptor (outer nuclear layer thickness) were analyzed using Photoshop (Adobe Photoshop 2024 version 25.5) as previously described<sup>130</sup>.

#### **5.3.10.2 Confocal Scanning Laser Ophthalmoscope (cSLO)**

Immediately afterward, a rigid, specialized contact lens adapted for mouse imaging (Heidelberg Engineering) was placed on the eye (back optic zone radius, 1.7 mm; diameter, 3.2 mm; power, Plano), and blue autofluorescence (BAF) imaging at the layer of the photoreceptor-RPE was obtained using Heidelberg Spectralis and SD-OCT instrument with a 25 D lens ( (HRA)CT2-MC; Heidelberg Engineering, Heidelberg, Germany). Afterward, mice were injected with a reversal agent (0.5 mg/mL atipamezole (Antisedan); Zoetis, Cat # 10000449, Parsippany, NJ) injection volume 5  $\mu$ L per gram mouse weight; and placed individually in cages on top of heated water pads to recover.

#### **5.3.11 Western Blot Protocol**

As described in Ferdous et al. 2019 and Ferdous et al. 2023, immunoblot experiments were conducted<sup>191,193</sup>. In brief, two dissected eye cups (containing both the retina and RPE/ Sclera) were collected from each animal. Protein was extracted via mechanical rending of tissue by a QIAGEN TissueLyser in a solution of radioimmunoprecipitation (RIPA) buffer containing protease inhibitors cOmplete™ mini protease inhibitor, Roche , Cat #118361530001,Indianapolis, IN ) and phosphatase inhibitors (PhosSTOP EASypack, Roche, Cat #04906845001, Indianapolis, IN). Protein concentration was determined using a Bicinchonic Acid (BCA) Assay (Pierce, Cat # 23225, Waltham, MA) and absorbance was measured at 562 nm using a Synergy H1 Hybrid Plate Reader (Biotek). After ascertaining protein concentration, the samples were diluted to 0.8 mg/mL and heated to 95 °C for 10 minutes to denature proteins before electrophoresis. Samples were run on a pre-cast Criterion gel (TGX Stain free Gel 4%-20%, Catalog # 567-8094, Bio-rad, Hercules, CA) along with 10 $\mu$ L of a molecular weight ladder (Catalog # 1610376, Bio-Rad, Hercules, CA) and run at 120V for approximately 90 mins.

#### **5.3.12 TUNEL Staining protocol**

The manufacturer instructions for the Promega DeadEnd TUNEL Fluorometric kit (Cat # G3250, Promega, Madison, WI) were followed. In brief, tissue sections were deparaffinized in 5 steps of xylene

for 2 min each. The tissue sections were then rehydrated in a graded ethanol series (100, 90, 80, 70, 60, and 50%) for 2 min each. The slides were then washed for 5 min in PBS (Cat # 46-013-CM, Corning™ Mediatech™, Manassas, VA) and mounted in the Sequenza system. Sections were incubated for 15 min in Z-fix (Cat # NC935141, Anatech™, Battlecreek, MI), washed twice in PBS for 5 min each, incubated in Proteinase K solution for 8 min, washed with PBS for 5 min, fixed with Z-fix for 5 min, washed with PBS for 5 min, incubated with rTDT enzyme and nucleotide mix in equilibration buffer for two hours, washed with 2× SSC for 5 min, counterstained with 2.5 m Hoechst 33342 in TBS for 10 min, and rinsed with TBS for 5 min. Coverslips were then mounted using VectaShield Vibrance and imaged using an A1R confocal on a Nikon Ti2 microscope.

### **5.3.13 Galectin-3 inhibitor experiments**

At baseline, animals were assessed by electroretinogram, spectral domain coherence tomography (SD-OCT), and confocal scanning laser ophthalmoscope (CSLO) to evaluate any inherent structural or functional features or defects. Animals were injected with 15mg/kg of TD139 (33DFTG; AOBIOUS, Inc., Cat # AOB37408, Scranton, PA) intraperitoneally daily beginning one day before light damage administration until day five post damage. Animals were then assessed using the same in vivo measures for retina architecture and structure changes.

### **5.3.14 Gene expression analysis**

#### **5.3.14.1 cDNA prep**

Eyes were collected between 10 AM and 2 PM (ZT3-ZT7) to ensure standardized gene expression. The cornea and iris were removed via an incision, followed by the lens, and the neuroretina was separated from the RPE/choroid eye cup. Retinas were flash-frozen in RNase-free tubes and pre-chilled on dry ice. RPE/choroid eye cups were incubated in RNAlater® Cell Reagent (Qiagen, Cat # 76106, Germantown, MD) for 10 minutes, with occasional agitation to release RPE cells. Cells were pelleted by centrifugation (>12,000 x g for 5 minutes), the supernatant was discarded, and the cells were stored at -80°C. RNA extraction was performed using the Qiagen RNeasy Mini Kit (Qiagen, Cat #74106),

Germantown, MD). Samples were homogenized in RLT lysis buffer with a stainless-steel bead, followed by ethanol addition and vortexing. The mixture was processed through an RNeasy column, washed with RW1 and RPE buffers, and eluted with nuclease-free water. The final RNA samples were stored at -80°C. cDNA synthesis was conducted using the Qiagen Quantitect RT kit (Qiagen, Cat # 205311, Germantown, MD).

#### **5.3.14.2 Digital droplet PCR (ddPCR) Reactions**

Reaction mixes containing reverse transcriptase, primers, RT buffer, and QX200™ ddPCR EvaGreen Supermix (Bio-Rad, Cat # 186–4034, Hercules, CA) were added to 2µL of cDNA template for a total volume of 20 µL /well on the plate Twin-Tec plate (Eppendorf, Cat # 951020320 Enfield, CT). Fill the empty well with RT Buffer and seal plate with tape film and spin down and mix. Plates were preheated at 95 C for 2 min/cycle. After using the droplet generator to generate droplets on the ddPCR plate, seal the droplet plate with foil film using the Biorad program. Then place the sealed Twin-Tec plate into ddPCR apparatus (QX200 Droplet Digital PCR (ddPCR™) System – Bio-Rad) and run the program as detailed in manufacturer’s manual.

#### **5.3.15 Imaris analysis**

The intensity, size, and distribution of Galectin-3 positive immune cells were analyzed using Imaris software (10.1.0, Bitplane, Inc.), in which individual cells were identified, segmented, and quantified morphologically. Before converting and uploading images to Imaris, the corneal flaps and optic nerve heads were removed via the crop tool in Photoshop. Subretinal immune cell counts were conducted using the spots function in Imaris (artifacts and cell particulates were manually rejected) so that only cells with intact soma were quantified. Cell counts were normalized against double-blind manual cell counts of the same samples.

### **5.3.16 Statistical analysis**

Statistical analysis was conducted using Prism 9.1.0 (on Mac OS X 14 Sonoma) (GraphPad Software, Inc., La Jolla, CA, USA). Data are presented as mean +/- standard deviation (SD), with statistical testing for individual datasets described in the Figure legends. A p-value <0.05 was considered statistically significant. Demographic distributions and sample sizes are summarized in Table 1. All statistical tests used are detailed in each Figure Legend.

## 5.4 RESULTS

### 5.4.1 Figure 1: Loss of Pigment Epithelium Derived Factor Modifies Sensitivity to Phototoxic Damage in C57BL/6J Animals

Expression of PEDF protects neurons and photoreceptors<sup>186,187,232</sup>. Conversely, loss of PEDF is linked to neurodegenerative disease phenotypes, including an autosomal dominant retinitis pigmentosa locus in human studies<sup>220,233</sup>. To determine if loss of PEDF sensitizes C57BL/6J mice to phototoxic damage, we crossed PEDF-null mice to mice with a hypomorphic mutation in the RPE65 gene, resulting in reduced sensitivity to light damage. We exposed these animals to 50,000 lux of light for 5 hours. We found that PEDF-null animals had more mottling in the fundus after light stress treatment than wildtype controls and experienced more retinal degeneration and thinning (see Figure. 1E-F). We quantified these changes amongst PEDF<sup>+/+</sup>, PEDF<sup>+/-</sup>, and PEDF<sup>KO/KO</sup>. We found that PEDF<sup>+/-</sup> behaved very similarly to PEDF<sup>+/+</sup> animals and showed minimal perturbations to ocular structure after light stress (Fig. 1G-H). However, PEDF<sup>KO/KO</sup> showed significantly increased losses of photoreceptor thickness and total retinal thickness compared to PEDF<sup>+/+</sup> and PEDF<sup>+/-</sup> animals (See Fig. 1G-H). Analysis: One-way ANOVA with Brown-Forsythe test and Barlett's correction. Retinal thickness: PEDF<sup>+/+</sup> vs. PEDF<sup>+/-</sup> p-value= not significant(ns); PEDF<sup>+/+</sup> vs. PEDF<sup>KO/KO</sup> \*\*p-value<0.01; PEDF<sup>+/-</sup> vs. PEDF<sup>KO/KO</sup> \*\*p-value0.01. Photoreceptor thickness: PEDF<sup>+/+</sup> vs. PEDF<sup>+/-</sup> = ns; PEDF<sup>+/+</sup> vs. PEDF<sup>KO/KO</sup> \*\*\*\*p-value<0.0001; PEDF<sup>+/-</sup> vs. PEDF<sup>KO/KO</sup> \*\*\*\*p-value<0.000. PEDF<sup>+/+</sup> n=5, PEDF<sup>+/-</sup> n=4, PEDF<sup>KO/KO</sup> n=4). This data suggest that PEDF was protective against increased phototoxic damage.

### 5.4.2 Figure 2: Loss of PEDF Increased Damaged-Associated Autofluorescent Dots at the Level of the RPE

We used cSLO to capture dynamic changes in the presence of autofluorescent dots associated with damage at the level of the photoreceptor-RPE interface. At baseline, there were no differences or abnormalities between PEDF<sup>+/+</sup> (2A-B) or PEDF<sup>KO/KO</sup> (2F-G) in the vasculature or at the level of the RPE interface. However, when assessing the same animals on Day 7, the number of damage-associated

puncta at the RPE-photoreceptor layer was significantly increased in the PEDF<sup>KO/KO</sup>(2H-J) animals compared to the PEDF<sup>+/+</sup> (2C-E). This data suggest that PEDF-null animals had an increased response to damage via the appearance of damage-associated foci at the RPE-photoreceptor interface.

### 5.4.3 Figure 3: Loss of PEDF Resulted in Regional Damage and Increased Apoptosis of Photoreceptor Cells.

We used H&E to quantify the number of nuclei remaining in the outer nuclear layer (ONL) after LIRD damage to assess the degree of the damage and morphological changes. PEDF<sup>+/+</sup> animals still had relatively normal morphology with intact RPE layer and photoreceptor inner and outer segments before and after LIRD (Figure 3A-B). However, the PEDF<sup>KO/KO</sup> animal displayed a significant loss of total retinal thickness, a drastically diminished ONL, an almost complete loss of photoreceptor inner and outer segments, and compromised RPE integrity (shown via white arrows: differences in RPE thickness; Fig. 3C-D). There were regional characteristics to this damage phenotype in the PEDF<sup>KO/KO</sup> animals, with retinal structures on the superior portion of the eye being more severely diminished compared to the inferior region of the eye (Fig.3E). A similar phenotype was also shown in day five after damage [data not shown]. (Analysis: One-way ANOVA with Brown-Forsythe test and Barlett's correction; ## p-value<0.01 and ### p-value< 0.001; PEDF<sup>+/+</sup> n=4, PEDF<sup>KO/KO</sup> n=4). This phenomenon was characteristic of light damage models, as described by Rapp and Williams<sup>166,196</sup> and our data confirmed that.

Previous light studies in rats have suggested that peak DNA damage occurs within the first 8-16 hours after damage<sup>234</sup>. To assess if PEDF<sup>KO/KO</sup> animals were still undergoing significant levels of active apoptosis at day 7, we stained for DNA fragmentation using TUNEL and immune cells using CX3CR1-GFP. PEDF<sup>KO/KO</sup> animals had significantly more apoptotic cells at day 7, resulting in a more depleted outer nuclear layer than wild-type controls. Additionally, there are more immune cells in the PEDF<sup>KO/KO</sup> subretinal space compared to the wild-type animals at the same time point (Fig. 3L-N; quantified in Fig. 3O: Analysis: One-way ANOVA with Tukey's multiple comparison tests: untreated vs. PEDF<sup>+/+</sup> p-

value=ns; untreated vs. PEDF<sup>KO/KO</sup> \*\*p-value <0.01; PEDF<sup>+/+</sup> vs PEDF<sup>KO/KO</sup> \*\*p-value<0.01. untreated n=3, PEDF<sup>+/+</sup> n=4, PEDF<sup>KO/KO</sup> n=3.) These data suggest that loss of PEDF increased regional loss of photoreceptors after light damage.

#### 5.4.4 Figure 4: PEDF<sup>KO/KO</sup> RPE Failed to Increase Rhodopsin Metabolism After Light Damage

Loss of PEDF in the RPE affects aging and RPE functional deficiency<sup>204,235</sup>. To assess changes in RPE function in the absence of PEDF, we performed a rhodopsin metabolism assay as a proxy for RPE phagocytic capacity, a critical function of the RPE. We found that at day seven after LIRD, PEDF<sup>+/+</sup> animals significantly increased rhodopsin metabolism in response to damage. However, PEDF<sup>KO/KO</sup> mice failed to significantly increase rhodopsin metabolism, although they showed increased damage compared to wild-type littermate controls (See Figure 4F; quantified in Fig. 4G: Two-way ANOVA with Tukey's multiple comparison test, \*p-value<0.05). Defects in phagocytosis of PEDF<sup>KO/KO</sup> mice have been previously documented<sup>210</sup>. These data suggest that loss of PEDF results in reduced capacity for phagocytosis by the RPE.

#### 5.4.3 Figure 5: The Loss of PEDF Led to significant deficits in Visual Function after Light Damage Exposure

We also assessed functional changes using electroretinograms to accompany the distinctive in vivo and post-mortem histology analysis that we performed. Under scotopic conditions, we found that at baseline until three days post-LIRD, there was no significant difference between genotypes in either a- or b-wave function. However, by days 5 and 7, there were significant defects in a- and b-wave amplitudes of PEDF<sup>KO/KO</sup> compared to wild-type littermates (Fig. 3A-B: Two-way ANOVA with Sidak's Multiple comparison correction. Scotopic a-wave- Day 5: PEDF<sup>+/+</sup> vs. PEDF<sup>KO/KO</sup> \*\*p-value<0.01. Day 7: \*\*p-value<0.01 n=3-7/group/timepoint. Scotopic b-wave: Day 5: \*p-value<0.05. Day 7: \*p-value<0.05). To accompany the rhodopsin metabolism analysis, we used c-wave analysis as a proxy to evaluate the RPE function. We found that after light damage, there is not a significant difference between PEDF<sup>+/+</sup> and

PEDF<sup>KO/KO</sup> animals until day seven post-LIRD damage (Fig5.C: Two-way ANOVA with Sidak's multiple comparison correction: PEDF<sup>+/+</sup> vs. PEDF<sup>KO/KO</sup>; Day 5-ns; Day 7 \*p-value<0.05). This datum aligns with the functional deficits observed in the RPE in our immunofluorescence data from Figure 4. We also assessed the scotopic and photopic waveforms of PEDF<sup>KO/KO</sup> compared to PEDF<sup>+/+</sup> at baseline and day seven post-LIRD. PEDF<sup>KO/KO</sup> animals have a slightly lower b-wave and c-wave amplitude compared to PEDF<sup>+/+</sup> littermate controls at baseline (Fig.5D); however, there were no defects in photopic function (Fig. 5F). On day seven after damage, both scotopic and photopic waveforms worsened in PEDF<sup>KO/KO</sup> animals compared to PEDF<sup>+/+</sup> animals (Fig. 5E and 5G). These data suggest that the loss of PEDF negatively affects the retina and RPE function and leads to increased damage after LIRD compared to PEDF<sup>+/+</sup> littermates.

#### 5.4.4 **Figure 6: Loss of PEDF Suppressed the Damage-Associated Increase in IGF-1 after Light Damage**

Studies of hypoxic trauma, diabetic retinopathy, and pharmacological damage in the eye have linked the expression of PEDF and insulin-like growth factor 1(IGF-1) to the protection of RPE cells and other ocular structures after insult<sup>80,236,237</sup>. To determine if loss of PEDF impacts the expression of IGF-1 after damage, we used immunofluorescence to stain retinal sections of PEDF<sup>+/+</sup> and PEDF<sup>KO/KO</sup> animals. We quantified the expression of IGF-1 from baseline until day seven post-damage. Notably, PEDF<sup>KO/KO</sup> animals showed significant reductions in IGF-1 starting at day three compared to wildtype littermates (Fig 6Q: Two-way ANOVA with Tukey's multiple comparison test, n=3-4 animals/group/timepoint. Day 3: \*\*\*\*p-value<0.0001; Day 5: \*\*\*\*<0.0001; Day 7: \*\*\*\*p-value<0.0001). Increased infiltrating Galectin-3 positive immune cells were found at the RPE-photoreceptor interface in PEDF<sup>KO/KO</sup> animals and significantly more damage via loss of ONL thickness compared to wildtype littermates (See Fig. 6A-P). To confirm these findings, we tested the protein expression of IGF-1 in PEDF<sup>+/+</sup> and PEDF<sup>KO/KO</sup> animals. At baseline, there is no significant difference in IGF-1 expression among PEDF<sup>+/+</sup> and PEDF<sup>KO/KO</sup> animals (Two-way ANOVA with Tukey's multiple comparison test. N=3-6 animals/group/timepoint.

Baseline: PEDF<sup>+/+</sup> vs. PEDF<sup>KO/KO</sup>=ns). PEDF<sup>+/+</sup> animals significantly increased IGF-1 expression by day seven after damage (PEDF<sup>+/+</sup> no damage vs. PEDF<sup>+/+</sup> Day 7 post \*p-value<0.05). Notably, the expression of IGF-1 in response to damage was significantly dampened in PEDF<sup>KO/KO</sup> compared to PEDF<sup>+/+</sup> animals at day 7 (PEDF<sup>+/+</sup> Day 7 vs. PEDF<sup>KO/KO</sup> Day 7 \*\*p-value<0.01). Immune cells, like microglia, with high expression of IGF1 are associated with neuroprotection<sup>238,239</sup>. We found that subretinal immune cells in the PEDF<sup>+/+</sup> animals on day 7 showed a prominent expression of IGF1 in the cell body/cytoplasm. However, the subretinal immune cells in the PEDF<sup>KO/KO</sup> had very little to no expression of IGF-1. These data may suggest that loss of PEDF results in global loss of IGF-1 expression and increased recruitment of IGF-1 deficient immune cells.

#### 5.4.5 **Figure 7: Loss of PEDF Increased Infiltration of Galectin-3+ Immune Cells Compared to PEDF<sup>+/+</sup>**

Pigment epithelium-derived factor regulates inflammatory responses in multiple diseases, including diabetic retinopathy, dry eye disease, and cancer studies<sup>58,63,81,215,217,240,241</sup>. Specifically, the 44-mer and 17-mer PEDF peptides have been associated with antagonizing IL-6 production, thus suppressing chorioretinal inflammation<sup>242</sup>. We used immunofluorescence staining of RPE flat mounts to evaluate how the loss of PEDF affects the recruitment of subretinal immune cells at different time points after LIRD. The number of subretinal immune cells in PEDF<sup>KO/KO</sup> and wildtype littermates is comparable at baseline. However, after LIRD, PEDF<sup>KO/KO</sup> animals had significantly more recruitment of subretinal immune cells by day five than wildtype littermates (See Fig. 7A-D; quantified in Fig. 7E: Two-way ANOVA with Sidak's multiple comparison test, Day 5: PEDF<sup>+/+</sup> vs. PEDF<sup>KO/KO</sup> \*\*p-value 0.01). The number of subretinal immune cells peaked on day 7 (\*\*\*\*p-value 0.0001). Additionally, the cells had higher expression of Galectin-3, a pleiotropic,  $\beta$ -galactoside-binding protein associated with reactive microglia, compared to wildtype littermate controls at day seven post<sup>180</sup>.

#### 5.4.6 **Figure 8: PEDF<sup>KO/KO</sup> Increased *lgals*, *nlrp3* gene Expression After LIRD Compared to PEDF<sup>+/+</sup>**

To determine if loss of PEDF differentially affects inflammasome activation after LIRD, we first used digital drop PCR to assess mRNA expression of both *Lgals3* and *Nlrp3* in both the retina (data not shown) and RPE. *Lgals3*, the gene that encodes Galectin-3, mRNA expression was significantly lower in the RPE of PEDF<sup>KO/KO</sup> animals compared to wildtype littermate controls at baseline (Two-way ANOVA with Tukey's multiple comparison test. \*p-value<0.05). However, the amount of the transcript significantly increases on day 7 in PEDF<sup>KO/KO</sup> animals compared to wildtype littermates at the same time point (\*\*p-value< 0.01). Additionally, *Nlrp3* mRNA in the RPE only increased significantly at day seven post-LIRD in PEDF<sup>KO/KO</sup> compared to wildtype littermates (\*p-value<0.05). The supplemental information can find the mRNA expression of LGALS3 and NLRP3 in RPE and SNAI1, IL-6, and IL1-beta expression in retina and RPE. The loss of PEDF differentially regulates genes that encode Galectin-3 and inflammasome-associated protein, *Nlrp3*, at baseline and after LIRD, implicating PEDF in regulating Galectin-3 gene expression.

#### 5.4.7 **Figure 9: Loss of PEDF Reduced Total Galectin-3 Expression Before and After LIRD**

Previous studies have identified immune cells recruited to the subretinal space as a unique subset enriched for Galectin-3<sup>243,244</sup>. To investigate the relationship between the loss of PEDF and Galectin-3 expression, we performed protein expression analysis via western blot at baseline and day seven post-LIRD in PEDF<sup>KO/KO</sup> compared to PEDF<sup>+/+</sup>. PEDF<sup>KO/KO</sup> animals, at baseline, had significantly lower Galectin-3 protein expression than those of PEDF<sup>+/+</sup> littermate controls (PEDF<sup>+/+</sup> vs. PEDF<sup>KO/KO</sup> Baseline \*\*\*\*p-value<0.0001). This data substantiated results from Figure 8A, which showed lower *Lgals3* mRNA expression in PEDF<sup>KO/KO</sup> animals at baseline. However, while the level of Galectin-3 protein expression in PEDF<sup>KO/KO</sup> animals increases after phototoxic damage, it remains suboptimal to PEDF<sup>+/+</sup> animals at the same time point (Two-way ANOVA with Tukey multiple comparison test,

n=3/group/timepoint. PEDF<sup>+/+</sup> vs PEDF<sup>KO/KO</sup> Day 7 \*\*\*p-value 0.001). These data suggest the loss of PEDF significantly affected the protein expression of Galectin-3 both before and after LIRD.

#### **5.4.8 Figure 10: Treatment with Galectin-3 inhibitor, TD139, Significantly Decreased PEDF Expression in PEDF<sup>+/+</sup> Animals after LIRD.**

Previous studies have correlated increased expression of Galectin-3 with poor clinical outcomes in multiple eye diseases<sup>176,179,181,182,245,246</sup>. Additionally, the inhibition Galectin-3 by genetic manipulation or pharmacological targeting dampened immune cell activity<sup>178</sup>. To determine if dampening the Galectin-3 expression would be protective after LIRD damage, we pharmacologically inhibited Galectin-3 in PEDF<sup>+/+</sup> animals using TD139 to determine if Galectin-3 inhibition was protective after LIRD. We found that treatment with Galectin-3 inhibitor (TD139) did not significantly affect Galectin-3 protein levels. However, we did notice significant differences in the visual function of animals without LIRD exposure (data not shown). Interestingly, we found that animals treated with Galectin-3 inhibitor had a worse damage phenotype than LIRD-only controls. Surprisingly, PEDF levels in animals treated with TD139 and LIRD were significantly lower than in the LIRD-only control group (One-way ANOVA with Tukey's multiple comparison test. n=3 animals/group. PEDF<sup>+/+</sup> No damage vs. PEDF<sup>+/+</sup> LIRD only: p-value=ns; PEDF<sup>+/+</sup> no damage vs. PEDF<sup>+/+</sup> LIRD + Gal-3 inhibitor \*\*\*p-value<0.001; PEDF<sup>+/+</sup> LIRD only vs. PEDF<sup>+/+</sup> LIRD + Gal-3 inhibitor \*p-value<0.01). These data suggest a potential correlation between PEDF and Galectin-3 expression since the inhibition of Galectin-3 significantly decreases PEDF expression.

## 5.5 DISCUSSION

The findings from this study reveal that PEDF plays a significant regulatory role in facilitating immune privilege and suppressing inflammation to protect vulnerable tissues from damage within the ocular microenvironment. Previous studies have evaluated and purported the protective role of PEDF against photoreceptor death in albino rat models under various light damage conditions; additionally, these studies showed that intravitreal supplementation with exogenous PEDF was protective<sup>183,247</sup>. However, the full mechanism for this protection has not been fully established. Previous studies were limited in that they primarily used albino animals, which are not fully translatable to normal vision in humans with pigmented eyes. This study aimed to examine the influence of PEDF on the outcome of visual function, Galectin-3 positive subretinal immune cell recruitment, and effects on the neurotrophic factor, IGF-1, after light damage. By employing a global deletion model of PEDF and comparing the multiple visual metrics to wildtype controls, we could identify phenotypic shifts during damage resolution that coincide with expression changes in IGF-1 and Galectin-3. Studying these molecular mechanisms may be the basis for better understanding and predicting the pathological onset of disease, reveal new pathway interactions for conserved biomarkers, and present new considerations for therapeutic approaches employing gene therapy. To our knowledge, our study is the first to evaluate the potential regulatory axis of PEDF-Galectin-3-IGF-1 in visual function. Additionally, according to our understanding, this is the first study to implicate PEDF in the modulation of Galectin-3 expression in the eye. Overall, our results implicate the loss of PEDF as an essential regulator of both IGF-1 and Galectin-3 expression after light damage, suggesting an additional level of RPE-mediated regulation of immunosuppression in the ocular microenvironment.

Immune privilege in the eye requires an intact RPE monolayer, which secretes factors that suppress the immune response, controls the maturation of immune cells, and leads to apoptosis of infiltrating macrophages, magnifying the role of RPE in facilitating immunomodulation<sup>43,49,50,248–252</sup>.

Studies of pigment epithelia derived from various ocular tissues suggest that immunosuppression is achieved by cell-cell contact, soluble factors, or both, depending on the source of epithelia. The retinal pigment epithelia predominantly utilize secreted, soluble factors to suppress immune cell activation. Previous studies have described the immunomodulatory functions of the RPE via the secretion of cytokines and neuropeptides, like alpha-melanocyte stimulating hormone ( $\alpha$ -MSH) and Neuropeptide Y (NPY)<sup>48,49,252,253</sup>. However, the complete mechanism by which the RPE participates in immunomodulation has not been fully elucidated.

Loss of PEDF is associated with aging and reductions in RPE functionality<sup>82,118</sup>. Here, we assessed the potential immunomodulatory effects of the secreted homeostatic marker, PEDF, on damage outcomes and inflammation. Previous studies have described overexpression of or supplementation with PEDF as protective of photoreceptors and motor neurons, improvements in mitochondrial function and cortical neurons after damage, and inhibition of inflammatory damage<sup>187,204,218,254–257</sup>. Additionally, deletion of PEDF is associated with aging, increased inflammation, and increased loss of visual function<sup>185,189,220,258</sup>. Notably, we found the increased presence of cell-sized white foci at the level of the RPE in our cSLO analysis of PEDF-null animals exposed to light damage. Currently, the field has not reached a unified consensus on identity of these puncta as immune cells, displaced RPE cells, aggregates of cellular debris or lipofuscin, or a combination of all of the above<sup>259–262</sup>. While defining the identity of these structures requires advanced studies outside the scope of this paper, there is agreement that the presence of autofluorescent dots at the RPE-photoreceptor interface is associated with pathology and damage. Our results confirm the findings of other studies since the loss of PEDF resulted in increased retinal thinning, more damage-associated auto-fluorescent dots at the RPE-photoreceptor interface, significant loss of the photoreceptor layer, and increased cell death compared to littermate controls.

Additionally, when evaluating the retinal function, we found that the RPE of PEDF<sup>KO/KO</sup> animals had a reduced capacity for rhodopsin metabolism after LIRD compared to littermate controls at the same

time point. Retinal function loss reduced scotopic *a*-, *b*, and *c*-wave amplitudes by five to seven days after light damage in PEDF<sup>KO/KO</sup> animals compared to littermate controls. These data suggest that PEDF is protective against excessive damage after phototoxic light exposure.

The RPE is the major contributor to IGF-1 secretion in the ocular environment<sup>263</sup>. The importance of IGF-1 as a neurotropic factor and a regulator of immune cell function has been described in the eye and other tissue types under normal and pathological conditions, like cancer and ischemia<sup>78,236,238,239,264,265</sup>. Additionally, decreases in IGF-1 expression have been correlated with aging, increased damage, and apoptosis in eye and brain studies<sup>266-268</sup>. To assess how the loss of PEDF may affect the expression and abundance of the neurotrophic factor, IGF-1, we first evaluated IGF-1 immunoreactivity in retinal sections of PEDF<sup>KO/KO</sup> animals compared to PEDF<sup>+/+</sup> animals at baseline. Baseline data showed no significant changes in IGF-1 expression between genotypes. However, after insult, there was a considerable loss in IGF-1 expression beginning on Day 3 of PEDF<sup>KO/KO</sup> animals, which increased to Day 7. We confirmed these findings via western blot analysis, showing a significant reduction in IGF1 protein expression in PEDF<sup>KO/KO</sup> compared to wild-type littermates at day 7. IGF-1 inhibits apoptosis of photoreceptors via the downregulation of caspase-3 and c-JUN signaling; thus, the reduced expression of IGF-1 may explain the increased degree of apoptosis observed in Fig.3B<sup>236,267,268</sup>. The presence of IGF-1 and Galectin-3 co-expression in neuroprotective immune cells has been reported previously<sup>77,238,239</sup>. We also assessed the presence of IGF-1 in recruited subretinal immune cells adhered to RPE flat mounts collected from PEDF<sup>+/+</sup> and PEDF<sup>KO/KO</sup> animals at day seven post-LIRD. We found that PEDF<sup>KO/KO</sup> animals had fewer IGF-1 positive immune cells (See Fig. 6W-Y) compared to the PEDF<sup>+/+</sup>(Fig.6T-V) at the same time point. IGF-1 modulates macrophage responsiveness and activity when challenged with a high-fat diet, shifting the transcriptional and morphological phenotypes to that of an M2-like proinflammatory macrophage<sup>269</sup>. A decrease in IGF-1 and PEDF expression has also been described in aging studies, which may suggest a similar mechanism as observed during our light damage experiments in the absence of PEDF<sup>270-273</sup>. The loss of IGF-1 expression with age likely affects microglia function and

sensitivity. The loss of PEDF leads to insult-initiated down-regulation of IGF-1 protein expression and reduced recruitment of IGF-1-expressing immune cells.

Multiple groups have described a unique subclass of immune cells enriched in Galectin-3, recruited during neurodegeneration in the brain and the eye<sup>72,73,75,77,177,180</sup>. In the eye, Galectin-3 enriched subretinal immune cells are recruited to the photoreceptor-RPE interface, suggesting that there may be a functional requirement for Galectin-3 in the subretinal space<sup>73,75,244</sup>. Elevated Galectin-3 expression is associated with poor prognostic outcomes<sup>176,179,181,182</sup>. Additionally, an ocular proteome study comparing AMD patients to age-matched controls found a significant increase in the secretion of Galectin-3 binding protein and Pigment epithelium-derived factor from the RPE<sup>17</sup>. However, the correlation between PEDF expression, Galectin-3 levels, and damage outcomes has yet to be investigated. We hypothesized that loss of PEDF will increase Galectin-3 expressing cells and global expression of Galectin-3, ultimately leading to increased inflammation in the ocular microenvironment. To evaluate this, we quantified the number of Galectin-3 expressing cells that adhered to the RPE in no damage controls and day seven between PEDF<sup>KO/KO</sup> compared to littermate controls (Fig. 7). At baseline, there was no difference between genotypes. However, after damage, we found that the total number of Galectin-3 positive cells was significantly increased in PEDF<sup>KO/KO</sup> animals compared to wildtype controls (See Fig. 7A-D), suggesting that without damage, there is no increased infiltration of immune cells. However, after damage initiation, PEDF<sup>KO/KO</sup> animals had significantly more Galectin-3 expressing cells infiltrating the subretinal space compared to wild-type littermates at the same time (Fig. 7E). Damage to the subretinal space, neurodegeneration, and aging are associated with an increased activation of inflammation signaling and recruitment of immune cells<sup>102,148,274–278</sup>. To investigate if PEDF<sup>KO/KO</sup> animals exhibit differential expression of Galectin-3 and inflammasome mediator Nlrp3, we used digital drop PCR. We found that Galectin-3 mRNA expression in the RPE from PEDF<sup>KO/KO</sup> was significantly reduced compared to wild-type littermates. However, after damage, there is a significant increase in *lgals3* and *nlrp3* expression at day 7 in PEDF<sup>KO/KO</sup> animals compared to the wildtype controls, which dampens the expression of these genes at the same time point.

In agreement with the gene expression data, Galectin-3 protein expression was significantly lower in PEDF<sup>KO/KO</sup> animals compared to PEDF<sup>+/+</sup>. On day 7, post-damage, PEDF<sup>+/+</sup> animals reduced Galectin-3 expression considerably compared to baseline expression; conversely, Galectin-3 increased in the PEDF<sup>KO/KO</sup> animals at the same time point. Notably, while Galectin-3 protein expression in PEDF<sup>KO/KO</sup> animals increased over baseline expression, there was significantly lower expression of Galectin-3 protein at day seven compared to PEDF<sup>+/+</sup>. These data may suggest that loss of PEDF affects the steady state of Galectin-3 expression. Interestingly, when we pharmacologically inhibited Galectin-3 activity in PEDF<sup>+/+</sup> animals during LIRD, we found it significantly decreased PEDF levels compared to LIRD-only controls (see Fig. 10), leading to poorer visual outcomes (data not shown). These data suggest that PEDF protects ocular function after LIRD via a novel Galectin-3-mediated mechanism.

PEDF suppresses eye diseases and cancer studies<sup>240,241,279</sup>. In this study, we hypothesized that the protective role of PEDF in the ocular microenvironment after damage includes regulation of inflammation and immune privilege via Galectin-3 mediated signaling. This study reports a putative relationship between Galectin-3 and PEDF, suggesting that Galectin-3 enriched immune cells within the subretinal space are a positive regulator of PEDF expression after light damage. However, the precise molecular signaling by which loss of PEDF impacts Galectin-3 and IGF-1 expression requires further study.

**Acknowledgments:** Supported by Grants from the National Institutes of Health (R01EY028450, R01EY021592, P30EY006360, U01CA242936, R01EY028859, T32EY07092, T32GM008490); by the Abraham J. and Phyllis Katz Foundation; by grants from the U.S. Department of Veterans Affairs and Atlanta Veterans Administration Center for Excellence in Vision and Neurocognitive Rehabilitation (RR&D I01RX002806, I21RX001924; VA RR&D C9246C); and an unrestricted grant to the Department of Ophthalmology at Emory University from Research to Prevent Blindness, Inc. We would also like to thank Dr. Hans Grossniklaus and Dr. Sue Crawford at Northwestern University Feinberg School of Medicine for gifting the PEDF knockout mice used in this study.

## 5.6 FIGURES AND TABLES

5.6.1 Table 1: Primary and Secondary Antibody Information

| <b>Antibody</b>                                 | <b>Antibody Type</b>       | <b>Species</b> | <b>Company and Catalog information</b>      | <b>Concentration</b> |
|---|----------------------------|----------------|---|----------------------|
| <b>Galectin-3</b>                               | Primary                    | Goat           | R&D Systems ( AF1197)                       | 1:250                |
| <b>ZO-1</b>                                     | Primary                    | Rat            | Sigma                                       | 1:250                |
| <b>IGF-1</b>                                    | Primary (conjugated AF546) | Mouse          | Santa Cruz (sc-518040)                      | 1:100                |
| <b>IBA-1</b>                                    | Primary                    | Rabbit         | Abcam (ab178847)                            | (1:1000)             |
| <b>Pentahydrate(bis-Benzamide)Hoechst 33258</b> | DNA nuclear Stain          | N/A            | Thermo-Fisher Catalog #: H3569              | [1:250]              |
| <b>TUNEL</b>                                    | N/A                        | N/A            | Promega DeadEnd TUNEL Fluometric Kit- G3250 |                      |
| <b>Mouse anti-Rhodopsin</b>                     | Primary                    | Mouse          | Abcam, ab3267                               | [1:250]              |
| <b>Rabbit anti-Best1</b>                        | Primary                    | Rabbit         | Abcam, ab14927                              | [1:250]              |
| <b>Donkey anti-Rat (AF488)</b>                  | Secondary                  | Rat            | Life Technologies, Catalog # A21208         | [1:1000]             |
| <b>Donkey anti-rabbit (AF568)</b>               | Secondary                  | Rabbit         | Life Technologies, Catalog # A10042         | [1:1000]             |
| <b>Donkey Anti-Mouse(AF488)</b>                 | Secondary                  | Mouse          | Life Technologies Catalog #A21202           | [1:1000]             |
| <b>Donkey Anti-Goat(AF647)</b>                  | Secondary                  | Goat           | Abcam Catalog # A32849                      | [1:1000]             |
|   |                            |                |   |                      |

5.6.2 Table 2: Digital Droplet PCR Primers

| <b>Gene</b>   | <b>Protein</b>    | <b>Primer Sequence</b> | <b>Size</b> | <b>Species</b> |
|---------------|-------------------|------------------------|-------------|----------------|
| <i>Hrpt</i>   | HRPT-<br>HEX(IDT) | Mm.PT.39a22214828      |             | Mouse          |
| <i>Il6</i>    | IL6               | dMmuCPE5095532         | <b>70</b>   | Mouse          |
| <i>Il1b</i>   | IL1B              | Mm.PT.58.41616450      | 119         | Mouse          |
| <i>Lgals3</i> | Galectin-<br>3    | Mm.PT.58.8335884       | 130         | Mouse          |
| <i>Nlrp3</i>  | NLRP3             | Mm.PT.58.13974318      | 90          | Mouse          |
| <i>Snai1</i>  | SNAI1             | Mm.PT.58.43057042      | 122         | Mouse          |
|               |                   |                        |             |                |

### 5.6.3 Figure 1: Loss of Pigment Epithelium Derived Factor Modifies Sensitivity to Phototoxic Damage in C57BL/6J Animals

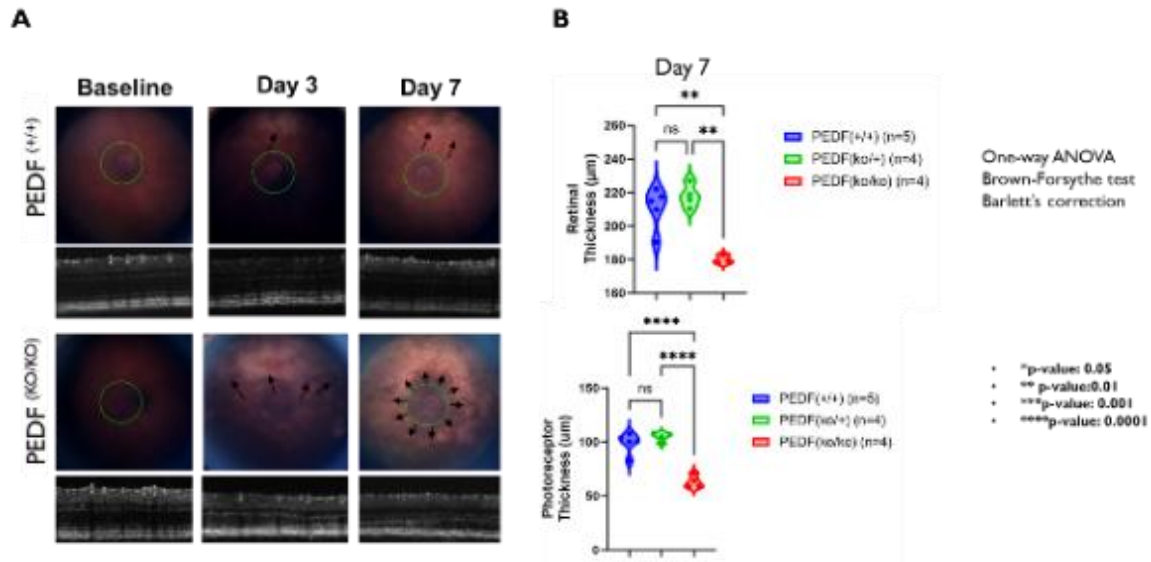


**Figure 1: Loss of Pigment Epithelium Derived Factor Modifies Sensitivity to Phototoxic Damage in C57BL/6J Animals**

Fundus and retinal C57BL/6J animals that express wild-type PEDF (PEDF +/+ ) or PEDF knockout (PEDF KO/KO) animals are shown. Figure 1A shows Spectral Domain Optical Coherence Tomography (SD-OCT) images of the Fundus and circular B-scans of the retinal architecture around the optic nerve. Top row: PEDF +/+ animals are shown in the top row at both baselines and on day seven post-LIRD. Bottom row: PEDF KO/KO animals at baseline and Day 7 Post LIRD. White arrows denote regions of damage-associated mottling of the fundus. Figure 1B shows the quantification of total retinal thickness and the thickness of the photoreceptor layer of PEDF +/+ n=5, PEDF KO/+ n=4, PEDF KO/KO= n=4 at Day 7 Post LIRD. One-way ANOVA Brown-Forsythe test with Barlett's correction. \* p-value< 0.05, \*\* p-value<0.01, \*\*\* p-value<0.001, \*\*\*\* p-value<0.0001.

5.6.4 **Figure 2: Loss of PEDF Increases Damaged-Associated Autofluorescent Dots at the Level of the RPE**

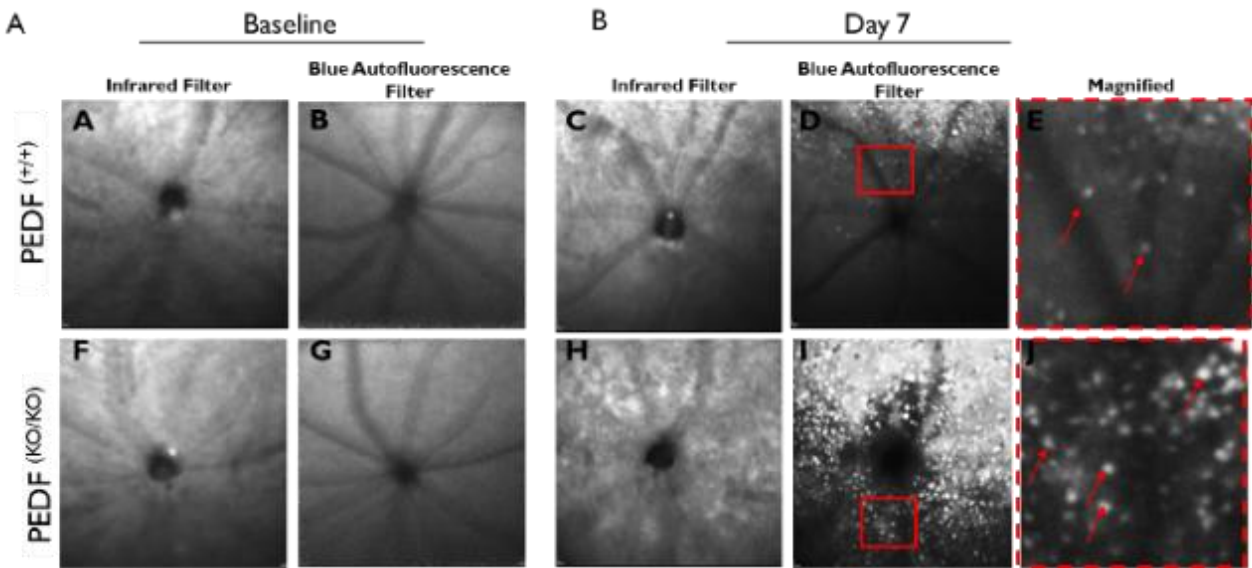


**Figure 2: Loss of PEDF Increases Damaged-Associated Autofluorescent Dots at the Level of the RPE.** Heidelberg Spectralis cSLO (confocal scanning laser ophthalmoscope) images show an increased accumulation of autofluorescent dots/granules at the level of the photoreceptor-RPE interface after phototoxic damage that is not present at baseline. Images were taken at -12 diopters at the level of the interdigitations of RPE and photoreceptors using both the infrared (to detect vascular architecture) and the blue autofluorescence filter (to detect fluorescent dots). Representative Images at baseline for PEDF<sup>+/+</sup> (2A-B) and PEDF<sup>KO/KO</sup> (2F-G) and at Day 7 Post LIRD (PEDF<sup>+/+</sup>: 2C-E; PEDF<sup>KO/KO</sup>: 2H-J). A Zoom (red box) of each representative image with red arrows highlighting individual dots.

### 5.6.5 Figure 3: Loss of PEDF Results in Regional Damage and Increases Apoptosis of Photoreceptor Cells.

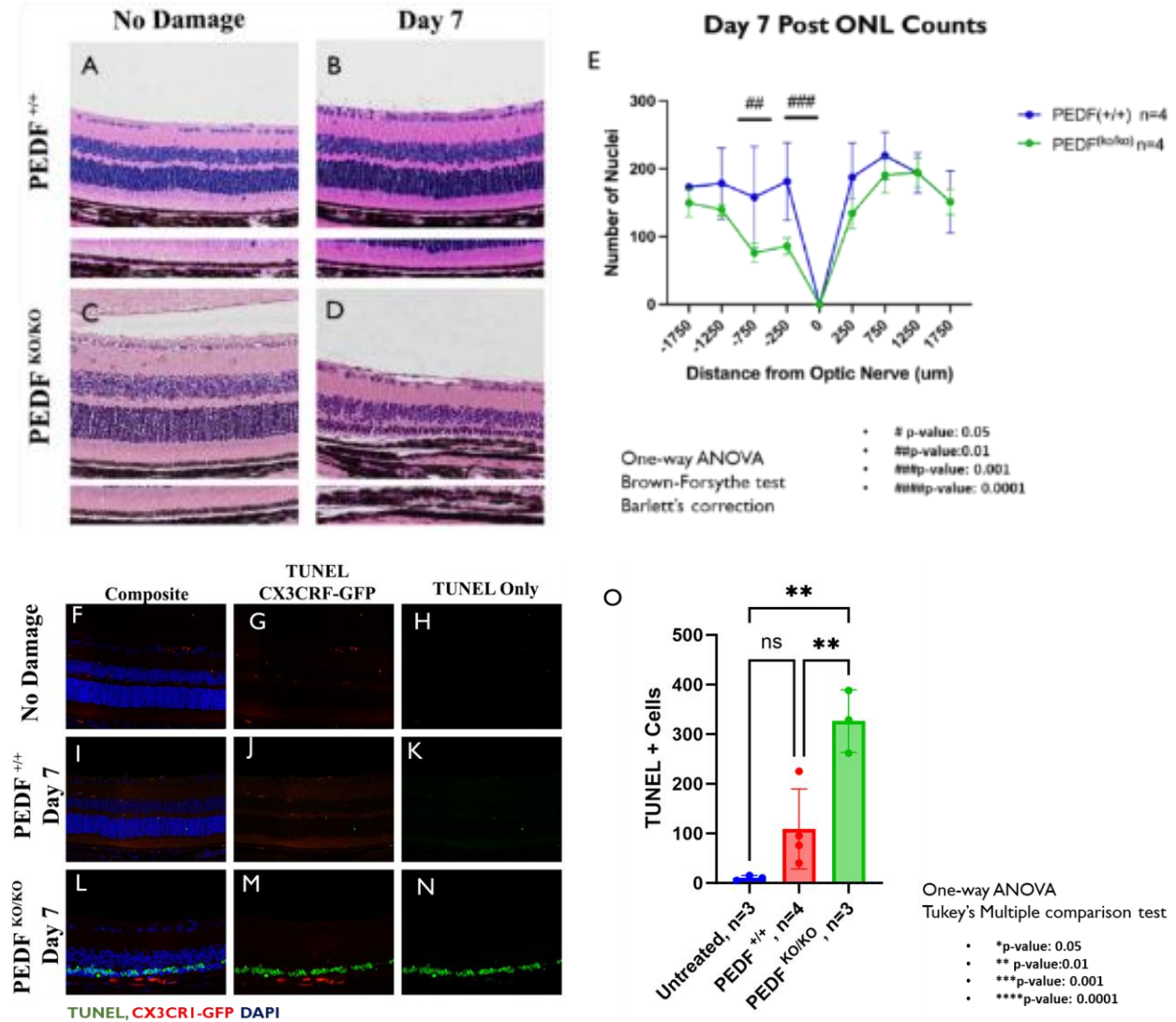


**Figure 3: Loss of PEDF Results in Regional Damage and Increases Apoptosis of Photoreceptor Cells.**

The morphology of the postmortem tissue shows significant regional alterations in retinal architecture.

Figure 3A-B shows a representative image of PEDF<sup>+/+</sup> with no damage and day seven post-LIRD.

Representative images of PEDF<sup>KO/KO</sup> animals with no damage (Figure 2C) and day seven post-damage (Figure 2D) are shown. Figure 2D shows severe loss of the outer nuclear layer (ONL), disruption of the photoreceptor inner and outer segment layer, and aberrations in the RPE monolayer in PEDF<sup>KO/KO</sup>

compared to PEDF<sup>+/+</sup> controls at day five post-light damage. Figure 3E quantifies ONL counts from -

1750 microns (superior) to 1750 microns (inferior) on either side of the optic nerve. The damage is regionally isolated to the superior portion of the retina and is significantly between PEDF KO/KO n=4 and PEDF <sup>+/+</sup> n=4. One-way ANOVA with Brown-Forsythe test and Barlett's correction. # p-value<0.05, ## p-value<0.01, ### p-value<0.001, ##### p-value <0.0001. The loss trend was the same on day seven post-LIRD (data not shown).

Figure 3F-N shows representative images of retinal sections stained for TUNEL (green), immune cells via CX3CR1-GFP (red), and cell nuclei (DAPI) of no damage control (3F-H), Day 7 PEDF <sup>+/+</sup> (3I-K) and, Day 7 PEDF <sup>KO/KO</sup> (3L-N). These data are quantified in Figure 3O and show that PEDF <sup>KO/KO</sup> have significantly more TUNEL-positive cells than either the untreated (\*\* p-value<0.01) or the PEDF <sup>+/+</sup> (\*\* p-value<0.01) group.

### 5.6.6 Figure 4: PEDF<sup>KO/KO</sup> RPE Fail to Increase Rhodopsin Metabolism after Light Damage

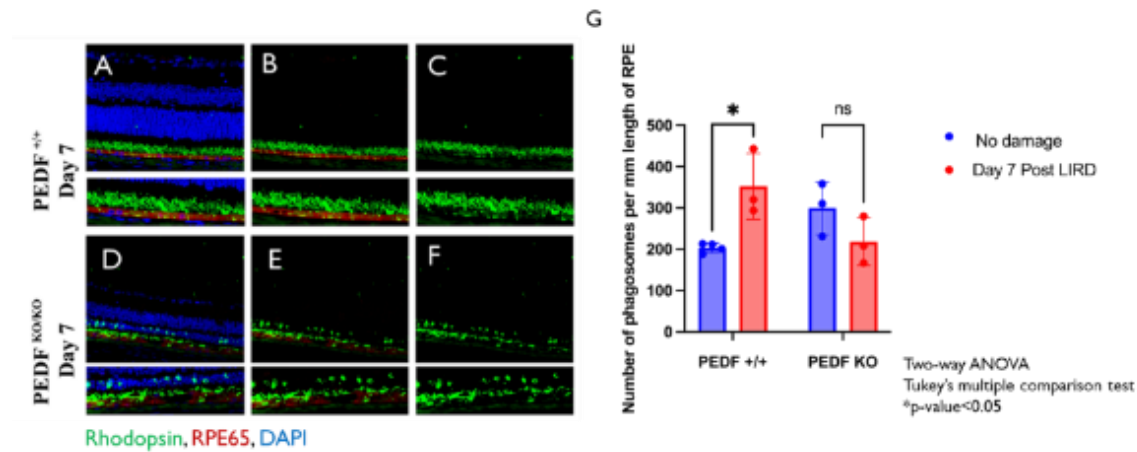


**Figure 4: PEDF<sup>KO/KO</sup> RPE Fail to Increase Rhodopsin Metabolism after Light Damage.**

Loss of PEDF results in a suboptimal production of phagosomes by the RPE after light-induced retinal damage. Figure 4A-F shows representative retinal immunofluorescence images of a PEDF<sup>+/+</sup> and PEDF<sup>KO/KO</sup> at day 7 Post-light damage. The sections were stained with Rhodopsin (green) to visualize shed rod outer segments and phagosomes, Best1 (red) was used to visualize the RPE monolayer, and cell nuclei were stained with DAPI (blue). Figure 4G, notably, the PEDF<sup>+/+</sup> animals significantly increase production to redress clearance demands at day seven post-LIRD compared to untreated PEDF<sup>+/+</sup> (Two-way ANOVA, Tukey's multiple comparison test, \*p-value<0.05). However, while PEDF<sup>KO/KO</sup> animals had a more significant accumulation of phagosomes at baseline, they failed to increase phagosome production after light damage.

### 5.6.7 Figure 5 The Loss of PEDF leads to significant deficits in visual function after light damage exposure.

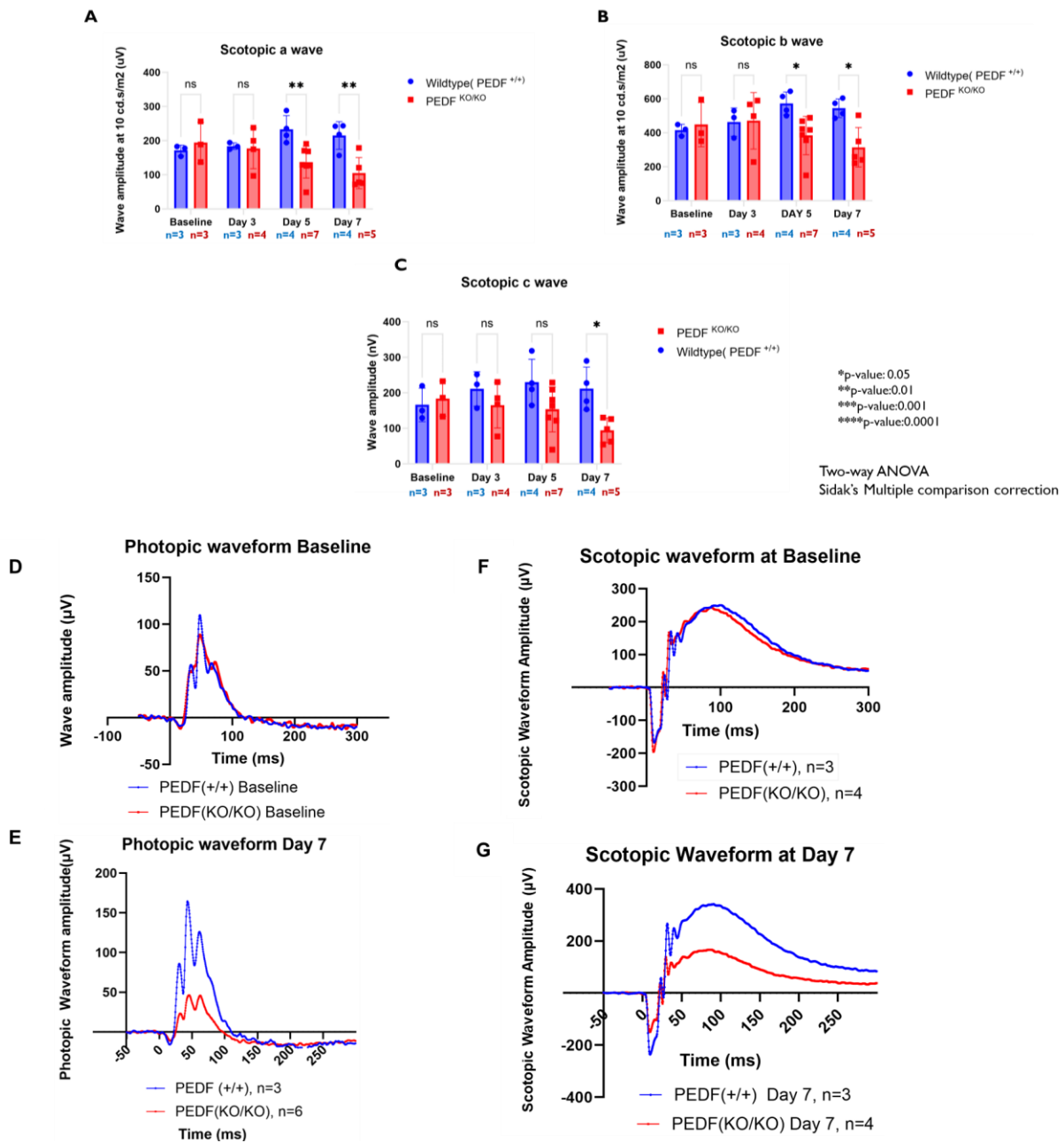


**Figure 5: The Loss of PEDF leads to significant deficits in visual function after light damage exposure.**

The figure shows the maximal visual output of *a*-wave, *b*-wave, and *c*-wave at a flash intensity of 10 candelas/second/meters<sup>2</sup> (cd.s/m<sup>2</sup>). These data show no statistically significant difference in the visual function of the PEDF<sup>KO/KO</sup> compared to PEDF<sup>+/+</sup> at baseline or on day three after light damage. However, after day three there is a notable decrease in visual function of PEDF<sup>KO/KO</sup> animals in both *a*- and *b*-wave amplitudes at 10Hz that persists to day 7 (*a*-wave: day 5: \*\* p-value<0.01; day 7: \*\* p-value<0.01 and *b*-wave: day 5: \*p-value <0.05; day 7: \*p-value<0.05. n=3-7/time point/group) see Figure 5A and 5B; Two-way ANOVA with Sidak's multiple comparison correction). Significant loss of the *c*-wave amplitudes is delayed to day seven post-light damage (See Fig. 2C: Two-way ANOVA with Sidak's multiple comparison corrections, day 7: \* p-value<0.01). The scotopic waveforms of PEDF KO/KO mice also reveal a slight depression in the waveform amplitude at baseline compared to PEDF<sup>+/+</sup> (n=3-4/genotype). This reduction in waveform amplitude is more pronounced at day seven post-LIRD (n=5/genotype; See Figures 5D and 5E). Photopic waveforms show a similar trend as scotopic waveforms with significantly reduced amplitudes in PEDF KO/KO at day 7 compared to PEDF<sup>+/+</sup> littermates (See Fig. 5F-G).

### 5.6.8 Figure 6: Loss of PEDF Suppresses the Damage-Associated Increase in IGF-1 after Light Damage

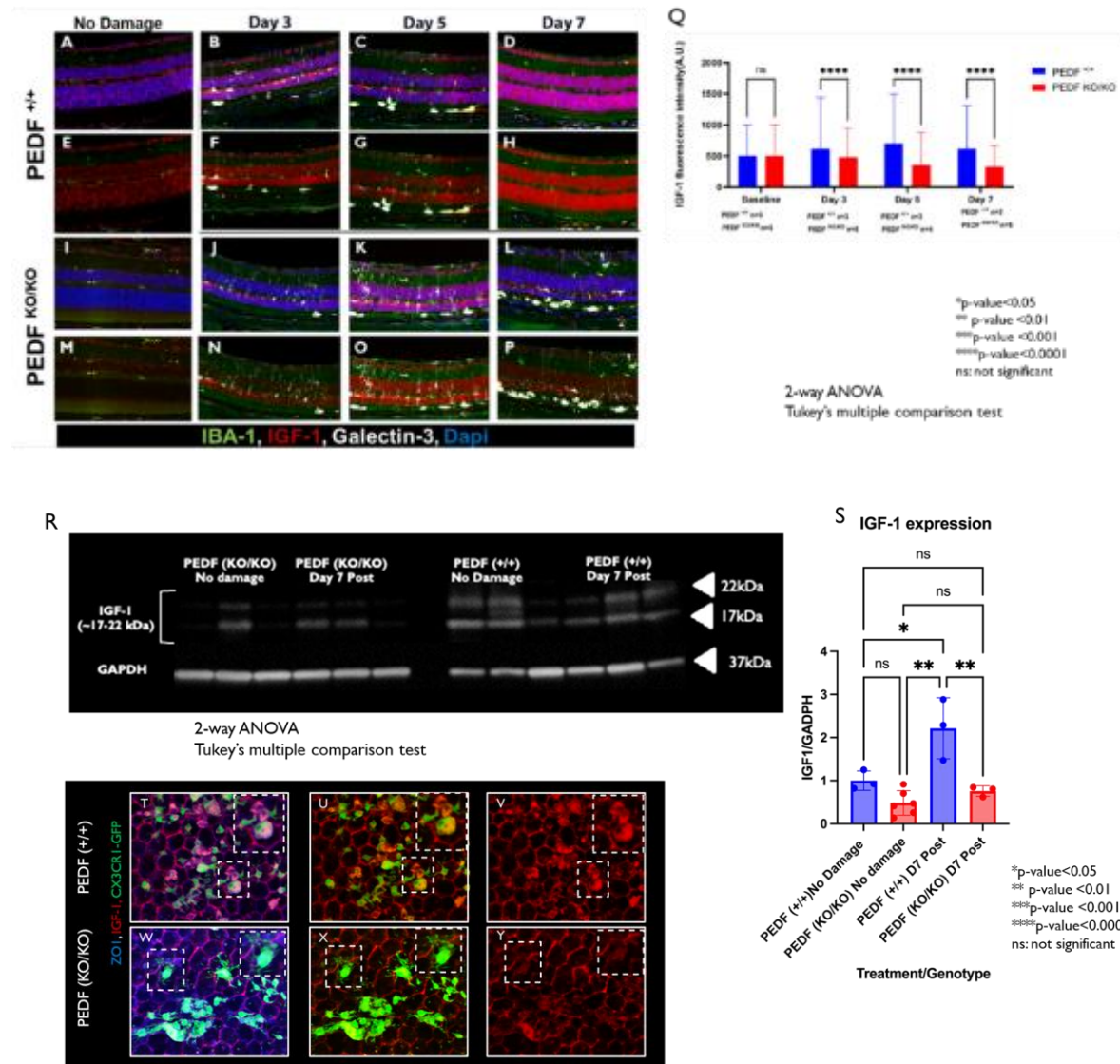


**Figure 6: Loss of PEDF Suppresses the Damage-Associated Increase in IGF-1 after Light Damage**

Retinal sections were collected at days 3, 5, and 7 post light damage and stained for the neurotrophic factor, IGF-1 (red), the immune cell marker, IBA1 (green), immune cell activation marker, Galectin-3 (white), and dapi (blue). Staining showed that at baseline, there was no significant difference between PEDF<sup>+/+</sup> and PEDF<sup>KO/KO</sup> animals without damage. Figure 6A-P is a representative image showing the

degree of expression of IGF-1 and Galectin-3 and the infiltration of immune cells from the retina to the subretinal space. After light damage, there is an increase in Galectin-3 positive cell expression in both genotypes at day 3, with the earliest deposition at the photoreceptor-RPE interface occurring at day 3. By day 7, only the PEDF<sup>KO/KO</sup> animals still have Galectin-3 positive cells at the interface of the photoreceptors-RPE. Additionally, when quantifying the immunofluorescent signal of IGF-1, there are statically significant differences between the PEDF<sup>+/+</sup> and PEDF<sup>KO/KO</sup> as early as day 3. The levels of IGF-1 continue to decrease until day seven post LIRD (see Fig. 6Q). Analysis: Two-way ANOVA with Tukey's multiple comparison test, n=3-5/ group/time point. \* p-value< 0.05, \*\* p-value<0.01, \*\*\* p-value<0.001, \*\*\*\* p-value<0.0001. In Figure 6R, we confirm this finding via total eye cup expression of IGF-1 normalized to GAPDH in no damage controls versus at day seven post-LIRD via western blot. Figure 6R quantifies the total expression of IGF-1 between PEDF<sup>+/+</sup> and PEDF<sup>KO/KO</sup> before and after LIRD. Analysis: Two-way ANOVA with Tukey's multiple comparison test, n=3-6/group/timepoint. Subretinal immune cells recruited to RPE in PEDF<sup>KO/KO</sup> have lower expression of IGF-1 than PEDF<sup>+/+</sup> animals. Figure 6T-Y shows a representative image of PEDF<sup>+/+</sup> (6T-V) and PEDF<sup>KO/KO</sup> (6W-Y) stained for ZO1(blue), IGF-1(red), and CX3CR1-GFP (green) to look for heterogeneity in the immune cell population.

**5.6.9 Figure 7: Loss of PEDF increases infiltration of Galectin-3<sup>+</sup> immune cells compared to PEDF<sup>+/+</sup>**

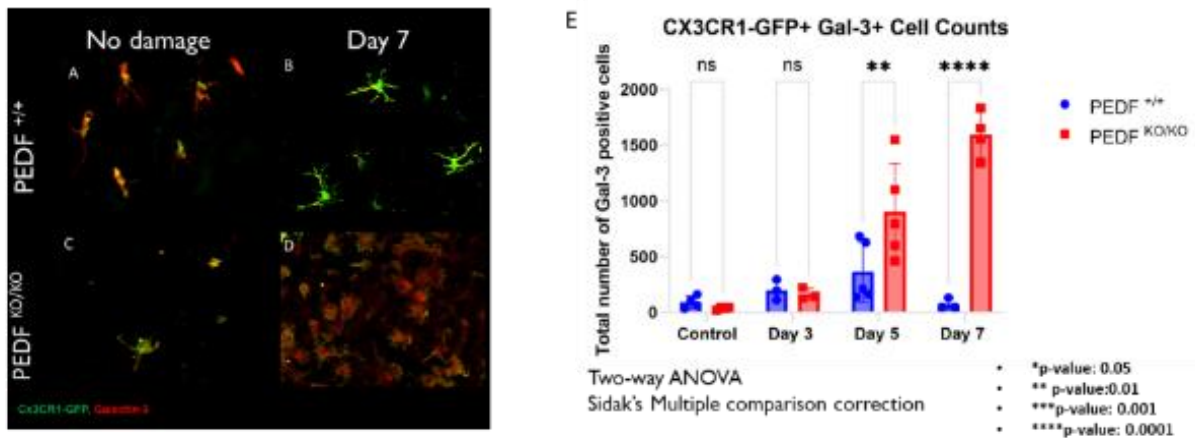


**Figure 7: Loss of PEDF increases infiltration of Galectin-3<sup>+</sup> immune cells compared to PEDF<sup>+/+</sup>**

We collected RPE flat mounts to assess if PEDF<sup>KO/KO</sup> animals showed an increased inflammatory profile and stained them for Galectin-3 (red) and CX3CR1-GFP(Green). We found that PEDF<sup>KO/KO</sup> animals were like PEDF<sup>+/+</sup> animals at baseline and up to day three post-LIRD damage. However, by day 5, there was the inflammation phenotype significantly increased in PEDF<sup>KO/KO</sup> animals compared to littermate controls \* p-value< 0.05, \*\* p-value<0.01, \*\*\* p-value<0.001, \*\*\*\* p-value<0.0001 (Analysis: Two-way ANOVA with sidak's multiple comparison correction. N=3-5 animals group/ time point. p-value: Day 5: \*\* vs Day 7 \*\*). Figure 7A-D shows a representative image of the subretinal immune cell morphology in PEDF<sup>+/+</sup> and PEDF<sup>KO/KO</sup> animals at baseline and Day 7. Figure 7E shows the total number of Gal-3 positive cells counted from baseline to day seven post-LIRD between PEDF<sup>+/+</sup> and PEDF<sup>KO/KO</sup>

**5.6.10 Figure 8: Loss of PEDF Increases Galectin-3 Gene Expression at Day 7 Post LIRD Compared to Wildtype Littermates**

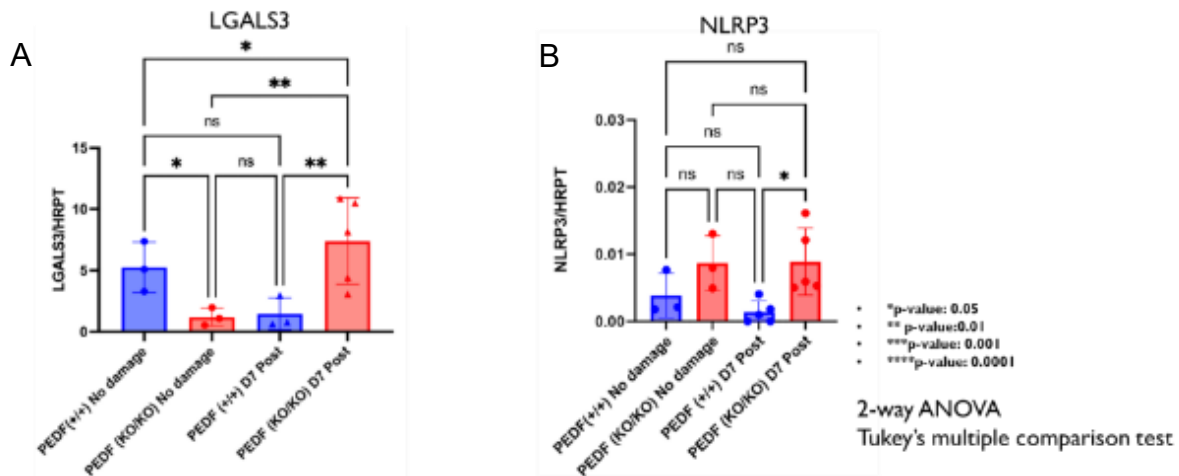


**Figure 8: Galectin-3 and NLRP3 gene expression are elevated in PEDF KO/KO at day seven compared to PEDF +/+.**

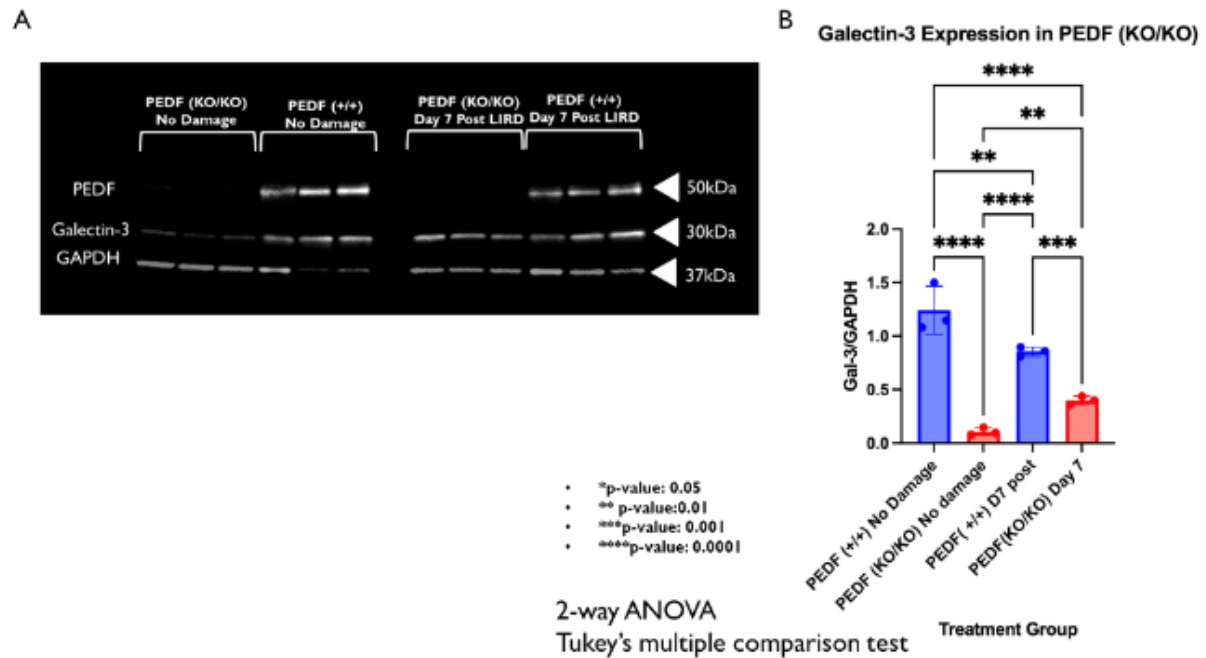
Retinal and RPE tissues were collected separately, and RNA was extracted from each tissue sample type.

Figure 9A quantifies *Lgals3* and *Nlrp3* gene expression normalized to HRPT in the retina between PEDF +/+ and PEDF<sup>KO/KO</sup> at baseline and Day 7 Post LIRD. Figure 9A-B shows the gene expression of *Lgals3*

and *Nlrp3* at the same time points in the RPE. The *Lgals3* expression in the RPE Two-way ANOVA;

PEDF<sup>KO/KO</sup> baseline vs. PEDF KO/KO Day 7: \*p-value<0.05; PEDF<sup>+/+</sup> Day 7 vs. PEDF<sup>KO/KO</sup> Day 7: \*p-value<0.05. However, only at day 7 in the RPE is *Nlrp3* expression significantly different in the PEDF<sup>KO/KO</sup> compared to littermate controls(\*p-value<0.05).

### 5.6.11 Figure 9: Loss of PEDF Reduces Total Galectin-3 Expression Before and After LIRD



### Figure 9: Loss of PEDF Reduces Total Galectin-3 Expression Before and After LIRD

PEDF<sup>KO/KO</sup> animals have significantly lower expression of Galectin-3 at baseline compared to littermate controls. Additionally, after damage, there is a suboptimal increase in Galectin-3 protein expression on day seven post-LIRD. PEDF<sup>+/+</sup> animals dampen Galectin-3 expression in response to LIRD damage at day 7, suggesting differential temporal regulation of the protein when PEDF is present compared to when it is not. Figure 9A shows a western blot that was probed for PEDF (50kDa), Galectin-3 (~30kDa), and GAPDH (~37kDa) loading control. The results from Figure 9A are quantified in Figure 9B and show that there are significant differences in Galectin-3 expression at both baselines (Two-way ANOVA with Tukey's multiple comparison correction. \*\*\*\* p-value<0.0001. sample sizes: 3 animals/group/time point) and at Day 7 (\*\*\*\*p-value<0.0001) between PEDF<sup>KO/KO</sup> and PEDF<sup>+/+</sup> animals. While Galectin-3 expression increases in the PEDF<sup>KO/KO</sup> animals at day seven compared to baseline, it is still dampened compared to the Gal-3 expression of PEDF<sup>+/+</sup> at the same time point.

5.6.12 Figure 10: Treatment with Galectin-3 inhibitor, TD139, significantly decreases PEDF expression in PEDF<sup>+/+</sup> animals after LIRD.

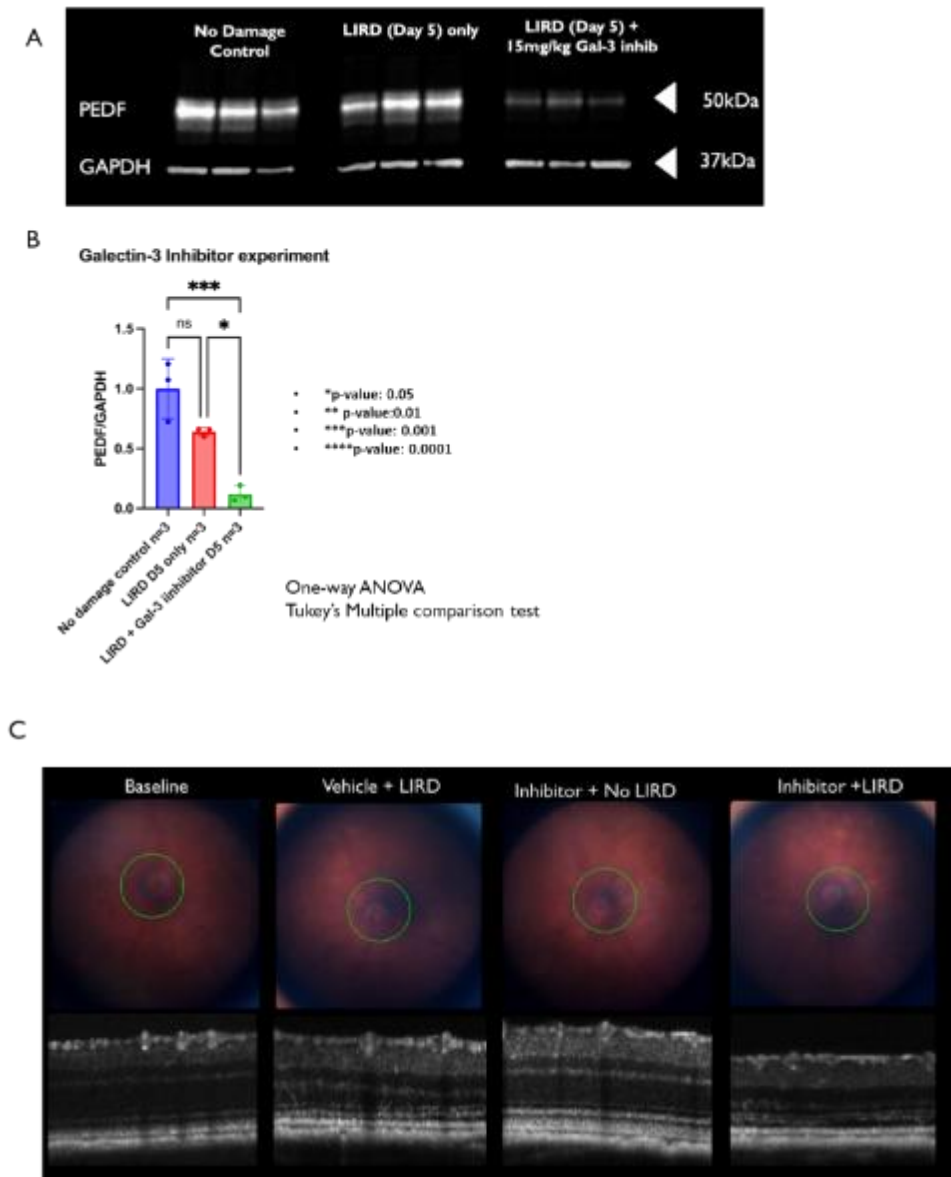
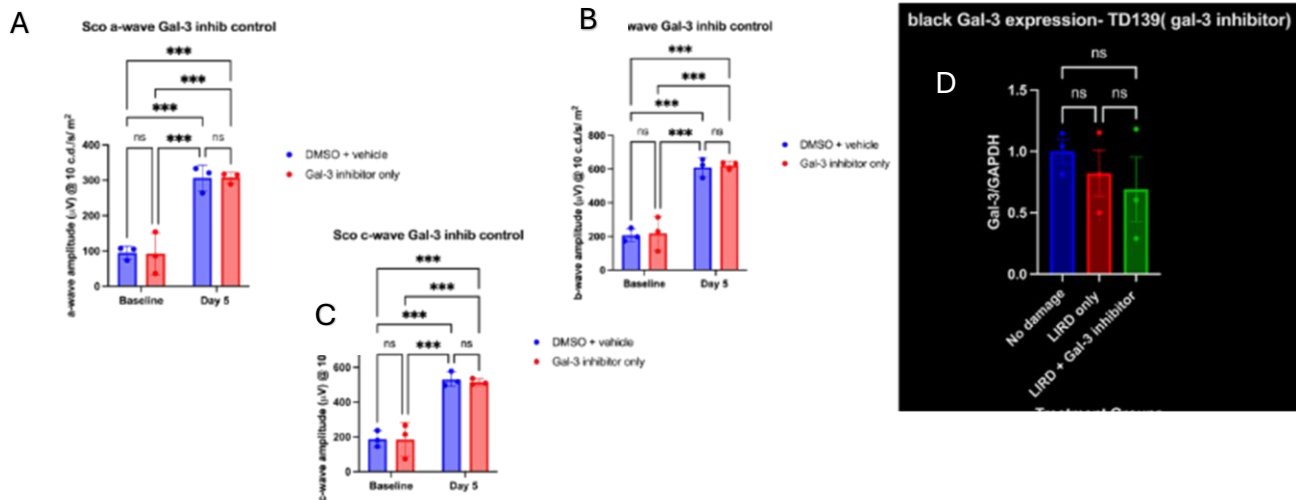


**Figure 10: Treatment with Galectin-3 inhibitor, TD139, significantly decreases PEDF expression in PEDF<sup>+/+</sup> animals after LIRD.**

Figure 10A shows a western blot exhibiting that PEDF<sup>+/+</sup> with no damage controls have high levels of PEDF, and exposing PEDF<sup>+/+</sup> animals to LIRD shows a decrease in PEDF levels. Still, it is not significantly different from no-damage controls. However, by adding the Galectin-3 inhibitor to

LIRD, there is a significant loss of PEDF compared to LIRD, and there is no damage control. 10B is a quantification of 10A. (One-way ANOVA with Tukey's multiple comparison test. No damage vs. LIRD only (Day 5 post) ns; not significant. No damage vs. LIRD (day 5) + Gal-3 inhibitor \*\*\*p-value<0.001. LIRD only (Day 5) vs. LIRD (Day 5) + Gal-3 inhibitor (\*p-value<0.05). 10C shows representative fundus and retinal images taken using SD-OCT, displaying the effects of TD139 treatment with and without LIRD. Treatment with an inhibitor in conjunction with LIRD significantly increased retinal thinning compared to the control of LIRD only.

### 5.6.13 Supplemental Figure 1: Treatment with TD139 Alone does not Deleteriously Affect Visual Function or Galectin-3 Protein Levels



### Supplemental Figure 1: Treatment with TD139 Alone does not Deleteriously Affect Visual Function or Galectin-3 Protein Levels

When comparing animals at baseline versus after 5 days of Galectin-3 inhibitor (TD139), we found that between the DMSO vehicle control and the experiment TD139 treated animals, there was not a statistically significant difference at baseline or at Day 5 (See figure S1 A-C). Additionally, when assessing total Gal-3 expression normalized to GAPDH of no damage, LIRD, only, and LIRD+ Gal-3 treated animals, the inhibitor did not deplete Galectin-3 levels, suggesting that its mode of function does not degrade Gal-3 protein. Taken together, these data show that inhibiting Galectin-3 activity using TD139 alone does not have deleterious off target effects on visual signaling or Gal-3 protein.

5.6.14 Figure 11: Schematic of Model Summary

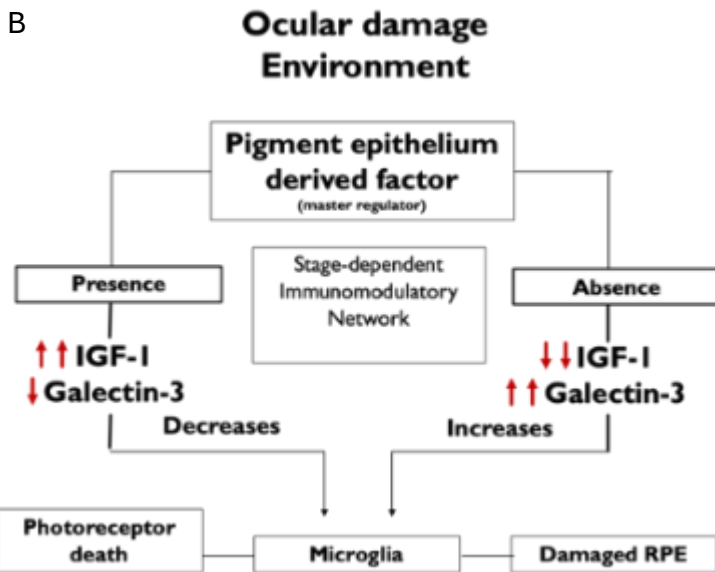
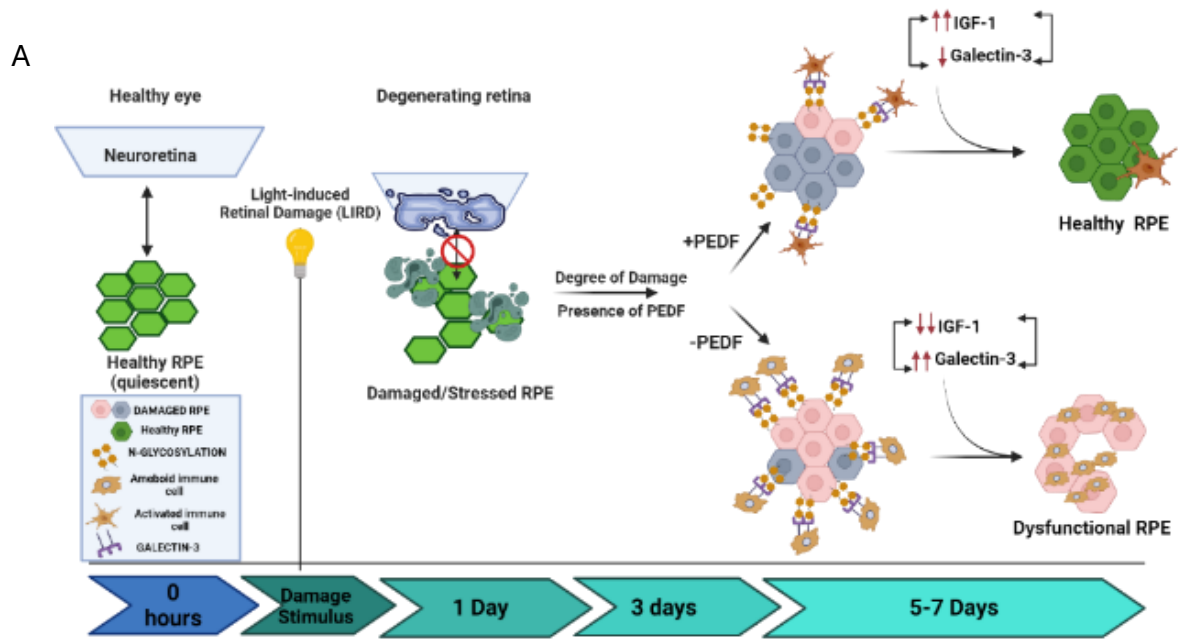


Fig 11A: Schematic summary illustrating significant differences between PEDF<sup>+/+</sup> and PEDF<sup>KO/KO</sup> animals and the impacts on IGF-1 and Galectin-3 expression.

Fig 11B: Shows the proposed immunomodulatory network influencing photoreceptor death, immune cells, and RPE cells.

Images made using Biorender.

## 6 CHAPTER 6: THE DISCUSSION

### 6.1 SUMMARY

Overall, the main objectives of this dissertation research were to 1) investigate the role of RPE in immunomodulation, 2) characterize how secreted factors from the RPE may affect outcomes of visual damage, and identify potential molecular targets for interventions that may aid in limiting inflammation-associated loss of vision. Secondly, this dissertation also investigated the role of Lysine demethylase 1 (Lsd1) in the proper organization and development of the neural retina. Lastly, this dissertation also evaluated how natural aging affects RPE morphometrics and visual function in wild-type C57BL/6J animals between the ages of 2 and 32 months.

*Lsd1* plays an indispensable role in the development and maturation of neurons within the brain; however, less was known about the role that *Lsd1* plays in the proper differentiation of retinal cell types. Previous studies by Popova et al. found that pharmacological inhibition of *Lsd1* reduced rod photoreceptors' development and shunt retinal progenitors' cells into development programs for other cell fates<sup>280</sup>. A previous study from our lab showed that the temporal localization of Lsd1 and its unique expression patterns likely play a role in retinal cell subtype speciation<sup>193</sup>. *Lsd1* localization within rod photoreceptors was particularly interesting because there was low expression compared to rods, and it formed a "ring-like" structure around the periphery of the nucleus, which coincided with the location of euchromatin. Using the data from those studies as a premise, we hypothesized that Lsd1 plays a role in the proper development and maturation of retinal cells. We made a mouse *Lsd1*<sup>f/f</sup> mouse line under the Chx10 promoter, expressed in embryonic neuroblast cells that later differentiate into inner nuclear layer cells, bipolar cells, and Muller glia. We found that the Chx10-specific deletion of Lsd1 would result in global morphological and structural ocular defects. We found that the loss of Lsd1 resulted in significant loss of a-, b-, and c-wave amplitudes, loss of retinal thickness, and loss of cells via apoptosis by TUNEL analysis<sup>191</sup>. Additional essential findings from this study are all described in Chapter 2.

Next, in Chapter 3, we created a study to build upon our knowledge of how aging affects RPE function and morphology with the topography of stress markers, like alpha-catenin and subretinal immune cell function. Currently, many studies explicitly characterizing changes in the aging RPE of mice are limited to data before or around the age of 24 months (correlating to 56-69 human years), which limits our understanding of changes in RPE morphology resulting in the cumulative loss of vision in seniors over 80 years of age<sup>(121-124)</sup>. In humans, RPE morphology is intact into middle age (38-47 years); however, by 80 years of age, there is a sudden decrease in visual function due to subtle changes in the RPE monolayer arrangement, integrity, and geometry, resulting in vision loss<sup>125</sup>. This change in RPE corresponds with a significant spike in the rate of visual disability in adults who are 80 years or older<sup>126</sup>. Thus, the data loss in this maturational cusp between 17 months and 32 months limits our understanding of early signs of aging and distress in RPE cells, resulting in vision loss. To address this gap, we utilized a C57BL/6J mouse model divided into three groups: young (P60-180), middle-aged (P365-P544), and aged (P730-P970), providing a comprehensive analysis of RPE aging. In this study, we aimed to extend our understanding of age-associated RPE changes to changes in the recruitment of subretinal immune cells and the breakdown of RPE cell borders, resulting in the cytoplasmic localization of alpha-catenin. We found region-specific differences in cytoplasmic alpha-catenin immunoreactivity, RPE area and eccentricity, and immune cell recruitment were most significant between our cohort's youngest and oldest groups. The middle-aged animals often displayed intermediary phenotypes that were distinct from the young group in some metrics and different from the oldest group in others, adding the premise of studying RPE changes in mice older than 24 months.

In Chapter 4, we aimed to redress the lack of comparative analysis of light damage in pigmented animals in the field. Previous studies using light damage models were done predominantly in albino rats and mice, presenting multiple limitations. For example, albino rats and mice spontaneously acquire lesions in the retina during ambient low light exposure with a rate of incidence of almost 55%<sup>281</sup>. This

phenomenon is less likely to happen in pigmented animals<sup>167</sup>. However, when using pigmented animals, similar damage patterns observed in albino animals required consecutive, multi-day exposures<sup>166,172</sup>. An additional limitation in previous studies was intrinsic strain differences when comparing albino strains to pigmented strains of animals, e.g., cone photoreceptor types and density differences and susceptibility to damage via elevated intraocular pressure.<sup>167,171,282</sup> This study utilized the increased retinal damage using LED light sources in conjunction with short exposure times during the dark phase (when diurnal animals are the most active) to maximize phototoxic damage susceptibility<sup>199,283</sup>. The works in this dissertation showed that utilizing the vitamin A cycle could create a line of pigmented photosensitive animals that are similar morphologically and functionally to the pigmented photoresistant animals before damage. However, after damage, pigmented photosensitive animals show severe defects in visual function via electroretinogram amplitudes, increased retinal thinning, prominent loss of the ONL (photoreceptors), and increased expression of galectin-3, inflammation-associated pattern-recognition receptor, and danger-associated molecular pattern<sup>284</sup>. Additionally, this study showed that PEDF is required for phototoxic protection since photoresistant animals without PEDF phenocopy the photosensitive animals' response to light damage. Chapter 4 characterized the light damage-associated phenotypes in pigmented animals and expounded on these findings by analyzing potential molecular determinants that may confer resistance and susceptibility to light damage.

Finally, in Chapter 5, we sought to investigate the relationship between PEDF and Galectin-3 expression, implicated in multiple studies involving ocular pathologies<sup>56,202,215,279,285-287</sup>. The immunosuppressive effects of RPE-secreted neuropeptides, Neuropeptide Y and alpha-MSH, have been well established. The RPE has an extra level of immune regulation via PEDF-Galectin-3 signaling.

In 2006, An et al. studied the secreted proteome of RPE cell cultures isolated from patients with AMD compared to control eyes<sup>17,68</sup>. Interestingly, they found a 3-fold increase in the secretion of four proteins in AMD eyes compared to controls. Among them were galectin-3 (Lgals3) and pigment

epithelium-derived factor (PEDF). Galectin-3, a member of the  $\beta$ -galactosidase binding protein family, is endogenously expressed in the cytosol and the nucleus of the RPE but can be secreted where it participates in cell lattice formation and cell-cell interaction<sup>69,70</sup>. Galectin-3 has been implicated in fine-tuning inflammatory responses due to its increased affinity for  $\beta$ -1, 6-N- glycosylation on the cell surface of RPE cells undergoing EMT and its increased secretion from RPE cells after damage<sup>69,70,74</sup>.

Coincidentally, O'koren et al. described that microglia recruited to the subretinal space during ocular damage enriched in Galectin-3, which changes the secretory profile and morphology of immune cells<sup>73</sup>. PEDF, a critical neurotrophic, non-inhibitory member of the serpin protease inhibitor family, has decreased expression during AMD, RP, diabetic retinopathy, and glaucoma<sup>209,184,211,288</sup>. Previous studies have implicated a correlation between the onset of disease/pathology, increased expression of Galectin-3 and inflammation, and reductions in PEDF expression; however, the potential immunomodulatory mechanism between PEDF and Galectin-3 is yet to be explored.

Previous studies of PEDF and light damage utilize albino animals and use exogenous supplementation with PEDF via intravitreal injections, which has drawbacks: 1) it may overshadow the impact of endogenous expression of PEDF, 2) studies in albino rats are not as translatable to normal human vision since there is pigmentation<sup>183,247</sup>. Chapter 5 has profiled changes in PEDF-null animals compared to wild-type littermates during LIRD. Typically, C57BL/6J (RPE65<sup>M450/M450</sup>) has reduced light damage risk due to slower visual cycle turnover. However, in the absence of PEDF, photoresistant animals show a significantly increased susceptibility to LIRD damage described in Chapter 4. We assessed and analyzed changes in severe loss retinal architecture via Spectral-domain optical coherence tomography (SD-OCT; Fig. 1), increased autofluorescence at the level of the RPE-photoreceptor interface (See Fig. 2), significant loss of ONL (H&E sections; Fig. 3), increased cellular apoptosis(See Fig 3B) and reduced phagocytotic capacity of the RPE (rhodopsin metabolism; Fig. 4). These changes in these structural changes in the retina coincide with functional defects in visual output (See Fig. 5). Next, we looked for changes in neurotrophic factors and biomarkers of inflammation. The expression of neurotrophic factor,

IGF-1, in PEDF-null animals and how that changes expression of subretinal microglia (IHC expression and protein quantification of IGF-1; Fig. 4). Additionally, I found that loss of PEDF results in dysregulation of galectin-3 at both the mRNA and protein expression level (qRT-PCR and protein quantification; Fig. 5). Finally, I've confirmed that the pharmacological blockade of galectin-3 activity phenocopies what was documented in my PEDF-null studies (protein quantification; Fig. 6). In figures 7 and 8, I have added simplified model summaries of how the factors I've discussed correlate with damage course and outcomes. T

## 6.2 FUTURE DIRECTION

This dissertation addressed a few important scientific questions regarding the role of PEDF in protection from light damage that extends beyond its neurotrophic attributes and proposed that it partially facilitates this protection via modulation of the immune responses via a Galectin-3 mediated mechanism. However, many unanswered questions still need to be addressed in future studies.

Further investigation of how PEDF may be modulating galectin-3 mRNA and protein expression is required. Galectin-3 has multifaceted roles ranging from development, cell differentiation, survival, and innate and adaptive immune cell tolerance<sup>284</sup>. While Gal-3 has multiple binding partners, there is no evidence, at present, that PEDF and Galectin-3 interact directly. So, the mechanism by which PEDF and the RPE modulate Galectin-3 during challenges remains in need of further study. Why does inhibition of Galectin-3 pharmacologically result in reduced expression of PEDF during challenge? Do Galectin-null mice exhibit reduced expression of PEDF? Are the impacts of PEDF on Galectin-3 during challenge temporally regulated? Is the relationship between PEDF and galectin-3 observed in the eye conserved in other tissues? One could look for direct interactions between PEDF or its known receptors and Galectin-3 via Co-immunoprecipitation, which would be relatively simple. Additionally, like Galectin-3, PEDF also has a nuclear localization sequence and has been shown to interact with Transportin SR2 in both normal RPE cells and several cancerous cell lines; however, less is known about the function of

PEDF within the nucleus or whether its localization is a sign of pathology<sup>52,289</sup>. The importance of galectin-3 and PEDF in the pathobiology of multiple diseases makes the potential co-regulatory relationship between the two a tantalizing scientific query to explore in the future.

### 6.3 SIGNIFICANCE AND IMPACT

The overarching theme of this dissertation is that RPE acts as a biosensor within the ocular environment, changing its shape and secreted factors to facilitate high-fidelity signaling and visual performance. One way the RPE functions as a biosensor is its effect on immune privilege. Immune privilege is the selective recruitment of immune cells to facilitate a limited inflammatory response during healing and repair to protect sensitive tissues within the CNS. The retinal pigment epithelium is required for immune privilege to exist within the eye<sup>249,250</sup>. The RPE facilitates this immunosuppression primarily by secreting factors like alpha-MSH and neuropeptide Y. However, this study expanded on this premise by identifying an extended level of regulation via PEDF-Galectin-3 signaling that may be important to other ocular pathologies with etiologies involving RPE dysfunction and dysregulated inflammatory responses.

Additionally, the study of epithelia in the eye modulating immune privilege via a PEDF-Galectin-3 signaling paradigm might be translatable to tumor microenvironment and granulomatous disease studies. Tumors recreate the immune-privileged microenvironment seen in the CNS via immunosuppression. Interestingly, both PEDF and Galectin-3 are dysregulated in multiple cancer subtypes, like breast and prostate cancers<sup>290-295</sup>, as well as in aging studies<sup>17</sup>. PEDF has suppressive effects on T-cells and regulates the maturation of dendritic cells<sup>215,285</sup>. Thus, this study of PEDF and Galectin-3 in the ocular microenvironment may tell us more about how the tumor microenvironment is structured and aid in improving the efficacy of therapeutic interventions.

## 7 All References (Chapters 3-5)

- 1 Strauss O. The retinal pigment epithelium in visual function. *Physiol Rev* 2005;**85**:845–81. <https://doi.org/10.1152/PHYSREV.00021.2004/ASSET/IMAGES/LARGE/Z9J0030503690006.JPEG>.
- 2 Boulton M, Dayhaw-Barker P. The role of the retinal pigment epithelium: topographical variation and ageing changes. *Eye (Lond)* 2001;**15**:384–9. <https://doi.org/10.1038/EYE.2001.141>.
- 3 Redmond TM, Yu S, Lee E, Bok D, Hamasaki D, Chen N, *et al.* Rpe65 is necessary for production of 11-cis-vitamin A in the retinal visual cycle. *Nat Genet* 1998;**20**:344–51. <https://doi.org/10.1038/3813>.
- 4 Bonilha VL. Age and disease-related structural changes in the retinal pigment epithelium. *Clin Ophthalmol* 2008;**2**:413. <https://doi.org/10.2147/OPHTH.S2151>.
- 5 Gu X, Neric NJ, Crabb JS, Crabb JW, Bhattacharya SK, Rayborn ME, *et al.* Age-Related Changes in the Retinal Pigment Epithelium (RPE). *PLoS One* 2012;**7**:e38673. <https://doi.org/10.1371/JOURNAL.PONE.0038673>.
- 6 Jackson GR, Owsley C, Curcio CA. Photoreceptor degeneration and dysfunction in aging and age-related maculopathy. *Ageing Res Rev* 2002;**1**:381–96. [https://doi.org/10.1016/S1568-1637\(02\)00007-7](https://doi.org/10.1016/S1568-1637(02)00007-7).
- 7 Ts'o MOM, Friedman E. The Retinal Pigment Epithelium: I. Comparative Histology. *Archives of Ophthalmology* 1967;**78**:641–9. <https://doi.org/10.1001/ARCHOPHT.1967.00980030643016>.
- 8 Chen M, Rajapakse D, Fraczek M, Luo C, Forrester J V., Xu H. Retinal pigment epithelial cell multinucleation in the aging eye – a mechanism to repair damage and maintain homeostasis. *Ageing Cell* 2016;**15**:436. <https://doi.org/10.1111/ACEL.12447>.
- 9 Gao H, Hollyfield JG. Aging of the human retina: Differential loss of neurons and retinal pigment epithelial cells. *Invest Ophthalmol Vis Sci* 1992;**33**:1–17.
- 10 Pang JJ, Chang B, Hawes NL, Hurd RE, Davisson MT, Li J, *et al.* Retinal degeneration 12 (rd12): A new, spontaneously arising mouse model for human Leber congenital amaurosis (LCA). *Mol Vis* 2005;**11**:152–62.
- 11 Lopez-Rodriguez R, Lantero E, Blanco-Kelly F, Avila-Fernandez A, Martin Merida I, del Pozo-Valero M, *et al.* RPE65-related retinal dystrophy: Mutational and phenotypic spectrum in 45 affected patients. *Exp Eye Res* 2021;**212**:108761. <https://doi.org/10.1016/J.EXER.2021.108761>.
- 12 Caruso RC, Aleman TS, Cideciyan A V., Roman AJ, Sumaroka A, Mullins CL, *et al.* Retinal Disease in Rpe65-Deficient Mice: Comparison to Human Leber Congenital Amaurosis Due to RPE65 Mutations. *Invest Ophthalmol Vis Sci* 2010;**51**:5304–13. <https://doi.org/10.1167/IOVS.10-5559>.
- 13 Tsujikawa M, Wada Y, Sukegawa M, Sawa M, Gomi F, Nishida K, *et al.* Age at Onset Curves of Retinitis Pigmentosa. *Archives of Ophthalmology* 2008;**126**:337–40. <https://doi.org/10.1001/ARCHOPHT.126.3.337>.
- 14 Chakravarthy U, Wong TY, Fletcher A, Pault E, Evans C, Zlateva G, *et al.* Clinical risk factors for age-related macular degeneration: a systematic review and meta-analysis. *BMC Ophthalmol* 2010;**10**:. <https://doi.org/10.1186/1471-2415-10-31>.

- 15 Inana G, Murat C, An W, Yao X, Harris IR, Cao J. RPE phagocytic function declines in age-related macular degeneration and is rescued by human umbilical tissue derived cells. *J Transl Med* 2018;**16**:63. <https://doi.org/10.1186/S12967-018-1434-6>.
- 16 Mercau ME, Akalu YT, Mazzoni F, Gyimesi G, Alberto EJ, Kong Y, *et al.* Inflammation of the retinal pigment epithelium drives early-onset photoreceptor degeneration in Mertk-associated retinitis pigmentosa. *Sci Adv* 2023;**9**:. [https://doi.org/10.1126/SCIADV.ADE9459/SUPPL\\_FILE/SCIADV.ADE9459\\_DATA\\_S1.ZIP](https://doi.org/10.1126/SCIADV.ADE9459/SUPPL_FILE/SCIADV.ADE9459_DATA_S1.ZIP).
- 17 An E, Lu X, Flippin J, Devaney JM, Halligan B, Hoffman E, *et al.* Secreted proteome profiling in human RPE cell cultures derived from donors with age related macular degeneration and age matched healthy donors. *J Proteome Res* 2006;**5**:2599–610. <https://doi.org/10.1021/PR060121J/ASSET/IMAGES/MEDIUM/PR060121JN00001.GIF>.
- 18 Cottingham K. Age-related macular degeneration and the RPE secretome. *J Proteome Res* 2006:2501. <https://doi.org/10.1021/pr062762k>.
- 19 Winkler TW, Grassmann F, Brandl C, Kiel C, Günther F, Strunz T, *et al.* Genome-wide association meta-analysis for early age-related macular degeneration highlights novel loci and insights for advanced disease. *BMC Med Genomics* 2020;**13**:1–18. <https://doi.org/10.1186/S12920-020-00760-7/FIGURES/3>.
- 20 Kauppinen A, Paterno JJ, Blasiak J, Salminen A, Kaarniranta K. Inflammation and its role in age-related macular degeneration. *Cellular and Molecular Life Sciences* 2016:1765–86. <https://doi.org/10.1007/s00018-016-2147-8>.
- 21 ten Berge JC, Fazil Z, van den Born I, Wolfs RCW, Schreurs MWJ, Dik WA, *et al.* Intraocular cytokine profile and autoimmune reactions in retinitis pigmentosa, age-related macular degeneration, glaucoma and cataract. *Acta Ophthalmol* 2019;**97**:185–92. <https://doi.org/10.1111/AOS.13899>.
- 22 Wolfensberger TJ. A short history of the retinal pigment epithelium 1998:1–4. [https://doi.org/10.1007/978-94-011-5137-5\\_1](https://doi.org/10.1007/978-94-011-5137-5_1).
- 23 Bertolotti E, Neri A, Camparini M, Macaluso C, Marigo V. Stem cells as source for retinal pigment epithelium transplantation. *Prog Retin Eye Res* 2014;**42**:130–44. <https://doi.org/10.1016/J.PRETEYERES.2014.06.002>.
- 24 George SM, Lu F, Rao M, Leach LL, Gross JM. The Retinal Pigment Epithelium: Development, Injury Responses, and Regenerative Potential in Mammalian and non-Mammalian Systems. *Prog Retin Eye Res* 2021;**85**:100969. <https://doi.org/10.1016/J.PRETEYERES.2021.100969>.
- 25 Raymond SM, Jackson IJ. The retinal pigmented epithelium is required for development and maintenance of the mouse neural retina. *Current Biology* 1995;**5**:1286–95. [https://doi.org/10.1016/S0960-9822\(95\)00255-7](https://doi.org/10.1016/S0960-9822(95)00255-7).
- 26 Heavner W, Pevny L. Eye Development and Retinogenesis. *Cold Spring Harb Perspect Biol* 2012;**4**:. <https://doi.org/10.1101/CSHPERSPECT.A008391>.
- 27 Martínez-Morales JR, Rodrigo I, Bovolenta P. Eye development: a view from the retina pigmented epithelium. *BioEssays* 2004;**26**:766–77. <https://doi.org/10.1002/BIES.20064>.
- 28 Schraermeyer U, Heimann K. Current Understanding on the Role of Retinal Pigment Epithelium and its Pigmentation. *Pigment Cell Res* 1999;**12**:219–36. <https://doi.org/10.1111/J.1600-0749.1999.TB00755.X>.
- 29 Imamura Y, Noda S, Hashizume K, Shinoda K, Yamaguchi M, Uchiyama S, *et al.* Drusen, choroidal neovascularization, and retinal pigment epithelium dysfunction in SOD1-

- deficient mice: A model of age-related macular degeneration. *Proc Natl Acad Sci U S A* 2006;**103**:11282–7. <https://doi.org/10.1073/PNAS.0602131103/ASSET/485CD330-EF95-4AE8-8D7B-97BCE3783CBF/ASSETS/GRAPHIC/ZPQ0300629400005.JPEG>.
- 30 Ferguson TA, Green DR. Autophagy and phagocytosis converge for better vision. *Autophagy* 2014;**10**:165. <https://doi.org/10.4161/AUTO.26735>.
- 31 Morimura H, Fishman GA, Grover SA, Fulton AB, Berson EL, Dryja TP. Mutations in the RPE65 gene in patients with autosomal recessive retinitis pigmentosa or leber congenital amaurosis. *Proc Natl Acad Sci U S A* 1998;**95**:3088–93. <https://doi.org/10.1073/PNAS.95.6.3088>.
- 32 Cai X, Conley SM, Naash MI. RPE65: Role in the visual cycle, human retinal disease, and gene therapy. *Ophthalmic Genet* 2009;**30**:57. <https://doi.org/10.1080/13816810802626399>.
- 33 Redmond TM, Yu S, Lee E, Bok D, Hamasaki D, Chen N, *et al.* Rpe65 is necessary for production of 11-cis-vitamin A in the retinal visual cycle. *Nature Genetics* 1998 **20**:4 1998;**20**:344–51. <https://doi.org/10.1038/3813>.
- 34 O’Neal TB, Luther EE. Retinitis Pigmentosa. *StatPearls* 2024.
- 35 Kutsyr O, Sánchez-Sáez X, Martínez-Gil N, de Juan E, Lax P, Maneu V, *et al.* Gradual Increase in Environmental Light Intensity Induces Oxidative Stress and Inflammation and Accelerates Retinal Neurodegeneration. *Invest Ophthalmol Vis Sci* 2020;**61**:. <https://doi.org/10.1167/IOVS.61.10.1>.
- 36 den Hollander AI, Roepman R, Koenekoop RK, Cremers FPM. Leber congenital amaurosis: Genes, proteins and disease mechanisms. *Prog Retin Eye Res* 2008;**27**:391–419. <https://doi.org/10.1016/J.PRETEYERES.2008.05.003>.
- 37 Xu H, Chen M, Forrester J V. Para-inflammation in the aging retina. *Prog Retin Eye Res* 2009;**28**:348–68. <https://doi.org/10.1016/J.PRETEYERES.2009.06.001>.
- 38 Xu H, Chen M, Manivannan A, Lois N, Forrester J V. Age-dependent accumulation of lipofuscin in perivascular and subretinal microglia in experimental mice. *Aging Cell* 2008;**7**:58–68. <https://doi.org/10.1111/J.1474-9726.2007.00351.X>.
- 39 Yi C, Liu J, Deng W, Luo C, Qi J, Chen M, *et al.* Old age promotes retinal fibrosis in choroidal neovascularization through circulating fibrocytes and profibrotic macrophages. *J Neuroinflammation* 2023;**20**:45. <https://doi.org/10.1186/S12974-023-02731-Y>.
- 40 Liu J, Copland DA, Theodoropoulou S, Chiu HAA, Barba MD, Mak KW, *et al.* Impairing autophagy in retinal pigment epithelium leads to inflammasome activation and enhanced macrophage-mediated angiogenesis. *Scientific Reports* 2016 **6**:1 2016;**6**:1–15. <https://doi.org/10.1038/srep20639>.
- 41 Carson MJ, Doose JM, Melchior B, Schmid CD, Ploix CC. CNS immune privilege: hiding in plain sight. *Immunol Rev* 2006;**213**:48. <https://doi.org/10.1111/J.1600-065X.2006.00441.X>.
- 42 Zhou R, Caspi RR. Ocular immune privilege. *F1000 Biol Rep* 2010;**2**:3. <https://doi.org/10.3410/B2-3>.
- 43 Streilein JW, Ma N, Wenkel H, Fong Ng T, Zamiri P. Immunobiology and privilege of neuronal retina and pigment epithelium transplants. *Vision Res* 2002;**42**:487–95. [https://doi.org/10.1016/S0042-6989\(01\)00185-7](https://doi.org/10.1016/S0042-6989(01)00185-7).
- 44 Cone RE, Pais R. Anterior Chamber-Associated Immune Deviation (ACAID): An Acute Response to Ocular Insult Protects from Future Immune-Mediated Damage? *Ophthalmol Eye Dis* 2009;**1**:33. <https://doi.org/10.4137/OED.S2858>.

- 45 Qiao H, Lucas K, Stein-Streilein J. Retinal Laser Burn Disrupts Immune Privilege in the Eye. *Am J Pathol* 2009;**174**:414. <https://doi.org/10.2353/AJPATH.2009.080766>.
- 46 Streilein JW, Ma N, Wenkel H, Fong Ng T, Zamiri P. Immunobiology and privilege of neuronal retina and pigment epithelium transplants. *Vision Res* 2002;**42**:487–95. [https://doi.org/10.1016/S0042-6989\(01\)00185-7](https://doi.org/10.1016/S0042-6989(01)00185-7).
- 47 Jiang LQ, Jorquera M, Streilein JW. Subretinal space and vitreous cavity as immunologically privileged sites for retinal allografts. *Invest Ophthalmol Vis Sci* 1993;**34**:3347–54.
- 48 Phan TA, Taylor AW. The neuropeptides  $\alpha$ -MSH and NPY modulate phagocytosis and phagolysosome activation in RAW 264.7 cells. *J Neuroimmunol* 2013;**260**:9–16. <https://doi.org/10.1016/J.JNEUROIM.2013.04.019>.
- 49 Benque IJ, Xia P, Shannon R, Ng TF, Taylor AW. The Neuropeptides of Ocular Immune Privilege,  $\alpha$ -MSH and NPY, Suppress Phagosome Maturation in Macrophages. *Immunohorizons* 2018;**2**:314–23. <https://doi.org/10.4049/IMMUNOHORIZONS.1800049>.
- 50 Taylor AW, Wayne Streilein J, Cousins SW. Alpha-melanocyte-stimulating hormone suppresses antigen-stimulated T cell production of gamma-interferon. *Neuroimmunomodulation* 1994;**1**:188–94. <https://doi.org/10.1159/000097167>.
- 51 Xu X, Zhang SSM, Barnstable CJ, Tombran-Tink J. Molecular phylogeny of the antiangiogenic and neurotrophic serpin, pigment epithelium derived factor in vertebrates. *BMC Genomics* 2006;**7**:248. <https://doi.org/10.1186/1471-2164-7-248>.
- 52 Tombran-Tink J, Aparicio S, Xu X, Tink AR, Lara N, Sawant S, *et al*. PEDF and the serpins: Phylogeny, sequence conservation, and functional domains. *J Struct Biol* 2005;**151**:130–50. <https://doi.org/10.1016/J.JSB.2005.05.005>.
- 53 Tombran-Tink J, Johnson L V. Neuronal differentiation of retinoblastoma cells induced by medium conditioned by human RPE cells. *Invest Ophthalmol Vis Sci* 1989;**30**:1700–7.
- 54 Tombran-Tink J, Chader GG, Johnson L V. PEDF: A pigment epithelium-derived factor with potent neuronal differentiative activity. *Exp Eye Res* 1991:411–4. [https://doi.org/10.1016/0014-4835\(91\)90248-D](https://doi.org/10.1016/0014-4835(91)90248-D).
- 55 Matsui T, Higashimoto Y, Yamagishi SI. Laminin receptor mediates anti-inflammatory and anti-thrombogenic effects of pigment epithelium-derived factor in myeloma cells. *Biochem Biophys Res Commun* 2014;**443**:847–51. <https://doi.org/10.1016/J.BBRC.2013.12.060>.
- 56 Ho TC, Fan NW, Yeh SI, Chen SL, Tsao YP. The Therapeutic Effects of a PEDF-Derived Short Peptide on Murine Experimental Dry Eye Involves Suppression of MMP-9 and Inflammation. *Transl Vis Sci Technol* 2022;**11**:. <https://doi.org/10.1167/TVST.11.10.12>.
- 57 Sugita Y, Becerra SP, Chader GJ, Schwartz JP. Pigment epithelium-derived factor (PEDF) has direct effects on the metabolism and proliferation of microglia and indirect effects on astrocytes. *J Neurosci Res* 1997;**49**:710–8. [https://doi.org/10.1002/\(SICI\)1097-4547\(19970915\)49:6<710::AID-JNR5>3.0.CO;2-A](https://doi.org/10.1002/(SICI)1097-4547(19970915)49:6<710::AID-JNR5>3.0.CO;2-A).
- 58 Singh RB, Blanco T, Mittal SK, Alemi H, Chauhan SK, Chen Y, *et al*. Pigment Epithelium-Derived Factor Enhances the Suppressive Phenotype of Regulatory T Cells in a Murine Model of Dry Eye Disease. *American Journal of Pathology* 2021;**191**:720–9. <https://doi.org/10.1016/j.ajpath.2021.01.003>.
- 59 Zhang T, Yin P, Zhang Z, Xu B, Che D, Dai Z, *et al*. Deficiency of pigment epithelium-derived factor in nasopharyngeal carcinoma cells triggers the epithelial–mesenchymal

- transition and metastasis. *Cell Death & Disease* 2017 8:6 2017;**8**:e2838–e2838. <https://doi.org/10.1038/cddis.2017.114>.
- 60 Yang X, Chung JY, Rai U, Esumi N. Cadherins in the retinal pigment epithelium (RPE) revisited: P-cadherin is the highly dominant cadherin expressed in human and mouse RPE in vivo. *PLoS One* 2018;**13**:. <https://doi.org/10.1371/journal.pone.0191279>.
- 61 Ishiyama N, Sarpal R, Wood MN, Barrick SK, Nishikawa T, Hayashi H, *et al*. Force-dependent allostery of the  $\alpha$ -catenin actin-binding domain controls adherens junction dynamics and functions. *Nat Commun* 2018;**9**:1–17. <https://doi.org/10.1038/s41467-018-07481-7>.
- 62 Ma W, Zhao L, Fontainhas AM, Fariss RN, Wong WT. Microglia in the mouse retina alter the structure and function of retinal pigmented epithelial cells: A potential cellular interaction relevant to AMD. *PLoS One* 2009;**4**:. <https://doi.org/10.1371/journal.pone.0007945>.
- 63 Takanohashi A, Yabe T, Schwartz JP. Pigment epithelium-derived factor induces the production of chemokines by rat microglia. *Glia* 2005;**51**:266–78. <https://doi.org/10.1002/glia.20203>.
- 64 Cevenini A, Orrù S, Mancini A, Alfieri A, Buono P, Imperlini E. Molecular Signatures of the Insulin-Like Growth Factor 1-Mediated Epithelial-Mesenchymal Transition in Breast, Lung and Gastric Cancers. *Int J Mol Sci* 2018;**19**:. <https://doi.org/10.3390/IJMS19082411>.
- 65 Ruberte J, Ayuso E, Navarro M, Carretero A, Nacher V, Haurigot V, *et al*. Increased ocular levels of IGF-1 in transgenic mice lead to diabetes-like eye disease. *Journal of Clinical Investigation* 2004;**113**:1149. <https://doi.org/10.1172/JCI19478>.
- 66 Salminen A, Kaarniranta K, Kauppinen A. Insulin/IGF-1 signaling promotes immunosuppression via the STAT3 pathway: impact on the aging process and age-related diseases. *Inflammation Research* 2021;**70**:1043. <https://doi.org/10.1007/S00011-021-01498-3>.
- 67 Wang, Angeline L., Kothary, Piyush, Del Monte M. *Effect of IGF-1 and Pigment Epithelium Derived Factor on Epo Production in hRPE Cells | IOVS | ARVO Journals*. Investigative Ophthalmology & Visual Science. n.d. URL: <https://iovs.arvojournals.org/article.aspx?articleid=2359007> (Accessed 9 June 2021).
- 68 Yuan X, Gu X, Crabb JS, Yue X, Shadrach K, Hollyfield JG, *et al*. Quantitative proteomics: Comparison of the macular bruch membrane/choroid complex from age-related macular degeneration and normal eyes. *Molecular and Cellular Proteomics* 2010;**9**:1031–46. <https://doi.org/10.1074/mcp.M900523-MCP200>.
- 69 Priglinger CS, Obermann J, Szober CM, Merl-Pham J, Ohmayer U, Behler J, *et al*. Epithelial-to-Mesenchymal Transition of RPE Cells In Vitro Confers Increased  $\beta$ 1,6-N-Glycosylation and Increased Susceptibility to Galectin-3 Binding. *PLoS One* 2016;**11**:. <https://doi.org/10.1371/JOURNAL.PONE.0146887>.
- 70 Hughes RC. Secretion of the galectin family of mammalian carbohydrate-binding proteins. *Biochim Biophys Acta Gen Subj* 1999:172–85. [https://doi.org/10.1016/S0304-4165\(99\)00177-4](https://doi.org/10.1016/S0304-4165(99)00177-4).
- 71 Caridi B, Doncheva D, Sivaprasad S, Turowski P. Galectins in the Pathogenesis of Common Retinal Disease. *Front Pharmacol* 2021;**12**:. <https://doi.org/10.3389/fphar.2021.687495>.

- 72 Rahimian R, Lively S, Abdelhamid E, Lalancette-Hebert M, Schlichter L, Sato S, *et al.* Delayed Galectin-3-Mediated Reprogramming of Microglia After Stroke is Protective 2018. <https://doi.org/10.1007/s12035-019-1527-0>.
- 73 O’Koren EG, Yu C, Klingeborn M, Wong AYW, Prigge CL, Mathew R, *et al.* Microglial Function Is Distinct in Different Anatomical Locations during Retinal Homeostasis and Degeneration. *Immunity* 2019;**50**:723-737.e7. <https://doi.org/10.1016/j.immuni.2019.02.007>.
- 74 Ronning KE, Karlen SJ, Miller EB, Burns ME. Molecular profiling of resident and infiltrating mononuclear phagocytes during rapid adult retinal degeneration using single-cell RNA sequencing. *Sci Rep* 2019;**9**:. <https://doi.org/10.1038/s41598-019-41141-0>.
- 75 Yu C, Saban DR. Identification of a Unique Subretinal Microglia Type in Retinal Degeneration Using Single Cell RNA-Seq. *Adv Exp Med Biol*, vol. 1185. Springer; 2019. p. 181–6.
- 76 Holtman IR, Raj DD, Miller JA, Schaafsma W, Yin Z, Brouwer N, *et al.* Induction of a common microglia gene expression signature by aging and neurodegenerative conditions: a co-expression meta-analysis. *Acta Neuropathol Commun* 2015;**3**:31. <https://doi.org/10.1186/S40478-015-0203-5/FIGURES/6>.
- 77 Lalancette-Hébert M, Swarup V, Beaulieu JM, Bohacek I, Abdelhamid E, Weng YC, *et al.* Galectin-3 is required for resident microglia activation and proliferation in response to ischemic injury. *Journal of Neuroscience* 2012;**32**:10383–95. <https://doi.org/10.1523/JNEUROSCI.1498-12.2012>.
- 78 O’Donnell SL, Frederick TJ, Krady JK, Vannucci SJ, Wood TL. IGF-I and microglia/macrophage proliferation in the ischemic mouse brain. *Glia* 2002;**39**:85–97. <https://doi.org/10.1002/glia.10081>.
- 79 Labandeira-Garcia JL, Costa-Besada MA, Labandeira CM, Villar-Cheda B, Rodríguez-Perez AI. Insulin-like growth factor-1 and neuroinflammation. *Front Aging Neurosci* 2017. <https://doi.org/10.3389/fnagi.2017.00365>.
- 80 Sivakumar V, Zhang Y, Ling EA, Foulds WS, Kaur C. Insulin-like growth factors, angiopoietin-2, and pigment epithelium-derived growth factor in the hypoxic retina. *J Neurosci Res* 2008;**86**:702–11. <https://doi.org/10.1002/JNR.21519>.
- 81 Yamagishi S, Koga Y, Sotokawauchi A, Hashizume N, Fukahori S, Matsui T, *et al.* Therapeutic Potential of Pigment Epithelium-derived Factor in Cancer. *Curr Pharm Des* 2019;**25**:313–24. <https://doi.org/10.2174/1381612825666190319112106>.
- 82 Bhutto IA, McLeod DS, Hasegawa T, Kim SY, Merges C, Tong P, *et al.* Pigment epithelium-derived factor (PEDF) and vascular endothelial growth factor (VEGF) in aged human choroid and eyes with age-related macular degeneration. *Exp Eye Res* 2006;**82**:99–110. <https://doi.org/10.1016/j.exer.2005.05.007>.
- 83 Pauleikhoff D, Harper CA, Marshall J, Bird AC. Aging Changes in Bruch’s Membrane: A Histochemical and Morphologic Study. *Ophthalmology* 1990;**97**:171–8. [https://doi.org/10.1016/S0161-6420\(90\)32619-2](https://doi.org/10.1016/S0161-6420(90)32619-2).
- 84 Gullapalli VK, Sugino IK, Van Patten Y, Shah S, Zarbin MA. Impaired RPE survival on aged submacular human Bruch’s membrane. *Exp Eye Res* 2005;**80**:235–48. <https://doi.org/10.1016/j.exer.2004.09.006>.
- 85 Feeney-Burns L, Ellersieck MR. Age-Related Changes in the Ultrastructure of Bruch’s Membrane. *Am J Ophthalmol* 1985;**100**:686–97. [https://doi.org/10.1016/0002-9394\(85\)90625-7](https://doi.org/10.1016/0002-9394(85)90625-7).

- 86 Rashid A, Bhatia SK, Mazzitello KI, Chrenek MA, Zhang Q, Boatright JH, *et al.* RPE cell and sheet properties in normal and diseased eyes. *Adv Exp Med Biol*, vol. 854. Springer New York LLC; 2016. p. 757–63.
- 87 Bhatia SK, Rashid A, Chrenek MA, Zhang Q, Bruce BB, Klein M, *et al.* Analysis of RPE morphometry in human eyes. *Mol Vis* 2016;**22**:898–916.
- 88 Foulds WS, Glasgow C. The Choroidal Circulation and Retinal Metabolism-An Overview. *Eye* 1990;**4**:243–8.
- 89 Gregory CY, Converse CA, Foulds WS. Effect of glycoconjugates on rod outer segment phagocytosis by retinal pigment epithelial explants in vitro assessed by a specific double radioimmunoassay procedure. *Curr Eye Res* 1990;**9**:65–77.  
<https://doi.org/10.3109/02713689009000056>.
- 90 Sparrow JR, Hicks D, Hamel CP. The retinal pigment epithelium in health and disease. *Curr Mol Med* 2010;**10**:802–23. <https://doi.org/10.2174/156652410793937813>.
- 91 Raymond SM, Jackson IJ. The retinal pigmented epithelium is required for development and maintenance of the mouse neural retina. *Curr Biol* 1995;**5**:1286–95.  
[https://doi.org/10.1016/S0960-9822\(95\)00255-7](https://doi.org/10.1016/S0960-9822(95)00255-7).
- 92 Yang S, Zhou J, Li D. Functions and Diseases of the Retinal Pigment Epithelium. *Front Pharmacol* 2021;**12**:727870. <https://doi.org/10.3389/FPHAR.2021.727870/BIBTEX>.
- 93 Wang Y, Grenell A, Zhong F, Yam M, Hauer A, Gregor E, *et al.* Metabolic signature of the aging eye in mice. *Neurobiol Aging* 2018;**71**:223–33.  
<https://doi.org/10.1016/J.NEUROBIOLAGING.2018.07.024>.
- 94 Gao H, Hollyfield JG. Aging of the human retina. Differential loss of neurons and retinal pigment epithelial cells. *Invest Ophthalmol Vis Sci* 1992;**33**:1–17.
- 95 Panda-Jonas S, Jonas JB, Jakobczyk-Zmija M. Retinal pigment epithelial cell count, distribution, and correlations in normal human eyes. *Am J Ophthalmol* 1996;**121**:181–9.  
[https://doi.org/10.1016/S0002-9394\(14\)70583-5](https://doi.org/10.1016/S0002-9394(14)70583-5).
- 96 Dorey CK, Wu G, Ebenstein D, Garsd A, Weiter JJ. Cell loss in the aging retina. Relationship to lipofuscin accumulation and macular degeneration. *Invest Ophthalmol Vis Sci* 1989;**30**:1691–9.
- 97 Bhutto I, Lutty G. Understanding age-related macular degeneration (AMD): Relationships between the photoreceptor/retinal pigment epithelium/Bruch’s membrane/choriocapillaris complex. *Mol Aspects Med* 2012;**33**:295. <https://doi.org/10.1016/J.MAM.2012.04.005>.
- 98 Boulton M, Docchio F, Dayhaw-Barker P, Ramponi R, Cubeddu R. Age-related changes in the morphology, absorption and fluorescence of melanosomes and lipofuscin granules of the retinal pigment epithelium. *Vision Res* 1990;**30**:1291–303.  
[https://doi.org/10.1016/0042-6989\(90\)90003-4](https://doi.org/10.1016/0042-6989(90)90003-4).
- 99 Holz FG, Bellmann C, Margaritidis M, Schütt F, Otto TP, Völcker HE. Patterns of increased in vivo fundus autofluorescence in the junctional zone of geographic atrophy of the retinal pigment epithelium associated with age-related macular degeneration. *Graefes Archive for Clinical and Experimental Ophthalmology* 1999;**237**:145–52.  
<https://doi.org/10.1007/S004170050209>.
- 100 Yi C, Liu J, Deng W, Luo C, Qi J, Chen M, *et al.* Old age promotes retinal fibrosis in choroidal neovascularization through circulating fibrocytes and profibrotic macrophages. *J Neuroinflammation* 2023;**20**:45. <https://doi.org/10.1186/S12974-023-02731-Y>.
- 101 Zhang Q, Presswalla F, Calton M, Charniga C, Stern J, Temple S, *et al.* Highly Differentiated Human Fetal RPE Cultures Are Resistant to the Accumulation and Toxicity

- of Lipofuscin-Like Material. *Invest Ophthalmol Vis Sci* 2019;**60**:3468. <https://doi.org/10.1167/IOVS.19-26690>.
- 102 Ardeljan D, Chan CC. Aging is not a disease: distinguishing age-related macular degeneration from aging. *Prog Retin Eye Res* 2013;**37**:68–89. <https://doi.org/10.1016/J.PRETEYERES.2013.07.003>.
- 103 Karampelas M, Sim DA, Keane PA, Papastefanou VP, Sadda SR, Tufail A, *et al*. Evaluation of retinal pigment epithelium-Bruch's membrane complex thickness in dry age-related macular degeneration using optical coherence tomography. *British Journal of Ophthalmology* 2013;**97**:1256. <https://doi.org/10.1136/BJOPHTHALMOL-2013-303219>.
- 104 Ehrlich R, Harris A, Kheradiya NS, Winston DM, Ciulla TA, Wirostko B. Age-related macular degeneration and the aging eye. *Clin Interv Aging* 2008;**3**:473. <https://doi.org/10.2147/CIA.S2777>.
- 105 Grossniklaus HE, Nickerson JM, Edelhauser HF, Bergman LAMK, Berglin L. Anatomic Alterations in Aging and Age-Related Diseases of the Eye. *Invest Ophthalmol Vis Sci* 2013;**54**:ORSF23. <https://doi.org/10.1167/IOVS.13-12711>.
- 106 Lambert NG, ElShelmani H, Singh MK, Mansergh FC, Wride MA, Padilla M, *et al*. Risk factors and biomarkers of age-related macular degeneration. *Prog Retin Eye Res* 2016:64–102. <https://doi.org/10.1016/j.preteyeres.2016.04.003>.
- 107 Fritsche LG, Chen W, Schu M, Yaspan BL, Yu Y, Thorleifsson G, *et al*. Seven new loci associated with age-related macular degeneration. *Nat Genet* 2013;**45**:433–9. <https://doi.org/10.1038/ng.2578>.
- 108 Fritsche LG, Igl W, Bailey JNC, Grassmann F, Sengupta S, Bragg-Gresham JL, *et al*. A large genome-wide association study of age-related macular degeneration highlights contributions of rare and common variants. *Nat Genet* 2016;**48**:134–43. <https://doi.org/10.1038/NG.3448>.
- 109 Chew EY, Clemons TE, SanGiovanni JP, Danis R, Ferris FL, Elman M, *et al*. Lutein + zeaxanthin and omega-3 fatty acids for age-related macular degeneration: the Age-Related Eye Disease Study 2 (AREDS2) randomized clinical trial. *JAMA* 2013;**309**:2005–15. <https://doi.org/10.1001/JAMA.2013.4997>.
- 110 van Asten F, Simmons M, Singhal A, Keenan TD, Ratnapriya R, Agrón E, *et al*. A Deep Phenotype Association Study reveals specific phenotype associations with genetic variants in age-related macular degeneration: Age-Related Eye Disease Study 2 (AREDS2) Report No. 14. *Ophthalmology* 2018;**125**:559. <https://doi.org/10.1016/J.OPHTHA.2017.09.023>.
- 111 Chew EY, Clemons T, Sangiovanni JP, Danis R, Domalpally A, McBee W, *et al*. The age-related eye disease study 2 (AREDS2): Study design and baseline characteristics (AREDS2 Report Number 1). *Ophthalmology* 2012;**119**:2282–9. <https://doi.org/10.1016/j.ophtha.2012.05.027>.
- 112 Black JRM, Clark SJ. Age-related macular degeneration: genome-wide association studies to translation. *Genetics in Medicine* 2016;**18**:283. <https://doi.org/10.1038/GIM.2015.70>.
- 113 Kassoff A, Kassoff J, Buehler J, Eglow M, Kaufman F, Mehu M, *et al*. A Randomized, Placebo-Controlled, Clinical Trial of High-Dose Supplementation With Vitamins C and E, Beta Carotene, and Zinc for Age-Related Macular Degeneration and Vision Loss: AREDS Report No. 8. *Archives of Ophthalmology* 2001;**119**:1417. <https://doi.org/10.1001/ARCHOPHT.119.10.1417>.
- 114 Denny JC, Ritchie MD, Basford MA, Pulley JM, Bastarache L, Brown-Gentry K, *et al*. PheWAS: demonstrating the feasibility of a phenome-wide scan to discover gene–disease

- associations. *Bioinformatics* 2010;**26**:1205.  
<https://doi.org/10.1093/BIOINFORMATICS/BTQ126>.
- 115 Varesi A, Chirumbolo S, Campagnoli LIM, Pierella E, Piccini GB, Carrara A, *et al.* The Role of Antioxidants in the Interplay between Oxidative Stress and Senescence. *Antioxidants (Basel)* 2022;**11**:. <https://doi.org/10.3390/ANTIOX11071224>.
- 116 Voisin A, Gaillard A, Balbous A, Leveziel N. Proteins Associated with Phagocytosis Alteration in Retinal Pigment Epithelial Cells Derived from Age-Related Macular Degeneration Patients. *Antioxidants* 2022;**11**:. <https://doi.org/10.3390/ANTIOX11040713>.
- 117 Ida H, Boylan SA, Weigel AL, Hjelmeland LM. Age-related changes in the transcriptional profile of mouse RPE/choroid. *Physiol Genomics* 2004;**15**:258–62.  
[https://doi.org/10.1152/PHYSIOLGENOMICS.00126.2003/SUPPL\\_FILE/SUPPTABLE.PDF](https://doi.org/10.1152/PHYSIOLGENOMICS.00126.2003/SUPPL_FILE/SUPPTABLE.PDF).
- 118 Ma JYW, Greferath U, Wong JHC, Fothergill LJ, Jobling AI, Vessey KA, *et al.* Aging induces cell loss and a decline in phagosome processing in the mouse retinal pigment epithelium. *Neurobiol Aging* 2023;**128**:1–16.  
<https://doi.org/10.1016/J.NEUROBIOLAGING.2023.03.003>.
- 119 Chen M, Rajapakse D, Fraczek M, Luo C, Forrester J V., Xu H. Retinal pigment epithelial cell multinucleation in the aging eye – a mechanism to repair damage and maintain homeostasis. *Aging Cell* 2016;**15**:436. <https://doi.org/10.1111/ACEL.12447>.
- 120 Baumann CW, Kwak D, Thompson LD V. Assessing onset, prevalence and survival in mice using a frailty phenotype. *Aging (Albany NY)* 2018;**10**:4042.  
<https://doi.org/10.18632/AGING.101692>.
- 121 Ma JYW, Greferath U, Wong JHC, Fothergill LJ, Jobling AI, Vessey KA, *et al.* Aging induces cell loss and a decline in phagosome processing in the mouse retinal pigment epithelium. *Neurobiol Aging* 2023;**128**:1–16.  
<https://doi.org/10.1016/J.NEUROBIOLAGING.2023.03.003>.
- 122 Yako T, Nakamura M, Otsu W, Nakamura S, Shimazawa M, Hara H. Mitochondria dynamics in the aged mice eye and the role in the RPE phagocytosis. *Exp Eye Res* 2021;**213**:108800. <https://doi.org/10.1016/J.EXER.2021.108800>.
- 123 Imamura Y, Noda S, Hashizume K, Shinoda K, Yamaguchi M, Uchiyama S, *et al.* Drusen, choroidal neovascularization, and retinal pigment epithelium dysfunction in SOD1-deficient mice: A model of age-related macular degeneration. *Proc Natl Acad Sci U S A* 2006;**103**:11282–7. <https://doi.org/10.1073/PNAS.0602131103/ASSET/485CD330-EF95-4AE8-8D7B-97BCE3783CBF/ASSETS/GRAPHIC/ZPQ0300629400005.JPEG>.
- 124 Chucair-Elliott AJ, Ocañas SR, Pham K, Machalinski A, Plafker S, Stout MB, *et al.* Age- and sex- divergent translomic responses of the mouse retinal pigmented epithelium. *Neurobiol Aging* 2024;**140**:41–59.  
<https://doi.org/10.1016/J.NEUROBIOLAGING.2024.04.012>.
- 125 Tarau IS, Berlin A, Curcio CA, Ach T. The Cytoskeleton of the Retinal Pigment Epithelium: from Normal Aging to Age-Related Macular Degeneration. *Int J Mol Sci* 2019;**20**:. <https://doi.org/10.3390/IJMS20143578>.
- 126 Pelletier AL, Rojas-Roldan L, Coffin J. Vision Loss in Older Adults 2016;**94**:.  
 127 Weikel KA, FitzGerald P, Shang F, Andrea Caceres M, Bian Q, Handa JT, *et al.* Natural history of age-related retinal lesions that precede AMD in mice fed high or low glycemic index diets. *Invest Ophthalmol Vis Sci* 2012;**53**:622–32. <https://doi.org/10.1167/IOVS.11-8545/-DCSUPPLEMENTAL>.

- 128 Kim Y-K, Yu H, Summers VR, Donaldson KJ, Ferdous S, Shelton D, *et al.* Morphometric Analysis of Retinal Pigment Epithelial Cells From C57BL/6J Mice During Aging. *Invest Ophthalmol Vis Sci* 2021;**62**:32–32. <https://doi.org/10.1167/IOVS.62.2.32>.
- 129 Sun N, Shibata B, Hess JF, Fitzgerald PG. An alternative means of retaining ocular structure and improving immunoreactivity for light microscopy studies. *Mol Vis* 2015;**21**:428.
- 130 Zhang N, Zhang X, Girardot PE, Chrenek MA, Sellers JT, Li Y, *et al.* Electrophysiologic and Morphologic Strain Differences in a Low-Dose NaIO<sub>3</sub>-Induced Retinal Pigment Epithelium Damage Model. *Transl Vis Sci Technol* 2021;**10**:. <https://doi.org/10.1167/TVST.10.8.10>.
- 131 Yonemura S, Wada Y, Watanabe T, Nagafuchi A, Shibata M.  $\alpha$ -Catenin as a tension transducer that induces adherens junction development. *Nature Cell Biology* 2010 **12**:6 2010;**12**:533–42. <https://doi.org/10.1038/ncb2055>.
- 132 Gates J, Peifer M. Can 1000 reviews be wrong? Actin, alpha-Catenin, and adherens junctions. *Cell* 2005;**123**:769–72. <https://doi.org/10.1016/J.CELL.2005.11.009>.
- 133 Del Priore L V., Kuo YH, Tezel TH. Age-related changes in human RPE cell density and apoptosis proportion in situ. *Invest Ophthalmol Vis Sci* 2002;**43**:3312–8.
- 134 Chen H, Lukas TJ, Du N, Suyeoka G, Neufeld AH. Dysfunction of the Retinal Pigment Epithelium with Age: Increased Iron Decreases Phagocytosis and Lysosomal Activity. *Invest Ophthalmol Vis Sci* 2009;**50**:1895–902. <https://doi.org/10.1167/IOVS.08-2850>.
- 135 Wong JHC, Ma JYW, Jobling AI, Brandli A, Greferath U, Fletcher EL, *et al.* Exploring the pathogenesis of age-related macular degeneration: A review of the interplay between retinal pigment epithelium dysfunction and the innate immune system. *Front Neurosci* 2022;**16**:1009599. <https://doi.org/10.3389/FNINS.2022.1009599/BIBTEX>.
- 136 Ferrington DA, Sinha D, Kaarniranta K. Defects in Retinal Pigment Epithelial Cell Proteolysis and the Pathology Associated with Age-related Macular Degeneration. *Prog Retin Eye Res* 2016;**51**:69. <https://doi.org/10.1016/J.PRETEYERES.2015.09.002>.
- 137 Pennesi ME, Neuringer M, Courtney RJ. Animal models of age related macular degeneration. *Mol Aspects Med* 2012;**33**:487. <https://doi.org/10.1016/J.MAM.2012.06.003>.
- 138 Jiang Y, Qi X, Chrenek MA, Gardner C, Boatright JH, Grossniklaus HE, *et al.* Functional principal component analysis reveals discriminating categories of retinal pigment epithelial morphology in mice. *Invest Ophthalmol Vis Sci* 2013;**54**:7274–83. <https://doi.org/10.1167/iov.13-12450>.
- 139 Jiang Y, Qi X, Chrenek MA, Gardner C, Dalal N, Boatright JH, *et al.* Analysis of mouse RPE sheet morphology gives discriminatory categories. *Adv Exp Med Biol* 2014;**801**:601–7. [https://doi.org/10.1007/978-1-4614-3209-8\\_76](https://doi.org/10.1007/978-1-4614-3209-8_76).
- 140 Boatright JH, Dalal N, Chrenek MA, Gardner C, Ziesel A, Jiang Y, *et al.* Methodologies for analysis of patterning in the mouse RPE sheet. *Mol Vis* 2015;**21**:40.
- 141 Drees F, Pokutta S, Yamada S, Nelson WJ, Weis WI.  $\alpha$ -catenin is a molecular switch that binds E-cadherin- $\beta$ -catenin and regulates actin-filament assembly. *Cell* 2005;**123**:903–15. <https://doi.org/10.1016/j.cell.2005.09.021>.
- 142 Maiden SL, Hardin J. The secret life of  $\alpha$ -catenin: moonlighting in morphogenesis. *J Cell Biol* 2011;**195**:543–52. <https://doi.org/10.1083/JCB.201103106>.

- 143 Kemler R. From cadherins to catenins: cytoplasmic protein interactions and regulation of cell adhesion. *Trends Genet* 1993;**9**:317–21. [https://doi.org/10.1016/0168-9525\(93\)90250-L](https://doi.org/10.1016/0168-9525(93)90250-L).
- 144 Coulombre JL, Coulombre AJ. Regeneration of neural retina from the pigmented epithelium in the chick embryo. *Dev Biol* 1965;**12**:79–92. [https://doi.org/10.1016/0012-1606\(65\)90022-9](https://doi.org/10.1016/0012-1606(65)90022-9).
- 145 Piskova T, Kozyrina AN, Di Russo J. Mechanobiological implications of age-related remodelling in the outer retina. *Biomaterials Advances* 2023;**147**:213343–213343. <https://doi.org/10.1016/J.BIOADV.2023.213343>.
- 146 Sarna, Tadeusz; Burke, Janice M.; Korytowski, Witold; Rozanowska, Malgorzata; Skumatz, Christine MB.; Zareba, Agnieszka; Zareba M. Loss of Melanin from human RPE with aging: Possible role of melanin photooxidation. *Exp Eye Res* 2003;**76**:89–98. [https://doi.org/10.1016/s0014-4835\(02\)00247-6](https://doi.org/10.1016/s0014-4835(02)00247-6).
- 147 Senabouth A, Daniszewski M, Lidgerwood GE, Liang HH, Hernández D, Mirzaei M, *et al.* Transcriptomic and proteomic retinal pigment epithelium signatures of age-related macular degeneration. *Nature Communications* 2022 *13:1* 2022;**13**:1–18. <https://doi.org/10.1038/s41467-022-31707-4>.
- 148 Ma W, Cojocar R, Gotoh N, Gieser L, Villasmil R, Cogliati T, *et al.* Gene expression changes in aging retinal microglia: Relationship to microglial support functions and regulation of activation. *Neurobiol Aging* 2013;**34**:2310–21. <https://doi.org/10.1016/j.neurobiolaging.2013.03.022>.
- 149 Ma W, Zhao L, Wong WT. Microglia in the Outer Retina and their Relevance to Pathogenesis of Age-Related Macular Degeneration (AMD). *Adv Exp Med Biol* 2012;**723**:37. [https://doi.org/10.1007/978-1-4614-0631-0\\_6](https://doi.org/10.1007/978-1-4614-0631-0_6).
- 150 Harry GJ. Microglia during development and aging. *Pharmacol Ther* 2013;**139**:313–26. <https://doi.org/10.1016/J.PHARMTHERA.2013.04.013>.
- 151 Lehmann K, Schmidt K-F, Löwel S. Vision and visual plasticity in ageing mice. *Restor Neurol Neurosci* 2012;**30**:161–78. <https://doi.org/10.3233/RNN-2012-110192>.
- 152 Gehrs KM, Anderson DH, Johnson L V., Hageman GS. Age-related macular degeneration—emerging pathogenetic and therapeutic concepts. *Ann Med* 2006;**38**:450. <https://doi.org/10.1080/07853890600946724>.
- 153 Nguyen T, Urrutia-Cabrera D, Liou RHC, Luu CD, Guymer R, Wong RCB. New Technologies to Study Functional Genomics of Age-Related Macular Degeneration. *Front Cell Dev Biol* 2020;**8**:. <https://doi.org/10.3389/FCELL.2020.604220>.
- 154 Wanner IB, Anderson MA, Song B, Levine J, Fernandez A, Gray-Thompson Z, *et al.* Glial scar borders are formed by newly proliferated, elongated astrocytes that interact to corral inflammatory and fibrotic cells via STAT3-dependent mechanisms after spinal cord injury. *J Neurosci* 2013;**33**:12870–86. <https://doi.org/10.1523/JNEUROSCI.2121-13.2013>.
- 155 Andersen GJ. Aging and Vision: Changes in Function and Performance from Optics to Perception. *Wiley Interdiscip Rev Cogn Sci* 2012;**3**:403. <https://doi.org/10.1002/WCS.1167>.
- 156 Marola OJ, MacLean M, Cossette TL, Diemler CA, Hewes AA, Reagan AM, *et al.* Genetic context modulates aging and degeneration in the murine retina. *BioRxiv* 2024. <https://doi.org/10.1101/2024.04.16.589625>.

- 157 Daruich A, Matet A, Moulin A, Kowalczyk L, Nicolas M, Sellam A, *et al.* Mechanisms of macular edema: Beyond the surface. *Prog Retin Eye Res* 2018;**63**:20–68. <https://doi.org/10.1016/J.PRETEYERES.2017.10.006>.
- 158 Zhang C, Lai MB, Pedler MG, Johnson V, Adams RH, Petrash JM, *et al.* Endothelial Cell-Specific Inactivation of TSPAN12 (Tetraspanin 12) Reveals Pathological Consequences of Barrier Defects in an Otherwise Intact Vasculature. *Arterioscler Thromb Vasc Biol* 2018;**38**:2691. <https://doi.org/10.1161/ATVBAHA.118.311689>.
- 159 Wavre-Shapton ST, Calvi AA, Turmaine M, Seabra MC, Cutler DF, Futter CE, *et al.* Photoreceptor phagosome processing defects and disturbed autophagy in retinal pigment epithelium of Cln3 $\Delta$ ex1-6 mice modelling juvenile neuronal ceroid lipofuscinosis (Batten disease). *Hum Mol Genet* 2015;**24**:7060–74. <https://doi.org/10.1093/HMG/DDV406>.
- 160 Ebrahimi KB, Handa JT. Lipids, Lipoproteins, and Age-Related Macular Degeneration. *J Lipids* 2011;**2011**:1–14. <https://doi.org/10.1155/2011/802059>.
- 161 Upadhyay M, Milliner C, Bell BA, Bonilha VL. Oxidative stress in the retina and retinal pigment epithelium (RPE): Role of aging, and DJ-1. *Redox Biol* 2020;**37**:101623. <https://doi.org/10.1016/J.REDOX.2020.101623>.
- 162 Ueda K, Kim HJ, Zhao J, Song Y, Dunaief JL, Sparrow JR. Iron promotes oxidative cell death caused by bisretinoids of retina. *Proc Natl Acad Sci U S A* 2018;**115**:4963–8. [https://doi.org/10.1073/PNAS.1722601115/SUPPL\\_FILE/PNAS.201722601SI.PDF](https://doi.org/10.1073/PNAS.1722601115/SUPPL_FILE/PNAS.201722601SI.PDF).
- 163 Biesemeier A, Yoeruek E, Eibl O, Schraermeyer U. Iron accumulation in Bruch's membrane and melanosomes of donor eyes with age-related macular degeneration. *Exp Eye Res* 2015;**137**:39–49. <https://doi.org/10.1016/J.EXER.2015.05.019>.
- 164 Beatty S, Koh HH, Phil M, Henson D, Boulton M. The Role of Oxidative Stress in the Pathogenesis of Age-Related Macular Degeneration. *Surv Ophthalmol* 2000;**45**:115–34. [https://doi.org/10.1016/S0039-6257\(00\)00140-5](https://doi.org/10.1016/S0039-6257(00)00140-5).
- 165 Ma JYW, Greferath U, Wong JHC, Fothergill LJ, Jobling AI, Vessey KA, *et al.* Aging induces cell loss and a decline in phagosome processing in the mouse retinal pigment epithelium. *Neurobiol Aging* 2023;**128**:1–16. <https://doi.org/10.1016/J.NEUROBIOLAGING.2023.03.003>.
- 166 Rapp L, Williams T. A parametric study of retinal light damage in albino and pigmented rats. *The Effects of Constant Light on Visual Processes Plenum Press, New York* 1980:133–59.
- 167 Wasowicz M, Morice C, Ferrari P, Callebert J, Versaux-Botteri C. Long-Term Effects of Light Damage on the Retina of Albino and Pigmented Rats. *Invest Ophthalmol Vis Sci* 2002;**43**:813–20.
- 168 Wenzel A, Remé CE, Williams TP, Hafezi F, Grimm C. The Rpe65 Leu450Met Variation Increases Retinal Resistance Against Light-Induced Degeneration by Slowing Rhodopsin Regeneration. *Journal of Neuroscience* 2001;**21**:53–8. <https://doi.org/10.1523/JNEUROSCI.21-01-00053.2001>.
- 169 Danciger M, Matthes MT, Yasamura D, Akhmedov NB, Rickabaugh T, Gentleman S, *et al.* A QTL on distal Chromosome 3 that influences the severity of light-induced damage to mouse photoreceptors. *Mammalian Genome* 2000;**11**:422–7. <https://doi.org/10.1007/S003350010081/METRICS>.
- 170 Danciger M, Lyon J, Worrill D, Hoffman S, Lem J, Reme CE, *et al.* New retinal light damage QTL in mice with the light-sensitive RPE65 LEU variant. *Mamm Genome* 2004;**15**:277–83. <https://doi.org/10.1007/S00335-003-2336-2>.

- 171 Gurdita A, Tan B, Joos KM, Bizheva K, Choh V. Pigmented and albino rats differ in their responses to moderate, acute and reversible intraocular pressure elevation. *Doc Ophthalmol* 2017;**134**:205. <https://doi.org/10.1007/S10633-017-9586-X>.
- 172 Rapp LM, Williams TP. The role of ocular pigmentation in protecting against retinal light damage. *Vision Res* 1980;**20**:1127–31. [https://doi.org/10.1016/0042-6989\(80\)90050-4](https://doi.org/10.1016/0042-6989(80)90050-4).
- 173 Ortín-Martínez A, Nadal-Nicolás FM, Jiménez-López M, Alburquerque-Béjar JJ, Nieto-López L, Garcia-Ayuso D, *et al.* Number and Distribution of Mouse Retinal Cone Photoreceptors: Differences between an Albino (Swiss) and a Pigmented (C57/BL6) Strain. *PLoS One* 2014;**9**:e102392. <https://doi.org/10.1371/JOURNAL.PONE.0102392>.
- 174 Grant S, Patel NN, Philp AR, Grey CNB, Lucas RD, Foster RG, *et al.* Rod photopigment deficits in albinos are specific to mammals and arise during retinal development. *Vis Neurosci* 2001;**18**:245–51. <https://doi.org/10.1017/S095252380118209X>.
- 175 Bhansali P, Rayport I, Rebsam A, Mason C. Delayed neurogenesis leads to altered specification of ventrotemporal retinal ganglion cells in albino mice. *Neural Dev* 2014;**9**:1–15. <https://doi.org/10.1186/1749-8104-9-11/FIGURES/8>.
- 176 Pitts KM, Neeson CE, Hall NE, Lin JB, Falah HK, Wang SL, *et al.* Neurodegeneration Markers Galectin-3 and Apolipoprotein E Are Elevated in the Aqueous Humor of Eyes With Glaucoma. *Transl Vis Sci Technol* 2022;**11**:. <https://doi.org/10.1167/TVST.11.11.1>.
- 177 Siew JJ, Chen HM, Chen HY, Chen HL, Chen CM, Soong BW, *et al.* Galectin-3 is required for the microglia-mediated brain inflammation in a model of Huntington's disease. *Nature Communications* 2019 10:1 2019;**10**:1–18. <https://doi.org/10.1038/s41467-019-11441-0>.
- 178 Tabel M, Wolf A, Szczepan M, Xu H, Jägle H, Moehle C, *et al.* Genetic targeting or pharmacological inhibition of galectin-3 dampens microglia reactivity and delays retinal degeneration. *J Neuroinflammation* 2022;**19**:229. <https://doi.org/10.1186/S12974-022-02589-6>.
- 179 Bauer PM, Zalis MC, Abdshill H, Deierborg T, Johansson F, Englund-Johansson U. Inflamed In Vitro Retina: Cytotoxic Neuroinflammation and Galectin-3 Expression. *PLoS One* 2016;**11**:. <https://doi.org/10.1371/JOURNAL.PONE.0161723>.
- 180 García-Revilla J, Boza-Serrano A, Espinosa-Oliva AM, Soto MS, Deierborg T, Ruiz R, *et al.* Galectin-3, a rising star in modulating microglia activation under conditions of neurodegeneration. *Cell Death & Disease* 2022 13:7 2022;**13**:1–11. <https://doi.org/10.1038/s41419-022-05058-3>.
- 181 Hata-Mizuno M, Uchino Y, Uchino M, Shimmura S, Ogawa Y, Tsubota K, *et al.* Analysis of the Association between Galectin-3 Concentration in Tears and the Severity of Dry Eye Disease: A Case-Control Study. *Journal of Clinical Medicine* 2022, Vol 11, Page 66 2021;**11**:66. <https://doi.org/10.3390/JCM11010066>.
- 182 Liu Y, Zhao C, Meng J, Li N, Xu Z, Liu X, *et al.* Galectin-3 regulates microglial activation and promotes inflammation through TLR4/MyD88/NF-κB in experimental autoimmune uveitis. *Clinical Immunology* 2022;**236**:108939. <https://doi.org/10.1016/J.CLIM.2022.108939>.
- 183 Cao W, Tombran-Tink J, Elias R, Sezate S, Mrazek D, McGinnis JF. In vivo protection of photoreceptors from light damage by pigment epithelium-derived factor. *Invest Ophthalmol Vis Sci* 2001;**42**:1646–52.

- 184 Hernández-Pinto A, Polato F, Subramanian P, Rocha-Muñoz A de la, Vitale S, de la Rosa EJ, *et al.* PEDF peptides promote photoreceptor survival in rd10 retina models. *Exp Eye Res* 2019;**184**:24. <https://doi.org/10.1016/J.EXER.2019.04.008>.
- 185 Dixit S, Polato F, Samardzija M, Abu-Asab M, Grimm C, Crawford SE, *et al.* PEDF deficiency increases the susceptibility of rd10 mice to retinal degeneration. *Exp Eye Res* 2020;**198**:108121. <https://doi.org/10.1016/J.EXER.2020.108121>.
- 186 Bilak MM, Corse AM, Bilak SR, Lehar M, Tombran-Tink J, Kuncel RW. Pigment Epithelium-derived Factor (PEDF) Protects Motor Neurons from Chronic Glutamate-mediated Neurodegeneration. *J Neuropathol Exp Neurol* 1999;**58**:719–28. <https://doi.org/10.1097/00005072-199907000-00006>.
- 187 Bilak MM, Patricia Becerra S, Vincent AM, Moss BH, Aymerich MS, Kuncel RW. Identification of the Neuroprotective Molecular Region of Pigment Epithelium-Derived Factor and Its Binding Sites on Motor Neurons. *Journal of Neuroscience* 2002;**22**:9378–86. <https://doi.org/10.1523/JNEUROSCI.22-21-09378.2002>.
- 188 Liu Y, Leo LF, McGregor C, Grivitchvili A, Barnstable CJ, Tombran-Tink J. Pigment epithelium-derived factor (PEDF) peptide eye drops reduce inflammation, cell death and vascular leakage in diabetic retinopathy in Ins2(Akita) mice. *Mol Med* 2012;**18**:1387–401. <https://doi.org/10.2119/MOLMED.2012.00008/FIGURES/12>.
- 189 Chen X, Xu M, Zhang X, Barnstable CJ, Li X, Tombran-Tink J. Deletion of the *Pedf* gene leads to inflammation, photoreceptor loss and vascular disturbances in the retina. *Exp Eye Res* 2022;**222**:109171. <https://doi.org/10.1016/J.EXER.2022.109171>.
- 190 Zhang Q, Chrenek MA, Bhatia S, Rashid A, Ferdous S, Donaldson KJ, *et al.* Comparison of histologic findings in age-related macular degeneration with RPE flatmount images. *Mol Vis* 2019;**25**:70–8.
- 191 Ferdous S, Shelton DA, Getz TE, Chrenek MA, L'Hernault N, Sellers JT, *et al.* Deletion of histone demethylase *Lsd1* (*Kdml1a*) during retinal development leads to defects in retinal function and structure. *Front Cell Neurosci* 2023;**17**:1104592. <https://doi.org/10.3389/FNCEL.2023.1104592/FULL>.
- 192 Huber G, Beck SC, Grimm C, Sahaboglu-Tekgoz A, Paquet-Durand F, Wenzel A, *et al.* Spectral Domain Optical Coherence Tomography in Mouse Models of Retinal Degeneration. *Invest Ophthalmol Vis Sci* 2009;**50**:5888–95. <https://doi.org/10.1167/IOVS.09-3724>.
- 193 Ferdous S, Grossniklaus HE, Boatright JH, Nickerson JM. Characterization of LSD1 Expression Within the Murine Eye. *Invest Ophthalmol Vis Sci* 2019;**60**:4619. <https://doi.org/10.1167/IOVS.19-26728>.
- 194 Akhtar-Schäfer I, Wang L, Krohne TU, Xu H, Langmann T. Modulation of three key innate immune pathways for the most common retinal degenerative diseases. *EMBO Mol Med* 2018;**10**:. <https://doi.org/10.15252/emmm.201708259>.
- 195 Marc RE, Jones BW, Watt CB, Vazquez-Chona F, Vaughan DK, Organisciak DT. Extreme retinal remodeling triggered by light damage: implications for age related macular degeneration. *Mol Vis* 2008;**14**:782.
- 196 Organisciak DT, Vaughan DK. Retinal light damage: Mechanisms and protection. *Prog Retin Eye Res* 2010:113–34. <https://doi.org/10.1016/j.preteyeres.2009.11.004>.
- 197 Organisciak DT, Wong H-M, Li Z-Y, Tsof MOM. The protective effect of ascorbate in retinal light damage of rats. *Invest Ophthalmol Vis Sci* 1985;**26**:1580–8.

- 198 Krigel A, Berdugo M, Picard E, Levy-Boukris R, Jaadane I, Jonet L, *et al.* Light-induced retinal damage using different light sources, protocols and rat strains reveals LED phototoxicity. *Neuroscience* 2016;**339**:296–307. <https://doi.org/10.1016/j.neuroscience.2016.10.015>.
- 199 Nakamura M, Yako T, Kuse Y, Inoue Y, Nishinaka A, Nakamura S, *et al.* Exposure to excessive blue LED light damages retinal pigment epithelium and photoreceptors of pigmented mice. *Exp Eye Res* 2018;**177**:1–11. <https://doi.org/10.1016/J.EXER.2018.07.022>.
- 200 Grant S, Patel NN, Philp AR, Grey CNB, Lucas RD, Foster RG, *et al.* Rod photopigment deficits in albinos are specific to mammals and arise during retinal development. *Vis Neurosci* 2001;**18**:245–51. <https://doi.org/10.1017/S095252380118209X>.
- 201 Jeffery G. The albino retina: an abnormality that provides insight into normal retinal development. *Trends Neurosci* 1997;**20**:165–9. [https://doi.org/10.1016/S0166-2236\(96\)10080-1](https://doi.org/10.1016/S0166-2236(96)10080-1).
- 202 Obermann J, Priglinger CS, Merl-Pham J, Geerlof A, Priglinger S, Götz M, *et al.* Proteome-wide Identification of Glycosylation-dependent Interactors of Galectin-1 and Galectin-3 on Mesenchymal Retinal Pigment Epithelial (RPE) Cells. *Mol Cell Proteomics* 2017;**16**:1528. <https://doi.org/10.1074/MCP.M116.066381>.
- 203 Jablonski MM, Tombran-Tink J, Mrazek DA, Iannaccone A. Pigment Epithelium-Derived Factor Supports Normal Development of Photoreceptor Neurons and Opsin Expression after Retinal Pigment Epithelium Removal. *The Journal of Neuroscience* 2000;**20**:7149. <https://doi.org/10.1523/JNEUROSCI.20-19-07149.2000>.
- 204 He Y, Leung KW ah, Ren Y, Pei J, Ge J, Tombran-Tink J. PEDF Improves Mitochondrial Function in RPE Cells During Oxidative Stress. *Invest Ophthalmol Vis Sci* 2014;**55**:6742–55. <https://doi.org/10.1167/IOVS.14-14696>.
- 205 Tombran-Tink J, Mazuruk K, Rodriguez IR, Chung D, Linker T, Englander E, *et al.* Organization, Evolutionary Conservation, Expression and Unusual Alu Density of the Human Gene for Pigment Epithelium-Derived Factor, a Unique Neurotrophic Serpin. *Molecular Vision*. 1996. URL: <http://www.molvis.org/molvis/v2/a11/> (Accessed 22 July 2024).
- 206 Karakousis PC, John SK, Behling K, Surace EM, Smith JE, Hendrickson A, *et al.* Localization of pigment epithelium derived factor (PEDF) in developing and adult human ocular tissues. *Mol Vis* 2001;**7**:154–63.
- 207 Longbottom R, Fruttiger M, Douglas RH, Martinez-Barbera JP, Greenwood J, Moss SE. Genetic ablation of retinal pigment epithelial cells reveals the adaptive response of the epithelium and impact on photoreceptors. *Proc Natl Acad Sci U S A* 2009;**106**:18728–33. [https://doi.org/10.1073/PNAS.0902593106/SUPPL\\_FILE/0902593106SI.PDF](https://doi.org/10.1073/PNAS.0902593106/SUPPL_FILE/0902593106SI.PDF).
- 208 Aymerich, Maria S., Alberdi, EM. , Martinez, A. , Becerra SP. Evidence for pigment epithelium derived factor receptors in the neural retina. *Invest Ophthalmol Vis Sci* 2001;**42**:3287–93.
- 209 Becerra SP, Fariss RN, Wu YQ, Montuenga LM, Wong P, Pfeffer BA. Pigment epithelium-derived factor in the monkey retinal pigment epithelium and interphotoreceptor matrix: apical secretion and distribution. *Exp Eye Res* 2004;**78**:223–34. <https://doi.org/10.1016/J.EXER.2003.10.013>.

- 210 Rebutini IT, Crawford SE, Becerra SP. PEDF Deletion Induces Senescence and Defects in Phagocytosis in the RPE. *International Journal of Molecular Sciences* 2022, Vol 23, Page 7745 2022;**23**:7745. <https://doi.org/10.3390/IJMS23147745>.
- 211 Ogata N, Matsuoka M, Imaizumi M, Arichi M, Matsumura M. Decreased levels of pigment Epithelium-derived factor in eyes with neuroretinal dystrophic diseases. *Am J Ophthalmol* 2004;**137**:1129–30. <https://doi.org/10.1016/j.ajo.2003.11.080>.
- 212 Rogers ME, Navarro ID, Perkumas KM, Niere SM, Allingham RR, Crosson CE, *et al*. Pigment Epithelium-Derived Factor Decreases Outflow Facility. *Invest Ophthalmol Vis Sci* 2013;**54**:6655. <https://doi.org/10.1167/IOVS.13-12766>.
- 213 Spranger J, Osterhoff M, Reimann M, Möhlig M, Ristow M, Francis MK, *et al*. Loss of the Antiangiogenic Pigment Epithelium-Derived Factor in Patients With Angiogenic Eye Disease. *Diabetes* 2001;**50**:2641–5. <https://doi.org/10.2337/DIABETES.50.12.2641>.
- 214 Ma B, Zhou Y, Liu R, Zhang K, Yang T, Hu C, *et al*. Pigment epithelium-derived factor (PEDF) plays anti-inflammatory roles in the pathogenesis of dry eye disease. *Ocul Surf* 2021;**20**:70–85. <https://doi.org/10.1016/J.JTOS.2020.12.007>.
- 215 Singh RB, Blanco T, Mittal SK, Taketani Y, Chauhan SK, Chen Y, *et al*. Pigment Epithelium-derived Factor secreted by corneal epithelial cells regulates dendritic cell maturation in dry eye disease. *Ocular Surface* 2020;**18**:460–9. <https://doi.org/10.1016/j.jtos.2020.05.002>.
- 216 Alberdi E, Aymerich MS, Becerra SP. Binding of Pigment Epithelium-derived Factor (PEDF) to Retinoblastoma Cells and Cerebellar Granule Neurons: EVIDENCE FOR A PEDF RECEPTOR \*. *Journal of Biological Chemistry* 1999;**274**:31605–12. <https://doi.org/10.1074/JBC.274.44.31605>.
- 217 Zamiri P, Masli S, Streilein JW, Taylor AW. Pigment Epithelial Growth Factor Suppresses Inflammation by Modulating Macrophage Activation. *Invest Ophthalmol Vis Sci* 2006;**47**:3912–8. <https://doi.org/10.1167/IOVS.05-1267>.
- 218 Park K, Jin J, Hu Y, Zhou K, Ma J-X. Overexpression of Pigment Epithelium-Derived Factor Inhibits Retinal Inflammation and Neovascularization. *Am J Pathol* 2011;**178**:688–98. <https://doi.org/10.1016/j.ajpath.2010.10.014>.
- 219 Polato F, Becerra SP. Pigment Epithelium-Derived Factor, a Protective Factor for Photoreceptors in Vivo. *Adv Exp Med Biol* 2016;**854**:699. [https://doi.org/10.1007/978-3-319-17121-0\\_93](https://doi.org/10.1007/978-3-319-17121-0_93).
- 220 Cayouette M, Smith SB, Becerra SP, Gravel C. Pigment Epithelium-Derived Factor Delays the Death of Photoreceptors in Mouse Models of Inherited Retinal Degenerations. *Neurobiol Dis* 1999;**6**:523–32. <https://doi.org/10.1006/NBDI.1999.0263>.
- 221 Taniwaki T, Hirashima N, Becerra SP, Chader GJ, Etcheberrigaray R, Schwartz JP. Pigment Epithelium-Derived Factor Protects Cultured Cerebellar Granule Cells Against Glutamate-Induced Neurotoxicity. *J Neurochem* 1997;**68**:26–32. <https://doi.org/10.1046/J.1471-4159.1997.68010026.X>.
- 222 Taniwaki T, Becerra SP, Chader GJ, Schwartz JP. Pigment epithelium-derived factor is a survival factor for cerebellar granule cells in culture. *J Neurochem* 1995;**64**:2509–17. <https://doi.org/10.1046/J.1471-4159.1995.64062509.X>.
- 223 An E, Lu X, Flippin J, Devaney JM, Halligan B, Hoffman E, *et al*. Secreted proteome profiling in human RPE cell cultures derived from donors with age related macular degeneration and age matched healthy donors. *J Proteome Res* 2006;**5**:2599–610. <https://doi.org/10.1021/pr060121j>.

- 224 Yuan X, Gu X, Crabb JS, Yue X, Shadrach K, Hollyfield JG, *et al.* Quantitative proteomics: Comparison of the macular bruch membrane/choroid complex from age-related macular degeneration and normal eyes. *Molecular and Cellular Proteomics* 2010;**9**:1031–46. <https://doi.org/10.1074/mcp.M900523-MCP200>.
- 225 Priglinger CS, Obermann J, Szober CM, Merl-Pham J, Ohmayer U, Behler J, *et al.* Epithelial-to-mesenchymal transition of RPE cells in vitro confers increased  $\beta$ 1,6-N-Glycosylation and Increased Susceptibility to Galectin-3 Binding. *PLoS One* 2016;**11**:e0146887. <https://doi.org/10.1371/journal.pone.0146887>.
- 226 Hughes RC. Secretion of the galectin family of mammalian carbohydrate-binding proteins. *Biochim Biophys Acta Gen Subj* 1999:172–85. [https://doi.org/10.1016/S0304-4165\(99\)00177-4](https://doi.org/10.1016/S0304-4165(99)00177-4).
- 227 Caridi B, Doncheva D, Sivaprasad S, Turowski P. Galectins in the Pathogenesis of Common Retinal Disease. *Front Pharmacol* 2021;**12**:. <https://doi.org/10.3389/fphar.2021.687495>.
- 228 Henderson NC, Sethi T. The regulation of inflammation by galectin-3. *Immunol Rev* 2009;**230**:160–71. <https://doi.org/10.1111/J.1600-065X.2009.00794.X>.
- 229 Li Z-Y, M Tso MO, Wongf H, Organisciakf DT. Amelioration of photic injury in rat retina by ascorbic acid: a histopathologic study. *Invest Ophthalmol Vis Sci* 1985;**26**:1589–98.
- 230 Sun N, Shibata B, Hess JF, Fitzgerald PG. An alternative means of retaining ocular structure and improving immunoreactivity for light microscopy studies. *Mol Vis* 2015;**21**:428.
- 231 Devera C, Dixon J, Chrenek MA, Baba K, Le YZ, Iuvone PM, *et al.* The Circadian Clock in the Retinal Pigment Epithelium Controls the Diurnal Rhythm of Phagocytic Activity. *Int J Mol Sci* 2022;**23**:5302. <https://doi.org/10.3390/IJMS23105302>.
- 232 Murakami Y, Ikeda Y, Yonemitsu Y, Onimaru M, Nakagawa K, Kohno RI, *et al.* Inhibition of Nuclear Translocation of Apoptosis-Inducing Factor Is an Essential Mechanism of the Neuroprotective Activity of Pigment Epithelium-Derived Factor in a Rat Model of Retinal Degeneration. *Am J Pathol* 2008;**173**:1326. <https://doi.org/10.2353/AJPATH.2008.080466>.
- 233 Cao W, Tombran-Tink J, Elias R, Sezate S, McGinnis JF. Role of Pigment Epithelium-Derived Factor (PEDF) in Photoreceptor Cell Protection. *New Insights Into Retinal Degenerative Diseases* 2001:119–26. [https://doi.org/10.1007/978-1-4615-1355-1\\_14](https://doi.org/10.1007/978-1-4615-1355-1_14).
- 234 Gordan WC, Casey DM, Lukiw WJ, Bazan NG. DNA Damage and Repair in Light-Induced Photoreceptor Degeneration. *Invest Ophthalmol Vis Sci* 2002:3511–21.
- 235 Chen Y, Yang J, Geng H, Li L, Li J, Cheng B, *et al.* Photoreceptor degeneration in microphthalmia (Mitf) mice: partial rescue by pigment epithelium-derived factor. *Dis Model Mech* 2019;**12**:. <https://doi.org/10.1242/DMM.035642>.
- 236 Liao R, Yan F, Zeng Z, Wang H, Qiu K, Xu J, *et al.* Insulin-like growth factor-1 activates PI3K/Akt signalling to protect human retinal pigment epithelial cells from amiodarone-induced oxidative injury. *Br J Pharmacol* 2018;**175**:125. <https://doi.org/10.1111/BPH.14078>.
- 237 Haurigot V, Villacampa P, Ribera A, Bosch A, Ramos D, Ruberte J, *et al.* Long-Term Retinal PEDF Overexpression Prevents Neovascularization in a Murine Adult Model of Retinopathy. *PLoS One* 2012;**7**:e41511. <https://doi.org/10.1371/JOURNAL.PONE.0041511>.

- 238 Arroba AI, Campos-Caro A, Aguilar-Diosdado M, Valverde ÁM. IGF-1, Inflammation and Retinal Degeneration: A Close Network. *Front Aging Neurosci* 2018;**10**:203. <https://doi.org/10.3389/FNAGI.2018.00203>.
- 239 Arroba AI, Álvarez-Lindo N, van Rooijen N, de la Rosa EJ. Microglia-mediated IGF-I neuroprotection in the rd10 mouse model of retinitis pigmentosa. *Invest Ophthalmol Vis Sci* 2011;**52**:9124–30. <https://doi.org/10.1167/IOVS.11-7736>.
- 240 Yamawaki T, Ito E, Mukai A, Ueno M, Yamada J, Sotozono C, *et al*. The ingenious interactions between macrophages and functionally plastic retinal pigment epithelium cells. *Invest Ophthalmol Vis Sci* 2016;**57**:5945–53. <https://doi.org/10.1167/iov.16-20604>.
- 241 Ueno S, Sudo T, Saya H, Sugihara E. Pigment epithelium-derived factor promotes peritoneal dissemination of ovarian cancer through induction of immunosuppressive macrophages. *Communications Biology* 2022 5:1 2022;**5**:1–16. <https://doi.org/10.1038/s42003-022-03837-4>.
- 242 Bernardo-Colón A, Lerner M, Becerra SP. Pigment epithelium-derived factor is an interleukin-6 antagonist in the RPE: Insight of structure-function relationships. *Front Physiol* 2022;**13**:. <https://doi.org/10.3389/FPHYS.2022.1045613>.
- 243 O’Koren EG, Yu C, Klingeborn M, Wong AYW, Prigge CL, Mathew R, *et al*. Microglial Function Is Distinct in Different Anatomical Locations during Retinal Homeostasis and Degeneration. *Immunity* 2019;**50**:723-737.e7. <https://doi.org/10.1016/j.immuni.2019.02.007>.
- 244 Yu C, Lad EM, Mathew R, Littleton S, Chen Y, Schlepckow K, *et al*. Microglia at Sites of Atrophy Restrict the Progression of Retinal Degeneration via Galectin-3 and Trem2 Interactions. *BioRxiv* 2023. <https://doi.org/10.1101/2023.07.19.549403>.
- 245 Kumar S, Ranawat CS, Bhandiwad C, Arya H, Mali M, Singh CP, *et al*. Galectin-3 as a Potential Biomarker of Microvascular Complications in Patients with Type 2 Diabetes. *Indian J Endocrinol Metab* 2022;**26**:490. [https://doi.org/10.4103/IJEM.IJEM\\_270\\_22](https://doi.org/10.4103/IJEM.IJEM_270_22).
- 246 Zhou ZY, Chang TF, Lin Z Bin, Jing YT, Wen LS, Niu YL, *et al*. Microglial Galectin3 enhances endothelial metabolism and promotes pathological angiogenesis via Notch inhibition by competitively binding to Jag1. *Cell Death & Disease* 2023 14:6 2023;**14**:1–15. <https://doi.org/10.1038/s41419-023-05897-8>.
- 247 Ortín-Martínez A, Valiente-Soriano FJ, García-Ayuso D, Alarcón-Martínez L, Jiménez-López M, Bernal-Garro JM, *et al*. A Novel In Vivo Model of Focal Light Emitting Diode-Induced Cone-Photoreceptor Phototoxicity: Neuroprotection Afforded by Brimonidine, BDNF, PEDF or bFGF. *PLoS One* 2014;**9**:. <https://doi.org/10.1371/JOURNAL.PONE.0113798>.
- 248 MEDAWAR PB. Immunity to Homologous Grafted Skin. III. The Fate of Skin Homographs Transplanted to the Brain, to Subcutaneous Tissue, and to the Anterior Chamber of the Eye. *Br J Exp Pathol* 1948;**29**:58.
- 249 Wayne J, Boston S. Immunological non-responsiveness and acquisition of tolerance in relation to immune privilege in the eye. *Eye* 1995 9:2 1995;**9**:236–40. <https://doi.org/10.1038/eye.1995.46>.
- 250 Qiao H, Lucas K, Stein-Streilein J. Retinal Laser Burn Disrupts Immune Privilege in the Eye. *Am J Pathol* 2009;**174**:414. <https://doi.org/10.2353/AJPATH.2009.080766>.
- 251 Lucas K, Karamichos D, Mathew R, Zieske JD, Stein-Streilein J. Retinal laser burn (RLB) induced neuropathy leads to substance P dependent loss of ocular immune privilege. *J Immunol* 2012;**189**:1237. <https://doi.org/10.4049/JIMMUNOL.1103264>.

- 252 Taylor AW, Hsu S, Ng TF. The Role of Retinal Pigment Epithelial Cells in Regulation of Macrophages/Microglial Cells in Retinal Immunobiology. *Front Immunol* 2021;**12**:3256. <https://doi.org/10.3389/FIMMU.2021.724601/BIBTEX>.
- 253 Kawanaka N, Taylor AW. Localized retinal neuropeptide regulation of macrophage and microglial cell functionality. *J Neuroimmunol* 2011;**232**:17. <https://doi.org/10.1016/J.JNEUROIM.2010.09.025>.
- 254 Zhang SX, Wang JJ, Gao G, Shao C, Mott R, Ma J. Pigment epithelium-derived factor (PEDF) is an endogenous antiinflammatory factor. *The FASEB Journal* 2006;**20**:323–5. <https://doi.org/10.1096/FJ.05-4313FJE>.
- 255 Kenealey J, Subramanian P, Comitato A, Bullock J, Keehan L, Polato F, *et al*. Small Retinoprotective Peptides Reveal a Receptor-binding Region on Pigment Epithelium-derived Factor \*. *Journal of Biological Chemistry* 2015;**290**:25241–53. <https://doi.org/10.1074/JBC.M115.645846>.
- 256 Sanchez A, Tripathy D, Yin X, Luo J, Martinez J, Grammas P. Pigment epithelium-derived factor (PEDF) protects cortical neurons in vitro from oxidant injury by activation of extracellular signal-regulated kinase (ERK) 1/2 and induction of Bcl-2. *Neurosci Res* 2012;**72**:1. <https://doi.org/10.1016/J.NEURES.2011.09.003>.
- 257 He T, Liu W, Shen CAA. Anti-inflammatory properties of pigment epithelium-derived factor. <https://doi.org/10.1177/1721727X221138857> 2022;**20**:. <https://doi.org/10.1177/1721727X221138857>.
- 258 Rebutini IT, Crawford SE, Becerra SP. PEDF Deletion Induces Senescence and Defects in Phagocytosis in the RPE. *International Journal of Molecular Sciences* 2022, Vol 23, Page 7745 2022;**23**:7745. <https://doi.org/10.3390/IJMS23147745>.
- 259 Zhang L, Cui X, Jauregui R, Park KS, Justus S, Tsai YT, *et al*. Genetic Rescue Reverses Microglial Activation in Preclinical Models of Retinitis Pigmentosa. *Molecular Therapy* 2018;**26**:1953. <https://doi.org/10.1016/J.YMTHE.2018.06.014>.
- 260 Secondi R, Kong J, Blonska AM, Staurengi G, Sparrow JR. Fundus Autofluorescence Findings in a Mouse Model of Retinal Detachment. *Invest Ophthalmol Vis Sci* 2012;**53**:5190–7. <https://doi.org/10.1167/IOVS.12-9672>.
- 261 Miura M, Makita S, Sugiyama S, Hong YJ, Yasuno Y, Elsner AE, *et al*. Evaluation of intraretinal migration of retinal pigment epithelial cells in age-related macular degeneration using polarimetric imaging. *Sci Rep* 2017;**7**:. <https://doi.org/10.1038/s41598-017-03529-8>.
- 262 Curcio CA, Zanzottera EC, Ach T, Balaratnasingam C, Freund KB. Activated Retinal Pigment Epithelium, an Optical Coherence Tomography Biomarker for Progression in Age-Related Macular Degeneration. *Invest Ophthalmol Vis Sci* 2017;**58**:BIO211–26. <https://doi.org/10.1167/IOVS.17-21872>.
- 263 Rajala A, Teel K, Bhat MA, Batushansky A, Griffin TM, Purcell L, *et al*. Insulin-like growth factor 1 receptor mediates photoreceptor neuroprotection. *Cell Death Dis* 2022;**13**:. <https://doi.org/10.1038/S41419-022-05074-3>.
- 264 Jones AL, Dhanapala L, Baldo TA, Sharafeldin M, Krause CE, Shen M, *et al*. Prostate Cancer Diagnosis in the Clinic Using an 8-Protein Biomarker Panel. *Anal Chem* 2021;**93**:1059–67. [https://doi.org/10.1021/ACS.ANALCHEM.0C04034/ASSET/IMAGES/LARGE/AC0C04034\\_0006.JPEG](https://doi.org/10.1021/ACS.ANALCHEM.0C04034/ASSET/IMAGES/LARGE/AC0C04034_0006.JPEG).

- 265 Bellver-Landete V, Bretheau F, Mailhot B, Vallières N, Lessard M, Janelle M-E, *et al.* Microglia are an essential component of the neuroprotective scar that forms after spinal cord injury n.d. <https://doi.org/10.1038/s41467-019-08446-0>.
- 266 Rodriguez-de la Rosa L, Fernandez-Sanchez L, Germain F, Murillo-Cuesta S, Varela-Nieto I, de la Villa P, *et al.* Age-related functional and structural retinal modifications in the Igf1<sup>-/-</sup> null mouse. *Neurobiol Dis* 2012;**46**:476–85. <https://doi.org/10.1016/J.NBD.2012.02.013>.
- 267 Kermer P, Klöcker N, Labes M, Bähr M. Insulin-Like Growth Factor-I Protects Axotomized Rat Retinal Ganglion Cells from Secondary Death via PI3-K-Dependent Akt Phosphorylation and Inhibition of Caspase-3 In Vivo. *Journal of Neuroscience* 2000;**20**:722–8. <https://doi.org/10.1523/JNEUROSCI.20-02-00722.2000>.
- 268 Politi LE, Rotstein NP, Salvador G, Giusto NM, Fernanda Insua M. Insulin-like growth factor-I is a potential trophic factor for amacrine cells. *J Neurochem* 2001;**76**:1199–211. <https://doi.org/10.1046/J.1471-4159.2001.00128.X>.
- 269 Spadaro O, Camell CD, Bosurgi L, Nguyen KY, Youm YH, Rothlin C V., *et al.* IGF1 shapes the macrophage activation in response to immunometabolic challenge. *Cell Rep* 2017;**19**:225. <https://doi.org/10.1016/J.CELREP.2017.03.046>.
- 270 Lee DC, Ruiz CR, Lebson L, Selenica MLB, Rizer J, Hunt JB, *et al.* Aging enhances classical activation but mitigates alternative activation in the CNS. *Neurobiol Aging* 2013;**34**:1610. <https://doi.org/10.1016/J.NEUROBIOLAGING.2012.12.014>.
- 271 Santos CL, Bobermin LD, Quincozes-Santos A. Aging changes the expression of adenosine receptors, insulin-like growth factor 1 (IGF1), and hypoxia-inducible factor 1 $\alpha$  (HIF1 $\alpha$ ) in hypothalamic astrocyte cultures. *Aging Brain* 2024;**5**:100104. <https://doi.org/10.1016/J.NBAS.2023.100104>.
- 272 Toth L, Czigler A, Hegedus E, Komaromy H, Amrein K, Czeiter E, *et al.* Age-related decline in circulating IGF-1 associates with impaired neurovascular coupling responses in older adults. *Geroscience* 2022;**44**:2771–83. <https://doi.org/10.1007/S11357-022-00623-2/FIGURES/5>.
- 273 Holtman IR, Raj DD, Miller JA, Schaafsma W, Yin Z, Brouwer N, *et al.* Induction of a common microglia gene expression signature by aging and neurodegenerative conditions: a co-expression meta-analysis. *Acta Neuropathol Commun* 2015;**3**:31. <https://doi.org/10.1186/s40478-015-0203-5>.
- 274 Fernandez CG, Hamby ME, McReynolds ML, Ray WJ. The role of apoE4 in disrupting the homeostatic functions of astrocytes and microglia in aging and Alzheimer’s disease. *Front Aging Neurosci* 2019;**10**:14. <https://doi.org/10.3389/fnagi.2019.00014>.
- 275 Chen M, Muckersie E, Forrester J V., Xu H. Immune Activation in Retinal Aging: A Gene Expression Study. *Invest Ophthalmol Vis Sci* 2010;**51**:5888–96. <https://doi.org/10.1167/IOVS.09-5103>.
- 276 Xu H, Chen M, Forrester J V. Para-inflammation in the aging retina. *Prog Retin Eye Res* 2009;**28**:348–68. <https://doi.org/10.1016/J.PRETEYERES.2009.06.001>.
- 277 Miller EB, Zhang P, Ching K, Pugh EN, Burns ME. In vivo imaging reveals transient microglia recruitment and functional recovery of photoreceptor signaling after injury. *Proc Natl Acad Sci U S A* 2019;**116**:16603–12. <https://doi.org/10.1073/pnas.1903336116>.
- 278 Karlen SJ, Miller EB, Wang X, Levine ES, Zawadzki RJ, Burns ME. Monocyte infiltration rather than microglia proliferation dominates the early immune response to

- rapid photoreceptor degeneration. *J Neuroinflammation* 2018;**15**:344.  
<https://doi.org/10.1186/s12974-018-1365-4>.
- 279 Ma B, Zhou Y, Liu R, Zhang K, Yang T, Hu C, *et al*. Pigment epithelium-derived factor (PEDF) plays anti-inflammatory roles in the pathogenesis of dry eye disease. *Ocul Surf* 2021;**20**:70–85. <https://doi.org/10.1016/J.JTOS.2020.12.007>.
- 280 Popova EY, Pinzon-Guzman C, Salzberg AC, Zhang SSM, Barnstable CJ. LSD1-Mediated Demethylation of H3K4me2 Is Required for the Transition from Late Progenitor to Differentiated Mouse Rod Photoreceptor. *Mol Neurobiol* 2016;**53**:4563.  
<https://doi.org/10.1007/S12035-015-9395-8>.
- 281 Rao GN. Light intensity-associated eye lesions of Fischer 344 rats in long-term studies. *Toxicol Pathol* 1991;**19**:148–55. <https://doi.org/10.1177/019262339101900209>.
- 282 Heiduschka P, Schraermeyer U. Comparison of visual function in pigmented and albino rats by electroretinography and visual evoked potentials. *Graefes Arch Clin Exp Ophthalmol* 2008;**246**:1559–73. <https://doi.org/10.1007/S00417-008-0895-3>.
- 283 de Imperial-Ollero JAM, Gallego-Ortega A, Ortín-Martínez A, Villegas-Pérez MP, Valiente-Soriano FJ, Vidal-Sanz M. Animal Models of LED-Induced Phototoxicity. Short- and Long-Term In Vivo and Ex Vivo Retinal Alterations. *Life* 2021;**11**:.  
<https://doi.org/10.3390/LIFE11111137>.
- 284 Díaz-Alvarez L, Ortega E. The Many Roles of Galectin-3, a Multifaceted Molecule, in Innate Immune Responses against Pathogens. *Mediators Inflamm* 2017;**2017**:.  
<https://doi.org/10.1155/2017/9247574>.
- 285 Singh RB, Blanco T, Mittal SK, Alemi H, Chauhan SK, Chen Y, *et al*. Pigment Epithelium-Derived Factor Enhances the Suppressive Phenotype of Regulatory T Cells in a Murine Model of Dry Eye Disease. *Am J Pathol* 2021;**191**:720.  
<https://doi.org/10.1016/J.AJPAT.2021.01.003>.
- 286 Hata-Mizuno M, Uchino Y, Uchino M, Shimmura S, Ogawa Y, Tsubota K, *et al*. Analysis of the Association between Galectin-3 Concentration in Tears and the Severity of Dry Eye Disease: A Case-Control Study. *J Clin Med* 2022;**11**:66.  
<https://doi.org/10.3390/JCM11010066>.
- 287 An E, Lu X, Flippin J, Devaney JM, Halligan B, Hoffman E, *et al*. Secreted proteome profiling in human RPE cell cultures derived from donors with age related macular degeneration and age matched healthy donors. *J Proteome Res* 2006;**5**:2599–610.  
<https://doi.org/10.1021/pr060121j>.
- 288 Wang Y, Subramanian P, Shen D, Tuo J, Becerra SP, Chan CC. Pigment epithelium-derived factor reduces apoptosis and pro-inflammatory cytokine gene expression in a murine model of focal retinal degeneration. *ASN Neuro* 2013;**5**:309–19.  
<https://doi.org/10.1042/AN20130028>.
- 289 Anguissola S, McCormack WJ, Morrin MA, Higgins WJ, Fox DM, Worrall DM. Pigment Epithelium-Derived Factor (PEDF) Interacts with Transportin SR2, and Active Nuclear Import Is Facilitated by a Novel Nuclear Localization Motif. *PLoS One* 2011;**6**:.  
<https://doi.org/10.1371/JOURNAL.PONE.0026234>.
- 290 Pereira JX, Dos Santos SN, Pereira TC, Cabanel M, Chammas R, De Oliveira FL, *et al*. Galectin-3 Regulates the Expression of Tumor Glycosaminoglycans and Increases the Metastatic Potential of Breast Cancer. *J Oncol* 2019;**2019**:9827147.  
<https://doi.org/10.1155/2019/9827147>.

- 291 Ilmer M, Mazurek N, Gilcrease MZ, Byrd JC, Woodward WA, Buchholz TA, *et al.* Low expression of galectin-3 is associated with poor survival in node-positive breast cancers and mesenchymal phenotype in breast cancer stem cells. *Breast Cancer Research* 2016;**18**:1–12. <https://doi.org/10.1186/S13058-016-0757-6/FIGURES/6>.
- 292 Nakajima K, Balan V, Raz A. Galectin-3: an immune checkpoint target for musculoskeletal tumor patients. *Cancer Metastasis Rev* 2021;**40**:297. <https://doi.org/10.1007/S10555-020-09932-4>.
- 293 Kashyap VK, Tripathi S, Elmi M, Dass JH, Dass CR, Au JHD. The Various Roles of PEDF in Cancer. *Cancers* 2024, Vol 16, Page 510 2024;**16**:510. <https://doi.org/10.3390/CANCERS16030510>.
- 294 Becerra SP, Notario V. The effects of PEDF on cancer biology: mechanisms of action and therapeutic potential. *Nature Reviews Cancer* 2013 13:4 2013;**13**:258–71. <https://doi.org/10.1038/nrc3484>.
- 295 Martinez-Marin D, Jarvis C, Nelius T, De Riese W, Volpert O V., Filleur S. PEDF increases the tumoricidal activity of macrophages towards prostate cancer cells in vitro. *PLoS One* 2017;**12**:e0174968. <https://doi.org/10.1371/JOURNAL.PONE.0174968>.